# Table of Contents

# List of Tables

# List of Figures

# Chapter 1

## Introduction, hypothesis, and scope

### 1.1. Introduction

Coal, being a product of the remains of most kingdoms of life (Hower et al., 2009, 2011b), is a complex product of various botanical and zoological precursor materials. During peatification, diagenesis, and subsequent coalification processes, the original matter is decomposed, altered, and transformed into coal. The organic chemistry of coal is chiefly a function of the starting materials, and any process that affects it subsequently. In addition to the organic fraction (macerals), coal contains an inorganic (mineral matter) fraction, which determines the grade of the coal (Snyman and Botha, 1993; O'Keefe et al., 2013). The organic fraction of coal forms the primary basis upon which to understand behaviour during potential applications including: combustion, liquefaction, gasification, carbonization, and, most importantly for current study, it aids in the general understanding of the origin of the organic components (van Krevelen, 1993, and references therein).

Previous studies have used various organic geochemical analytical methods to elucidate the composition of the maceral components of coal, and to constrain the origin pathways thereof (e.g., Austen et al., 1966; Retcofsky et al., 1968, 1981; Dyrkacz and Horwitz, 1982; Dyrkacz et al., 1984; Meuzelaar et al., 1984; Silbernagel et al., 1984a, 1984b, 1986; Senftle et al., 1986; Spiker and Hatcher, 1987; Nip et al., 1988, 1992; Solum et al., 1989; White et al., 1989; Supaluknari et al., 1990; Powell et al., 1991; Haenel, 1992; van Krevelen, 1993, and references therein; Hartgers et al., 1994; Mastalerz and Bustin, 1994, 1997; Hatcher and Clifford, 1997, and references therein; Maroto-Valer et al., 1998; Więckowski et al., 2000; Davidson, 2004, and references therein; Suggate and Dickinson, 2004; Rimmer et al., 2006; Erdenetsogt et al., 2010, 2017; Cao et al., 2011, 2013; Chen et al., 2012; Mastalerz et al., 2013; Valentim et al., 2016; Radlinski and Mastalerz, 2018; Zieger et al., 2018). However, the overwhelming majority of these previous studies have addressed vitrinite-rich coals of the northern hemisphere, which have been shown to be both compositionally and genetically distinct from southern hemisphere counterparts (Plumstead, 1961; Falcon and Snyman, 1986; Falcon, 1986; Cairncross and Cadle,

1988; Falcon and Ham, 1988; Snyman, 1989; Cairncross et al., 1990; Diessel, 1992, 2010; Snyman and Botha, 1993; Taylor et al., 1998; Van Niekerk et al., 2008; O'Keefe et al., 2013).

Organic geochemical studies on coals from the various South African coalfields have used analytical techniques such as flash-pyrolysis gas chromatography mass spectrometry (flash-pyrolysis GCMS), gas chromatography (GC) with flame-ionization detection (FID), solid-state nuclear magnetic resonance (NMR), wide angle X-ray diffraction-carbon fraction analysis (WAXRD-CFA), fourier transform infrared spectroscopy (FTIR), computer controlled scanning electron microscopy (CCSEM), matrix assisted laser desorption ionization-time-of-flight mass spectrometry (MALDI-TOF-MS), X-ray photoelectron spectroscopy (XPS), high-resolution transmission electron microscopy (HRTEM), small-angle X-ray scattering (SAXS), amongst others, primarily to understand changes associated with various coal conversion processes (e.g., Van Niekerk et al., 2008; Van Niekerk and Mathews, 2010; Malumbazo et al., 2011; Strydom et al., 2011; Hattingh et al., 2013; Coetzee et al., 2015; Okolo et al., 2015; Roberts et al., 2015a, 2015b; Louw et al., 2016; Sehume et al., 2017; Phiri et al., 2017, 2018). In addition, Fabiańska and Kruszewska (2003) investigated the relationship between petrographic composition and geochemistry obtained using liquid gas chromatography-mass spectrometry (GC-MS) using coals from the Main Karoo Basin (MKB) as well as the Waterberg and Soutpansberg Coalfields. A number of other studies report on the concentration of various trace elements present in South African coals (e.g., Cairncross et al., 1990; Wagner and Hlatshwayo, 2005; Pone et al., 2007; Bergh et al., 2011; Lusilao-Makiese et al., 2012; Wagner and Tlotleng, 2012; Kolker et al., 2017). However, the vast majority of these geochemical studies were not concerned with the origin pathways for macerals present in the coals.

The present study incorporates the use of selected organic geochemical techniques in an investigation into the origin pathways for macerals present in iso-rank inertinite-rich and vitrinite-rich South African coal samples from the Witbank Coalfield. The geochemical techniques used include: electron spin resonance (ESR); carbon-13 cross-polarization magic-angle-spinning solid-state nuclear magnetic resonance ($^{13}$C CP-MAS SS NMR); and, stable nitrogen and carbon isotope ($\delta^{15}$N and $\delta^{13}$C) values along with the concentration of nitrogen functionalities determined using X-ray photoelectron spectroscopy (XPS). The molecular chemistry of inertinite-rich and vitrinite-rich coals is also compared using results from a

pyrolysis gas chromatograph (py-GC) equipped with a thermal desorption unit (TDU) coupled to a time of flight (TOF) mass spectrometer (MS) (py-GC/MS).

### 1.2. Coal use and geological setting

On an annual basis, South Africa produces approximately 245 million tonnes of coal (Steyn and Minnitt, 2010). Of the total production, approximately half (112 million tonnes) is used for electricity generation by the state-owned power-utility, Eskom. The electricity generated accounts for more than 90% of the total produced in South Africa (Beidari et al., 2017). Roughly a quarter of total annual coal production (~65 million tonnes) is exported to international markets, with the remainder consumed domestically by Sasol Synthetic Fuels, general industry, and households (Steyn and Minnitt, 2010). In spite of the general worldwide drive towards a reduction in the utilization of fossil fuels as a result of climate change, coal still remains an attractive energy option owing primarily to its relatively low cost and global abundance. Globally, and within South Africa's power generation sector, the focus appears to be on the deployment of high efficiency low emissions (HELE) technologies coupled with carbon capture and storage (CCS), rather than the complete and immediate abandonment of coal as a source of primary energy. Although there appears to be some interest by the South African government in procuring additional nuclear energy sometime in the future, this is not expected to be operational in the short-term owing chiefly to opposition from environmental groups, some sections of the general public, and, perhaps most importantly, funding constraints. As a result, the South African government is in the process of increasing the amount of energy derived from renewable sources. However, coal is expected to remain a significant contributor to the South African energy-mix in the short- to medium-term at the very least.

South African coal deposits are accommodated within the extensive Karoo Supergroup, and are generally Permian in age. The MKB, a type-deposit for coal formation in southern Africa, is interpreted to have been a large retro-arc foreland basin brought about by a combination of varying tectonic stresses concentrated mainly at the southern margin of the Gondwana supercontinent (Cairncross and Cadle, 1988; Cairncross, 1989, 1990, 2001; Cadle et al., 1993; Hancox and Götz, 2014; Hancox, 2016, and references therein). A large depression developed as a result of subduction, compression, collision, and terrane accretion, within which a thick sedimentary record is preserved. Sedimentary fill attains the greatest thickness in the south-west

direction where the basin terminates against the Cape Fold Belt, thinning out towards the north-eastern margin of the Kaapvaal Craton. The two margins are interpreted to represent proximal and distal facies respectively (Cairncross, 1989, 2001; Cadle et al., 1993; Hancox and Götz, 2014). The basin preserves a large, near complete sedimentary succession deposited during Gondwana, in climatic conditions ranging from cold to cool, and from dry to wet, environments (Cairncross and Cadle, 1988; Cairncross, 1989, 1990, 2001; Cadle et al., 1993). Northwards of the MKB, an intracratonic Karoo sub-basin developed on a rift, graben, or half-graben, and preserved what came to be known as the Waterberg Coalfield (Cairncross, 1990, 2001; Hancox and Götz, 2014). In general, the sedimentary fill of the northward sub-basins is comparable to that of the MKB, though structurally, the depositional environments differ.

The coalfields of South Africa are geographically subdivided into 19 distinct entities, based on sedimentation, basement highs, and sub-basins, as well as coal origin, distribution and quality (Cairncross, 1990; Hancox and Götz, 2014, and references therein; Hancox, 2016). In the MKB, the main coal-bearing lithostratigraphic units are the Vryheid Formation (Ecca Group), the Emakwezeni Formation (Beaufort Group), and the Molteno Formation (Stormberg Group). In addition, the Grootegeluk Formation (Ecca Group) is present in the northwards coalfields (Waterberg and Soutpansberg). Vertically, the sedimentary sequences are capped by a relatively thick deposit of basaltic lavas known as the Drakensberg Group. The location of the Witbank Coalfield, from which the sample of the present study was obtained, is shown in Figure 1.1.


**Figure 1.1:** The position of the Witbank Coalfield (circled) of South Africa (after Hancox and Götz, 2014).

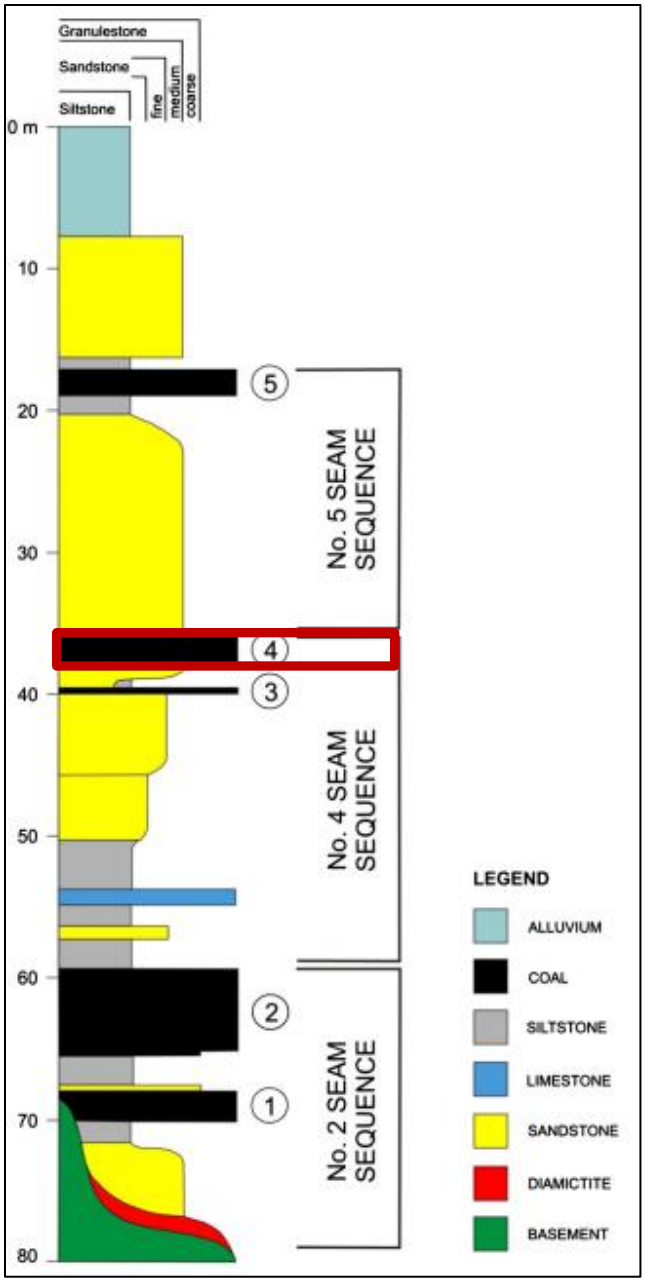


**Figure 1.2:** Generalized stratigraphy of the Vryheid Formation, Witbank Coalfield. Coal seams are numbered from No. 1 (bottom) to No. 5 (top) (after Hancox and Götz, 2014). The No. 4 Seam is in some localities split into two (Holland et al., 1989).

For over a century, the Witbank Coalfield of South Africa has been supplying both thermal and metallurgical coal to both local and international markets (Cairncross and Cadle, 1988; Cairncross et al., 1990; Snyman and Botha, 1993; Hancox and Götz, 2014, and references therein). A number of the country's more mature, likely to be soon retired, coal-fired power-stations were constructed within the confines of this coalfield. The coalfield extends over a distance of 90 km and 50 km in the east-west and north-south direction, respectively. To the

south, the coalfield terminates against pre-Karoo rocks, whereas a paleo-high of similar rocks separates it from the southward Highveld Coalfield. A total of five coal seams (Figure 1.2) are recognized within the coalfield (numbered 1 to 5 from the bottom to the top of the sequence), and are hosted within the Vryheid Formation (Cairncross and Cadle, 1988; Cairncross, 1989; Holland et al., 1989; Cairncross et al., 1990; Hancox and Götz, 2014). The coal seams overlie a diamictite (tillite) unit and are subdivided into individual entities by a combination of alluvium, siltstone, limestone, and sandstone (Cairncross and Cadle, 1988; Cairncross, 1989; Holland et al., 1989; Cairncross et al., 1990; Cadle et al., 1993; Hancox and Götz, 2014).

Holland et al. (1989) conducted a depositional environment and petrographical study in the coalfield using borehole cores. They concluded that the thick and persistent No.'s 1, 2, and 4 Seams, associated with high inertinite and mineral matter contents, were deposited in shallow, upper deltaic plain settings. The higher vitrinite content, thin and discontinuous No. 3 Seam is interpreted to represent a lower delta environment (Holland et al., 1989). Furthermore, the coal deposits of the older No.'s 1 and 2 Seams are related to glaciofluvial settings, whereas the coal seams above represent fluvial deposition (Cairncross and Cadle, 1988; Cairncross, 1989; Holland et al., 1989; Cairncross et al., 1990; Hancox and Götz, 2014). The productive No. 4 Seam (Figure 1.2) is split into two units in some localities – referred to as the No. 4 Lower and No. 4 Upper – by an approximately 2.5 m thick siltstone parting (Holland et al., 1989). The sample used in the current study was obtained from the latter coal seam (known as the "No. 4 Seam Upper"). The coalfield contains medium rank C bituminous coals, which are affected by igneous intrusions in places (Snyman and Botha, 1993; Gröcke et al., 2009; Hancox and Götz, 2014; Bussio and Roberts, 2016). These coals are typically inertinite-rich with a high mineral matter content (Falcon and Snyman, 1986; Falcon, 1986, 1989; Hagelskamp and Snyman, 1988; Holland et al., 1989; Snyman, 1989; Cadle et al., 1993; Snyman and Botha, 1993; Van Niekerk et al., 2008; O'Keefe et al., 2013; Hancox and Götz, 2014).

### 1.3. Macerals, with a focus on inertinite

Organic coal components are classified into three main groups on the basis of reflectance and morphology (Falcon and Snyman, 1986; Snyman, 1989; Teichmüller, 1989; Diessel, 1992; van Krevelen, 1993; International Committee for Coal and Organic Petrology (ICCP), 1998, 2001; Taylor et al., 1998; O'Keefe et al., 2013; Pickel et al., 2017). Owing to abundance in northern

hemisphere coals, vitrinite group macerals are perhaps the most extensively studied. In terms of reflectance, vitrinite is typically intermediate between liptinite and inertinite at the rank of bituminous coal (ICCP, 1998, 2001; Pickel et al., 2017). The observed petrographic characteristics are related to the chemical composition of the maceral groups; for example, hydrogen and volatile matter content decrease in the order: liptinite > vitrinite > inertinite (van Krevelen, 1993; ICCP, 1998, 2001; Pickel et al., 2017).

South African coals are generally rich in inertinite (Falcon and Snyman, 1986; Falcon, 1986; Cairncross and Cadle, 1988; Falcon and Ham, 1988; Hagelskamp and Snyman, 1988; Holland et al., 1989; Snyman, 1989; Cadle et al., 1993; Taylor et al., 1998; Glasspool, 2003a, 2003b; Van Niekerk et al., 2008; O'Keefe et al., 2013). The inertinite group comprises of a range of macerals, namely (in no particular order); fusinite, semifusinite, micrinite, macrinite, secretinite, funginite, and inertodetrinite (ICCP, 2001). Semifusinite present in South African coals may exhibit different levels of reflectance within the same sample, with a low- (reactive) and higher-reflecting (inert) submaceral (Falcon and Snyman, 1986; Hagelskamp and Snyman, 1988; Snyman, 1989; Cadle et al., 1993; Van Niekerk et al., 2008 and, references therein; Richards et al., 2013; Okolo et al., 2015). The low reflecting semifusinite is termed reactive semifusinite, and has been shown to enhance the cokability of medium rank bituminous coals (Falcon and Snyman, 1986; Falcon and Ham, 1988; Hagelskamp and Snyman, 1988; Snyman, 1989; Snyman and Botha, 1993; Richards et al., 2013).

At the rank of bituminous coal, inertinite group macerals have consistently been shown to be more aromatic than vitrinite counterparts (Dyrkacz et al., 1984; Maroto-Valer et al., 1994, 1998; Van Niekerk et al., 2008; Van Niekerk and Mathews, 2010; Moroeng et al., 2017). In terms of elemental composition, the hydrogen content of inertinite has is lower than that in corresponding vitrinite group macerals (Dyrkacz et al., 1984; Maroto-Valer et al., 1994, 1998; Van Niekerk et al., 2008; Van Niekerk and Mathews, 2010; Moroeng et al., 2017). The opposite has been reported with regards to carbon content. The corresponding hydrogen-carbon (H/C) atomic ratio is thus higher for vitrinite macerals when compared to inertinite macerals at similar rank. For bituminous coals, this ratio is characteristic for different maceral groups when comparison is made between iso-rank macerals (Dyrkacz et al., 1984; van Krevelen, 1993; Maroto-Valer et al., 1994, 1998; Van Niekerk et al., 2008). In general, the H/C atomic ratio is lower for higher

density, inertinite group macerals. Owing to their higher inertinite content, South African coals may thus be observed to have a greater aromatic fraction than vitrinite-rich coals at the bituminous rank.

### 1.4. Brief overview of previous work on the origin of inertinite in South African coals

With regards to the origin of inertinite macerals in general, multiple origin pathways have been proposed to account for the varied morphologies and reflectance values of macerals of this group. These include: (1) freeze-drying of gelified plant matter; (2) aerial oxidation; (3) fungal alteration; (4) inertinite formed from the remains of organisms (e.g., funginite) as well as from the partially digested excretion and/or regurgitation products thereof (e.g., the so-called copromacrinite); (5) inertinite formed from inherently carbon-rich plant matter; and, (6) charring of plant matter (Austen et al., 1966; Scott, 1989, 2002, 2010; Teichmüller, 1989; Jones and Chaloner, 1991; Diessel, 1992, 2010; van Krevelen, 1993; Moore et al., 1996; Moore and Shearer, 1997; Guo and Bustin, 1998; Taylor et al., 1998; ICCP, 2001; Glasspool, 2003a, 2003b; Scott and Glasspool, 2007; Hower et al., 2009, 2011a, 2011b, 2013; O'Keefe and Hower, 2011; Richardson et al., 2012; Jasper et al., 2013; O'Keefe et al., 2013; Valentim et al., 2016). In each case, the formation pathway determines not only the reflectance (and hence chemical composition), but also the anatomical structure or absence thereof, exhibited by the maceral produced.

Although multiple origin pathways for inertinite formation are generally recognized globally (ICCP, 2001; Hower et al., 2009, 2011a, 2011b, 2013; O'Keefe and Hower, 2011; Richardson et al., 2012; O'Keefe et al., 2013; Valentim et al., 2016), the various inertinite macerals present in South African coals have historically been chiefly attributed to aerial oxidation of plant matter in a cold climate, with the degree of oxidation responsible for the maceral produced (Falcon and Snyman, 1986; Falcon, 1986; Hagelskamp and Snyman, 1988; Snyman, 1989; Cadle et al., 1993; Snyman and Botha, 1993). However, the view that the processes responsible for the formation of inertinite present in South African coals were wholly exclusive of those recognized in other regions of the world is, at best, difficult to accept. If the cool, oxidizing conditions were solely responsible for the preservation of morphology, and subsequent formation of inertinite macerals in the coals, it would not be unreasonable to imagine similar macerals to be completely absent in coals formed in tropical climates such as the Pennsylvanian coals of the northern hemisphere.

It is important to mention that most work on the origin of inertinite macerals in South African coals was undertaken in the late 1980's (e.g., Falcon and Snyman, 1986; Falcon, 1986, 1989; Hagelskamp and Snyman, 1988; Snyman, 1989; Cadle et al., 1993; Snyman and Botha, 1993). Following which, there was a general paucity until the work of Glasspool (2003a, 2003b). This latter work disagrees with the earlier studies regarding the origin of the inertinite macerals, with Glasspool (2003a, p. 966) stating "...the abundance of Gondwana semifusinite has been explained-to have formed as a direct result of sub-aerial exposure in a cold climate setting. This hypothesis is not accepted. No mechanism by which cold climate alone can form high reflecting inertinites has so far been satisfactorily demonstrated. Conversely, wildfires can be demonstrated to produce a wide suite of inertinite morphologies and reflectances".

Glasspool (2003a, 2003b) was thus the first to show, through the description of what he termed "fossil charcoal", that inertinite macerals present in South African coals are likely to have a pyrogenic origin. Macroscopic charcoal associated with the clastic sedimentary rocks of the Vryheid Formation (Vereeniging Coalfield) has also been documented (Jasper et al., 2013). According to Jasper et al. (2013), these remnants of gymnosperm wood possess the widely documented properties of charcoal, namely: black streak, silky luster, splintery appearance, preserved anatomical structure, and homogenized cell walls (see also, Scott, 1989, 2010; Jones and Chaloner, 1991; Scott and Glasspool, 2007; Glasspool and Scott, 2010). Despite this, the now firmly entrenched view that the inertinite macerals are oxidation- and cold climate-derived continues to persist and is often cited as fact in the published literature (e.g., Van Niekerk et al., 2008; O'Keefe et al., 2013). This is surprising, since no other process has been demonstrated to produce charcoal (Scott, 1989, 2002, 2010; Jones and Chaloner, 1991; Guo and Bustin, 1998; Glasspool, 2003a, 2003b; Scott and Glasspool, 2007; Ascough et al., 2008, 2010; Diessel, 2010; Jasper et al., 2013). The controversy stems, in part, from the glacial/post-glacial climatic conditions prevailing in Gondwana in contrast to the more tropical conditions of Laurasia (Falcon, 1986; Cairncross and Cadle, 1988; Cairncross, 1989; Snyman and Botha, 1993). The Gondwana conditions were previously assumed to have hindered the development of extensive wild and/or peat fires. However, as Jasper et al. (2013) argued in their paper, the concentration of free oxygen in the atmosphere peaked at around 30% in the Early Permian falling to around 20% in the Late Permian (see also, Berner, 1999; Diessel, 2010; Glasspool and Scott, 2010). Thus,

with the atmospheric oxygen exceeding the minimum 13% required to sustain a fire (Bowman et al., 2009), plants would likely have been prone to fires even while wet (Jasper et al., 2013).

With the mounting body of evidence regarding the existence of charcoal directly associated with the coal seams of South Africa (Glasspool, 2003a, 2003b) as well as charcoal associated with clastic sedimentary units of similar age (Jasper et al., 2013), the skepticism regarding the occurrence of fires within and around the peat-forming environments of Gondwana South Africa is surely no longer sustainable. In which case, and contrary to earlier opinions, fires are likely to have played an important role in the formation of the inertinite macerals present in the coals of this region. Along with the occurrence of macroscopic charcoal, the pyrogenic origin of inertinite macerals, and thus the occurrence of palaeo-wildfires, is typically supported using geochemical and petrological evidence (e.g., Austen et al., 1966; Scott, 1989, 2010; Jones and Chaloner, 1991; Simoneit et al., 1993; Scott and Glasspool, 2007; Belcher et al., 2009; Bowman et al., 2009; Marynowski and Simoneit, 2009; Glasspool and Scott, 2010; Bird and Ascough, 2012; Jasper et al., 2013; Slater et al., 2015). The evidence put forward by Glasspool (2003a, 2003b) and Jasper et al. (2013) for a pyrogenic origin of South African inertinite macerals is based chiefly on palaeoecology and palynology, specifically not considering the geochemistry of the coals. Because of this, the present study attempts to reconcile the organic geochemistry of the coals with petrographically observed morphology and reflectance of the macerals, and ultimately examine the sustainability of a pyrogenic origin for inertinite macerals present in a South African coal from the Witbank Coalfield.

### 1.5. Hypothesis

Numerous studies have demonstrated that wood charring produces charcoal with morphologies and reflectance levels comparable to those observed in some inertinite macerals (e.g., Scott, 1989, 2002, 2010; Teichmüller, 1989; Jones and Chaloner, 1991; Guo and Bustin, 1998; Scott and Glasspoool, 2007; Ascough et al., 2008, 2010). The structure of a fusinite precursor, in particular, is typically preserved reflecting the negligible role played by organisms in the formation of this maceral. In contrast, some macerals such as macrinite exhibit no structure reflecting pronounced decomposition by organisms present within a peat-forming environment (Guo and Bustin, 1998; Hower et al., 2009, 2011a, 2011b, 2013; Richardson et al., 2012; O'Keefe et al., 2013). Within this context, the main hypothesis of the current research is

articulated as follows: **The structures exhibited by certain inertinite macerals present in South African coals of the Witbank Coalfield suggest that the formation of fusinite (Figure 1.3) and semifusinite (Figure 1.4) is preceded by charring of plant matter. Furthermore, charring occurred before humification-related degradation**.

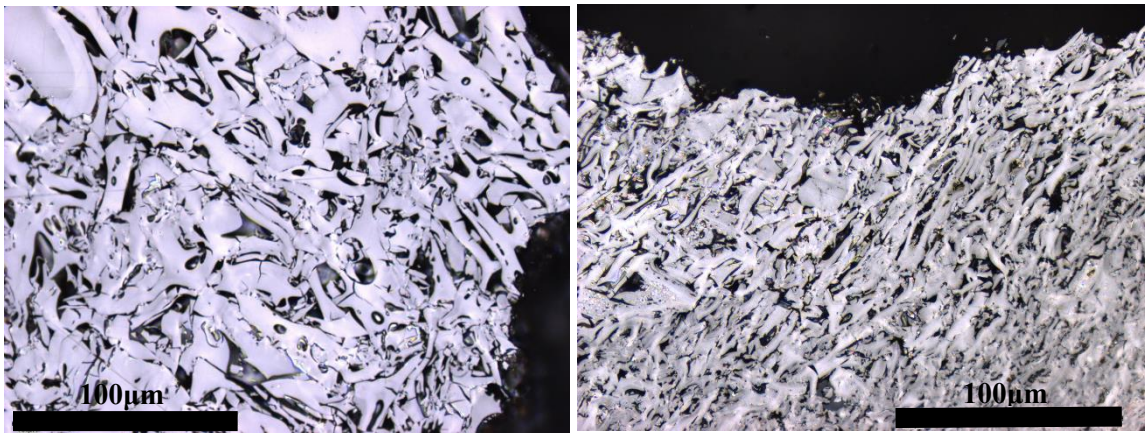


**Figure 1.3:** Fusinites observed in a Witbank coal, South Africa. 500x magnification, reflected light with oil immersion. Scale is indicated.

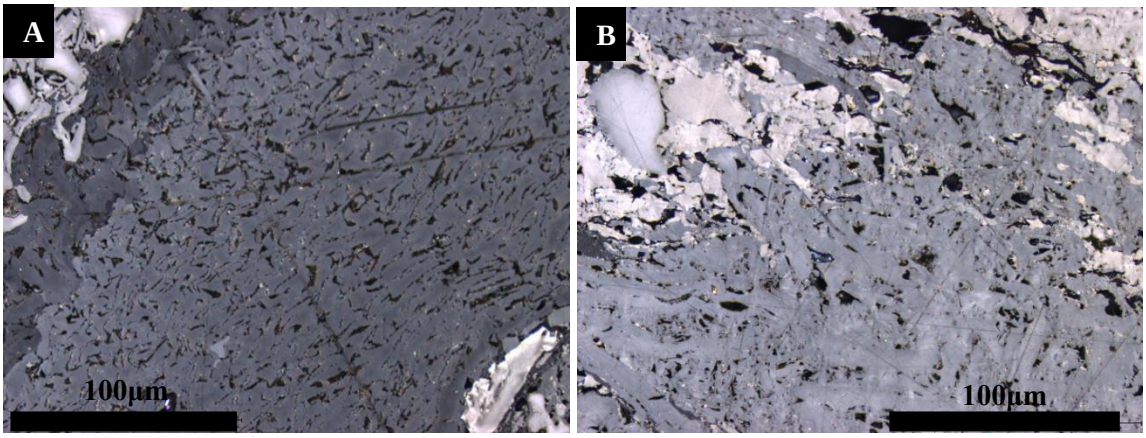


**Figure 1.4:** A – dark grey (reactive) and, B – light grey (inert) semifusinites observed in a Witbank coal, South Africa. 500x magnification, reflected light with oil immersion. Scale is indicated.

### 1.6. Aim and objectives

The overarching aim of the present study is to investigate the contribution of fire-affected plant matter in the formation of a Witbank coal using ESR, $^{13}C$ CP-MAS SS NMR, and $\delta^{15}N$ and $\delta^{13}C$ values and the concentration of nitrogen functionalities determined using XPS.

This thesis is presented by publication, and hence, each main objective is captured in a publication, summarized as follows:

1. To characterize and compare a vitrinite-rich and an inertinite-rich coal sample as well as the parent coal based on ESR properties, and test the sustainability of a fire-origin for the dominant inertinite macerals. The ESR properties are discussed in conjunction with detailed petrographic (maceral and mean random vitrinite reflectance analysis), elemental, proximate analysis, and fraction of aromaticity inferred from the H/C atomic ratio (Chapter 2).

**Published as:** Moroeng, O.M., Keartland, J.M., Roberts, R.J., Wagner, N.J., 2018. Characterization of coal using Electron Spin Resonance: Implications for the formation of inertinite macerals in the Witbank Coalfield, South Africa. International Journal of Coal Science & Technology 5(3), 385-398.

2. To investigate the origin of fusinite and semifusinite macerals in the inertinite-rich sample based on detailed petrographic composition (maceral, microlithotype, and mean random vitrinite reflectance) as well as $^{13}C$ CP-MAS SS NMR chemical-structural parameters. The chapter focusses on the aromatic cluster sizes present in each sample, and compares these to the sizes that would be expected following charring of lignin-rich, woody plant matter (Chapter 3).

**Published as:** Moroeng, O.M., Wagner, N.J., Brand, D.J., Roberts, R.J., 2018. A Nuclear Magnetic Resonance study: Implications for coal formation in the Witbank Coalfield, South Africa. International Journal of Coal Geology 188, 145-155.

3. To quantify and compare the $\delta^{15}N$ and $\delta^{13}C$ values and the concentrations of various nitrogen functionalities determined using XPS (N-pyridinic, N-pyrrolic, N-quaternary, and N-oxide complexes) for the vitrinite-rich and inertinite-rich samples, and constrain origin pathways for the major maceral components present in each coal sample (Chapter 4). In addition to the measured $\delta^{15}N$ and $\delta^{13}C$ values, the chapter uses the relative shifts in $\delta^{15}N$ and $\delta^{13}C$ values reported by others following laboratory charring of various modern woods.

**Submitted as:** Moroeng, O.M., Wagner, N.J., Hall, G., Roberts, R.J., Using $\delta^{15}N$ and $\delta^{13}C$ and nitrogen functionalities to support a fire-origin for certain inertinite macerals in a No. 4 Seam

Upper Witbank coal, South Africa. Submitted to Organic Geochemistry (Submission no.: OG-3813).

4. To examine the differences and/or similarities in the molecular chemistry of vitrinite-rich and inertinite-rich samples at the bituminous coal rank using py-GC/MS and the $^{13}C$ CP-MAS SS NMR chemical-structural parameters (Chapter 5).

**To be submitted as:** Moroeng, O.M., Mhuka, V., Nindi, M.M., Roberts, R.J., Wagner, N.J., Comparative study of a vitrinite-rich and an inertinite-rich Witbank coal using pyrolysis-gas chromatography, South Africa. To be submitted to Energy & Fuels.

### 1.7. Scope

The study consists of four standalone research articles (Chapter 2 to Chapter 5). In addition to basic chemical and petrographic characterization, each chapter includes a different analytical method to investigate the organic geochemistry of the parent, inertinite-rich, and vitrinite samples from the No. 4 Seam Upper, Witbank Coalfield. For Chapters 2 to 4, the geochemical results were specifically discussed within the context of charring of plant matter. In Chapter 5, organic molecular chemistry obtained using py-GC/MS was used to compare the composition of the inertinite-rich and vitrinite-rich samples.

A run-of-mine bituminous coal sample weighing approximately 50 kg was obtained from the No. 4 Seam Upper, Witbank Coalfield, South Africa. Subsequently, the entire sample (as received) was crushed and a quarter reserved to represent the "parent sample". The remaining material was subjected to float-sink density-fractionation following South African National Standard (SANS) 7936 (2010) to create inertinite-rich and vitrinite-rich sub-samples. Because these samples are of exactly the same bituminous coal rank, differences in the various geochemical parameters were interpreted to largely reflect coal-formation processes.

The investigation will largely take the form of a comparative study. Given that coal organic chemistry is highly dependent on rank, it was imperative that the vitrinite-rich and inertinite-rich samples are derived from the same coal sample so that rank-dependent variations between the samples may be eliminated. The differences observed in the chemistry of the samples may then be interpreted to reflect differences in the chemistry of the dominant macerals present in each sample. The geochemistry of the vitrinite-rich sample was interpreted to reflect formation driven

by humification and gelification processes (Teichmüller, 1989; Diessel, 1992; van Krevelen, 1993; Hatcher and Clifford, 1997; ICCP, 1998; Taylor et al., 1998; Hower et al., 2013; O'Keefe et al., 2013). The chemistry of this sample was therefore compared with that of the inertinite-rich sample of the same coal, so that the origin pathway(s) for the dominant inertinite macerals of the inertinite-rich sample may be best constrained.

- The ESR analytical technique (Chapter 2) was chosen specifically because it was one of the lines evidence used earlier-on to support of a fire-origin for fusinite (Austen et al., 1966), which has subsequently become widely accepted to represent fossilized charcoal (Scott, 1989, 2002, 2010; Teichmüller, 1989; Diessel, 1992, 2010; ICCP, 2001; Scott and Glasspool, 2007; Hower et al., 2013; O'Keefe et al., 2013).

- The $^{13}C$ CP-MAS SS NMR analysis was used to determine the average aromatic cluster sizes present in each sample (Chapter 3), as well as the proportions of chemical functional groups present in the samples (Chapter 5). The average aromatic cluster size of the vitrinite-rich sample was compared with that of the inertinite-rich sample. For the latter sample, the cluster size was also compared to what would be expected following charring of woody plant matter.

- Humification-related degradation of plant matter, resulting in the formation of unstructured macerals (Guo and Bustin, 1998; Richardson et al., 2012; Hower et al., 2013; O'Keefe et al., 2013) e.g., collotelinite and collodetrinite, leads to the expulsion of the isotopically lighter, $^{14}N$ along with cellulose (Spiker and Hatcher, 1987; Rimmer et al., 2006; Skrzypek et al., 2010). At the same time, the vitrinization processes result in the formation of N-quaternary, whereas N-pyrrolic may result from charring (Schulten and Schnitzer, 1998, and references therein; Kelemen et al., 2006). The $\delta^{15}N$ and $\delta^{13}C$ values and the concentration of nitrogen functionalities (determined using XPS) were therefore used to constrain the origin pathways for the major organic components present in the density-fractionated samples. The discussion based on the measured isotopic values also considers the relative shifts in $\delta^{15}N$ and $\delta^{13}C$ values previously observed by others during laboratory experiments on various modern woods (Chapter 4).

- Lastly, along with the $^{13}C$ CP-MAS SS NMR chemical-structural parameters reported in Chapter 3, py-GC/MS was used to compare the organic molecular chemistry of the inertinite-rich and vitrinite-rich samples in an attempt to understand the impact of origin pathways on coal pyrolysis products (Chapter 5).

It is important to mention that no attempt was made understand the implications of the organic geochemical results of the present study in terms of coal utilization in various processes, since the main focus is on the origin of certain macerals present in the coals samples. This is in spite of the results of the study possibly having implications on the utilization of the coal. The supposed impact may be further explored in the future.

### 1.8. Contribution to science

There are some notable research publications regarding the origin of coals in South Africa. However, the author has no knowledge of any, in the available published literature, that have used ESR to assess coal-forming processes. Although $^{13}C$ CP-MAS SS NMR chemical-structural parameters and the concentration of nitrogen functionalities have been reported for various South African coals, these were, for example, used to assess changes and following solvent extraction or acid treatment, and/or, to assess char structure or composition following coal pyrolysis under various operational conditions (e.g., Van Niekerk et al., 2008; Van Niekerk and Mathews, 2010; Malumbazo et al., 2011; Strydom et al., 2011; Hattingh et al., 2013; Okolo et al., 2015; Roberts et al., 2015a, 2015b; Phiri et al., 2017, 2018), without emphasis on the origin of the coals. Similarly, $\delta^{13}C$ values have previously been reported to assess the effect of igneous intrusions on coal (Gröcke et al., 2009), with no particular focus on the origin pathways for the macerals present in the coals.

The present study provides detailed petrographic (maceral, microlithotype, and mean random vitrinite reflectance) and selected organic geochemical analyses for a bituminous South African Witbank Permian coal, and density-fractionated vitrinite-rich and inertinite-rich samples thereof. In addition, the present study is one of the few (e.g., Glasspool, 2003a, 2003b; Jasper et al., 2013) to attempt to constrain the origin pathways for macerals present in South African coals since the late 1980's (e.g., Falcon and Snyman, 1986; Falcon, 1986, 1989; Hagelskamp and Snyman, 1988; Snyman, 1989; Cadle et al., 1993; Snyman and Botha, 1993), and the first to do so using relatively advanced organic geochemical methods which have been widely used on the

generally vitrinite-rich coals of the Carboniferous from the northern hemisphere. The combined use of ESR, $^{13}C$ CP-MAS SS NMR, and $\delta^{15}N$ and $\delta^{13}C$ values along with the concentration of nitrogen functionalities in the evaluation of the origin pathways for the dominant macerals of the density-fractionated Witbank coal samples is considered to be a significant contribution to science. Moreover, the study contributes to knowledge on the formation of coal macerals in general.

Although the main finding of the study, i.e., charring as a pathway for the formation of inertinite in South African coals, has been proposed by others (e.g., Glasspool, 2003a, 2003b; Jasper et al., 2013), the present study is the first to reach the finding via the use of organic geochemistry of a South African coal sample. The possible presence of low-temperature lignin pyrolysis products in the density-fractionated inertinite-rich Witbank coal sample (Chapter 3 of this study, and published as Moroeng et al., 2018), in addition to the widely documented polycyclic aromatic compounds (Chapter 5), is of particular significance. Chapters 2 and 4, based on ESR properties and $\delta^{15}N$ and $\delta^{13}C$ values along with the concentration of nitrogen functionalities, respectively; attempt to provide additional evidence of charring for the dominant macerals of the inertinite-rich sample. Whereas, Chapter 5 compares the molecular chemistry of the inertinite-rich and vitrinite-rich samples with the aid of py-GC/MS.

### 1.9. References


Ascough, P.L., Bird, M.I., Scott, A.C., Collinson, M.E., Cohen-Ofri, I., Snape, C.E., Le Manquais, K., 2010. Charcoal reflectance measurements: implications for structural characterization and assessment of diagenetic alteration. Journal of Archaeological Science 37, 1590-1599.

Ascough, P.L., Bird, M.I., Wormald, P., Snape, C.E., Apperley, D., 2008. Influence of production variables and starting material on charcoal stable isotopic and molecular characteristics. Geochimica et Cosmochimica Acta 72, 6090-6102.

Austen, D.E.G., Ingram, D.J.E. Given, P.H., Binder, C.R., Hill, L.W., 1966. Electron Spin Resonance Study of Pure Macerals. In: Given, P.H., (Ed.). Coal Science, Advances in Chemistry, 55. American Chemical Society, Washington DC, pp. 344-362.

Beidari, M., Lin, S.-J., Lewis, C., 2017. Decomposition Analysis of $CO_2$ Emissions from Coal-Sourced Electricity Production in South Africa. Aerosol and Air Quality Research 17, 1043-1051.

Belcher, C.M., Finch, P., Collinson, M.E., Scott, A.C., Grassineau, N.V., 2009. Geochemical evidence for combustion of hydrocarbons during the K-T impact event. Proceedings of the National Academy of Sciences of the United States of America 106 (11), 4112-4117.

Bergh, J.P., Falcon, R.M.S., Falcon, L.M., 2011. Trace element concentration reduction by beneficiation of Witbank Coalfield no. 4 Seam. Fuel Processing Technology 92 (4), 812-816.

Berner, R.A., 1999. Atmospheric oxygen over Phanerozoic time. Proceedings of the National Academy of Sciences of the United States of America 96 (20), 10955-10957.

Bird, M.I., Ascough, P.L., 2012. Isotopes in pyrogenic carbon: A review. Organic Geochemistry 42, 1529-1539.

Bowman, D.M.J.S., Balch, J.K., Artaxo, P., Bond, W.J., Carlson, J.M., Cochrane, M.A., D'Antonio, C.M., DeFries, R.S., Doyle, J.C., Harrison, S.P., Johnston, F.H., Keeley, J.E., Krawchuk, M.E., Kull, C.A., Marston, J.B., Moritz, M.A., Prentice, I.C., Roos, C.I., Scott, A.C., Swetnam, T.W., van der Werf, G.R., Pyne, S.J., 2009. Fire in the Earth System. Science, New Series 24 (5926), 481-484.

Bussio, J.P., Roberts, J.R., 2016. A large scale investigation into changes in coal quality caused by dolerite dykes in Secunda, South Africa-implications for the use of proximate analysis on a working mine. Journal of African Earth Sciences 117, 401-409.

Cadle, A.B., Cairncross, B., Christie, A.D.M., Roberts, D.L., 1993. The Karoo Basin of South Africa: type basin for coal-bearing deposits of southern Africa. International Journal of Coal Geology 23, 117-157.

Cairncross, B., 1989. Paleodepositional environments and tectonosedimentary controls of the postglacial Permian coals, Karoo Basin, South Africa. International Journal of Coal Geology 12 (1-4), 365-380.

Cairncross, B., 1990. Tectono-sedimentary settings and controls of the Karoo Basin Permian coals, South Africa. International Journal of Coal Geology 16 (1-3), 175-178.

Cairncross, B., 2001. An overview of the Permian (Karoo) coal deposits of Southern Africa. Journal of African Earth Sciences 33, 529-562.

Cairncross, B., Cadle, A.B., 1988. Palaeoenvironmental control on coal formation, distribution and quality in the Permian Vryheid Formation, East Witbank Coalfield, South Africa. International Journal of Coal Geology 9 (4), 343-370.

Cairncross, B., Hart, R.J., Wills, J.P., 1990. Geochemistry and sedimentology of coal seams from the Permian Witbank Coalfield, South Africa; a means of identification. International Journal of Coal Geology 16 (4), 309-325.

Cao, X., Chappell, M.A., Schimmelmann, A., Mastalerz, M., Li, Y., Hu, W., Mao, J., 2013. Chemical structure changes in kerogen from bituminous coal in response to dike intrusions as investigated by advanced solid-state $^{13}C$ NMR spectroscopy. International Journal of Coal Geology 108, 53-64.

Cao, X., Mastalerz, M., Chappell, M.A., Miller, L.F., Li, Y., Mao, J., 2011. Chemical structures of coal lithotypes before and after $CO_2$ adsorption as investigated by advanced solid-state $^{13}C$ nuclear magnetic resonance spectroscopy. International Journal of Coal Geology 88 (1), 67-74.

Chen, Y., Mastalerz, M., Schimmelmann, A., 2012. Characterization of chemical functional groups in macerals across different coal ranks via micro-FTIR spectroscopy. International Journal of Coal Geology 104, 22-33.

Coetzee, G.H., Sakurovs, R., Neomagus, H.W.J.P., Morpeth, L., Everson, R.C., Mathews, J.P., Bunt, J.R., 2015. Pore development during gasification of South African inertinite-rich chars evaluated using small angle X-ray scattering. Carbon 95, 250-260.

Davidson, R.M., 2004. Studying the structural chemistry of coal. IEA Clean Coal Centre. 121pp.

Diessel, C.F.K., 1992. Coal-Bearing Depositional Systems. Springer-Verlag, Berlin Heidelberg, 721pp.

Diessel, C.F.K., 2010. The stratigraphic distribution of inertinite. International Journal of Coal Geology 81 (4), 251-268.

Dyrkacz, G.R., Bloomquist, C.A.A., Ruscic, L., 1984. Chemical variations in coal macerals separated by density gradient centrifugation. Fuel 63, 1166-1173.

Dyrkacz, G.R., Horwitz, E.P., 1982. Separation of coal macerals. Fuel 61 (1), 3-12.

Erdenetsogt, B-.O., Lee, I., Ko, Y-.J., 2017. Carbon isotope analysis and a solid state $^{13}C$ NMR study of Mongolian lignite: Changes in stable carbon isotopic composition during diagenesis. Organic Geochemistry 113, 293-302.

Erdenetsogt, B-.O., Lee, I., Lee, S.K., Ko, Y-.J., Bat-Erdene, D., 2010. Solid-state C-13 CP/MAS NMR study of Baganuur coal, Mongolia: Oxygen-loss during coalification from lignite to subbituminous rank. International Journal of Coal Geology 82 (1-2), 37-44.

Fabiańska, M.J., Kruszewska, K.K.J., 2003. Relationship between petrographic and geochemical characterisation of selected South African coals. International Journal of Coal Geology 54 (1-2), 95-114.

Falcon, M.S., Snyman, C.P., 1986. An Introduction to Coal Petrography: Atlas of Petrographic Constituents in the Bituminous Coals of Southern Africa. Geological Society of South Africa, Johannesburg, 27pp.

Falcon, R., Ham, A.J., 1988. The characteristics of Southern African coals. The Journal of the South African Institute of Mining and Metallurgy 88 (5), 145-161.

Falcon, R.M.S., 1986. A brief review of the origin, formation, and distribution of coal in southern Africa. In: Anhaeusser, C.R., Maske, S. (Eds.), Mineral Deposits of Southern Africa, Vols. I and II. Geological Society of South Africa, Johannesburg, pp. 1879-1898.

Falcon, R.M.S., 1989. Macro-and micro-factors affecting coal-seam quality and distribution in southern Africa with particular reference to the No. 2 seam, Witbank coalfield, South Africa. International Journal of Coal Geology 12 (1-4), 681-731.

Glasspool, I., 2003a. Palaeoecology of selected South African export coals from the Vryheid Formation, with emphasis on the role of heterosporous lycopods and wildfire derived inertinite. Fuel 82, 959-970.

Glasspool, I.J., 2003b. Hypautochthonous–allochthonous coal deposition in the Permian, South African, Witbank Basin No. 2 seam; a combined approach using sedimentology, coal petrology and palaeontology. International Journal of Coal Geology 53, 81-135.

Glasspool, I.J., Scott, A.C., 2010. Phanerozoic concentrations of atmospheric oxygen reconstructed from sedimentary charcoal. Nature Geoscience Letters 3, 627-630.

Gröcke, D.R., Rimmer, S.M., Yoksoulian, L.E., Cairncross, B., Tsikos, H., van Hunen, J., 2009. No evidence for thermogenic methane release in coal from the Karoo-Ferrar large igneous province. Earth and Planetary Science Letters 277, 204-212.

Guo, Y., Bustin, R.M., 1998. FTIR spectroscopy and reflectance of modern charcoals and fungal decayed woods: implications for studies of inertinite in coals. International Journal of Coal Geology 37, 29-53.

Haenel, M.W., 1992. Recent progress in coal structure research. Fuel 71, 1211-1223.

Hagelskamp, H.H.B., Snyman, C.P., 1988. On the origin of low-reflecting inertinites in coals from the Highveld Coalfield, South Africa. Fuel 67, 307-313.

Hancox, J.P., 2016. The Coalfields of South-Central Africa: A Current Perspective. In: Wilson, M.G.C., (Ed.). The Great Mineral Fields of Africa (Special Issue of the 35 IGC, Cape Town, South Africa 27 August – 4 September 2016). Episodes, Journal of International Geoscience 37 (2), 407-428.

Hancox, J.P., Götz, A.E., 2014. South Africa's coalfields – a 2014 perspective. International Journal of Coal Geology 132, 170-254.

Hartgers, W.A., Sinninghe Damste, J.S., de Leeuw, J.W., Ling, Y., Dyrkacz, G.R., 1994. Molecular Characterization of Flash Pyrolyzates of Two Carboniferous Coals and Their Constituting Maceral Fractions. Energy & Fuels 8 (5), 1055-1067.

Hatcher, P.G., Clifford, D.J., 1997. The organic geochemistry of coal: from plant materials to coal. Organic Geochemistry 27 (5-6), 251-257, 259-274.

Hattingh, B.B., Everson, R.C., Neomagus, H.W.J.P., Bunt, J.R., Van Niekerk, D., Jordaan, J.H.L., Mathews, J.P., 2013. Elucidation of the Structural and Molecular Properties of Typical South African Coals. Energy & Fuels 27 (6), 3161-3172.

Holland, M.J., Cadle, A.B., Pinheiro, R., Falcon, R.M.S., 1989. Depositional environments and coal petrography of the Permian Karoo Sequence: Witbank Coalfield, South Africa. International Journal of Coal Geology 11, 143-169.

Hower, J.C., O'Keefe, J.M.K., Eble, C.F., Raymond, A., Valentim, B., Volk, T.J., Richardson, A.R., Satterwhite, A.B., Hatch, R.S., 2011a. Notes on the origin of inertinite macerals in coal: Evidence for fungal and arthropod transformations of degraded macerals. International Journal of Coal Geology 86 (2-3), 231-240.

Hower, J.C., O'Keefe, J.M.K., Eble, C.F., Volk, T.J., Richardson, A.R., Satterwhite, A.B., Hatch, R.S., Kostova, I.J., 2011b. Notes on the origin of inertinite macerals in coals: Funginite associations with cutinite and Suberinite, International Journal of Coal Geology 85 (1), 186-190.

Hower, J.C., O'Keefe, J.M.K., Wagner, N.J., Dai, S., Wang, X., Xue, W., 2013. An investigation of Wulantuga coal (Cretaceous, Inner Mongolia) macerals: Paleopathology of faunal and

fungal invasions into wood and the recognizable clues for their activity. International Journal of Coal Geology 114, 44-53.

Hower, J.C., O'Keefe, J.M.K., Watt, M.A., Pratt, T.J., Eble, C.F., Stucker, J.D., Richardson, A.R., Kostova, I.J., 2009. Notes on the origin of inertinite macerals in coals: Observations on the importance of fungi in the origin of Macrinite. International Journal of Coal Geology 80 (2), 135-143.

International Committee for Coal and Organic Petrology (ICCP)., 1998. The new vitrinite classification. (ICCP System 1994). Fuel 77 (5), 349-358.

International Committee for Coal and Organic Petrology (ICCP)., 2001. The new inertinte classification (ICCP System 1994). Fuel 80 (4), 459-47.

Jasper, A., Guerra-Sommer, M., Abu Hamad, A.M.B., Bamford, M., Cerruti Bernardes-de-Oliveira, M.E., Tewari, R., Uhl, D., 2013. The burning of Gondwana: Permian fires on the southern continent – A palaeobotanical approach. Gondwana Research 24 (1), 148-160.

Jones, T.P., Chaloner, W.G., 1991. Fossil charcoal, its recognition and palaeoatmospheric significance. Palaeogeography, Palaeoclimatology, Palaeoecology (Global and Planetary Change Section) 97, 39-50.

Kelemen, S.R., Afeworki, M., Gorbaty, M.L., Kwiatek, P.J., Sansone, M., Walters, C.C., 2006. Thermal Transformations of Nitrogen and Sulfur Forms in Peat Related to Coalification. Energy & Fuels 20, 635-652.

Kolker, A., Senior, C., van Alphen, C., Koenig, A., Geboy, N., 2017. Mercury and trace element distribution in density separates of a South African Highveld (#4) coal: Implications for mercury reduction and preparation of export coal. International Journal of Coal Geology 170, 7-13.

Louw, E.B., Mitchell, G.D., Wang, J., Winans, R.E., Mathews, J.P., 2016. Constitution of Drop-Tube-Generated Coal Chars from Vitrinite- and Inertinite-Rich South African Coals. Energy & Fuels 30 (1), 112-120.

Lusilao-Makiese, J., Tessier, E., Amouroux, D., Hlanganani, T., Chimuka, L., Cukrowska, E.M., 2012. Speciation of mercury in South African coals. Toxicological & Environmental Chemistry 94 (9), 1688-1706.

Malumbazo, N., Wagner, N.J., Bunt, J.R., Van Niekerk, D., Assumption, H., 2011. Structural analysis of chars generated from South African inertinite coals in a pipe-reactor combustion unit. Fuel Processing Technology 92 (4), 743-749.

Maroto-Valer, M.M., Love, G.D., Snape, C.E., 1994. Relationship between carbon aromaticities and H/C ratios for bituminous coals. Fuel 73 (12), 1926-1928.

Maroto-Valer, M.M., Taulbee, D.N., Andresén, J.M., Hower, J.C., Snape, C.E., 1998. Quantitative $^{13}C$ NMR study of structural variations within the vitrinite and inertinite maceral groups for a semifusinite-rich bituminous coal. Fuel 77 (8), 805-813.

Marynowski, L., Simoneit, B.R.T., 2009. Widespread Upper Triassic to Lower Jurrasic wildfire records from Poland: Evidence from charcoal and pyrolytic polycyclic aromatic hydrocarbons. Palaios 24 (12), 785-798.

Mastalerz, M., Bustin, R.M., 1994. Variation in reflectance and chemistry of vitrinite and vitrinite precursors in a series of Tertiary Coals, Arctic Canada. Organic Geochemistry 22(6), 921-933.

Mastalerz, M., Bustin, R.M., 1997. Variation in the chemistry of macerals in coals of the Mist Mountain Formation, Elk Valley coalfield, British Columbia, Canada. International Journal of Coal Geology 33 (1), 43-59.

Mastalerz, M., Hower, J.C., Taulbee, D.N., 2013. Variations in chemistry of macerals as reflected by micro-scale analysis of a Spanish coal. Geologica Acta 11 (4), 483-493.

Meuzelaar, H.L.C., Harper, A.M., Hill, G.H., Given, P.H., 1984. Characterization and classification of Rocky Mountain coals by Curie-point pyrolysis mass spectrometry. Fuel 63 (5), 640-652.

Moore, T.A. Shearer, J.C., Miller, S.L., 1996. Fungal origin of oxidized plant material in the Palangkaraya peat deposit, Kalimantan Tengah, Indonesia: Implications for 'inertinite' formation in coal. International Journal of Coal Geology 30, 1-23.

Moore, T.A., Shearer, J.C., 1997. Evidence for Aerobic Degradation of Palangka Raya Peat and Implications for its Sustainability. In: Rieley, J.O., Page, S.E., (Eds.). Tropical Peatlands. Samara Publishing Limited, Cardigan, pp.157-167.

Moroeng, O.M., Roberts, R.J., Bussio, J.P., Dixon, R.D., 2017. Self-heating Potential of Coal inferred from Elemental Data – A Case-study of the Witbank Coalfield of South Africa. Energy & Fuels 31 (11), 11811-11817.

Moroeng, O.M., Wagner, N.J., Brand, D.J., Roberts, R.J., 2018. A Nuclear Magnetic Resonance study: Implications for coal formation in the Witbank Coalfield, South Africa. International Journal of Coal Geology 188, 145-155.

Nip, M., De Leeuw, J.W., Crelling, J.C., 1992. Chemical structure of bituminous coal and its constituting maceral fractions as revealed by flash pyrolysis. Energy & Fuels 6 (2), 125-136.

Nip, M., De Leeuw, J.W., Schenck, P.A., 1988. The characterization of eight maceral concentrates by means of Curie point pyrolysis-gas chromatography and Curie point pyrolysis-gas chromatography-mass spectrometry. Geochimica et Cosmochimica Acta 52 (3), 637-648.

O'Keefe, J.M.K., Bechtel, A., Christanis, K., Dai, S., DiMichele, W.A., Eble, C.F., Esterle, J.S., Mastalerz, M., Raymond, A.L., Valentim, B.V., Wagner, N.J., Ward, C.R., Hower, J.C., 2013. On the fundamental difference between coal rank and coal type. International Journal of Coal Geology 118, 58-87.

O'Keefe, J.M.K., Hower, J.C., 2011. Revisiting Coos Bay, Oregon: A re-examination of funginite–huminite relationships in Eocene subbituminous coals. International Journal of Coal Geology 85 (1), 34-42.

Okolo, G.N., Neomagus, H.W.J.P., Everson, R.C., Roberts, M.J., Bunt, J.R., Sakurovs, R., Mathews, J.P., 2015. Chemical-structural properties of South African bituminous coals: Insights from wide angle XRD-carbon fraction analysis, ATR-FTIR, solid state $^{13}C$ NMR, and HRTEM techniques. Fuel 158, 779-792.

Phiri, Z., Everson, R.C., Neomagus, H.W.J.P., Wood, B.J., 2017. The effect of acid demineralising bituminous coals and de-ashing the respective chars on nitrogen functional forms. Journal of Analytical and Applied Pyrolysis 125, 127-135.

Phiri, Z., Everson, R.C., Neomagus, H.W.J.P., Wood, B.J., 2018. Transformation of nitrogen functional forms and the accompanying chemical-structural properties emanating from pyrolysis of bituminous coals. Applied Energy 216, 414-427.

Pickel, W., Kus, J., Flores, D., Kalaitzidis, S., Christanis, K., Cardott, B.J., Misz-Kennan, M., Rodrigues, S., Hentschel, A., Hamor-Vido, M., Crosdale, P., Wagner, N., ICCP., 2017. Classification of liptinite – ICCP System 1994. International Journal of Coal Geology 169, 40-61.

Plumstead, E.P., 1961. Ancient plants and drifting continents. South African Journal of Science 57 (7), 173-181.

Pone, J.D.N., Hein, K.A.A., Stracher, G.B., Annegarn, H.J., Finkleman, R.B., Blake, D.R., McCormack, J.K., Schroeder, P., 2007. The spontaneous combustion of coal and its by-products in the Witbank and Sasolburg coalfields of South Africa. International Journal of Coal Geology 72 (2), 124-140.

Powell, T.G., Boreham, C.J., Smyth, M., Russell, N., Cook, A.C., 1991. Petroleum source rock assessment in non-marine sequences: pyrolysis and petrographic analysis of Australian coals and carbonaceous shales. Organic Geochemistry 17 (3), 375-394.

Radlinski, A.P., Mastalerz, M., 2018. Neutron scattering study of vitrinite: Insights into sub-micrometer inclusions in North American Carboniferous coals of bituminous rank. International Journal of Coal Geology 186, 145-154.

Retcofsky, H.L., Stark, J.M., Friedel, R.A., 1968. Electron Spin Resonance in American Coals. Analytical Chemistry 40 (11), 1699-1704.

Retcosfky, H.L., Hough, M.R., Maguire, M.M., Clarkson, R.B., 1981. Nature of the Free Radicals in Coals, Pyrolyzed Coals, Solvent-Refined Coal, and Coal Liquefaction Products. In: Gorbaty, M.L., Ouchi, K., (Eds.). Coal Structure, Advances in Chemistry, 192. American Chemical Society, Washington DC, pp 37-58.

Richards, J.M., Naude, G., Theron, S.J., McCullum, M., 2013. Petrological characterization of coal: an evolving science. The Journal of the Southern African Institute of Mining and Metallurgy 113, 865-875.

Richardson, A.R., Eble, C.F., Hower, J.C., O'Keefe, J.M.K., 2012. A critical re-examination of the petrology of the No. 5 Block coal in eastern Kentucky with special attention to the origin of inertinite macerals in the splint lithotypes. International Journal of Coal Geology 98, 41-49.

Rimmer, S.M., Rowe, H.D., Taulbee, D.N., Hower, J.C., 2006. Influence of maceral content on $\delta^{13}C$ and $\delta^{15}N$ in a Middle Pennsylvanian coal. Chemical Geology 225, 77-90.

Roberts, M.J., Everson, R.C., Neomagus, H.W.J.P., Okolo, G.N., Van Niekerk, D., Mathews, J.P., 2015a. The characterization of slow-heated inertinite- and vitrinite-rich coals from the South African coalfields. Fuel 158, 591-601.

Roberts, M.J., Everson, R.C., Neomagus, H.W.J.P., Van Niekerk, D., Mathews, J.P., Branken, D.J., 2015b. Influence of maceral composition on the structure, properties and behaviour of chars derived from South African coals. Fuel 142, 9-20.

Schulten, H.-R., Schnitzer, M., 1998. The chemistry of soil organic nitrogen: a review. Biology and Fertility of Soils 26, 1-15.

Scott, A.C., 1989. Observations on the nature and origin of fusain. International Journal of Coal Geology 12, 443-475.

Scott, A.C., 2002. Coal petrology and the origin of coal macerals: a way ahead? International Journal of Coal Geology 50, 119-134.

Scott, A.C., 2010. Charocoal recognition, taphonomy and uses in palaeoenvironmental analysis. Palaeogeography, Palaeoclimatology, Palaeoecology 291, 11-39.

Scott, A.C., Glasspool, I.J., 2007. Observations and experiments on the origin and formation of inertinite group macerals. International Journal of Coal Geology 70 (1-3), 53-66.

Sehume, T.Z., Strydom, C.A., Bunt, J.R., Schobert, H.H., 2017. Effectivity of Phenol during Solvent Extraction of a South African Bituminous Coal under Mild Conditions. Energy & Fuels 31 (12), 13655-13665.

Senftle, J.T., Larter, S.R., Bromley, B.W., Brown, J.H., 1986. Quantitative chemical characterization of vitrinite concentrates using pyrolysis-gas chromatography. Rank variation of pyrolysis products. Organic Geochemistry 9 (6), 345-350.

Silbernagel, B.G., Gebhard, L.A., Dyrkacz, G.R., 1984b. Electron Spin Resonance of Isolated Coal Macerals. In: Petrakis, L., Fraissard, J.P., (Eds.). Magnetic Resonance. Introduction, Advanced Topics and Applications to Fossil Energy. D. Reidel Publishing Company, pp. 645-653.

Silbernagel, B.G., Gebhard, L.A., Dyrkacz, G.R., Bloomquist, C.A.A., 1986. Electron spin resonance of isolated coal macerals. Fuel 65, 558-565.

Silbernagel, B.G., Gebhard, L.A., Dyrkacz, G.R., Bloomquist, C.A.A., 1984a. Electron Spin Resonance of Isolated Coal Macerals, Preliminary Survey. In: Winans, R.E., Crelling, J.C., (Eds.). Chemistry and Characterization of Coal Macerals. ACS Symposium Series, American Chemical Society, Washington DC, pp. 121-135.

Simoneit, B.R.T., Rogge, W.F., Mazurek, M.A., Standley, L.J., Hilderman, L.M., Cass, G.R., 1993. Lignin pyrolysis products, lignans, and resin acids as specific tracers of plant classes in emissions from biomass combustion. Environmental Science and Technology 27, 2533-2541.

Skrzypek, G., Jezierski, P., Szynkiewicz, A., 2010. Preservation of primary stable isotope signatures of peat-forming plants during early decomposition – observation along an altitudinal transect. Chemical Geology 273, 238-249.

Slater, B.J., McLoughlin, S., Hilton, J., 2015. A high-latitude Gondwana lagerstätte: The Permian permineralised peat biota of the Prince Charles Mountains, Antarctica. Gondwana Research 27, 1446-1473.

Snyman, C.P., 1989. The role of coal petrography in understanding the properties of South African coal. In: Pickhardt, W., (Ed.). Erich Stach Memorial Issue. International Journal of Coal Geology 14, 83-101.

Snyman, C.P., Botha, W.J., 1993. Coal in South Africa. Journal of African Earth Sciences 16 (1/2), 171-180.

Solum, M.S, Pugmire, R.J., Grant, D.M., 1989. $^{13}C$ Solid-state NMR of Argonne Premium Coals. Energy & Fuels 3, 187-193.

South African National Standards (SANS) 7936:2010 (ISO 7936:1992). Hard coal – Determination and presentation of float and sink characteristics – General directions for apparatus and procedures.

Spiker, E.G., Hatcher, P.G., 1987. The effects of early diagenesis on the chemical and stable carbon isotopic composition of wood. Geochimica et Cosmochimica Acta 51 (6), 1385-1391.

Steyn, M., Minnitt, R.C.A., 2010. Thermal coal products in South Africa. The Journal of Southern African Institute of Mining and Metallurgy 110 (10), 593-599.

Strydom, C.A., Bunt, J.R., Schobert, H.H., Raghoo, M., 2011. Changes to the organic functional groups of an inertinite rich medium rank bituminous coal during acid treatment processes. Fuel Processing Technology 92, 764-770.

Suggate, R.P., Dickinson, W.W., 2004. Carbon NMR of coals: the effects of coal type and rank. International Journal of Coal Geology 57, 1-22.

Supaluknari, S., Burgar, I., Larkins, F.P., 1990. High-resolution solid-state $^{13}C$ NMR studies of Australian coals. Organic Geochemistry 15 (5), 509-519.

Taylor, G.H., Teichmüller, M., Davis, A., Diessel, C.F.K., Littke, R., Robert, P., 1998. Organic Petrology. Gebrüder Borntraeger, Berlin, 704pp.

Teichmüller, M., 1989. The genesis of coal from the viewpoint of coal petrology. In: Lyons, P.C., Alpern, B., (Eds.). Peat and Coal: Origin, Facies, and Depositional Models. International Journal of Coal Geology 12, 1-87.

Valentim, B., Algarra, M., Guedes, A., Ruppert, L.F., Hower, J.C., 2016. Notes on the origin of copromacrinite based on nitrogen functionalities and $\delta^{13}C$ and $\delta^{15}N$ determined on samples from the Peach Orchard coal bed, southern Magoffin County, Kentucky. International Journal of Coal Geology 160-161, 63-72.

van Krevelen, D.W., 1993. Coal: Typology-Physics-Chemistry-Constitution. 3rd Ed. Elsevier Science Publishers, Amsterdam, The Netherlands, 979pp.

Van Niekerk, D., Mathews, J.P., 2010. Molecular representations of Permian-aged vitrinite-rich and inertinite-rich South African coals. Fuel 89, 73-82.

Van Niekerk, D., Mitchell, G.D., Mathews, J.P., 2010. Petrographic and reflectance analysis of solvent-swelled and solvent-extracted South African vitrinite-rich and inertinite-rich coals. International Journal of Coal Geology 81, 45-52.

Van Niekerk, D., Pugmire, R.J., Solum, M.S., Painter, P.C., Mathews, J.P., 2008. Structural characterization of vitrinite-rich and inertinite-rich Permian-aged South African bituminous coals. International Journal of Coal Geology 76, 290-300.

Wagner, N.J., Hlatshwayo, B., 2005. The occurrence of potentially hazardous trace elements in five Highveld coals, South Africa. International Journal of Coal Geology 63 (3-4), 228-246.

Wagner, N.J., Tlotleng, M.T., 2012. Distribution of selected trace elements in density fractionated Waterberg coals from South Africa. International Journal of Coal Geology 94, 225-237.

White, A., Davies, M.R., Jones, S.D., 1989. Reactivity and characterization of coal maceral concentrates. Fuel 68, 511-519.

Więckowski, A.B., Wojtowicz, W., Pilawa, B., 2000. EPR characteristics of petrographically complex coal samples from durain and clarain. Fuel 79, 1137-1141.

Zieger, L., Littke, R., Schwarzbauer, J., 2018. Chemical and structural changes in vitrinites and megaspores from Carboniferous coals during maturation. International Journal of Coal Geology 185, 91-102.

# Chapter 2

## Characterization of coal using Electron Spin Resonance: Implications for the formation of inertinite macerals in the Witbank Coalfield, South Africa

**ABSTRACT**

Coal contains a significant concentration of free radicals as a result of the coalification process. One of the experimental methods sensitive to the presence of free radicals is electron spin resonance (ESR), and the differences in ESR spectra for different macerals may provide insight into coal-forming processes. In this study, ESR data along with the H/C atomic ratio (to infer the aromatic fraction) are used to characterize coal samples with the aim of assessing a fire-origin for dominant inertinite macerals. A medium rank C bituminous Witbank No. 4 Seam Upper coal (the parent) was density-fractionated to create a vitrinite-rich and an inertinite-rich sample. The parent sample consists of 42 vol. % vitrinite, 48 vol. % inertinite, 4 vol. % liptinite, and 6 vol. % mineral matter. The density-fractionated samples are vitrinite-rich (81 vol. % total vitrinite, dominated by collotelinite and collodetrinite), and inertinite-rich (63 vol. % total inertinite, dominated by fusinite, semifusinite, and inertodetrinite). The H/C ratio is 0.74 for the inertinite-rich sample, and 0.85 for the vitrinite-rich counterpart, suggesting the former is more aromatic. The ESR spectra obtained for the three samples were found to fit best using a Lorentzian distribution. The fit is noticeably better for the aromatic inertinite-rich sample, for which the spectrum is symmetric. This is attributed to pronounced electron mobility and exchange interactions resulting from the higher spin density and greater degree of aromaticity. The higher radical content of the inertinite-rich and parent samples is attributed to the presence of specific inertinite macerals, namely: fusinite, semifusinite, and inertodetrinite. And, owing to the greater radical content of the inertinite-rich sample, the dominant inertinite macerals are interpreted to have formed through charring of plant matter. The degree of charring, in part controlled by the moisture content of the vegetation, determined whether fusinite or semifusinite was formed. Inertodetrinite, as a secondary maceral, represents fragments of charred matter.

**Keywords:** Main Karoo Basin; Radical contents; Origin pathways; Charring; Fusinite; Semifusinite; Inertodetrinite.

## 2.1. Introduction

South African coals of the Main Karoo Basin, much like other Gondwana Permian coals, have high inertinite contents, comprised of a significant amount semifusinite and inertodetrinite (Falcon, 1986a; Hagelskamp and Snyman, 1988; Snyman, 1989; Taylor et al., 1998; Glasspool, 2003a, 2003b; Van Niekerk et al., 2008, and references therein; Hower et al., 2012; O'Keefe et al., 2013). Inertinite has been shown to have higher carbon and lower hydrogen contents, as well as higher aromaticity than other maceral groups at the bituminous coal rank (Dyrkacz et al., 1984; Falcon, 1986b; White et al., 1989; Maroto-Valer et al., 1994, 1998a; Davidson, 2004; Van Niekerk et al., 2008; Van Niekerk and Mathews, 2010; Moroeng et al., 2017). As a result, free radicals formed during coalification are better preserved (Retcofsky et al., 1968; Levine et al., 1982). Radical properties have been used to understand the origin and chemistry of organic matter globally, including coal and its constituent macerals (Austen et al., 1966; Retcofsky et al., 1968, 1981; Grandy and Petrakis, 1979; Petrakis and Grandy, 1981; Silbernagel et al., 1984a, 1984b, 1986; Kwan and Yen, 1979; Fowler et al., 1987; van Krevelen, 1993, and references therein; Więckowski et al., 2000; Binet et al., 2002; Ikoma et al., 2002; Davidson, 2004; Liu et al., 2014; Zhou et al., 2017). For South African coals, there appears to be no information available in the published literature regarding the use of electron spin resonance (ESR) to determine the properties of the coals.

According to van Krevelen (1993), free radicals (i.e. unpaired electrons) in coal were discovered in 1954 by two research teams working independently. Following the discovery, there was an initial concerted focus on the origin and influence of the radicals on the chemical behaviour of coal in various technological applications (Austen et al., 1958, 1966; Retcofsky et al., 1968, 1981; Grandy and Petrakis, 1979; Petrakis and Grandy, 1981; van Krevelen, 1993, and references therein). An immediate observation made was that the radicals were primarily associated with the organic fraction of coal, rather than the mineral matter (Retcosfky et al., 1981).

In terms of elemental composition, coal is particularly distinctive from other fossil fuels: it has a significantly lower hydrogen and higher oxygen content in comparison to both petroleum and oil shale (Levine et al., 1982). The hydrogen deficiency of coal ensures the survival of early formed radicals throughout the coalification process (Retcofsky et al., 1968; Levine et al., 1982). The

concentration of radicals varies with coal rank, increasing as a function of rank advance and the concomitant expulsion of hydrogen, reflecting the pronounced alteration expected of mature coals (Retcofsky et al., 1968; Kwan and Yen, 1979; van Krevelen, 1993; Więckowski et al., 2000; Qiu et al., 2007). The aromatization of the coal macromolecule is suggested to be related to radical preservation (Austen et al., 1966; Kwan and Yen, 1979). The maceral constituents of coal have been found to have varying radical contents (Austen et al., 1966; Grandy and Petrakis, 1979; Silbernagel et al., 1984a, 1984b, 1986; van Krevelen, 1993, and references therein; Więckowski et al., 2000). At the bituminous rank, inertinite group macerals generally have a higher radical content than vitrinite and liptinite counterparts.

Austen et al. (1966) offer three possibilities for the origin of radicals in coal. Firstly, stable radicals are associated with the original organic matter and survive coalification. The radicals form as a result of enzymatic reactions, as well as the oxidation of organic matter during diagenesis. However, since radicals in the initial organic matter would mostly be localized on oxygen atoms, which are progressively expelled during coalification, it is unlikely that these are present in coal of bituminous rank (Austen et al., 1966). Indeed, with an increase in maturity from lignite to bituminous coal, the proportion of radicals localized on oxygen atoms is decreased (Austen et al., 1966). Radicals in such coals may instead be associated with carbon atoms, as molecular products of reactions related to oxygen expulsion (Austen et al., 1966). Secondly, the radicals form due to an increase in temperature during coalification (Austen et al., 1966; Qiu et al., 2007). The decomposition of methyl and methoxyl, hydroxyl, and carboxyl functional groups through homolytic fission with methane, water, and carbon dioxide as products respectively, results in the formation of radical species. The radicals are subsequently immobilized by the coal structure (Austen et al., 1966; Retcofsky et al., 1968). As the aromatic structure grows with increasing rank, bond breakage is also enhanced and the stable structure required to accommodate and shield the radicals is progressively established. The final mechanism proposed by Austen et al. (1966) is also related to a temperature rise. Radioactive decay of elements within mineral constituents of coal provides the heat required for the breaking of bonds in the organic fraction, resulting in the formation of radicals (Austen et al., 1966). All these three radical-generating processes, so far as they are related to homolytic bond fission during coalification, have subsequently been supported by others (e.g., Retcosfsky et al., 1968; Kwan and Yen, 1979; van Krevelen, 1993).

Variations in the radical content of iso-rank macerals are indicative of differences in the degree of thermal alteration of the botanical precursors, thus suggesting differences in origin pathways. The typically high radical content of inertinite macerals suggests pre-diagenesis metamorphism of the botanical precursor (Austen et al., 1966; Retcofsky et al., 1968; Silbernagel et al., 1984a, 1984b, 1986; Więckowski et al., 2000). There are numerous studies on the ESR properties of coal and constituent macerals in the published literature. However, these studies generally address vitrinite-rich northern hemisphere coals (Austen et al., 1966; Retcofsky et al., 1968, 1981; Silbernagel et al., 1984a, 1984b, 1986; Kwan and Yen, 1979; Fowler et al., 1987; Więckowski et al., 2000; Qiu et al., 2007; Liu et al., 2014; Zhou et al., 2017), which have been shown to be both compositionally and genetically distinct from southern hemisphere counterparts (Plumstead, 1961; Falcon, 1986a; Cairncross and Cadle, 1988; Falcon and Ham, 1988; Hagelskamp and Snyman, 1988; Snyman, 1989; Cairncross et al., 1990; Taylor et al., 1998; Glasspool, 2003a, and references therein; Van Niekerk et al., 2008; O'Keefe et al., 2013). The main consequence of this is a somewhat skewed focus on vitrinite macerals and vitrinite-rich coals, and the results may not be applicable to inertinite-rich South African coals of the Main Karoo Basin.

The present study employs ESR and the fraction of aromaticity inferred from the H/C atomic ratio in the characterization of a parent coal from the No. 4 Seam Upper, Witbank Coalfield, situated in the Main Karoo Basin of South Africa. A vitrinite-rich and an inertinite-rich sample were prepared through density-fractionation. The ESR properties for the three samples are discussed in conjunction with other coal parameters, including detailed petrographic analysis. The results are used to test whether a fire-origin hypothesis holds for the dominant inertinite macerals present in the coal samples. A fire-origin was proposed for the macerals based on the carbon-13 cross-polarization magic-angle-spinning solid-state nuclear magnetic resonance ($^{13}$C CP-MAS SS NMR) structural parameters (Moroeng et al., 2018). A similar conclusion was reached in a submitted research article based on stable nitrogen and carbon ($\delta^{15}$N and $\delta^{13}$C) isotopes (Moroeng et al., under review).

## 2.2. Materials and methods

### 2.2.1. Sample, preparation, and basic characterization

A medium rank C bituminous coal sample from the No. 4 Seam Upper of the Witbank Coalfield was obtained from an operating coal mine. The entire sample (~50 kg) was crushed and screened to between –2 mm and –0.5 mm. A quarter of the material was set aside to represent what is herein referred to as the "parent sample". The remaining material (~17 kg) was subjected to float-sink density separation following South African National Standard (SANS) 7936 (2010) to create a vitrinite-rich (RD = 1.3) and inertinite-rich (RD = 1.8) products. A rotary splitter was used to homogenously split each sample into amounts appropriate for the different analyses. These include: proximate; elemental; gross calorific value (CV); petrographic; ESR; carbon-13 cross-polarization magic-angle-spinning solid-state nuclear magnetic resonance ($^{13}$C CP-MAS SS NMR); stable nitrogen and carbon isotope ($\delta^{15}$N and $\delta^{13}$C); and, pyrolysis (py) thermal desorption (TD) – gas chromatography (GC) – time of flight (TOF) mass spectrometry (MS). For the present study, only the ESR results are reported.

The samples were prepared for petrographic analysis as polished blocks following SANS standard 7404-2 (2015), and the macerals qualified and quantified following SANS standard 7404-3 (2016) using a Zeiss AxioImager m2M reflected-light microscope retrofitted with Hilgers Diskus Fossil components and software, at a total magnification of 500x using immersion oil. The mean random vitrinite reflectance (%RoVmr) was determined following SANS 7404-5 (2016). The maceral nomenclature adopted follows that of the International Committee for Coal and Organic Petrology for bituminous coals (ICCP, 1998, 2001; Pickel et al., 2017). Proximate, elemental, and CV analyses were performed at a commercial laboratory (Bureau Veritas, Centurion, South Africa) following prescribed SANS standards; SANS 17247 (2006), SANS 17246 (2011), SANS 334 (1992), and SANS 1928 (2009), respectively.

### 2.2.2. Electron spin resonance analysis

The ESR analyses were undertaken using a Bruker ESP300E continuous wave X-band ESR spectrometer at ambient temperature (~23 °C). For each coal sample, the following parameters were determined: ESR spectrum, linewidths as a function of microwave power, and the area under the absorption spectrum as a function of microwave power. The variation of the spectrum

area as a function of microwave power was fitted to a power law, as described later, and the exponents of the power law extracted.

For each coal sample, a representative (prepared using a rotatory splitter) sub-sample was prepared for the ESR analysis. The ESR experiments were conducted on material with particle sizes between –2 mm and –0.5 mm. Milling and demineralization of the samples were considered unnecessary. Fine milling may result in the formation of radicals through bond cleavage as demonstrated by Liu et al. (2014). Although the presence of inorganic matter in coal may affect the resulting ESR spectra, acid-based demineralization may also lead to the loss of oxygenated radicals. Furthermore, the resonance peaks of metal ions are far removed from that of corresponding organic matter (Binet et al., 2002; Qiu et al., 2007). In addition, the ESR spectra of coal samples with varying amounts of mineral matter has also been found to be comparable (Retcosky et al., 1981; Silbernagel et al., 1986; Qiu et al., 2007, and references therein).

### 2.3. Results

#### 2.3.1. Basic characterization and aromaticity inferred from H/C atomic ratio

The proximate and elemental analyses of the parent coal and the density-fractionated samples are presented in Tables 2.1 and 2.2. The H/C atomic ratio was used estimate the aromatic fraction for bituminous rank coals (Maroto-Valer et al., 1994, 1998a; Mazumdar, 1999; Van Niekerk et al., 2008; Moroeng et al., 2017), and is applicable for density-fractionated samples (Maroto-Valer et al., 1998b; Davidson, 2004). Based on this, the inertinite-rich sample (H/C = 0.74) has the higher aromatic fraction compared to the vitrinite-rich counterpart (H/C = 0.85). The lower volatile content (VM = 28.5 wt. %) for the inertinite-rich sample is consistent with the higher aromatic fraction (Van Niekerk et al., 2008, and references therein), as inferred from the H/C ratio. For the inertinite-rich sample, the H/C atomic ratio is within the range ($0.51 < H/C < 0.75$) previously reported by Maroto-Valer et al. (1998b) for various inertinite-rich coals at the bituminous range of rank.

**Table 2.1:** Proximate analysis and calorific value (CV) (air dried) of the parent, inertinite-rich, and vitrinite-rich samples.

| Sample | Proximate Analysis (wt. %) | | | | Gross Calorific value (MJ/kg) |
|---|---|---|---|---|---|
| | Moisture | Ash | Volatile matter | Fixed carbon | |
| **Parent** | 3.10 | 12.50 | 30.70 | 53.70 | 27.69 |
| **Inertinite-rich** | 3.00 | 13.40 | 28.50 | 55.10 | 27.14 |
| **Vitrinite-rich** | 3.10 | 4.20 | 38.60 | 54.10 | 30.91 |

**Table 2.2:** Elemental analyses (air dried) for the parent, inertinite-rich, and vitrinite-rich samples.

| Sample | Elemental Analysis (wt. %) | | | | | H/C |
|---|---|---|---|---|---|---|
| | C | H | N | O | S | |
| **Parent** | 67.40 | 4.40 | 1.80 | 8.61 | 2.24 | 0.78 |
| **Inertinite-rich** | 67.60 | 4.17 | 1.68 | 9.57 | 0.64 | 0.74 |
| **Vitrinite-rich** | 75.00 | 5.33 | 2.07 | 9.58 | 0.76 | 0.85 |

Maceral group compositions for the parent, inertinite-rich, and vitrinite-rich samples are presented in Figure 2.1, and the detailed maceral composition is given in Table 2.3. The sample is a medium rank C bituminous coal (0.65 %RoVmr) as determined on the parent sample. The principal vitrinite macerals are collodetrinite and collotelinite with subordinate amounts of corpogelinite. As may be expected, the proportion of these macerals is greatest in the vitrinite-rich sample. Semifusinite constitutes a significant proportion of both the parent and inertinite-rich samples at approximately 18 vol. % and 29 vol. % respectively. In contrast, this maceral constitutes 5 vol. % of the vitrinite-rich sample. Inertodetrinite is the second most abundant inertinite maceral at 24 vol. % in the inertinite-rich sample and 20 vol. % in the parent sample. The fusinite content is similar for the parent and inertinite-rich samples at approximately 8 vol. %, and 4 vol. for the vitrinite-rich sample. The petrographic composition of the inertinite-rich sample is consistent with the higher fraction of aromaticity relative to the vitrinite-rich counterpart, as inferred from the H/C atomic ratio and in agreement with the findings by Van Niekerk et al. (2008).

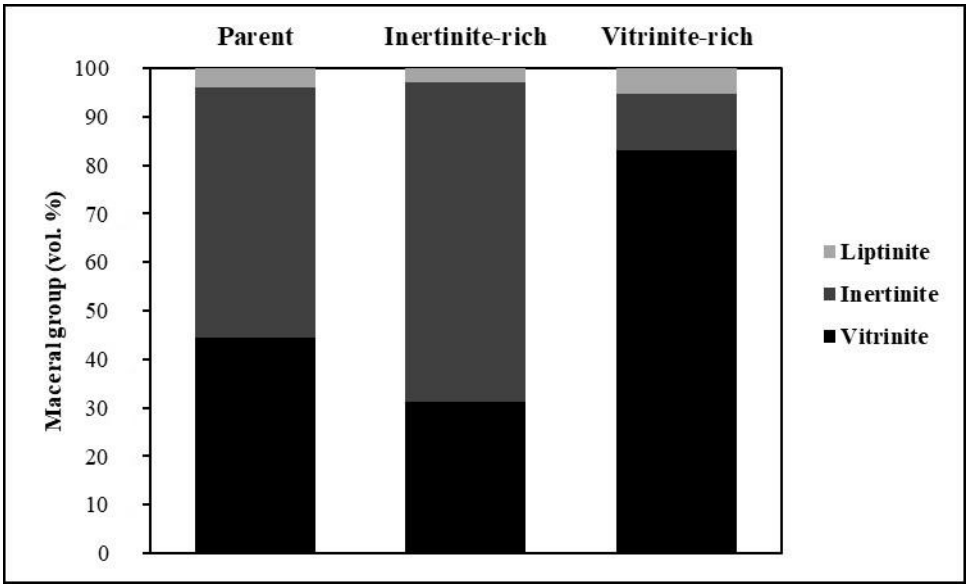


**Figure 2.1:** Distribution of maceral groups (mineral-matter-free basis) for the parent, inertinite-rich and vitrinite-rich samples.

**Table 2.3:** Maceral composition (vol. %) for the parent, inertinite-rich, and vitrinite-rich samples. (%RoVmr = mean random vitrinite reflectance).

| | **Parent** | **Inertinite-rich** | **Vitrinite-rich** |
|---|---|---|---|
| Telinite | 0.2 | 0.0 | 2.4 |
| Collotelinite | 12.0 | 12.4 | 35.3 |
| Vitrodetrinite | 0.0 | 0.0 | 0.0 |
| Collodetrinite | 28.0 | 15.4 | 36.3 |
| Corpogelinite | 1.4 | 0.5 | 6.9 |
| Gelinite | 0.0 | 1.3 | 0.0 |
| Pseudovitrinite | 0.0 | 0.2 | 0.4 |
| **Total vitrinite** | **41.6** | **29.8** | **81.3** |
| Fusinite | 8.6 | 8.3 | 3.9 |
| Semifusinite | 18.3 | 28.9 | 4.7 |
| Micrinite | 0.4 | 0.2 | 0.0 |
| Macrinite | 0.2 | 0.2 | 0.4 |
| Secretinite | 1.2 | 1.2 | 0.6 |
| Funginite | 0.0 | 0.0 | 0.0 |
| Inertodetrinite | 19.8 | 23.8 | 1.8 |
| **Total inertinite** | **48.5** | **62.6** | **11.4** |
| Sporinite | 3.3 | 2.9 | 2.9 |
| Cutinite | 0.4 | 0.0 | 2.0 |
| Resinite | 0.0 | 0.0 | 0.2 |
| Alginite | 0.0 | 0.0 | 0.0 |
| Liptodetrinite | 0.0 | 0.0 | 0.0 |
| Exsudatinite | 0.0 | 0.0 | 0.0 |
| **Total liptinite** | **3.7** | **2.9** | **5.1** |
| Silicate | 3.1 | 3.1 | 0.2 |
| Sulphide | 2.4 | 1.2 | 0.8 |
| Carbonate | 0.8 | 0.6 | 1.4 |

| | | | |
|---|---|---|---|
| **Total minerals** | **6.3** | **4.9** | **2.4** |
| **%RoVmr** | **0.65** | | |
| **Std. Dev.** | **0.067** | | |

### 2.3.2. Electron spin resonance: Spectral amplitudes, line-shapes, and line-widths

For each sample, measurements of the ESR spectrum were taken at a microwave power of approximately 2.6 mW, where 10 sweeps were taken to improve the signal-to-noise ratio. An attempt was made to fit the experimental data, the derivative of the absorption curve, to Gaussian and Lorentzian distributions; the latter is by far the best fit for all three samples (Figure 2.2). A Gaussian distribution is typically observed in low rank coals with higher rank coals (>90% carbon) exhibiting a Lorentzian spectra line-shape (Retcofsky et al., 1968). However, in the present case, the highest carbon content is only 75% for the vitrinite-rich sample. A Lorentzian distribution suggests a random distribution of radicals with the shape and associated linewidth resulting from dipole-dipole interactions (Silbernagel et al., 1984b).

The presence of a single peak in the spectra for the parent, inertinite-rich, and vitrinite-rich samples is due to the presence of radicals in the organic fraction of the coals. Furthermore, a single well-defined peak suggests the absence of radicals in the inorganic fraction (Binet et al., 2002). However, there are some notable differences between the spectral distributions for the three samples. Firstly, the spectrum peak for the inertinite-rich sample is markedly narrower than the other two samples with the vitrinite-rich sample exhibiting the broadest peak (Figure 2). In addition, the peak amplitudes appear roughly the same for both the parent and inertinite-rich samples. This is indicative of the intensity of the ESR signal and is proportional to the number of radicals in the samples. The vitrinite-rich sample has a much lower peak, indicative of a much lower radical content. Furthermore, the Lorentzian fit is evidently poorer for this sample in addition to the experimental spectrum showing slight asymmetry. Conversely, the spectra are largely symmetric and more pronounced for the inertinite-rich sample and, to a slightly lesser extent, the parent coal.

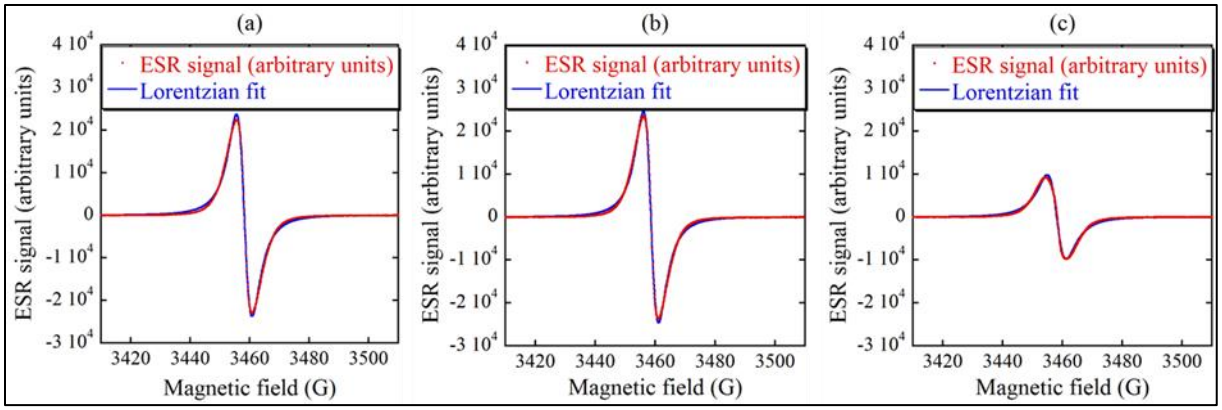


**Figure 2.2:** ESR spectra for (a) the parent, (b) inertinite-rich, and (c) vitrinite-rich coal samples.

Measurements of the linewidth as a function of microwave power (Figure 2.3) were taken in the 0.80 – 280 mW range in steps of 2dB. The behaviour of the parent coal is similar to that exhibited by the inertinite-rich sample. The behaviour of the vitrinite-rich sample is altogether different. At a microwave power of 1 mW, the linewidths for both the parent and inertinite-rich samples are roughly 4.4 gauss (G). The corresponding linewidth for the vitrinite-rich sample is markedly higher at approximately 5.5 G. The linewidth for the vitrinite-rich sample then decreases with increasing power, reaching a minimum of ~5.1 G at around 100 mW. The decrease in the corresponding linewidths for the other two samples are less pronounced, only reaching a minimum at a power of ~80 mW then rising again more rapidly. Linewidths for the vitrinite-rich sample as a function of increasing microwave power are consistently higher than those for both the parent and inertinite-rich samples. It must be noted that the minimum linewidth for the inertinite-rich sample at a power just below 100 mW is lower for the parent sample. The linewidth for low rank coals with a carbon content of less than 90% is reported to be within the range 5.9 – 8.0 G (Retcofsky et al., 1968). This appears to be higher than the values obtained for the samples of the present study. It has also been shown that the variation in width is not due to the presence of radical species with varying g-values and is, thus, not due to radicals localized on different host molecules or atoms (Retcofsky et al., 1968).

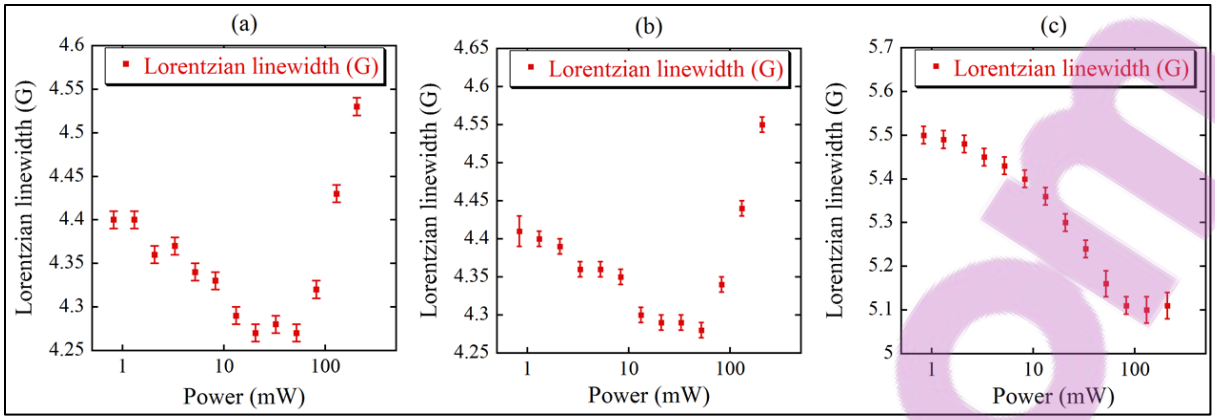


**Figure 2.3:** Lorentzian linewidth as a function of microwave power for (a) the parent, (b) inertinite-rich, and (c) vitrinite-rich coal samples.

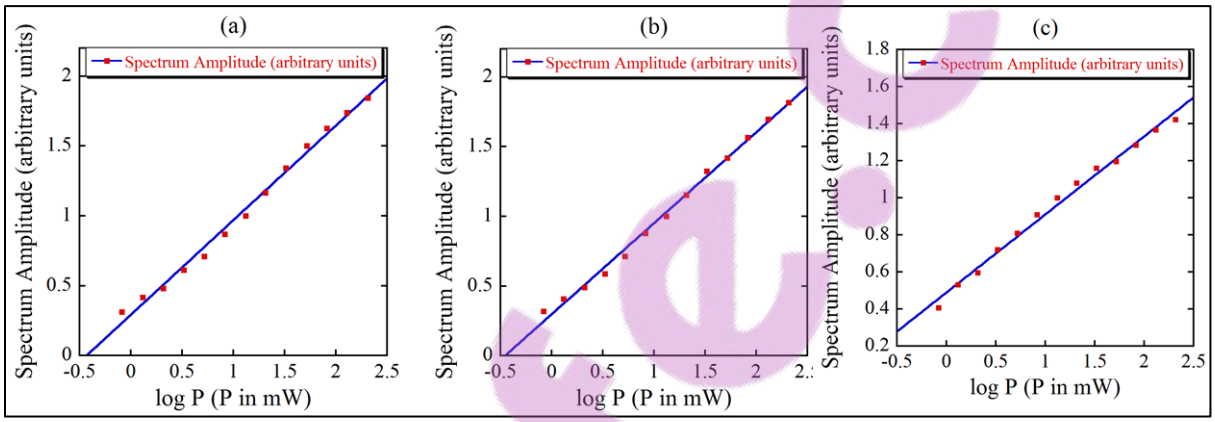


**Figure 2.4**: Spectrum amplitude as a function of microwave power for (a) the parent, (b) inertinite-rich, and (c) vitrinite-rich samples. The exponents for each of the power law fits are (a) 0.68 ± 0.02, (b) 0.65 ± 0.01, and (c) 0.42 ± 0.01.

The area under the absorption curve (integral of the derivative spectra obtained) for each sample was similarly measured as a function of microwave power (Figure 2.4). Each derivative spectrum was integrated numerically to obtain the absorption curve, and the area under the curve was determined numerically. This produces a result that is proportional to the number of unpaired electrons in each sample. The peak amplitude was determined from a double integral of the experimentally obtained derivative for each microwave power. Amplitude is plotted as a function of microwave power for each sample in Figure 4. The data were subsequently fitted using a regression power law of the form:

$$A = A_0 P^n \qquad \text{(Eq. 2.1)}$$

Where $A$ is the amplitude of the ESR signal; $P$ is the microwave power; and $A_0$ and $n$ are obtained from fitting the data.

In a case where a saturation peak is not observed, and the resonance line is homogeneously broadened, we expect $n \approx 0.5$. The resulting exponents for each sample are provided in the caption to Figure 4. The exponents for the parent and inertinite-rich samples are comparable at 0.68 and 0.65, respectively. As such, the parent and inertinite-rich samples have similar radical contents, with similar relaxation times. However, the slight broadening of the spectral line-shape for the parent sample suggests small differences in the radical properties of the two samples. The power law exponent for the vitrinite-rich sample is significantly lower, and suggests that the radical concentration is lower than for the other two samples, and that the radicals may be in a different chemical environment. This observation is in agreement with previous studies (e.g., Austen et al., 1966; Retcofsky et al., 1968; Silbernagel et al., 1984a, 1984b, 1986). The parent and inertinite-rich samples thus exhibit similar behaviour as is the case with both the spectra line-shape and width. None of the three samples showed a saturation peak over the power range explored. This suggests that the spin-lattice relaxation rate is high for all three samples at room temperature (~23 °C), i.e. $T_1$ is small. The difference in the exponents obtained for the parent and inertinite-rich samples on one hand, and the vitrinite-rich sample on the other, suggest that the spectral lines may originate from different environments. It would be of interest to perform saturation measurements at low temperatures, where the relaxation rate is lower, as this may uncover unresolved fine structure in the ESR spectra.

### 2.4. Discussion

#### 2.4.1. Radical properties for vitrinite-rich and inertinite-rich Witbank coals

Based on the petrographic composition and elemental analysis including the H/C atomic ratio, the parent sample is most comparable to the inertinite-rich sample. The ESR properties are largely consistent with this observation. The high collotelinite and collodetrinite content of the vitrinite-rich sample appears to be responsible for the deviation from a pure Lorentzian fit, resulting in a lower peak amplitude and slightly asymmetric distribution. Peak narrowing of a Lorentzian distribution, as observed in the line-shape of the inertinite-rich sample, is interpreted to reflect pronounced radical mobility, i.e., the migration of radical electrons between neighbouring molecular hosts (Retcofsky et al., 1968; Kwan and Yen, 1979; Silbernagel et al., 1984a, 1984b, 1986). In addition, exchange interactions between neighbouring radicals can also effect narrowing of the spectrum peak (Silbernagel et al., 1984b; Kwan and Yen, 1979). The former phenomenon inevitably requires that the individual host molecules be relatively close to

each other, whereas the latter necessitates a high spin density. The peak narrowing exhibited by the line-shape for the inertinite-rich sample suggests an increase in either or both radical motion and exchange interactions.

The greater aromatic fraction of both the inertinite-rich and parent samples is consistent with the likelihood of pronounced radical migration. With increasing aromaticity, the merging and condensation of aromatic rings (Solum et al., 1989; Haenel, 1992; Davidson, 2004; Suggate and Dickinson, 2004; Van Niekerk et al., 2008; Chen et al., 2012) implies that a molecular host becomes progressively larger (Kwan and Yen, 1979). Spatially, greater aromaticity suggests that the area over which a radical electron is able to move is therefore also enlarged. In addition, the reduction in distance between adjacent molecules (Van Niekerk et al., 2008) implies that a radical electron is better able to interchange hosts. Larger aromatic cluster sizes as well as the greater degree of condensation associated with higher aromaticity are thus consistent with prominent radical mobility (Kwan and Yen, 1979; Więckowski et al., 2000). The higher spin densities for the parent and inertinite-rich samples, coupled with greater aromaticity, permits greater exchange interactions between adjacent radical species. Owing to greater aromatic fraction, radicals in the inertinite-rich sample may be associated with larger aromatic molecular hosts (Figure 2.5) (Van Niekerk et al., 2008).

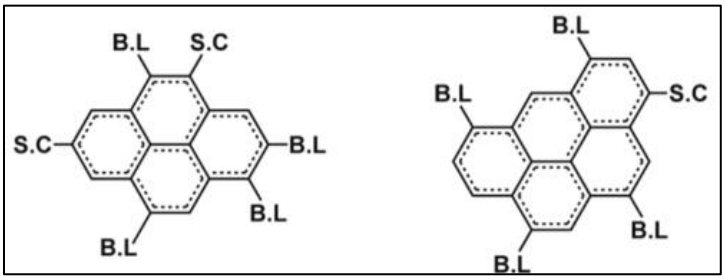


**Figure 2.5:** Representations of the average molecular host size and attachments for vitrinite-rich Waterberg and inertinite-rich Highveld coal. S.C= side chains, B.L= bridges and loops (Van Niekerk et al., 2008).

The considerably broader and less than perfect spectrum fit for the vitrinite-rich sample, coupled with lower aromaticity, is attributable to reduced radical migration and exchange interactions. According to Silbernagel et al. (1986), individual molecular hosts should, in this case, be viewed as somewhat isolated from one another. As a result of lower aromaticity, the cluster sizes are presumably smaller in comparison to those found in the inertinite-rich counterpart (Van Niekerk et al., 2008). Van Niekerk et al. (2008) also found that for bituminous coals of comparable rank,

the interplanar distances determined using X-ray diffraction (XRD) were 3.97Å for vitrinite-rich Waterberg and 3.42Å for inertinite-rich Highveld coals. The reduced interplanar distance along with larger cluster sizes for the more aromatic inertinite-rich Highveld sample (Figure 2.5) is a reflection of a more condensed molecular structure. This would, in turn, result in resonance stabilization leading to relatively unreactive and stable radicals (Austen et al., 1958). Therefore, with a narrowed ESR peak, the aromatic clusters and other molecules which serve as radical hosts are closer to one another. This implies that radical mobility is enhanced in a greater aromatic fraction coal. It should be mentioned that Moroeng et al. (2018) report the average aromatic cluster size for the inertinite-rich sample (determined using $^{13}C$ CP-MAS SS NMR) to be comprised of six-aromatic carbons (a single ring), implying a reduction in resonance stabilization for the radicals of this sample.

Conversely, in a sample with a broadened peak, the hosts are further apart, thus impeding radical motion resulting in the restriction of a radical electron to a single host. This coupled with a lower spin density is consistent with a reduction in exchange interactions due to the larger distance between molecular hosts and, consequently, radical electrons. With smaller hosts, with less a condensed molecular structure, resonance stabilization is diminished resulting in more reactive radical species (Austen et al., 1958). Notwithstanding lower aromaticity and spin density, radical motions and exchange interactions are present, albeit minimized, in the vitrinite-rich sample. Given that rank-dependent variations can be completely excluded (samples created from the same coal), the observed differences are attributable only to variations amongst the dominant macerals present in the density-fractionated samples.

Radical motions and exchange interactions are thus greatest in the inertinite-rich sample. These phenomena appear to decrease as a function of aromaticity and evidently, inertinite content in the order: inertinite-rich sample > parent sample > vitrinite-rich sample. In particular, radical mobility and exchange interactions appear to be greatest in a Witbank coal dominated by fusinite, semifusinite, and inertodetrinite; and reduced in a sample with a greater proportion of collotelinite and collodetrinite. These observations are consistent with the widely accepted view that the compositional differences between inertinite and vitrinite macerals derive mainly from genetic, depositional environment-specific variations. Metamorphosis of inertinite-forming

precursors before diagenesis and/or incorporation into a peat-forming environment has been suggested by Austen et al. (1966) and Silbernagel et al. (1984b).

### 2.4.2. On the formation of the inertinite macerals in the Witbank Coalfield

Vitrinite-rich and inertinite-rich samples derived from the same coal have lower and higher radical contents, respectively. This suggests independent origin pathways for the dominant macerals present in each coal sample. Differences in the pathways must have occurred before the precursors for the dominant macerals of each density-fractionated sample underwent diagenesis in a classic peat-forming environment, wherein geochemical coalification, affecting the sum total of coal-forming materials, took place. Any other process affecting the materials during coalification should have imparted similar characteristics on all coal-forming materials. The dominant macerals of vitrinite-rich sample, collotelinite and collodetrinite, formed through humification and gelification of woody tissues in a water-logged setting (Teichmüller, 1989; Diessel, 1992; van Krevelen, 1993; ICCP, 1998; Taylor et al., 1998; Hower et al., 2013; O'Keefe et al., 2013). Vitrinite formation is thus consistent with the lower radical content for the vitrinite-rich sample, thus lacking the pronounced, heat-induced alteration associated with fusinite genesis.

The high inertinite content in the coals of the Main Karoo Basin of South Africa, has historically been attributed to aerial oxidation and incomplete degradation of plant matter as a result of a cold climate (Falcon, 1986a, 1989; Hagelskamp and Snyman, 1988; Snyman, 1989; Cadle et al., 1993; Van Niekerk et al., 2008; O'Keefe et al., 2013). At the same time, others contend that the inertinite component of the coals of the Main Karoo Basin is a product of charring of plant matter (Glasspool, 2003a, 2003b; Jasper et al., 2013; Moroeng et al., 2018). Given the complexity associated with coal formation, and consequent chemical and physical characteristics, it seems unlikely that inertinite genesis was the same in all the coal-forming regions of the world, or even, within a singular peat-forming environment (Austen et al., 1966; Diessel, 1992; Moore et al., 1996; Moore and Shearer, 1997; Taylor et al., 1998; ICCP, 2001; Hower et al., 2011b; Richardson et al., 2012; Jasper et al., 2013), what some commonly refer to as multiple origin pathways (Hower et al., 2011a, 2013; O'Keefe and Hower, 2011; O'Keefe et al., 2013; Moroeng et al., 2018).

Austen et al. (1966) report high radical contents for fusinite-rich coals relative to fusinite-impoverished counterparts, and found that the spin density of the former coals did not change during pyrolysis experiments at temperatures below 550 °C. As a result, Austen et al. (1966, p. 357) concluded that "fusinites achieved both their carbon contents and their high unpaired spin concentration before incorporation into the sediment and most probably by exposure to elevated temperatures". The relatively high temperatures required for inertinite formation can be provided by peat- or wildfires, or alternatively, by thermophilic bacteria and/or fungal activity (Austen et al., 1966; Scott, 1989, 2002, 2010; Diessel, 1992; Moore et al., 1996; Moore and Shearer, 1997; Glasspool, 2003a, 2003b; Scott and Glasspool, 2007; Hower et al., 2011a, 2011b, 2013; Richardson et al., 2012; Jasper et al., 2013; O'Keefe et al., 2013; Moroeng et al., 2018). However, when organisms degrade plant matter, anatomical structure is destroyed (Guo and Bustin, 1998; Hower et al., 2011a, 2011b, 2013; Richardson et al., 2012; O'Keefe et al., 2013). Furthermore, macerals produced through fungal activity possess indistinct cell walls (Taylor et al., 1998), and fungal hyphae length has been observed to correlate with the fusinitized sections of a plant organ (Moore et al., 1996; Moore and Shearer, 1997). In contrast, wood charring produces anatomical structures similar to those observed in inertinite macerals (Scott, 1989, 2002, 2010; Teichmüller, 1989; Jones and Chaloner, 1991; Guo and Bustin, 1998; Scott and Glasspool, 2007; Ascough et al., 2010), noted by Moroeng et al. (2018) for the inertinite macerals of the coal samples of the present study. If the same line of reasoning applied by Austen et al. (1966) with regards to fusinite genesis is applied to the dominant inertinite macerals of the inertinite-rich sample, the high radical content of this sample can be interpreted to suggest that the major components were subjected to thermally driven pre-diagenesis metamorphism.

Fusinite and semifusinite macerals present in the inertinite-rich Witbank coal sample of this study likely represent charred plant matter. The preservation of anatomical structure and reflectance of semifusinite, coupled with the higher radical content for the inertinite-rich sample, suggest charring of botanical precursor, albeit to a lesser degree than corresponding fusinite within the same coal sample. In this sense, a fusinite-rich section of a coal particle may be interpreted to represent the outermost layers of a plant organ. The inner, comparatively lower-reflectance portions of the same particle may then represent semifusinite. During charring, the outermost layers of a plant organ would have been directly exposed to the fire, whereas the inner portions would have been shielded and may thus, have remained relatively unaffected by the

elevated temperature (Scott, 2010). This process accounts for a gradational boundary between fusinite and adjacent semifusinite, as shown in Figures 2.6 and 2.7. In the absence of a gradational contact between inertinite macerals as shown in Figure 2.8, the botanical organs can be interpreted to have been distinct and discrete. However, fusinite and semifusinite would still have formed from woody plant organs. The degree of charring, controlled in part, by moisture and perhaps size of the affected plant organ, would then have determined whether fusinite or semifusinite was formed.

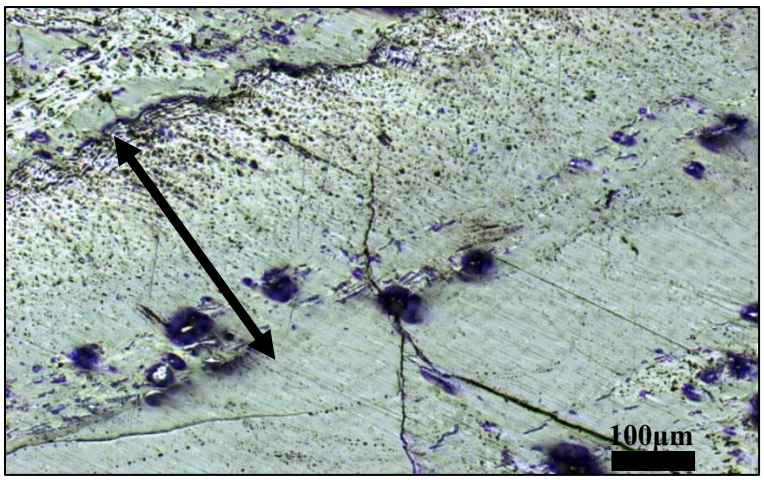


**Figure 2.6:** Fusinite grading into semifusinite and, finally into vitrinite, observed in the inertinite-rich sample. 100x magnification, reflected light in air (Photomicrograph, H. Dorland). Scale is indicated.


**Figure 2.7:** Mosaic photomicrograph showing fusinite (right; well-preserved structure, high reflectance) grading into semifusinite (structured still, lower reflectance), and finally into vitrinite (bottom left; unstructured, lowest reflectance) observed in the inertinite-rich sample. 500x magnification, reflected light under oil immersion. Scale is indicated.

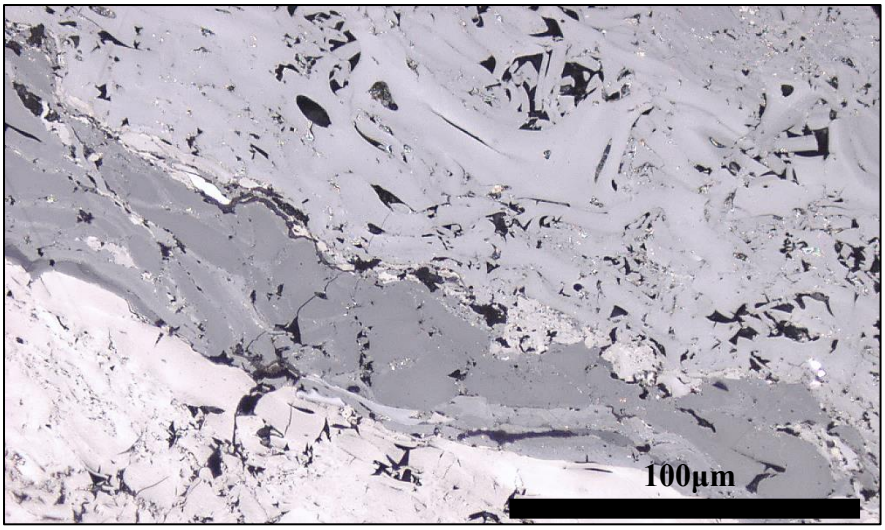


**Figure 2.8:** Inertinite macerals with varying reflectances observed in the inertinite-rich sample. 500x magnification, reflected light with oil immersion. Scale is indicated.

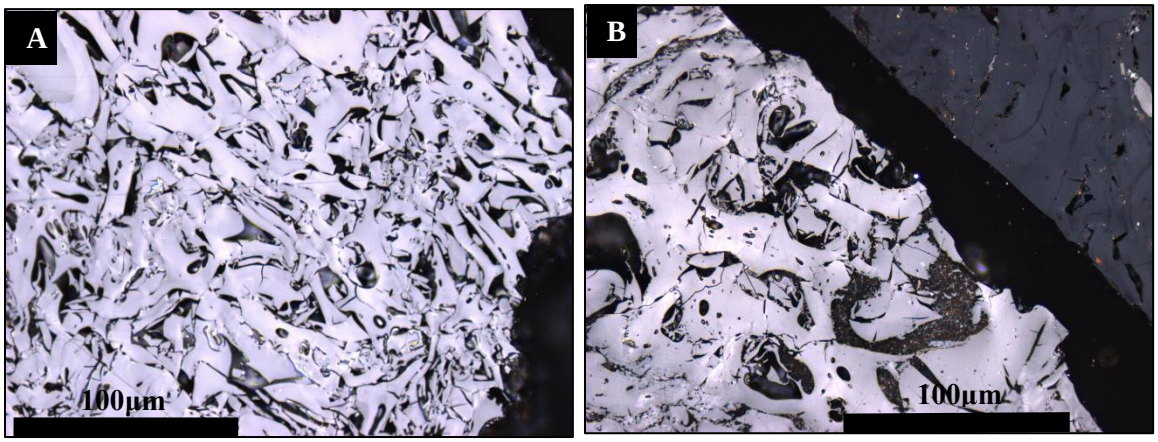


**Figure 2.9:** A and B – fusinites observed in the inertinite-rich sample. 500x magnification, reflected light with oil immersion. Scale is indicated.

A fusinite particle of uniformly high reflectance (Figure 2.9) may be interpreted to reflect charring when the botanical precursor had already died and was dried out, and was thus, more readily and evenly charred. The preservation of anatomical structure suggests negligible degradation by organisms (Guo and Bustin, 1998; Richardson et al., 2012; Hower et al., 2013; O'Keefe et al., 2013), and thus, the plant matter in question must have been located either at the top, above the water level, or outside the peat-forming environment before charring. Following this line of reasoning, the formation of semifusinite may represent charring while plant matter was still wet, potentially alive or recently deceased, with the increased moisture content hindering both complete charring and the attainment of very high reflectances. According to Jasper et al. (2013), the increased atmospheric oxygen content during the Permian Period would

have rendered wet vegetation more flammable. In this sense, the relatively high semifusinite content of the coals of the Main Karoo Basin likely represents coal-forming environments wherein incomplete/partial charring was prevalent. Charred and disintegrated plant matter could have resulted in smaller fragments blown into, or transported into the peat-forming environment through some other sedimentary process, resulting in the formation of inertodetrinite (Figure 2.10).

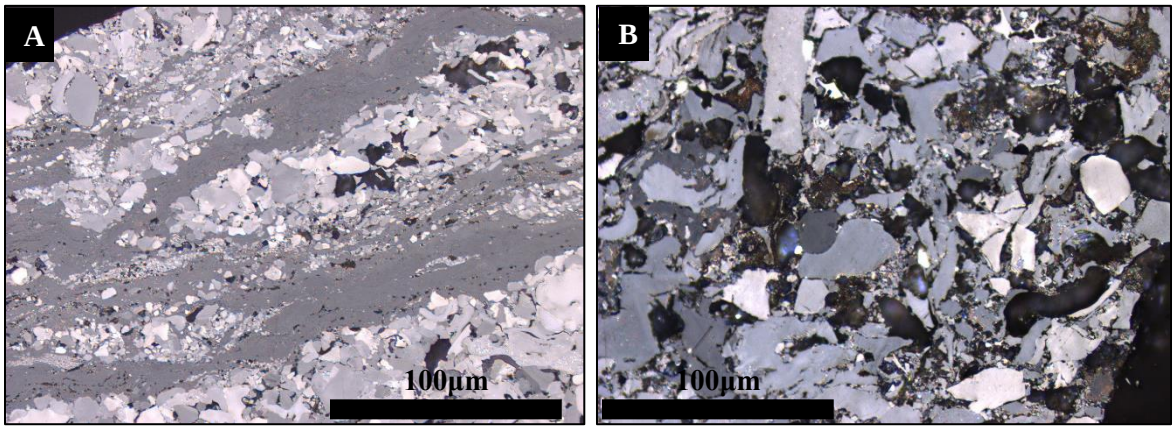


**Figure 2.10:** A – alternating layers of inertodetrinite and vitrinite; B – inertodetrinite, observed in the inertinite-rich sample. 500x magnification, reflected light with oil immersion. Scale is indicated.

Glasspool (2003b) notes the inherent contradiction required to reconcile the water-logged environments generally required for peat accumulation alongside the relatively dry conditions required for the formation of fire-derived inertinite macerals, and thus account for the high radical content of the inertinite-rich sample of this study. This is attributed to an interchange between periods of pronounced saturation and relatively drier periods (Glasspool, 2003b). Similar conditions, specifically the changes in climatic conditions are also invoked in the present case and appear to be particularly applicable given the general alternation of bright and dull coloured banding present in the coals, broadly corresponding to vitrinite-rich and inertinite-rich bands (Falcon, 1989). The dry periods could thus coincide with periods of pronounced wild- and peat-fire events (Hope et al., 2005), resulting in the formation of a significant amount of fire-derived inertinite macerals, with the wetter periods giving rise to mostly vitrinite macerals. Gondwana climatic conditions are generally interpreted to have been varied, ranging from cold to cool, and dry to wet (Falcon 1986a; Cairncross, 1989, 2001; Cadle et al., 1993). However, more recent studies have shown that the climate was warming during the formation of the younger coal seams of the Main Karoo Basin (Ruckwied et al., 2014). Furthermore, the

occurrence of fires, i.e., the proposed pathway for the formation of the dominant inertinite macerals, within and around Gondwana peat-forming environments, including in South Africa, has been established based on the presence of fossilized charcoal (e.g., Glasspool, 2003a, 2003b; Jasper et al., 2013; Slater et al., 2015).

### 2.5. Conclusion

For the first time, ESR was used to characterize an inertinite-rich and a vitrinite-rich sample of the same coal from the No. 4 Seam Upper, Witbank Coalfield (South Africa). In addition, the H/C atomic ratio was used to infer the fraction of aromaticity. The medium rank C bituminous parent coal sample density-fractionated. Semifusinite and inertodetrinite were the dominant macerals of the inertinite-rich sample (62.6% total inertinite), whereas the vitrinite-rich sample (81.3% total vitrinite) was dominated by collotelinite and collodetrinite. The radical (unpaired electrons) content as determined by ESR is highest in the inertinite-rich sample, followed by the parent sample, with the vitrinite-rich sample having the lowest radical content. The H/C ratios suggest that the fraction of aromaticity follows the same trend, with the inertinite-rich and vitrinite-rich samples having a higher and lower aromatic fraction, respectively. The ESR properties were used to examine the sustainability of a fire-origin for the dominant inertinite macerals. The main findings of the study can be summarized as follows:

- In addition to having the higher radical content, the inertinite-rich sample also has a narrowed ESR spectrum peak. This reflects radical mobility and exchange interactions between adjacent radicals. The higher aromatic fraction of this sample suggests proximity of radicals, and that the radicals interchange between molecular hosts.

- Owing to a higher radical concentration in the inertinite-rich sample, the dominant inertinite macerals of this coal sample are suggested to have formed in a similar manner as is widely accepted for fusinite, i.e., through charring of botanical precursors.

- It is argued that a coal particle – comprised of fusinite grading into semifusinite – reflects differences in degrees of charring for these macerals, controlled by the inherent moisture content and size of the botanical organ. Thus, semifusinite formation reflects moderate charring, whereas fusinite is indicative of near complete charring.

- Based on the degree of charring, and given a sufficiently thick plant organ, an individual organ may form both macerals with a gradational contact separating the two. In the case where the contact is sharp, the two macerals have been formed from individual plant organs that were subsequently superimposed.

- Inertodetrinite represents charred/partially charred plant matter that was subsequently fragmented.

**2.6. References**


Ascough, P.L., Bird, M.I., Scott, A.C., Collinson, M.E., Cohen-Ofri, I., Snape, C.E., Le Manquais, K., 2010. Charcoal reflectance measurements: implications for structural characterization and assessment of diagenetic alteration. Journal of Archaeological Science 37, 1590-1599.

Austen, D.E.G., Ingram, D.J.E., Given, P.H., Binder, C.R., Hill, L.W., 1966. Electron Spin Resonance Study of Pure Macerals. In: Given, P.H., (Ed.). Coal Science, Advances in Chemistry, 55. American Chemical Society, Washington DC, pp. 344-362.

Austen, D.E.G., Ingram, D.J.E., Tapley, J.G., 1958. The investigation of free radicals trapped in low temperature carbons. Transactions of the Faraday Society 54, 400-408.

Binet, L., Gourier, D., Derenne, S., Robert, F., 2002. Heterogeneous distribution of paramagnetic radicals in the insoluble organic matter from the Orgueil and Murchison meteorites. Geochimica et Cosmochimica Acta 66 (23), 4177-4186.

Cadle, A.B., Cairncross, B., Christie, A.D.M., Roberts, D.L., 1993. The Karoo Basin of South Africa: type basin for coal-bearing deposits of southern Africa. International Journal of Coal Geology 23, 117-157.

Cairncross, B., Cadle, A.B., 1988. Palaeoenvironmental control on coal formation, distribution and quality in the Permian Vryheid Formation, East Witbank Coalfield, South Africa. International Journal of Coal Geology 9 (4), 343-370.

Cairncross, B., Hart, R.J., Wills, J.P., 1990. Geochemistry and sedimentology of coal seams from the Permian Witbank Coalfield, South Africa; a means of identification. International Journal of Coal Geology 16 (4), 309-325.

Chen, Y., Mastalerz, M., Schimmelmann, A., 2012. Characterization of chemical functional groups in macerals across different coal ranks via micro-FTIR spectroscopy. International Journal of Coal Geology 104, 22-33.

Davidson, R.M., 2004. Studying the structural chemistry of coal. IEA Clean Coal Centre. 121pp.

Diessel, C.F.K., 1992. Coal-Bearing Depositional Systems. Springer-Verlag, Berlin Heidelberg, 721pp.

Dyrkacz, G.R., Bloomquist, C.A.A., Ruscic, L., 1984. Chemical variations in coal macerals separated by density gradient centrifugation. Fuel 63, 1166-1173.

Falcon, R., Ham, A.J., 1988. The characteristics of Southern African coals. The Journal of the South African Institute of Mining and Metallurgy 88 (5), 145-161.

Falcon, R.M., 1986b. Spontaneous combustion of the organic matter in discards from the Witbank coalfield. The Journal of the South African Institute of Mining and Metallurgy 86 (7), 243-250.

Falcon, R.M.S., 1986a. A brief review of the origin, formation, and distribution of coal in southern Africa. In: Anhaeusser, C.R., Maske, S., (Eds.). Mineral Deposits of Southern Africa, Vols. I and II. Geological Society of South Africa, Johannesburg, pp.1879-1898.

Falcon, R.M.S., 1989. Macro-and micro-factors affecting coal-seam quality and distribution in southern Africa with particular reference to the No. 2 seam, Witbank coalfield, South Africa. International Journal of Coal Geology 12 (1-4), 681-731.

Fowler, T.G., Bartle, K.D., Kandiyoti, R., 1987. Low temperature processes in a bituminous coal studied by in situ electron spin resonance spectroscopy. Fuel 66 (10), 1407-1412.

Glasspool, I., 2003a. Palaeoecology of selected South African export coals from the Vryheid Formation, with emphasis on the role of heterosporous lycopods and wildfire derived inertinite. Fuel 82, 959–970.

Glasspool, I.J., 2003b. Hypautochthonous-allochthonous coal deposition in the Permian, South African, Witbank Basin No. 2 seam; a combined approach using sedimentology, coal petrology and palaeontology. International Journal of Coal Geology 53, 81-135.

Grandy, D.W., Petrakis, L., 1979. Esr investigation of free radicals in solvent-refined coal materials. Fuel 58, 239-240.

Guo, Y., Bustin, R.M., 1998. FTIR spectroscopy and reflectance of modern charcoals and fungal decayed woods: implications for studies of inertinite in coals. International Journal of Coal Geology 37, 29-53.

Haenel, M.W., 1992. Recent progress in coal structure research. Fuel 71, 1211-1223.

Hagelskamp, H.H.B., Snyman, C.P., 1988. On the origin of low-reflecting inertinites in coals from the Highveld Coalfield, South Africa. Fuel 67, 307-313.

Hope, G., Chokkalingam, U., Anwar, S., 2005. The stratigraphy and fire history of the Kutai Peatlands, Kalimantan, Indonesia. Quaternary Research 64, 407-417.

Hower, J.C., O'Keefe, J.M.K., Eble, C.F., Raymond, A., Valentim, B., Volk, T.J., Richardson, A.R., Satterwhite, A.B., Hatch, R.S., 2011a. Notes on the origin of inertinite macerals in coal: Evidence for fungal and arthropod transformations of degraded macerals. International Journal of Coal Geology 86 (2-3), 231-240.

Hower, J.C., O'Keefe, J.M.K., Eble, C.F., Volk, T.J., Richardson, A.R., Satterwhite, A.B., Hatch, R.S., Kostova, I.J., 2011b. Notes on the origin of inertinite macerals in coals: Funginite associations with cutinite and Suberinite. International Journal of Coal Geology 85 (1), 186-190.

Hower, J.C., O'Keefe, J.M.K., Wagner, N.J., Dai, S., Wang, X., Xue, W., 2013. An investigation of Wulantuga coal (Cretaceous, Inner Mongolia) macerals: Paleopathology of faunal and fungal invasions into wood and the recognizable clues for their activity. International Journal of Coal Geology 114, 44-53.

Hower, J.C., Wagner, N.J., O'Keefe, J.M.K., Drew, J.W., Stucker, J.D., Richardson, A.R., 2012. Maceral types in some Permian southern African coals. International Journal of Coal Geology 100, 93-107.

Ikoma, T., Ito, O., Tero-Kubota, S., 2002. Exploring Radicals in Carbonaceous Solids by Means of Pulsed EPR Spectroscopy. Energy & Fuels 16, 40-47.

International Committee for Coal and Organic Petrology (ICCP)., 1998. The new vitrinite classification. (ICCP System 1994). Fuel 77 (5), 349-358.

International Committee for Coal and Organic Petrology (ICCP)., 2001. The new inertinite classification (ICCP System 1994). Fuel 80 (4), 459-471.

Jasper, A., Guerra-Sommer, M., Abu Hamad, A.M.B., Bamford, M., Cerruti Bernardes-de-Oliveira, M.E., Tewari, R., Uhl, D., 2013. The burning of Gondwana: Permian fires on the southern continent – A palaeobotanical approach. Gondwana Research 24 (1), 148-160.

Jones, T.P., Chaloner, W.G., 1991. Fossil charcoal, its recognition and palaeoatmospheric significance. Palaeogeography, Palaeoclimatology, Palaeoecology (Global and Planetary Change Section) 97, 39-50.

Kwan, C.L., Yen, T.F., 1979. Electron Spin Resonance Study of Coal by Line Width and Line Shape Analysis. Analytical Chemistry 51 (8), 1225-1229.

Levine, D.G., Schlosberg, R.H., Silbernagel, B.G., 1982. Understanding the chemistry and physics of coal structure (A Review). Proceedings of the National Academy of Sciences of the United States of America 79, 3365-3370.

Liu, J., Jiang, X., Shen, J., Zhang, H., 2014. Chemical properties of superfine pulverized coal particles. Part 1. Electron paramagnetic resonance analysis of free radical characteristics. Advanced Powder Technology 25 (3), 916-925.

Maroto-Valer, M.M., Andresén, J.M. Snape, C.E., 1998b. Verification of the linear relationship between carbon aromaticities and H/C ratios for bituminous coals. Fuel 77 (7), 783-785.

Maroto-Valer, M.M., Love, G.D., Snape, C.E., 1994. Relationship between carbon aromaticities and H/C ratios for bituminous coals. Fuel 73 (12), 1926-1928.

Maroto-Valer, M.M., Taulbee, D.N., Andresén, J.M., Hower, J.C., Snape, C.E., 1998a. Quantitative $^{13}C$ NMR study of structural variations within the vitrinite and inertinite maceral groups for a semifusinite-rich bituminous coal. Fuel 77 (8), 805-813.

Mazumdar, B.K., 1999. On the relationship between carbon aromaticities and H/C ratios for bituminous coals. Fuel 78, 1239-1241.

Moore, T.A. Shearer, J.C., Miller, S.L., 1996. Fungal origin of oxidized plant material in the Palangkaraya peat deposit, Kalimantan Tengah, Indonesia: Implications for 'inertinite' formation in coal. International Journal of Coal Geology 30, 1-23.

Moore, T.A., Shearer, J.C., 1997. Evidence for Aerobic Degradation of Palangka Raya Peat and Implications for its Sustainability. In: Rieley, J.O., Page, S.E., (Eds.). Tropical Peatlands. Samara Publishing Limited, Cardigan, pp.157-167.

Moroeng, O.M., Roberts, R.J., Bussio, J.P., Dixon, R.D., 2017. Self-heating Potential of Coal inferred from Elemental Data – A Case-study of the Witbank Coalfield of South Africa. Energy & Fuels 31 (11), 11811-11817.

Moroeng, O.M., Wagner, N.J., Brand, D.J., Roberts, R.J., 2018. A Nuclear Magnetic Resonance study: Implications for coal formation in the Witbank Coalfield, South Africa. International Journal of Coal Geology 188, 145-155.

Moroeng, O.M., Wagner, N.J., Hall, G., Roberts, R.J. (under review) Using $\delta^{15}N$ and $\delta^{13}C$ and nitrogen functionalities to support a fire-origin for certain inertinite macerals in a No. 4 Seam Upper Witbank coal, South Africa. Organic Geochemistry.

O'Keefe, J.M.K., Bechtel, A., Christanis, K., Dai, S., DiMichele, W.A., Eble, C.F., Esterle, J.S., Mastalerz, M., Raymond, A.L., Valentim, B.V., Wagner, N.J., Ward, C.R., Hower, J.C., 2013. On the fundamental difference between coal rank and coal type. International Journal of Coal Geology 118, 58-87.

O'Keefe, J.M.K., Hower, J.C., 2011. Revisiting Coos Bay, Oregon: A re-examination of funginite–huminite relationships in Eocene subbituminous coals. International Journal of Coal Geology 85 (1), 34-42.

Petrakis, L., Grandy, D.W., 1981. Free radicals in coals and coal conversion. 4. Investigation of the free radicals in selected macerals upon liquefaction. Fuel 60, 120-124.

Pickel, W., Kus, J., Flores, D., Kalaitzidis, S., Christanis, K., Cardott, B.J., Misz-Kennan, M., Rodrigues, S., Hentschel, A., Hamor-Vido, M., Crosdale, P., Wagner, N., ICCP. 2017. Classification of liptinite – ICCP System 1994. International Journal of Coal Geology 169, 40-61.

Plumstead, E.P., 1961. Ancient plants and drifting continents. South African Journal of Science 57 (7), 173-181.

Qiu, N., Li, H., Jin, Z., Zhu, Y., 2007. Temperature and time effect on the concentrations of free radicals in coal: Evidence from laboratory pyrolysis experiments. International Journal of Coal Geology 69, 220-228.

Retcofsky, H.L., Stark, J.M., Friedel, R.A., 1968. Electron Spin Resonance in American Coals. Analytical Chemistry 40 (11), 1699-1704.

Retcosfky, H.L., Hough, M.R., Maguire, M.M., Clarkson, R.B., 1981. Nature of the Free Radicals in Coals, Pyrolyzed Coals, Solvent-Refined Coal, and Coal Liquefaction Products.

In: Gorbaty, M.L., Ouchi, K., (Eds.). Coal Structure, Advances in Chemistry, 192. American Chemical Society, Washington DC, pp 37-58.

Richardson, A.R., Eble, C.F., Hower, J.C., O'Keefe, J.M.K., 2012. A critical re-examination of the petrology of the No. 5 Block coal in eastern Kentucky with special attention to the origin of inertinite macerals in the splint lithotypes. International Journal of Coal Geology 98, 41-49.

Ruckwied, K., Götz, A.E., Jones, P., 2014. Palynological records of the Permian Ecca Group (South Africa): Utilizing climatic icehouse–greenhouse signals for cross basin correlations. Palaeogeography, Palaeoclimatology, Palaeoecology 413, 167-172.

Scott, A.C., 1989. Observations on the nature and origin of fusain. International Journal of Coal Geology 12, 443-475.

Scott, A.C., 2002. Coal petrology and the origin of coal macerals: a way ahead? International Journal of Coal Geology 50, 119-134.

Scott, A.C., 2010. Charcoal recognition, taphonomy and uses palaeoenvironmental analysis. Palaeogeography, Palaeoclimatology, Palaeoecology 291, 11-39.

Scott, A.C., Glasspool, I.J., 2007. Observations and experiments on the origin and formation of inertinite group macerals. International Journal of Coal Geology 70 (1-3), 53-66.

Silbernagel, B.G., Gebhard, L.A., Dyrkacz, G.R., 1984b. Electron Spin Resonance of Isolated Coal Macerals. In: Petrakis, L., Fraissard, J.P., (Eds.). Magnetic Resonance. Introduction, Advanced Topics and Applications to Fossil Energy. D. Reidel Publishing Company, pp. 645-653.

Silbernagel, B.G., Gebhard, L.A., Dyrkacz, G.R., Bloomquist, C.A.A., 1986. Electron spin resonance of isolated coal macerals. Fuel 65, 558-565.

Silbernagel, B.G., Gebhard, L.A., Dyrkacz, G.R., Bloomquist, C.A.A., 1984a. Electron Spin Resonance of Isolated Coal Macerals, Preliminary Survey. In: Winans, R.E., Crelling, J.C., (Eds.). Chemistry and Characterization of Coal Macerals. ACS Symposium Series, American Chemical Society, Washington DC, pp. 121-135.

Slater, B.J., McLoughlin, S., Hilton, J., 2015. A high-altitude Gondwana lagerstätte: The Permian permineralised peat biota of the Prince Charles Mountains, Antarctica. Gondwana Research 27, 1446-1473.

Snyman, C.P., 1989. The role of coal petrography in understanding the properties of South African coal. In: Pickhardt, W., (Ed.). Erich Stach Memorial Issue. International Journal of Coal Geology 14, 83-101.

Solum, M.S, Pugmire, R.J., Grant, D.M., 1989. $^{13}C$ Solid-state NMR of Argonne Premium Coals. Energy & Fuels 3, 187-193.

South African National Standards (SANS) 17246:2011 (ISO 17246:2010). Coal - Proximate analysis.

South African National Standards (SANS) 17247:2006 (ISO 17247:2005). Coal - Ultimate analysis.

South African National Standards (SANS) 1928:2009 (ISO 1928:2009). Solid mineral fuels - Determination of gross calorific value by the bomb calorific method, and calculation of net calorific value.

South African National Standards (SANS) 334:1992 (ISO 334:1992). Solid mineral fuels - Determination of total sulfur - Eschka method.

South African National Standards (SANS) 7404-2:2015 (ISO 7404-2:2009). Methods for the petrographic analysis of coals Part 2: Methods of preparing coal samples.

South African National Standards (SANS) 7404-3:2016 (ISO 7404-3:2009). Methods for the petrographic analysis of coals - Part 3: Method of determining maceral group.

South African National Standards (SANS) 7936:2010 (ISO 7936:1992). Hard coal – Determination and presentation of float and sink characteristics – General directions for apparatus and procedures.

Suggate, R.P., Dickinson, W.W., 2004. Carbon NMR of coals: the effects of coal type and rank. International Journal of Coal Geology 57, 1-22.

Taylor, G.H., Teichmüller, M., Davis, A., Diessel, C.F.K., Littke, R., Robert, P., 1998. Organic Petrology. Gebrüder Borntraeger, Berlin, 704pp.

Teichmüller, M., 1989. The genesis of coal from the viewpoint of coal petrology. In: Lyons, P.C., Alpern, B., (Eds.). Peat and Coal: Origin, Facies, and Depositional Models. International Journal of Coal Geology 12, 1-87.

van Krevelen, D.W., 1993. Coal: Typology-Physics-Chemistry-Constitution, 3rd Ed. Elsevier Science Publishers. Amsterdam, The Netherlands, 979pp.

Van Niekerk, D., Mathews, J.P., 2010. Molecular representations of Permian-aged vitrinite-rich and inertinite-rich South African coals. Fuel 89, 73-82.

Van Niekerk, D., Pugmire, R.J., Solum, M.S., Painter, P.C., Mathews, J.P., 2008. Structural characterization of vitrinite-rich and inertinite-rich Permian-aged South African bituminous coals. International Journal of Coal Geology 76, 290-300.

White, A., Davies, M.R., Jones, S.D., 1989. Reactivity and characterization of coal maceral concentrates. Fuel 68, 511-519.

Więckowski, A.B., Wojtowicz, W., Pilawa, B., 2000. EPR characteristics of petrographically complex coal samples from durain and clarain. Fuel 79, 1137-1141.

Zhou, Q., Liu, Q., Shi, L., Yuxin, Y., Liu, Z., 2017. Behaviors of coking and radicals during reaction of volatiles generated from fixed-bed pyrolysis of a lignite and a subbituminous coal. Fuel Processing Technology 161, 304-310.

# Chapter 3

## A Nuclear Magnetic Resonance study: Implications for coal formation in the Witbank Coalfield, South Africa


### ABSTRACT

In this study, carbon-13 cross-polarization magic-angle-spinning solid-state nuclear magnetic resonance ($^{13}$C CP-MAS SS NMR) was undertaken on a parent coal sample and its density-fractionated derivatives, an inertinite-rich and a vitrinite-rich sample, obtained from the Witbank Coalfield of South Africa (medium rank C bituminous coal). The formation of inertinite macerals has been extensively researched and the conclusions remain largely controversial. However, most research has been confined to northern hemisphere coals, which are typically dominated by vitrinite. South African coals are widely known for their high inertinite content. Earlier workers have ascribed the inertinite macerals, in their diversity, to aerial oxidation. However, this oxidation-only pathway fails to recognize that inertinite macerals can form through other processes such as charring of plant matter. Microscopically, charred matter possesses anatomical structures that closely resembles those observed in inertinite macerals, with lignin and/or cell walls largely preserved, perhaps mechanically fragmented or compressed in some instances. Based on the NMR structural parameters, the average aromatic cluster size in the inertinite-rich sample (petrographically dominated by fusinite, semifusinite of varying reflectance, and inertodetrinite) corresponds to monocyclic, 6-aromatic carbon rings. In the vitrinite-rich sample of the same coal, the cluster sizes are larger, corresponding to multi-ring aromatic hydrocarbons. The 6-carbon rings in the inertinite-rich sample are interpreted to correspond to guaiacol and syringol, the principal products of low-temperature (below 400 °C) lignin pyrolysis. Since charring depletes cellulose and moisture, fire-affected plant matter is interpreted to have a lower compaction potential than vitrinite-forming material, sustaining 6-aromatic carbon ring isolation in the former. Lignin-derived aromatic rings in compactable plant matter merge to form the multi-ring clusters present in the collotelinite- and collodetrinite-rich sample of the same coal.



**Keywords:** $^{13}$C CP-MAS SS NMR; Karoo Basin; Coal-formation; Charring; Monocyclic aromatic rings; Semifusinite; Fusinite.

### 3.1. Introduction

The formation of inertinite macerals in coal through peat fire and/or wildfire combustion has been the subject of controversial discussion for some time (Austen et al., 1966; Hunt and Smyth, 1989; Scott, 1989, 2002, 2010; Teichmüller, 1989; Diessel, 1992, 2010; Moore et al., 1996; Shearer and Moore 1996; Moore and Shearer, 1997; Guo and Bustin, 1998; International Committee for Coal and Organic Petrology (ICCP), 2001; Glasspool, 2003a, 2003b; Scott and Glasspool, 2007; Hower et al., 2009, 2011a, 2011b; O'Keefe and Hower, 2011; Richardson et al., 2012; O'Keefe et al., 2013). South African coals, specifically those of the Witbank-Highveld, are rich in inertinite, dominated by semifusinite and inertodetrinite, with variable proportions of fusinite. A low-reflecting semifusinite is recognized, termed reactive semifusinite due its coking and combustion properties, with reflectance values more comparable to that of vitrinite rather than other inertinite macerals within the same or adjacent microlithotypes of the same coal (Falcon and Ham, 1988; Hagelskamp and Snyman, 1988; Snyman, 1989; Cadle et al., 1993; Glasspool, 2003a, 2003b; Van Niekerk et al., 2008, 2010; O'Keefe et al., 2013; Richards et al., 2013). The main point of contention between different workers relates to whether some inertinite macerals, including those from South African coals, owe their (partial or complete) inert character to prehistoric fires and/or aerial oxidation (e.g., Falcon, 1986; Hagelskamp and Snyman, 1988; Snyman, 1989; Cadle et al., 1993; ICCP, 2001; Glasspool, 2003a, 2003b). Various workers have argued for and against the formation of inertinite macerals through charring, with fusinite generally accepted as representing fossilized charcoal (Austen et al., 1966; Falcon, 1986; Hagelskamp and Snyman, 1988; Hunt and Smyth, 1989; Scott, 1989, 2002, 2010; Teichmüller, 1989; Jones and Chaloner, 1991; Diessel, 1992, 2010; Cadle et al., 1993; Moore et al., 1996; Shearer and Moore 1996; Moore and Shearer, 1997; Guo and Bustin, 1998; ICCP, 2001; Glasspool, 2003a, 2003b; Scott and Glasspool, 2007; Hower et al., 2009, 2011a, 2011b; O'Keefe and Hower, 2011; Richardson et al., 2012; O'Keefe et al., 2013).

Globally, plants started forming in the late Silurian, although initially sparsely distributed and with limited differentiation compared to the various organs of present-day plants; the plant structures were simple (Plumstead, 1961; Remy et al., 1994; Diessel, 2010). In the Permian, specifically during the formation of the upper coal seams of the Witbank Coalfield (South Africa), Glossopterid gymnosperms became abundant and were the major coal-forming plants (Falcon, 1986; Bamford, 2004; Ruckwied et al., 2014; Slater et al., 2015). Aside from the

availability of vegetation, the main prerequisite for the formation of macerals through charring is the occurrence of fires within the coal-forming environments. The occurrence of wild-fires during coal-forming periods, as early as the Devonian and specifically in the Permian, is well-documented in the fossil record and is dependent, in part, on the availability of free oxygen in the atmosphere (Jones and Chaloner, 1991; Diessel, 2010; Glasspool and Scott, 2010; Scott, 2010; Slater et al., 2015). Similar processes continue to operate in modern peat-forming environments (Hope et al., 2005). Charring of plant matter before incorporation into peat would increase the rigidity of the coal-forming material so that it will be less affected by humification-related decomposition and confining pressures during diagenesis and subsequent coalification (Austen et al., 1966; Scott, 1989, and references therein; Jones and Chaloner, 1991; Diessel, 1992; Ascough et al., 2010). The charring process also imparts distinctive physical morphologies on fire-affected plant matter, and subsequently, on the macerals produced (Scott, 1989, 2010; Jones and Chaloner, 1991; Guo and Bustin, 1998).

The basic building units for the polycyclic aromatic clusters in coal, namely 6-carbon monocyclic rings, have been found to exist as aromatic alcohols in the lignin component of wood (Saiz-Jimenez and de Leeuw, 1986; Kirk and Farrell, 1987; Teichmüller, 1989; Haenel, 1992; Simoneit et al., 1993; Hatcher and Clifford, 1997, and references therein; Kawamoto, 2017). During the early stages of coal-formation, the cellulose component is preferentially eliminated through either enzymatic action or charring (Hatcher and Clifford, 1997; Spiker and Hatcher, 1987; Guo and Bustin, 1998; Czimczik et al., 2002; Yang et al., 2007). Coalification to higher coal ranks parallels an increase in aromaticity, which involves the condensation and merging of individual aromatic rings to form multi-ringed clusters (Solum et al., 1989; Haenel, 1992; Davidson, 2004; Suggate and Dickinson, 2004; Van Niekerk et al., 2008), physically manifested by cellular wall and bordered pit distortion (Hatcher and Clifford, 1997). The deformation is accompanied by major chemical and structural changes to the lignin macromolecule, with vitrinite becoming visually lustrous and more homogenous at the rank of bituminous coal (Hatcher and Clifford, 1997). Despite the structural changes observed at this coal rank, the chemical structure largely remains that of lignin although having been subjected to demethylation, dehydroxylation, and the expulsion of side chains. Low-temperature charring of lignin-rich wood produces phenolic moieties, thus preserving 6-carbon ring monocyclicity, with

multi-ring aromatic clusters only forming at high temperatures (Saiz-Jimenez and de Leeuw, 1986; Simoneit et al., 1993; Kawamoto, 2017).

In this contribution, solid-state carbon-13 cross-polarization magic-angle-spinning solid-state nuclear magnetic resonance ($^{13}$C CP-MAS SS NMR) evidence for the presence of wood-derived (lignin) charring products in an inertinite-rich coal is provided. A medium rank C bituminous coal was obtained from the No. 4 Seam Upper of the Witbank Coalfield, South Africa. Density fractionation was performed to prepare samples corresponding to an inertinite-rich and a vitrinite-rich sample of the same coal. The aromatic cluster sizes in each sample were determined using $^{13}$C CP-MAS SS NMR. These were subsequently used to infer the coalification pathways for the inertinite macerals specifically. Both the detailed maceral and microlithotype compositions are presented, with the latter used to understand the associations between the individual macerals. Published NMR parameters for a vitrinite-rich Waterberg and an inertinite-rich Highveld coal (Van Niekerk et al., 2008) are included for comparison. This study focusses primarily on the formation of fusinite and semifusinite, and given that inertodetrinite is a secondary maceral it is largely omitted from the discussions. Similar, woody botanical precursors are assumed for vitrinite and the specific inertinite macerals, fusinite and semifusinite (ICCP, 1998, 2001; O'Keefe et al., 2013), so that the differences observed in the NMR data derive mainly from the coalification process. The present paper forms part of a larger project considering the origin and geochemistry of inertinite-rich coals in the No. 4 Seam Upper of the Witbank Coalfield using advanced analytical techniques.

## 3.2. Materials and methods

### 3.2.1. Samples and basic characterization

The coal sample (~50 kg) was received from an operating mine in the Witbank Coalfield (Seam 4 Upper), South Africa. In order to concentrate the vitrinite and inertinite components, the sample was crushed to –2 mm and the fines (–0.5 mm) removed. A quarter of the particles were retained to represent the "parent", and the rest of the sample (~17 kg) was subjected to float-sink experiments (South African National Standards (SANS) 7936, 2010). The density fractionation was performed in low and high-density liquids (low-density, RD = 1.3; high-density, RD = 1.8) to create separate samples enriched in vitrinite and inertinite respectively. The liptinite content of Witbank coals is below 5 vol. % and should not influence the separation or subsequent analysis.

Following density fractionation, a representative portion of each sample was mounted in epoxy resin and polished for petrographic analysis (SANS 7404-2, 2015).

Further representative samples were crushed (–212 µm) and split using a rotary splitter for the determination of proximate and ultimate/elemental analyses as well as calorific value (CV). These analyses were undertaken at a commercial laboratory (Bureau Veritas, Centurion, South Africa) following prescribed SANS standards (SANS 334, 1992; SANS 17247, 2006; SANS 1928, 2009; SANS 17246, 2011).

### 3.2.2. Petrographic analysis

A minimum of 500 unique points were recorded on each polished block to quantify and qualify the maceral components (SANS 7404-3, 2016) using a Zeiss AxioImager m2M reflected light microscope retrofitted with Hilgers Diskus Fossil components and software, at a total magnification of x500 using immersion oil. The terminology used follows that used by Taylor et al. (1998) and the International Committee for Coal and Organic Petrology (ICCP, 1998, 2001; Pickel et al., 2017). The mean random vitrinite reflectance (%RoVmr) was determined as per SANS standard 7404-5 (2016) on the parent sample.

The microlithotype composition of each sample was determined by a 500 point-count in 50 by 50 µm areas following the method described in Teichmüller (1989), Diessel (1992), as well as Hower and Wagner (2012). Depending on which of the three maceral groups or a combination of two or all three dominated the area under observation, the microlithotype group was classed as mono-, bi-, or trimaceral, respectively. In addition to vitrite and liptite, the inertite microlithotype was further subdivided into semifusite, fusite/secretite, and inertodetrite depending on the dominant inertinite maceral. When the area under observation also contained a proportion of mineral matter it was classed as a carbominerite. Areas comprising only mineral matter (more than 60% of the field of view) were classified as minerite. It is beneficial to undertake microlitholitype analyses in order to gain an understanding of the size of the maceral components and their associations.

### 3.2.3. Nuclear magnetic resonance

$^{13}C$ SS NMR has been widely used in the past to characterize the complex molecular structure of coal and other carbonaceous materials, as reported by Solum et al. (1989), Supaluknari et al.

(1990), Edwards and Choate (1993), Hu et al. (2001), Suggate and Dickinson (2004), Van Niekerk et al. (2008), Erdenetsogt et al. (2010), De Goede et al. (2010) and Mao et al. (2010). The methodology developed by Solum et al. (1989) and Hu et al. (2001) has improved the understanding of the carbon skeletal structure of coal. They utilized cross-polarization, magic angle spinning ($^{13}$C CP-MAS), variable contact time (VCT) and dipolar dephasing (CP-DD-MAS) techniques, which provided a direct measurement of the different carbon functionalities in coals. Ultimately, twelve carbon structural parameters can be determined from the combination of these experiments. The method relies on the integration of selected chemical shift ranges assigned to various carbon functional groups. Additionally, the structural parameters can be used to estimate the aromatic cluster size and extent of bridging between clusters in coal samples. This method has been widely employed by other researchers in the field, such as Supaluknari et al. (1990), Edwards and Choate (1993), Hu et al. (2001), Suggate and Dickinson (2004), Van Niekerk et al. (2008), De Goede et al. (2010) and Mao et al. (2010).

The NMR experiments discussed were mostly carried out on low magnetic field instruments (60-100MHz) and generally, broad resonances were observed for the aromatic and aliphatic carbon signals. Several research groups have used higher magnetic field instruments (200-300MHz) and have successfully demonstrated an increased insensitivity and spectral resolution (e.g., Supaluknari et al., 1990). However, the CP-MAS spectra obtained at the higher field with the sample spinning rate at 3-5 kHz were usually obscured by spinning sidebands, which made spectral interpretation difficult, as mentioned by Mao et al. (2010). Chemical-shift anisotropy (CSA) is known to manifest as spinning sidebands and their intensity correlates with increasing magnetic field strength. Therefore, the intensity of the downfield sideband is an important consideration in the total intensity of the total aromatic/anomeric and aliphatic carbon content at the higher field strengths. One way to address this problem is through using a sideband suppression pulse sequence such as Total Suppression of Sidebands (TOSS). Supaluknari et al. (1990) reported a combined CP-MAS/TOSS technique that they used to characterize 29 Australian coals. By using CP-MAS/TOSS together with CP-MAS/TOSS/DD, they could estimate the structural parameters of the different coals similarly to Solum et al. (1989). Thus, their findings indicated more accurate measurements of carbon fractions. Supaluknari et al. (1990) also investigated the dynamics of cross-polarization with the variable contact time experiment. Their findings suggest that there is an optimum contact time of ~1.5 ms which is

suitable for a single contact time experiment in the absence of the more time-consuming variable contact time experiment. In the same way, while a full DD interrupt delay array analysis is useful for the ratio estimation of protonated and non-protonated carbons, the approach is tedious. Supaluknari et al. (1990) have indicated that for coal it is adequate to use only two spectra, one taken at an interrupted decoupling time constant, td = 0 (CP-MAS/TOSS) and one taken at td = 40μs (CP-MAS/TOSS/DD), as this delay provides the best suppression of protonated carbons.

In a study by Mao et al. (2010), advanced solid-state NMR has been employed in the characterization of coal. The techniques used in the study included quantitative direct polarization/magic angle spinning (DP-MAS) at a high MAS rate of 14kHz, CP-MAS/TOSS, CP-MAS/TOSS/DD, $^{13}C$ CSA filtering and two-dimensional (2D) $^{1}H$-$^{13}C$ heteronuclear correlation NMR (HETCOR) experiments. Direct polarization combined with spectral editing techniques, allowed Mao et al. (2010) to quantify eleven different types of functional groups with confidence. Unfortunately, neither the CP-MAS/TOSS/DD or DP-MAS/TOSS/DD pulse sequence are currently commercially available for Agilent users, even though their required CP-MAS/TOSS or DP-MAS/TOSS counterparts are. The experiments, while probably slightly more quantitative because of the direct polarization techniques, each took several days to run. Delay times of up to 30s were reported and the number of scans for different experiments varied from 4000 to over 70 000 scans. While the CP-MAS experiment can only be regarded as a semi-quantitative technique, it is practically more feasible than DP-MAS to evaluate differences between coal samples where the sample's cross-polarization dynamics are similar. CP-MAS is much more cost effective and, more importantly, their required DP-MAS/TOSS/DD and CP-MAS/TOSS/DD versions needed for the dipolar dephasing experiments are not available commercially. Thus, CP-MAS in combination with a CP-DD experiment at 12 kHz MAS still holds excellent value, at high field, for the relative comparison of coal samples. We, like others, dealt with the sidebands by subtracting the downfield sideband signal area from the corresponding upfield area in the calculations. The use of CP with DD NMR experiments is still popular for coal analysis (Malumbazo et al., 2011; Hattingh et al., 2013; Okolo et al., 2015).

$^{13}C$ CP-MAS NMR combined with CP-MAS/DD experiments was thus chosen to compare the coal samples, closely following the method described by Solum et al. (1989). These two experiments were performed on each sample to determine the structural differences between the

vitrinite-rich and inertinite-rich samples, as well as the parent coal. The structural parameters were calculated based on Solum et al. (1989) and Suggate and Dickinson (2004). As mentioned, there are minor variations in structural parameters regardless of whether single-pulse-excitation (SPE) or cross-polarization (CP) is chosen for NMR coal analysis (Davidson, 2004; Van Niekerk et al., 2008). Furthermore, demineralization has also been shown to result in only minor variations in the CP-NMR results, specifically so far as inertinite-rich coals are concerned (Van Niekerk et al., 2008). As a result, the CP-MAS NMR and CP-MAS/DD experiments were conducted without pretreatment of the samples.

The spectra were acquired using an Agilent VNMRS 500 MHz two-channel NMR spectrometer using 4 mm zirconia rotors and a 4 mm Chemagnetics TM T3 HXY MAS probe. All CP spectra were recorded with the latest VnmrJ 4.2 instrument software at ambient temperature with optimized high-power proton decoupling; a relaxation delay of 3 s and 10 000 scans were collected for obtaining sufficient signal-to-noise ratio. The power parameters were optimized for the Hartmann-Hahn match; the radio frequency fields were $\gamma$CB1C = $\gamma$HB1H $\approx$ 56 kHz. The contact time selected for CP was 2 ms. The free induction decay recorded 2000 points and was Fourier transformed with a 125 Hz line broadening. Magic-angle-spinning (MAS) rate of 12 kHz and Admantane was used as an external chemical shift standard with the upfield methyl peak referenced to 38.4 ppm.

The DD experiments were carried out under the same CP parameters with the interrupted decoupling constant of the tancpxidref sequence set to 40 μs, after first evaluating an incremental array of 10-100 μs time constants.

With regard to spectra processing, the integration reset points were adapted from Solum et al. (1989) and Mestrenova 11.02 “preset integral regions table” was made to ensure that the exact same regions were integrated reproducibly. The individual spectra were each phased and baseline corrected manually before integration. All spectra were processed in the same manner and by the same person to minimize operator bias. The absolute integral values were transferred to a Microsoft Excel spreadsheet for calculation of the coal structural parameters as per Solum et al. (1989). No variable contact time was performed as suggested by Solum et al. (1989), because of the long acquisition times. A contact time of 2 ms was used for all experiments and a correction factor of 1.3, derived from Solum et al. (1989), was used to correct the intensity of the

bridgehead aromatic carbons (peak 135-90 ppm for DD) for the loss of magnetization during the interrupted decoupling.

## 3.3. Results

### 3.3.1. Basic characterization

The proximate and elemental analysis results are presented in Tables 3.1 and 3.2. In agreement with published literature (Van Niekerk et al., 2008), the inertinite-rich and vitrinite-rich samples have the lowest and highest H/C atomic ratio, respectively. The vitrinite-rich sample has the greatest proportion of volatile matter at 38.6 wt. % in comparison to 28.5 wt. % for the inertinite-rich coal sample.

**Table 3.1:** Proximate analysis and calorific value (CV) (air-dried) of the parent coal, inertinite-rich, and vitrinite-rich samples.

| Sample | Proximate Analysis (wt. %) | | | | Gross Calorific value (MJ/kg) |
|---|---|---|---|---|---|
| | Moisture | Ash | Volatile matter | Fixed carbon | |
| **Parent** | 3.1 | 12.5 | 30.7 | 53.7 | 27.69 |
| **Inertinite-rich** | 3.0 | 13.4 | 28.5 | 55.1 | 27.14 |
| **Vitrinite-rich** | 3.1 | 4.2 | 38.6 | 54.1 | 30.91 |

**Table 3.2:** Elemental analysis (air dried) of the parent coal, inertinite-rich, and vitrinite-rich samples.

| Sample | Elemental Analysis (wt. %) | | | | | H/C |
|---|---|---|---|---|---|---|
| | C | H | N | O | S | |
| **Parent** | 67.4 | 4.4 | 1.8 | 8.61 | 2.24 | 0.78 |
| **Inertinite-rich** | 67.6 | 4.17 | 1.68 | 9.57 | 0.64 | 0.74 |
| **Vitrinite-rich** | 75.0 | 5.33 | 2.07 | 9.58 | 0.76 | 0.85 |

### 3.3.2. Maceral analysis and coal rank determination

The parent coal sample is comprised of 42 vol. % vitrinite, 48% inertinite, 4% liptinite and 6% observable mineral matter (Table 3.3). This sample can be considered to be relatively rich in vitrinite compared to typical unwashed Witbank coals, where vitrinite values are typically below 25%. The density fractionated samples consist of 81% vitrinite (vitrinite-rich sample) and 63% inertinite (inertinite-rich sample). The low-density float sample is thus considered to be enriched in vitrinite and the high-density float sample enriched in inertinite. Collotelinite and collodetrinite were found to be the most abundant vitrinite macerals and fusinite, semifusinite, and inertodetrinite the most abundant inertinite macerals. A comparatively high proportion of reactive semifusinite was recorded for the inertinite-rich sample. The liptinite content is below 5 vol. % and the observable mineral content is low; dominated by silicates in the parent and

inertinite-rich samples and carbonates in the vitrinite-rich samples. The %RoVmr value indicates that the coal is medium rank C bituminous and is neither heat affected nor contaminated as indicated by the low standard deviation.

**Table 3.3:** Maceral composition (mineral-included basis; vol. %) of the parent coal, inertinite-rich, and vitrinite-rich samples.

| | **Parent** | **Inertinite-rich** | **Vitrinite-rich** |
|---|---|---|---|
| Telinite | 0.2 | 0.0 | 2.4 |
| Collotelinite | 12.0 | 12.4 | 35.3 |
| Vitrodetrinite | 0.0 | 0.0 | 0.0 |
| Collodetrinite | 28.0 | 15.4 | 36.3 |
| Corpogelinite | 1.4 | 0.5 | 6.9 |
| Gelinite | 0.0 | 1.3 | 0.0 |
| Pseudovitrinite | 0.0 | 0.2 | 0.4 |
| **Total vitrinite** | **41.6** | **29.8** | **81.3** |
| Fusinite | 8.6 | 8.3 | 3.9 |
| Reactive semifusinite | 1.4 | 7.1 | 0.2 |
| Inert semifusinite | 16.9 | 21.8 | 4.5 |
| Micrinite | 0.4 | 0.2 | 0.0 |
| Macrinite | 0.2 | 0.2 | 0.4 |
| Secretinite | 1.2 | 1.2 | 0.6 |
| Funginite | 0.0 | 0.0 | 0.0 |
| Reactive inertodetrinite | 0.8 | 2.1 | 0.8 |
| Inert inertodetrinite | 19.0 | 21.7 | 1.0 |
| **Total inertinite** | **48.5** | **62.6** | **11.4** |
| Sporinite | 3.3 | 2.9 | 2.9 |
| Cutinite | 0.4 | 0.0 | 2.0 |
| Resinite | 0.0 | 0.0 | 0.2 |
| Alginite | 0.0 | 0.0 | 0.0 |
| Liptodetrinite | 0.0 | 0.0 | 0.0 |
| Exsudatinite | 0.0 | 0.0 | 0.0 |
| **Total liptinite** | **3.7** | **2.9** | **5.1** |
| Silicate | 3.1 | 3.1 | 0.2 |
| Sulphide | 2.4 | 1.2 | 0.8 |
| Carbonate | 0.8 | 0.6 | 1.4 |
| **Total minerals** | **6.3** | **4.9** | **2.4** |
| **%RoVmr** | **0.65** | | |
| **Std. Dev.** | **0.067** | | |

### 3.3.3. Microlithotype analysis

**Table 3.4:** Microlithotype composition (mineral-included basis; vol. %) of the parent coal, inertinite-rich, and vitrinite-rich samples.

| **Group** | **Microlithotype** | **Parent** | **Inertinite-rich** | **Vitrinite-rich** |
|---|---|---|---|---|
| **Monomaceral** | Vitrite | 30.2 | 19.7 | 69.6 |
| | Semifusite | 12.1 | 14.8 | 2.7 |

| | | | | |
|---|---|---|---|---|
| | Fusite/secretite | 5.4 | 6.4 | 1.2 |
| | Inertodetrite | 9.0 | 16.1 | 0.0 |
| | Liptite | 0.0 | 0.2 | 0.0 |
| **Bimaceral** | Vitrite+semifusite/fusite | 3.1 | 4.7 | 3.5 |
| | Vitrite+Inertodetrite | 3.5 | 5.4 | 2.2 |
| | Semifusite+inertodetrite | 1.8 | 2.3 | 0.0 |
| | Vitrite+Liptite | 4.7 | 1.8 | 9.8 |
| | Intertite+Liptite | 3.3 | 2.7 | 1.0 |
| **Trimaceral** | Duroclarite (V>I, L) | 11.7 | 13.0 | 3.9 |
| | Clarodurite (I>V, L) | 1.8 | 0.2 | 0.0 |
| | Vitrinertoliptite (L>I, V) | 0.0 | 0.0 | 0.0 |
| **Carbominerite** | Carbargillite/clays | 2.1 | 1.8 | 0.2 |
| | Carbosilicate/quartz | 4.1 | 7.4 | 0.2 |
| | Carbopyrite | 1.9 | 2.1 | 3.3 |
| | Carbankerite | 1.4 | 0.8 | 2.0 |
| | Carbopolyminerite | 0.2 | 0.0 | 0.2 |
| **Minerite** | Minerite | 3.7 | 0.6 | 0.2 |

Abbreviations: V – vitrinite, L – liptinite, I – inertinite.

The microlithotype compositions are presented in Table 3.4 and build on the data obtained in the maceral analysis. In general, the samples are dominated by monomaceral microlithotypes, which is beneficial for subsequent analysis and interpretation thereof. The vitrinite-rich, low density sample is dominated by vitrite, and the inertinite-rich, high density sample is comprised of various inertite microlithotypes with an abundance of semifusite/fusite/secretite (21.2 vol. %). Duroclarite was fairly common in the parent and inertinite-rich sample but depleted in the low-density sample. The carbominerites reflect the mineral proportions determined in the maceral analysis.

### 3.3.4. Nuclear magnetic resonance

NMR spectra of the parent and the vitrinite-rich sample exhibit two distinct peaks, corresponding to aromatic and aliphatic carbons (Figures 3.1 and 3.2). In contrast, the NMR spectrum for the inertinite-rich sample (Figure 3.3) reveals the presence of five peaks corresponding to aliphatic oxygen, carbonyl carbons, and a spinning sideband, in addition to the regions exhibited by the other two samples. The $^{13}C$ CP-MAS NMR spectra for the parent and the vitrinite-rich sample are generally comparable to the spectra of coals from the Petersburg Formation (Pennsylvanian Springfield Coal Member, Illinois) found by others using advanced, direct polarization SS $^{13}C$ NMR and spectral-editing techniques (Cao et al., 2011, 2013), although the latter techniques are quantitatively more accurate. In both studies (Cao et al., 2011, 2013), two broad bands corresponding to aromatic and aliphatic carbons were identified in the spectra of their coals. In

contrast to the five peaks identified in the spectrum of the inertinite-rich sample of the present study, Cao et al. (2011) found the spectrum of a fusain lithotype to exhibit an aromatic and an aliphatic band only. Whether this is due to differences in petrographic composition, or the NMR technique(s) used, is beyond the scope of the current study.

Despite the relative under-enrichment of the inertinite-rich sample, both empirical (proximate and ultimate analyses, Tables 3.1 and 3.2) and fundamental (petrographic analyses, Tables 3.3 and 3.4) coal characterization methods demonstrate that this sample is chemically and petrographically distinct from both the parent and the vitrinite-rich sample. The $^{13}C$ CP-NMR structural parameters (Figures 1 to 3, Table 5) corroborate the observation that the three samples are indeed dissimilar.

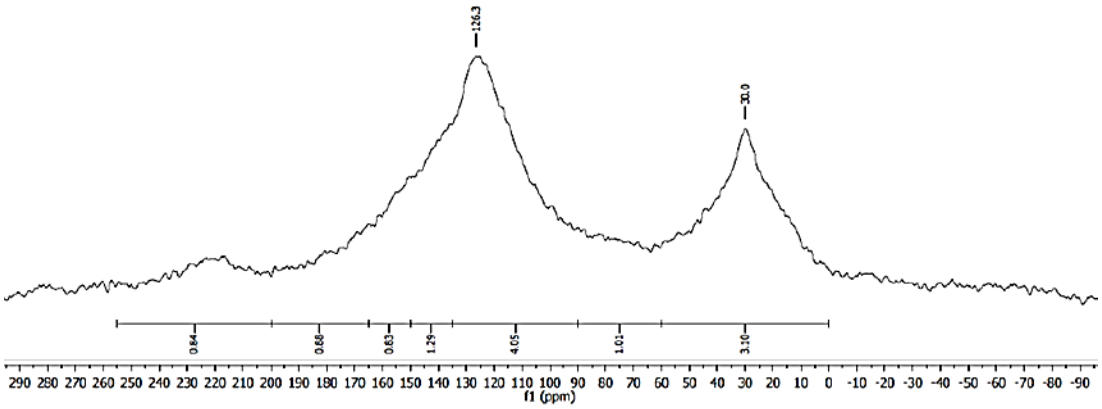


**Figure 3.1:** $^{13}C$ CP-MAS NMR spectrum of the parent coal sample.

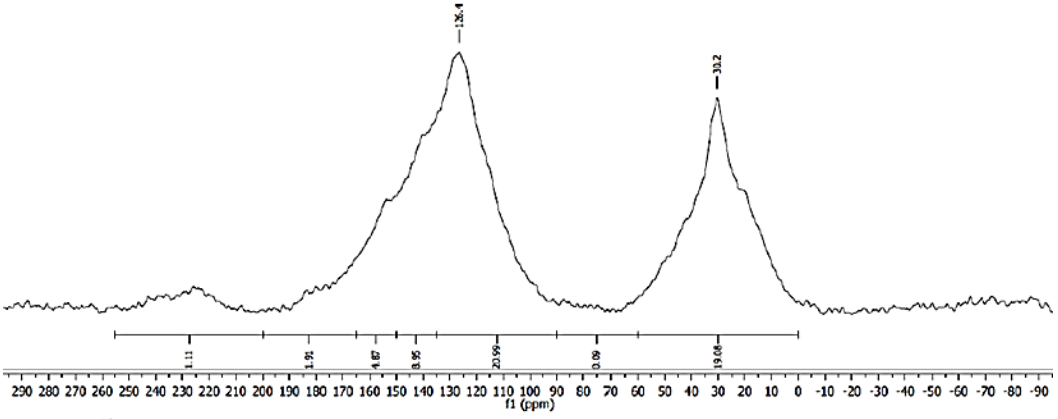


**Figure 3.2:** $^{13}C$ CP-MAS NMR spectrum of the vitrinite-rich coal sample.

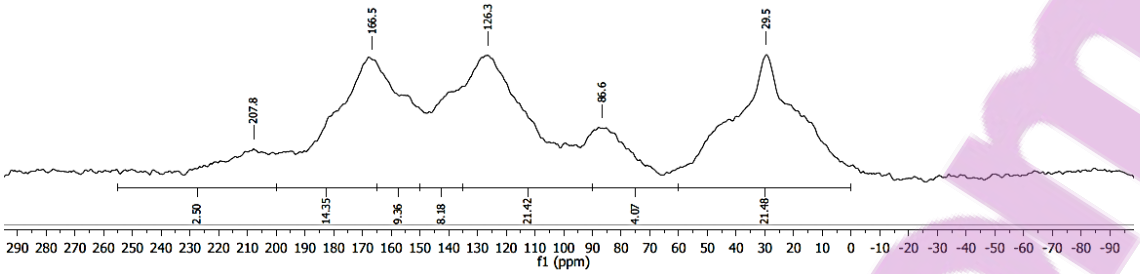


**Figure 3.3:** $^{13}$C CP-MAS NMR spectrum of the inertinite-rich coal sample.

Based on the NMR structural parameters (Table 3.5), the parent sample has the marginally higher fraction of aromaticity ($f_a$) of 0.73, followed closely by the inertinite-rich sample at $f_a$ =0.72, with the vitrinite-rich at only $f_a$ = 0.68. The $f_a$ values are within the range previously reported for bituminous coals (see Davidson, 2004, p. 18). As per proximate analyses, the inertinite-rich sample has the slightly higher fixed carbon content and lowest volatile matter, as would be expected from an inertinite-rich coal. In addition, owing to the lower H/C atomic ratio of the inertinite-rich sample (Table 3.2), it might be anticipated that this sample would have the greater fraction of aromaticity (Davidson, 2004; Van Niekerk et al., 2008).

**Table 3.5:** Structural parameters from solid-state $^{13}$C CP-NMR for the parent coal, inertinite-rich, and vitrinite-rich samples.

| | **Parent** | **Inertinite-rich** | **Vitrinite-rich** |
|---|---|---|---|
| $f_a$ | 0.73 | 0.72 | 0.68 |
| $f_a^*$ | 0.64 | 0.52 | 0.65 |
| $f_{al}$ | 0.27 | 0.28 | 0.32 |
| $f_{al}^o$ | 0.084 | 0.05 | 0.002 |
| $f_a^{CO}$ | 0.09 | 0.19 | 0.04 |
| $f_a^P$ | 0.09 | 0.13 | 0.09 |
| $f_a^S$ | 0.13 | 0.11 | 0.17 |
| $f_a^N$ | 0.39 | 0.25 | 0.48 |
| $f_a^H$ | 0.25 | 0.28 | 0.17 |
| $f_a^B$ | 0.17 | 0.01 | 0.22 |
| $f_a^{N*}$ | 0.05 | 0.04 | 0.10 |
| $f_{al}^H$ | 0.22 | 0.24 | 0.22 |
| $X_b$ | 0.26 | 0.02 | 0.34 |
| **C** | 13.9 | 5.80 | 17.3 |
| **#Cluster/100** | 4.58 | 9.10 | 3.74 |
| **σ + 1** | 4.77 | 2.59 | 6.87 |

Parameters: $f_a$ – Fraction Aromatics, $f_a^*$ – Corrected Fraction Aromatics (excl. CO), $f_{al}$ – Fraction Aliphatics, $f_{al}^o$ – Fraction Aliphatic C's bonded to oxygen, $f_a^{CO}$ – Fraction CO, $f_a^P$ – Fraction Phenolics, $f_a^S$ – Fraction Alkylated Aromatics, $f_a^N$ – Fraction Non-Protonated C's in aromatic region, $f_a^H$ – Fraction Protonated C's in aromatic region, $f_a^B$ – Fraction Bridgehead C's, $f_a^{N*}$ – Fraction Non-Protonated C's + Methyl groups in Aliphatics, $f_{al}^H$ – Aliphatic

CH+CH2, $X_b$ – Mole fraction of Aromatic Bridgehead C's, C – Average # of Aromatic C's per cluster, #Cluster/100 – Average # of clusters per 100 Aromatic C's, $\sigma + 1$ – #of attachment per cluster.

The inertinite-rich sample has an average of approximately six aromatic carbons per cluster (C = 5.80) which corresponds to a benzene or phenolic ring. And the number of clusters per 100 aromatic carbons is significantly higher in the inertinite-rich sample (#Cluster/100 = 9.10) than in the parent and especially the vitrinite-rich sample (#Cluster/100 = 2.59), hence the greater aromatic fraction. The increased number of monocyclic rings seems to account for the higher aromaticity of the inertinite-rich sample in spite of a 6-carbon ring being the smallest unit of a multi-ring aromatic hydrocarbon. The 17-aromatic carbon ring cluster (determined in the vitrinite-rich sample; C = 17.3) is one carbon short of the four-ringed, structural isomers tetracene and chrysene. This implies that the individual, monocyclic rings – likely from a woody, lignin-rich precursor (Haenel, 1992; Hatcher and Clifford, 1997) – have been fused to form larger systems in the course of coal formation. However, the number of clusters per 100 carbons is lower for the vitrinite-rich sample compared to the inertinite-rich sample. Although the clusters in the inertinite-rich sample are smaller, their total population is greater than that in the other two samples.

### 3.4. Discussion

Inertinite formation is generally attributed to multiple origin pathways, including: (1) being primary, i.e., formed from inherently carbon-rich plant matter; (2) freeze-drying; (3) aerial oxidation; (4) fungal activity; and (5) charring of plant matter (Austen et al., 1966; Hunt and Smyth, 1989; Scott, 1989, 2002, 2010; Teichmüller, 1989; Jones and Chaloner, 1991; Diessel, 1992, 2010; Moore et al., 1996; Shearer and Moore 1996; Moore and Shearer, 1997; Guo and Bustin, 1998; Taylor et al., 1998; ICCP, 2001; Glasspool, 2003a, 2003b; Scott and Glasspool, 2007; Hower et al., 2009, 2011a, 2011b; O'Keefe and Hower, 2011; Richardson et al., 2012; O'Keefe et al., 2013). In general, multiple pathways account for the wide range of morphologies exhibited by inertinite macerals (ICCP, 2001; Hower et al., 2011a; O'Keefe and Hower, 2011; O'Keefe et al., 2013). However, in South Africa, the high inertinite content (inertinite macerals of varying reflectance and morphologies) in the coals is ascribed primarily to aerial oxidation coupled with incomplete degradation of plant matter as a result of cool Permian climate (e.g., Falcon, 1986; Hagelskamp and Snyman, 1988; Cadle et al., 1993) with fusinite indicative of severe oxidation (Snyman, 1989). However, a fire origin is in general accepted globally for

fusinite formation (Scott, 1989, 2010; Jones and Chaloner, 1991; ICCP, 2001). An oxidation-only pathway for the high inertinite content of South African coals fails to appreciate this.

The Witbank Coalfield (the coalfield of interest in the present study) is interpreted to have formed on the edge of a large delta draining into an inland sea in the Main Karoo Basin (Cairncross, 2001; Cadle et al., 1993). A warming climate provided seasonal glacial melt from Dwyka ice in the Cargonian Highlands to the north and introduced water and sediments into the swamps with periodic flooding and meandering rivers (Glasspool 2003a, 2003b; Ruckwied et al., 2014). The presence of vitrinite macerals in the coals (Figure 3.4), with some localities having higher values than others, supports periods of wet peat-forming environments (ICCP, 1998; Glasspool, 2003a). The typically high inertinite content of the Witbank coals implies that other processes were also active.

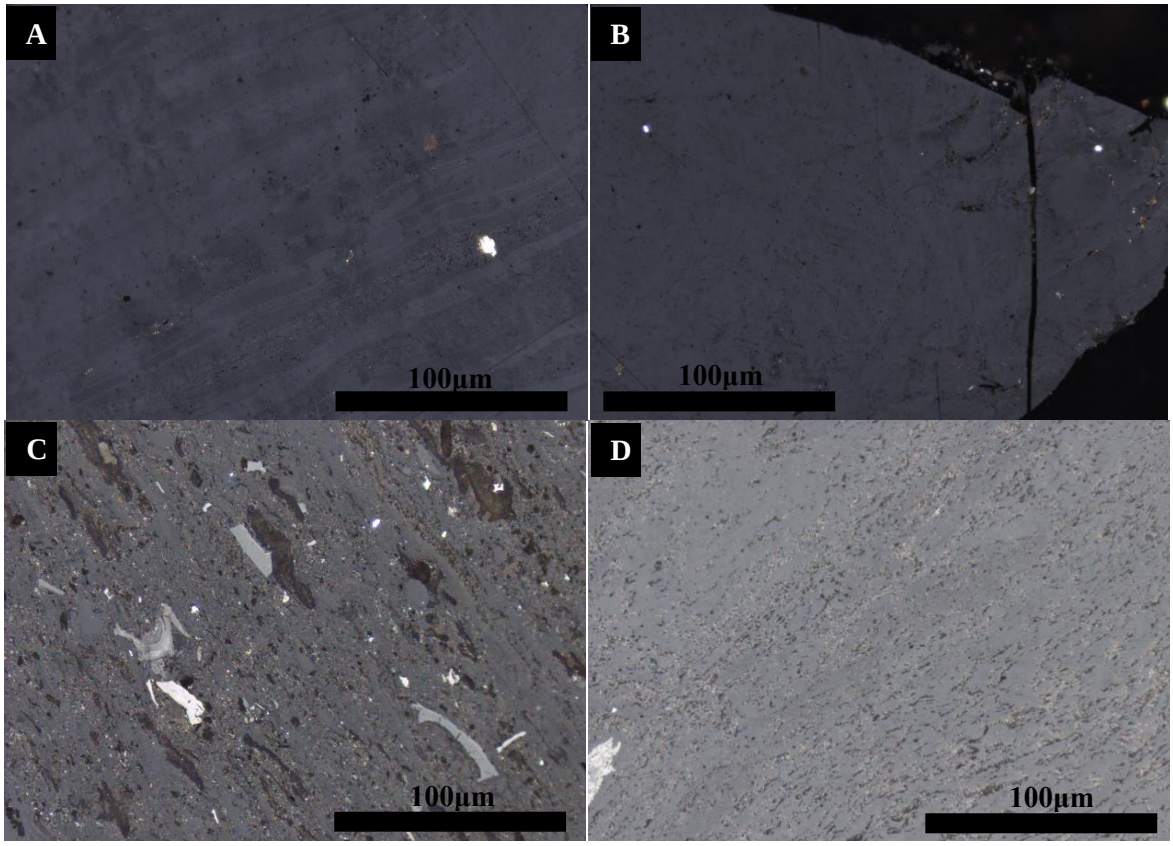


**Figure 3.4:** Vitrite monomacerals observed in the vitrinite-rich sample. A, B – vitrite (collotelinite); C, D – vitrite (collodetrinite). 500x magnification, reflected light with oil immersion. Scale is indicated.

At the onset, the variable reflectance of the inertinite macerals (Figure 3.5), also noted by others when discussing Gondwana coals (e.g., Falcon and Ham, 1988; Hagelskamp and Snyman, 1988;

Snyman, 1989; Taylor et al., 1998), can be interpreted to disqualify a primary origin (Moore and Shearer, 1997). A lack of pronounced degradation is supported by the presence of anatomical structure in the macerals (Guo and Bustin, 1998; Richardson et al., 2012; O'Keefe et al., 2013). Taylor et al. (1998) attributes the dominance of semifusinite in Gondwana coals to gelification followed by "freeze-drying" as a result of colder seasons. However, Ruckwied et al. (2014) have shown that the plants that gave rise to the coal seams above the No. 2 Seam of the Witbank Coalfield, such as Gangamopteris and Glossopteris, are better suited to temperate climatic conditions. Because of this, freeze-drying of gelified plant matter appears improbable. Thus, any process requiring cold climates are unsuitable for inertinite formation in the No. 4 Seam of the Witbank.

When considering aerial oxidation, it becomes apparent that the water level in a peat-forming environment would have to be significantly lowered to expose the amount of peat required to produce the volume of inertinite present in the coals (Hunt and Smyth, 1989). Alternatively, a reduced subsidence rate may result in the exposure of peat constituents, enabling aerial oxidation (Cadle et al., 1993). Furthermore, the water level would have to be lowered for prolonged periods to allow the time required for aerobic processes to begin to take root (Moore and Shearer, 1997). But a nearly permanently low water level may be considered counterproductive to the conditions generally required for the accumulation of a significant amount of peat (O'Keefe et al., 2013), and specifically for humification and gelification processes (Teichmüller, 1989; ICCP, 1998). Furthermore, Moore et al. (1996) and Moore and Shearer (1997) found that a lowered water level enhances alteration of plant matter through fungal activity.

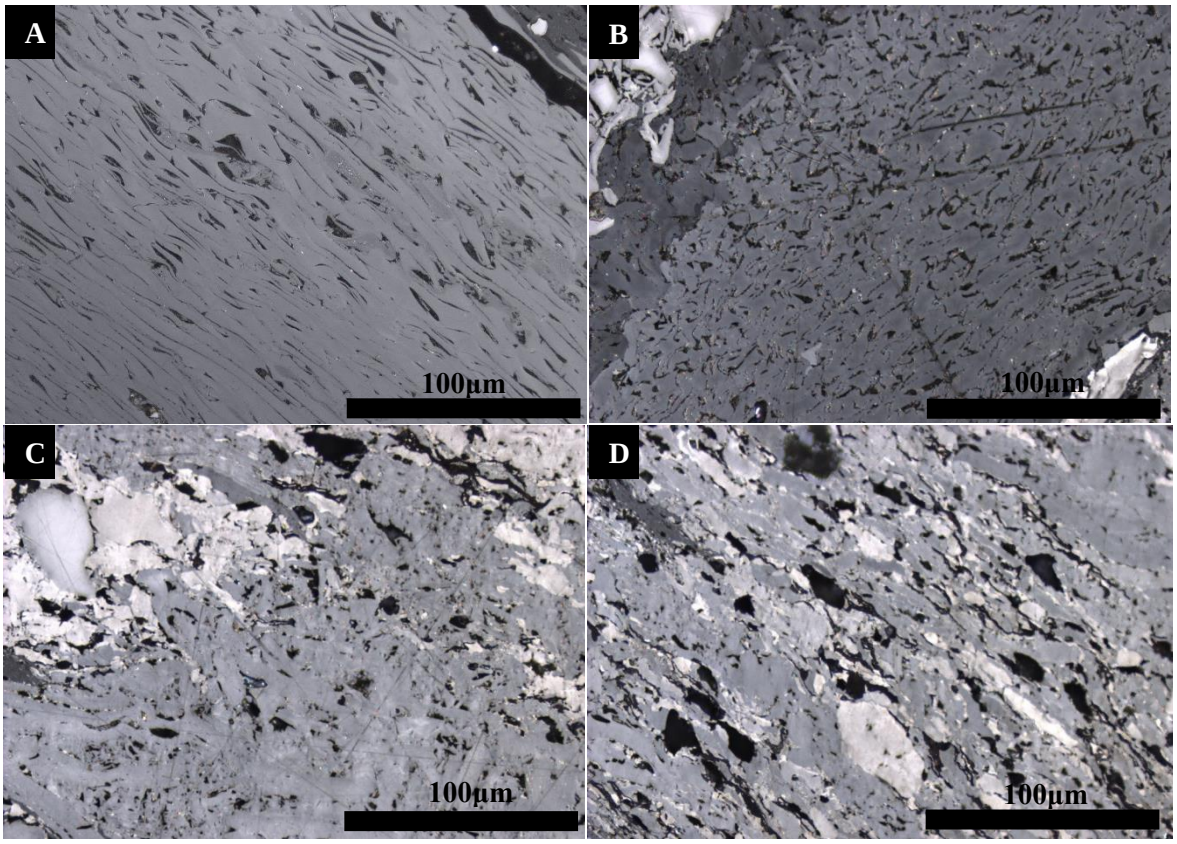


**Figure 3.5:** Inertite monomacerals observed in the inertinite-rich sample. A – fusite; B, C – semifusites of varying reflectance; D – inertodetrite and semifusite. 500x magnification, reflected light with oil immersion. Scale is indicated.

Moore et al. (1996) and Moore and Shearer (1997) concluded that carbonized material, corresponding to inertinite macerals in the upper layers (0.5 – 1.5 m) of the 6 m thick Palangka Raya peat deposit (Central Kalimantan, Indonesia), formed through fungal activity as opposed to being primary or combustion-derived. This was based on the correlation of fungal hyphae length with carbonized roots (Moore et al., 1996; Moore and Shearer, 1997). A more recent discussion by Hower et al. (2011b) on the association of fungi with plant roots, lends credence to the carbonization of root-derived inertinite by fungi. Funginite i.e., fungal remains (ICCP, 2001), has also been observed in association with macrinite, cutinite, and suberinite (Hower et al., 2009, 2011a, 2011b). It is important to mention that funginite is completely absent in the samples of the current study and other petrographic studies of South African coals (e.g., Hagelskamp and Snyman, 1988; Snyman, 1989). Suberinite is also not recorded (due to the higher rank), along with typically low proportion of both cutinite and macrinite (Table 3.3). These observations may be interpreted to suggest: (1) the absence of fungal colonies within the peat-forming environment; (2) that the prevailing conditions were not conducive to fungal preservation; and/or

(3) participation of fungi in coal-formation was limited for some reason. However, the presence of both anthropods and fungi in Gondwana coal-forming environments has recently been conclusively established, based on a study of silicified peat from Antarctica (Slater et al., 2015). Fusinite produced by fungal activity has been found to possess "only indistinct cell walls" (Taylor et al., 1998), so is in no way comparable to either the fusinite or semifusinite observed in most Witbank coals (e.g., Figure 3.5). It is worth mentioning that Moore et al. (1996) found a scarcity of wood, the precursor to fusinite and semifusinite, at the top of the Palangka Raya peat deposit, where fungal activity had been most pronounced.

As with a cold climate (Taylor et al., 1998), processes requiring low water levels for prolonged periods of time such as fungal activity (Moore et al., 1996; Moore and Shearer, 1997) and aerial oxidation (Falcon, 1986; Hagelskamp and Snyman, 1988; Hunt and Smyth, 1989; Snyman, 1989; Cadle et al., 1993) may also be considered inappropriate for inertinite formation in the No. 4 Seam Upper of the Witbank Coalfield. Importantly, the processes outlined above cannot, on their own, account for the selective preservation of lignin-derived monocyclic aromatic compounds in inertinite while simultaneously forming multi-ring clusters in vitrinite within the same peat or coal as determined by the NMR analysis (Table 3.5). An opposing argument may be made that 6-aromatic carbon rings present in the inertinite-rich sample were merged along with those in the vitrinite-rich sample, only to be subsequently detached. However, the selectivity with which such a process would have to ensue seems impractical. Aside from the thermodynamic requirements, the multi-ring clusters present in the vitrinite-rich sample would have to survive unscathed with only those present in the inertinite-rich sample, within the same coal or peat, affected.

### 3.4.1. Charring as an alternative pathway for inertinite formation in the Witbank Coalfield

Charring of plant matter provides an alternative pathway for inertinite formation (Austen et al., 1966; Scott, 1989, 2002, 2010; Teichmüller, 1989; Jones and Chaloner, 1991; Diessel, 1992, 2010; Moore et al., 1996; Moore and Shearer, 1997; Guo and Bustin, 1998; ICCP, 2001; Glasspool, 2003a, 2003b; Scott and Glasspool, 2007; O'Keefe and Hower, 2011; O'Keefe et al., 2013). Owing to the number of studies that have demonstrated that wood charring produces charcoal possessing anatomical structures comparable to those exhibited by inertinite macerals and that a range of reflectance values can be produced depending on the degree of charring (e.g., Scott, 1989, 2010; Teichmüller, 1989; Jones and Chaloner, 1991; Guo and Bustin, 1998;

Ascough et al., 2010), it appears more than probable that the fusinite and semifusinite macerals of the Witbank Coalfield, No. 4 Seam Upper, are fire-derived. Previously, Glasspool (2003a, 2003b) concluded that inertinite macerals in the No.'s 1, 2 and 4 Seams of the Witbank Coalfield were formed through charring of dead and living, i.e., standing vegetation. However, Glasspool (2003a, 2003b) did not consider NMR structural parameters. A wet, forested peat-forming environment is corroborated by the presence of vitrinite macerals (Tables 3.3 and 3.4, Figure 3.4) (ICCP, 1998; Glasspool, 2003a).

Three aromatic alcohols; p-coumaryl, coniferyl, and sinapyl are the major constituents of the lignin component of wood (Kirk and Farrell, 1987; Simoneit et al., 1993; Kawamoto, 2017), and form the primary basis upon which coal derives its aromaticity (Spiker and Hatcher, 1987). The proportion of these alcohols is specific for each of the three classes of plants; namely, gymnosperms, angiosperms, and grass, with the former being more enriched in coniferyl alcohol (Saiz-Jimenez and de Leeuw, 1986; Simoneit et al., 1993). Upon exposure to high temperatures, new functionalities are created at the expense of the alcohol moieties. The chemistry of the charred products depends on the temperature regime at which the resultant charcoal was generated (Belcher et al., 2009; Asmadi et al., 2011; Kawamoto, 2017).

Charcoal produced from wood charring experiments and fossilized charcoal particles has been found to be particularly enriched in pyrosynthetic polycyclic aromatic hydrocarbons (pPAHs) (Belcher et al., 2009; Marynowski and Simoneit, 2009; Ascough et al., 2010; Asmadi et al., 2011). pPAHs begin to form at temperatures above 400 °C, becoming particularly abundant at 700 °C with larger cluster sizes generally reflecting high charring temperatures (Belcher et al., 2009; Ascough et al., 2010; Asmadi et al., 2011; Kawamoto, 2017). However, even in the case of high temperature wood charring, pPAH enriched charcoal may become suspended in water, owing to hydrophobicity, and may become redeposited (Belcher et al., 2009). Marynowski and Simoneit (2009) found an abundance of pPAHs in charcoal fragments embedded within fine-grained sedimentary rocks (mudstones and siltstones), possibly reflecting redeposited charcoal generated at high temperatures.

At lower temperatures (below 400 °C) however, guaiacol (2-methoxyphenol) and syringol (2, 6-dimethoxyphenol) are the two main products of charred lignin-rich wood (Saiz-Jimenez and de Leeuw, 1986; Simoneit et al., 1993; Asmadi et al., 2011; Kawamoto, 2017). The two are

methoxy-substituted phenols consisting of a 6-aromatic carbon ring core, to which the methoxy moieties are attached. These phenolic groups are produced during low-temperature pyrolysis of lignin and are stable at temperatures below 400 °C (Asmadi et al., 2011; Kawamoto, 2017). The presence of 6-aromatic carbon rings in the inertinite-rich sample of the present study, coupled with the greater number of oxygenated moieties, is therefore in agreement with what would be expected from coal derived from the low-temperature charring of a woody, lignin-rich botanical precursor. The cellulose component of the wood would have been expelled at lower temperatures, possibly at 320 °C, according to Guo and Bustin (1998). The larger aromatic clusters present in the vitrinite-rich sample of the present study are in agreement with published literature regarding the formation of multi-ring clusters during the course of coalification (e.g., Solum et al., 1989; Haenel, 1992; Davidson, 2004; Suggate and Dickinson, 2004; Van Niekerk et al., 2008, 2010) and suggest the absence of low-temperature charring products.

Peat is widely considered to have the highest compaction potential among naturally occurring soils (Stout and Spackman, 1989; van Asselen et al., 2009). The compaction potential derives chiefly from the high moisture content, initially occurring between and within the peat constituents when the peat undergoes autocompaction (Shearer and Moore, 1996). Moreover, humification-related degradation of plant matter during biochemical coalification induces additional compaction (Stout and Spackman, 1989; van Asselen et al., 2009). Following burial, the peat is further subjected to compaction due to overburden material and further by the occurrence of anaerobic humification (van Asselen et al., 2009). Thus, the preceding discussion assumes that peat constituents, in their totality, have similar moisture contents and that an applied load along with biological compaction, affects the individual constituents of peat, equally.

At bituminous rank, inertinite-rich coals have a higher macro-porosity than vitrinite counterparts (Unsworth et al., 1989; Van Niekerk and Mathews, 2010). This may be interpreted to suggest that inertinite-forming materials have a lower compaction potential than vitrinite-forming counterparts. Given that vitrinite and inertinite (specifically fusinite and semifusinite) macerals may be derived from similar plant organs (ICCP, 1998, 2001), the rigidity (lower compaction potential) of inertinite-forming plant matter may be responsible for the higher macro-porosity. The “possession of rigidity before incorporation into peat” by fire-derived inertinite-forming

plant matter has previously been proposed by Scott (1989, and references therein), albeit based on physical rather than chemical structural observations. Since charring depletes both cellulose and moisture (Guo and Bustin, 1998; Czimczik et al., 2002; Yang et al., 2007), the discharge of these components would only have a negligible impact on the compactability of fire-affected plant matter.

The formation of phenolic moieties, and expulsion of moisture and cellulose during the low-temperature charring of wood (Saiz-Jimenez and de Leeuw, 1986; Simoneit et al., 1993; Guo and Bustin, 1998; Czimczik et al., 2002; Yang et al., 2007; Kawamoto, 2017), likely provides the conditions for rigidity, since the compaction potential of the charred plant matter would be minimized. In other words, when the charred material is incorporated into a peat-forming environment, it has lost its deformability and becomes more rigid, and thus, remains relatively unaffected when pressure is introduced during compaction. Physically, rigidity may be manifested by the preservation of anatomical structure as is typically observed in inertinite macerals, specifically fusinite (Figure 3.5A). However, on a molecular level, a low compaction potential (i.e., rigidity) appears to drive the preservation of aromatic compound monocyclicity, i.e., 6-aromatic carbon rings.

It is generally accepted that the formation of fusite and semifusite monomaceral microlithotypes are associated with relatively dry conditions when compared to vitrite counterparts (Teichmüller, 1989; ICCP, 1998, 2001). To reconcile this, Glasspool (2003b) suggested seasonality during coal formation in the Witbank Coalfield. In a coal formed from both gelified (vitrite) and fire-derived components (fusite and semifusite), monomacerals might be expected to predominate over bi- and trimacerals, as each process would require time. The vitrite macerals would have formed during relatively wet periods. These periods would interchange with drier periods during which wild-fires may occur, producing thick bands of fusite and semifusite. Evidence for the occurrence of fires in Gondwana coal-forming environments has been documented in silicified peat from Antarctica (Slater et al., 2015). The presence of anatomical structure in the inertite macerals suggests that precursors were neither degraded by organisms nor gelified (Guo and Bustin, 1998; Richardson et al., 2012; O'Keefe et al., 2013) prior to charring.

A possible analogue for the formation of coal through combustion or charring of plant matter is the 8000 year-old peat deposit in the Kutai Peatlands (Kalimantan, Indonesia) (Hope et al.,

2005). Episodic drying of relatively short periods (starting from more 3000 years ago and then in A.D.1527; 1846; 1877 – 1878; 1899 – 1890; 1914; 1982 – 3; 1997 – 8) was, in each case, found to coincide with major fire events during which a significant amount of charcoal was generated (Hope et al., 2005). Given the high proportion of inertite reported in the present study (Tables 3.3 and 3.4), the fire required to produce fusite and semifusite would have occurred within relatively short time-span(s), thus possibly within the time ranges reported by Hope et al. (2005). In contrast, the formation of vitrite would have taken longer, given low peat accumulation rates, possibly in the range of 1 – 4 mm per year (Taylor et al., 1998) as well as the time required for subsequent humification and gelification.

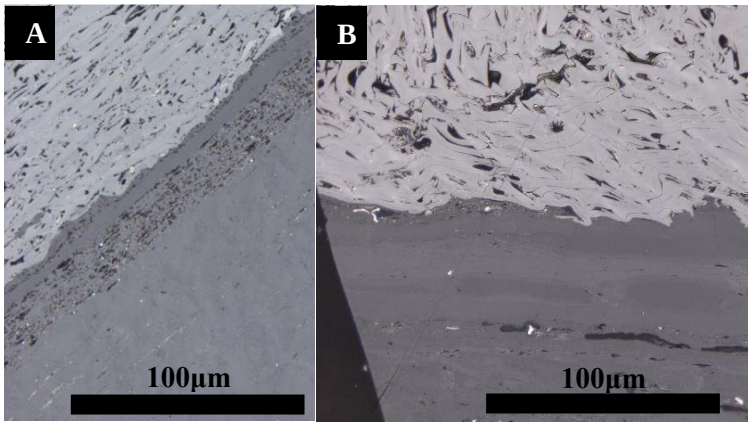


**Figure 3.6:** A, B – vitrite (bottom) with fusite (top), observed in the inertinite-rich sample. 500x magnification, reflected light with oil immersion. Scale is indicated.

Charring of living vegetation, as suggested by Glasspool (2003a, 2003b), would likely have occurred before degradation by the organisms that were present in the swamp. The well-preserved anatomical structure of the inertite macerals (Figure 3.5), supports charring before humification-related degradation. Subsequently, when the fire-affected plant matter was included in the peat-forming environment, some primary components of wood including cellulose would have been lost (Guo and Bustin, 1998; Czimczik et al., 2002; Yang et al., 2007), possibly rendering the inertite-forming material less susceptible to subsequent diagenetic alteration (Jones and Chaloner, 1991; Ascough et al., 2010; Scott, 2010). Charring of wet vegetation, resulting in variable and incomplete combustion, may also account for the partially degraded cellular structure (Jones and Chaloner, 1991) and varied reflectance readings of semifusite (Figure 3.5B-D). Fusite (Figure 3.5A) would have been produced through charring of mostly dead and dry plant matter, thus having been subjected to the highest temperatures, resulting in the highest

reflectances. The fire-affected plant matter would subsequently have been buried with the vitrinized material, producing sharp boundaries (Figure 3.6). The inertite precursor was possibly incorporated into the peat at the location of charring or alternatively, specifically when considering smaller particles, brought into the swamp by water and/or wind. The increased rigidity, corresponding to the low compaction potential of fusite and semifusite-forming plant matter, would hinder polymerization of aromatic rings. Since the low-temperature charring of lignin-rich wood produces monocyclic aromatic rings, the rigidity of the charred material would preserve this monocyclicity as well as the anatomical structure of the woody precursor. In contrast, the destruction of structure in the vitrite macerals would be accompanied by the amalgamation of lignin-derived aromatic rings.

### 3.4.2. Comparison with inertinite-rich Highveld and vitrinite-rich Waterberg coals

Van Niekerk et al. (2008) report NMR structural parameters for an inertinite-rich Highveld and a vitrinite-rich Waterberg sample (Table 3.6). The samples in Van Niekerk et al.'s (2008) study were obtained from two different coalfields and have %RoVmr values of 0.71 and 0.75, respectively. The Waterberg Coalfield is believed to have formed in a graben/half-graben, whereas the coal deposits of the Main Karoo Basin were formed in a deltaic foreland basin (Cairncross, 2001; Hancox and Götz, 2014). Within the Main Karoo Basin, the Witbank Coalfield is located on the uppermost delta plain setting, whereas the Highveld is interpreted to be lower, with the two separated by the Smithfield Ridge (Figure 3.7). The original vegetation and climates in the two coalfields are considered to have been similar and the coals are considered to be genetically related (Hancox and Götz, 2014).

**Table 3.6:** Maceral composition (vol. %; mmf), %RoVmr and solid-state 13C CP-NMR structural parameters for inertinite-rich Highveld and vitrinite-rich Waterberg coals (Van Niekerk et al., 2008).

| | **Highveld** | **Waterberg** |
|---|---|---|
| | **Petrography** | |
| **Vitrinite** | 11.2 | 91.8 |
| **Inertinite** | 87.7 | 5.8 |
| **Liptinite** | 1.1 | 2.4 |
| **%RoVmr** | 0.71 | 0.75 |
| | **NMR structural parameters** | |
| $f_a$ | 0.85 | 0.74 |
| $f_a^C$ | 0.03 | 0.04 |
| $f_a^O$ | 0.01 | 0.01 |
| $f_a^{OO}$ | 0.02 | 0.03 |
| $f_a'$ | 0.82 | 0.70 |

| | | |
|---|---|---|
| $f_a^H$ | 0.28 | 0.23 |
| $f_a^N$ | 0.54 | 0.47 |
| $f_a^P$ | 0.07 | 0.08 |
| $f_a^S$ | 0.18 | 0.18 |
| $f_a^B$ | 0.29 | 0.21 |
| $f_{al}$ | 0.15 | 0.26 |
| $f_{al}^H$ | 0.11 | 0.17 |
| $f_{al}^*$ | 0.04 | 0.09 |
| $f_{al}^O$ | 0.03 | 0.04 |
| $X_b$ | 0.354 | 0.30 |
| C | 18 | 15 |
| σ + 1 | 5.30 | 5.40 |

Parameters: $f_a$ —total of $sp^2$ carbon, $f_a^C$ —carbonyl/ carboxyl and amid carbon, $f_a^O$ —aldehyde and ketone fraction, $f_a^{OO}$ —acid, ester or amide fraction, $f_a'$ —aromatic carbon, $f_a^H$ —protonated aromatic carbons, $f_a^N$ —nonprotonated aromatic carbons, $f_a^P$ —phenols or phenolic ethers $f_a^S$ —alkylated aromatic carbons, $f_a^B$ —aromatic bridgehead carbons, $f_{al}$ —total $sp^2$ carbon, $f_{al}^H$ —CH or CH2, $f_{al}^*$ —methyl and methoxy groups, $f_{al}^O$ — total aliphatic carbon bonded to an oxygen. $X_b$ – mole fraction of aromatic bridgehead carbons, C –average # of aromatic C's per cluster, σ + 1 – #of attachment per cluster.

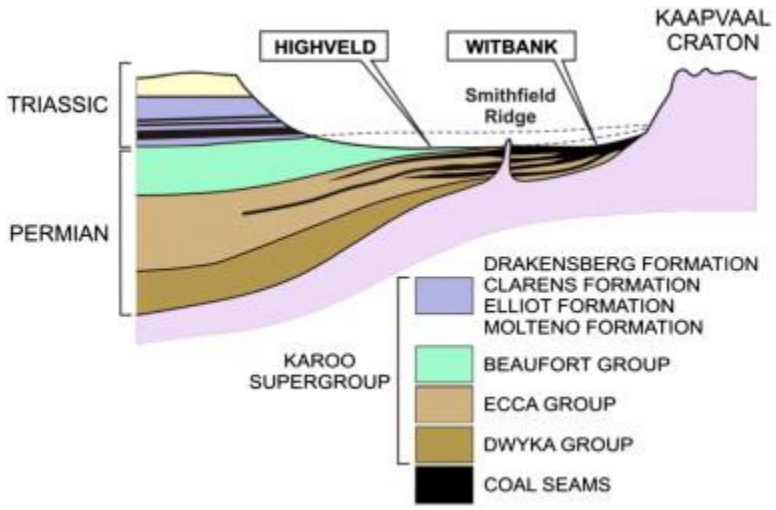


**Figure 3.7:** North-south cross-section through the Witbank and Highveld Coalfields (Hancox and Götz, 2014).

In general, the Waterberg sample is comparable to the low density, vitrinite-rich sample of the present study both in terms of vitrinite content and NMR structural parameters. Whereas, the Highveld sample is markedly different from the Witbank, inertinite-rich sample used in the present study. Of particular interest are the larger aromatic cluster sizes (18 carbons per cluster) for the inertinite-rich Highveld coal sample (Table 3.6) corresponding to a 4-ringed member (more similar to the vitrinite-rich sample of the present study). The seam from which the Highveld sample was obtained is not reported in Van Niekerk et al. (2008), making a direct

comparison of the results difficult. However, following the line of reasoning herein evoked, the formation of multi-ring clusters can be interpreted to imply an absence of low-temperature charring products, thus perhaps precluding a fire-origin for the inertinite macerals of the specific coal seam from which the Highveld sample in Van Niekerk et al. (2008) was obtained. Looking elsewhere in the literature, a relatively high inertodetrinite content (maximum 49 vol. %, mmf), with minor proportions of fusinite and semifusinite, has been documented in the No. 4 Seam Lower of the Highveld Coalfield (Hagelskamp and Snyman, 1988). This perhaps suggests a different origin pathway for inertinte in the Highveld Coalfield. Furthermore, the dominance of inertodetrinite appears to affect NMR parameters (cluster sizes) differently, when compared to a coal dominated by fusinite and semifusinite.

### 3.5. Conclusion

The presence of 6-aromatic carbon rings, interpreted to be guaiacol and syringol (the low-temperature pyrolysis products of lignin), was established in an inertinite-rich South African coal from the Witbank Coalfield using solid-state NMR-derived structural parameters. The inertinite-rich, high density fractionated sample has an average of 6-aromatic carbons per cluster, as opposed to 17 in the vitrinite-rich sample of the same coal. However, the number of clusters per 100 aromatic carbons is higher in the inertinite-rich sample, hence the greater aromatic fraction. Thus, it is suggested that the botanical precursor(s) to fusinite and semifusinite were charred before incorporation into the peat-forming environment, with charring expelling cellulose and moisture. When the fire-affected plant material was buried with the vitrinite-forming matter, the charred plant matter was less susceptible to compaction, i.e., rigid, given that peat compaction is driven by humification-related degradation and moisture expulsion. The reduced compaction and humification potential ensured the preservation of anatomical structure and the monocyclic combustion products. The widely observed preservation of physical morphology by fire-derived inertinite macerals may correspond to the retention of aromatic ring monocyclicity on a molecular level. In the vitrinite-rich density fractionated sample of the same coal, the 6-carbon rings polymerize to form multi-cyclic clusters. This is accompanied by the destruction of physical morphology and hence humification. Thus, it is proposed that the semifusinite component of No. 4 Seam Upper coal from the Witbank Coalfield is derived from charring of living vegetation; whereas, the fusinite component is derived from charring of dry and/or dead

vegetation. Both components can become incorporated into peat at the place of formation or, specifically in the case of smaller fusinite particles, transported by wind or water.

### 3.6. References


Ascough, P.L., Bird, M.I., Scott, A.C., Collinson, M.E., Cohen-Ofri, I., Snape, C.E., Le Manquais, K., 2010. Charcoal reflectance measurements: implications for structural characterization and assessment of diagenetic alteration. Journal of Archaeological Science 37, 1590-1599.

Asmadi, M., Kawamoto, H., Saka, S., 2011. Thermal reactions of guaiacol and syringol as lignin model aromatic nuclei. Journal of Analytical and Applied Pyrolysis 92, 88-98.

Austen, D.E.G., Ingram, D.J.E. Given, P.H., Binder, C.R., Hill, L.W., 1966. Electron Spin Resonance Study of Pure Macerals. In: Given, P.H., (Ed.). Coal Science, Advances in Chemistry, 55. American Chemical Society, Washington DC, pp. 344-362.

Bamford, M.K., 2004. Diversity of the Woody Vegetation of Gondwanan Southern Africa. Gondwana Research 7 (1), 153-164.

Belcher, C.M., Finch, P., Collinson, M.E., Scott, A.C., Grassineau, N.V., 2009. Geochemical evidence for combustion of hydrocarbons during the K-T impact event. Proceedings of the National Academy of Sciences of the United States of America 106 (11), 4112-4117.

Cadle, A.B., Cairncross, B., Christie, A.D.M., Roberts, D.L., 1993. The Karoo Basin of South Africa: type basin for coal-bearing deposits of southern Africa. International Journal of Coal Geology 23, 117-157.

Cairncross, B., 2001. An overview of the Permian (Karoo) coal deposits of Southern Africa. Journal of African Earth Sciences 33, 529-562.

Cao, X., Chappell, M.A., Schimmelmann, A., Mastalerz, M., Li, Y., Hu, W., Mao, J., 2013. Chemical structure changes in kerogen from bituminous coal in response to dike intrusions as investigated by advanced solid-state $^{13}C$ NMR spectroscopy. International Journal of Coal Geology 108, 53-64.

Cao, X., Mastalerz, M., Chappell, M.A., Miller, L.F., Li, Y., Mao, J., 2011. Chemical structures of coal lithotypes before and after $CO_2$ adsorption as investigated by advanced solid-state $^{13}C$ nuclear magnetic resonance spectroscopy. International Journal of Coal Geology 88 (1), 67-74.

Czimczik, C., Preston, C.M., Schimdt, M.W.I., Werner, R.A., Schulze, E.-D., 2002. Effects of charring on mass, organic carbon, and stable carbon isotope composition of wood. Organic Geochemistry 33, 1207-1223.

Davidson, R.M., 2004. Studying the structural chemistry of coal. IEA Clean Coal Centre, 121pp.

De Goede, S., Rabe, T., Bekker, R., Mtongana, S., Edwards, J., 2010. Characterization of Combustion Chamber Deposits Formed in Direct Injection Spark Ignition (DISI) Engines during an On-road Vehicle. SAE International 2010-01-2155.

Diessel, C.F.K., 1992. Coal-Bearing Depositional Systems. Springer-Verlag, Berlin Heidelberg, 721pp.

Diessel, C.F.K., 2010. The stratigraphic distribution of inertinite. International Journal of Coal Geology 81 (4), 251-268.

Edwards, J.C., Choate, P.J., 1993. Average Molecular Structure of Gasoline Engine Combustion Chamber Deposits Obtained by Solid-State $^{13}C$, $^{31}P$, and $^{1}H$ Nuclear Magnetic Resonance Spectroscopy. SAE International Technical Paper 932811.

Erdenetsogt, B-.O., Lee, I., Lee, S.K., Ko, Y-.J., Bat-Erdene, D., 2010. Solid-state C-13 CP/MAS NMR study of Baganuur coal, Mongolia: Oxygen-loss during coalification from lignite to subbituminous rank. International Journal of Coal Geology 82 (1-2), 37-44.

Falcon, R., Ham, A.J., 1988. The characteristics of Southern African coals. The Journal of the South African Institute of Mining and Metallurgy 88 (5), 145-161.

Falcon, R.M.S., 1986. A brief review of the origin, formation, and distribution of coal in southern Africa. In: Anhaeusser, C.R., Maske, S. (Eds.), Mineral Deposits of Southern Africa, Vols. I and II. Geological Society of South Africa, Johannesburg, pp. 1879-1898.

Glasspool, I., 2003a. Palaeoecology of selected South African export coals from the Vryheid Formation, with emphasis on the role of heterosporous lycopods and wildfire derived inertinite. Fuel 82, 959-970.

Glasspool, I.J., 2003b. Hypautochthonous–allochthonous coal deposition in the Permian, South African, Witbank Basin No. 2 seam; a combined approach using sedimentology, coal petrology and palaeontology. International Journal of Coal Geology 53, 81-135.

Glasspool, I.J., Scott, A.C., 2010. Phanerozoic concentrations of atmospheric oxygen reconstructed from sedimentary charcoal. Nature Geoscience Letters 3, 627-630.

Guo, Y., Bustin, R.M., 1998. FTIR spectroscopy and reflectance of modern charcoals and fungal decayed woods: implications for studies of inertinite in coals. International Journal of Coal Geology 37, 29-53.

Haenel, M.W., 1992. Recent progress in coal structure research. Fuel 71, 1211-1223.

Hagelskamp, H.H.B., Snyman, C.P., 1988. On the origin of low-reflecting inertinites in coals from the Highveld Coalfield, South Africa. Fuel 67, 307-313.

Hancox, J.P., Götz, A.E., 2014. South Africa's coalfields – A 2014 perspective. International Journal of Coal Geology 132, 170-254.

Hatcher, P.G., Clifford, D.J., 1997. The organic geochemistry of coal: from plant materials to coal. Organic Geochemistry 27 (5-6), 251-257, 259-274.

Hattingh, B.B., Everson, R.C., Neomagus, H.W.J.P., Bunt, J.R., Van Niekerk, D., Jordaan, J.H.L. and Mathews, J.P., 2013. Elucidation of the Structural and Molecular Properties of Typical South African Coals. Energy & Fuels 27, 3161-3172.

Hope, G., Chokkalingam, U., Anwar, S., 2005. The stratigraphy and fire history of the Kutai Peatlands, Kalimantan, Indonesia. Quaternary Research 64, 407-417.

Hower, J.C., Wagner, N.J., 2012. Notes on the methods of the combined maceral/microlithotype determination in coal. International Journal of Coal Geology 95, 47-53.

Hower, J.C., O'Keefe, J.M.K., Eble, C.F., Raymond, A., Valentim, B., Volk, T.J., Richardson, A.R., Satterwhite, A.B., Hatch, R.S., 2011a. Notes on the origin of inertinite macerals in coal: Evidence for fungal and arthropod transformations of degraded macerals. International Journal of Coal Geology 86 (2-3), 231-240.

Hower, J.C., O'Keefe, J.M.K., Eble, C.F., Volk, T.J., Richardson, A.R., Satterwhite, A.B., Hatch, R.S., Kostova, I.J., 2011b. Notes on the origin of inertinite macerals in coals: Funginite associations with cutinite and suberinite. International Journal of Coal Geology 85 (1), 186-190.

Hower, J.C., O'Keefe, J.M.K., Watt, M.A., Pratt, T.J., Eble, C.F., Stucker, J.D., Richardson, A.R., Kostova, I.J., 2009. Notes on the origin of inertinite macerals in coals: Observations on the importance of fungi in the origin of macrinite. International Journal of Coal Geology 80 (2), 135-143.

Hu, J.Z., Solum, M.S., Taylor, C.M.V., Pugmire, R.J., Grant, D.M., 2001. Structural Determination in Carbonaceous Solids Using Advanced Solid State NMR Techniques. Energy & Fuels 15 (1), 14-22.

Hunt, J.W., Smyth, M., 1989. Origin of inertinite-rich coals of Australian cratonic basins. International Journal of Coal Geology 11, 23-46.

International Committee for Coal and Organic Petrology (ICCP). (1998)., The new vitrinite classification (ICCP system 1994). Fuel 77 (5), 349-358.

International Committee for Coal and Organic Petrology (ICCP). (2001)., The new inertinite classification (ICCP System 1994). Fuel 80 (4), 459-471.

Jones, T.P., Chaloner, W.G., 1991. Fossil charcoal, its recognition and palaeoatmospheric significance. Palaeogeography, Palaeoclimatology, Palaeoecology (Global and Planetary Change Section) 97, 39-50.

Kawamoto, H., 2017. Lignin pyrolysis reactions. Journal of Wood Science 63 (2), 117-132.

Kirk, K.T., Farrell, R.L., 1987. Enzymatic "combustion": the microbial degradation of lignin. Annual Review of Microbiology 41, 465-505.

Malumbazo, N., Wagner, N.J., Bunt, J.R., Van Niekerk D., Assumption, H., 2011. Structural analysis of chars generated from South African inertinite coals in a pipe-reactor combustion unit. Fuel Processing Technology 92, 743-749.

Mao, J.D., Schimmelmann, A., Mastalerz, M., Hatcher, P.G., Li, Y., 2010. Structural Features of a Bituminous Coal and Their Changes during Low-Temperature Oxidation and Loss of Volatiles Investigated by Advanced Solid-State NMR Spectroscopy. Energy & Fuels 24 (4), 2536-2544.

Marynowski, L., Simoneit, B.R.T., 2009. Widespread Upper Triassic to Lower Jurrasic wildfire records from Poland: Evidence from charcoal and pyrolytic polycyclic aromatic hydrocarbons. Palaios 24 (12), 785-798.

Moore, T.A. Shearer, J.C., Miller, S.L., 1996. Fungal origin of oxidized plant material in the Palangkaraya peat deposit, Kalimantan Tengah, Indonesia: Implications for 'inertinite' formation in coal. International Journal of Coal Geology 30, 1-23.

Moore, T.A., Shearer, J.C., 1997. Evidence for Aerobic Degradation of Palangka Raya Peat and Implications for its Sustainability. In: Rieley, J.O., Page, S.E., (Eds.). Tropical Peatlands. Samara Publishing Limited, Cardigan, pp.157-167.

O'Keefe, J.M.K., Hower, J.C., 2011. Revisiting Coos Bay, Oregon: A re-examination of funginite–huminite relationships in Eocene subbituminous coals. International Journal of Coal Geology 85 (1), 34-42.

O'Keefe, J.M.K., Bechtel, A., Christanis, K., Dai, S., DiMichele, W.A., Eble, C.F., Esterle, J.S., Mastalerz, M., Raymond, A.L., Valentim, B.V., Wagner, N.J., Ward, C.R., Hower, J.C., 2013. On the fundamental difference between coal rank and coal type. International Journal of Coal Geology 118, 58-87.

Okolo, G.N., Neomagus, H.W.J.P., Everson, R.C., Roberts, M.J., Bunt, J.R., Sakurovs, R., Mathews, J.P., 2015. Chemical-structural properties of South African bituminous coals: Insights from wide angle XRD-carbon fraction analysis, ATR-FTIR, solid state $^{13}C$ NMR, and HRTEM techniques. Fuel 779-792.

Pickel, W., Kus, J., Flores, D., Kalaitzidis, S., Christanis, K., Cardott, B.J., Misz-Kennan, M., Rodrigues, S., Hentschel, A., Hamor-Vido, M., Crosdale, P., Wagner, N., ICCP., 2017. Classification of liptinite – ICCP System 1994. International Journal of Coal Geology 169, 40-61.

Plumstead, E.P., 1961. Ancient plants and drifting continents. South African Journal of Science 57 (7), 173-181.

Remy, W., Taylor, T.N., Hass, H., Kerp, H., 1994. Four hundred-million-year-old vesicular arbuscular mycorrhizae. Proceedings of the National Academy of Sciences of the United States of America 91 (25), 11841-11843.

Richards, J.M., Naude, G., Theron, S.J., McCullum, M., 2013. Petrological characterization of coal: an evolving science. The Journal of the Southern African Institute of Mining and Metallurgy 113, 865-875.

Richardson, A.R., Eble, C.F., Hower, J.C., O'Keefe, J.M.K., 2012. A critical re-examination of the petrology of the No. 5 Block coal in eastern Kentucky with special attention to the origin of inertinite macerals in the splint lithotypes. International Journal of Coal Geology 98, 41-49.

Ruckwied, K., Götz, A.E., Jones, P., 2014. Palynological records of the Permian Ecca Group (South Africa): Utilizing climatic icehouse–greenhouse signals for cross basin correlations. Palaeogeography, Palaeoclimatology, Palaeoecology 413, 167-172.

Saiz-Jimenez, C., de Leeuw, J.W., 1986. Lignin pyrolysis products: Their structures and their significance as biomarkers. Organic Geochemistry 10, (4-6), 869-876.

Scott, A.C., 1989. Observations on the nature and origin of fusain. International Journal of Coal Geology 12, 443-475.

Scott, A.C., 2002. Coal petrology and the origin of coal macerals: a way ahead? International Journal of Coal Geology 50, 119-134.

Scott, A.C., 2010. Charcoal recognition, taphonomy and uses in palaeoenvironmental analysis. Palaeogeography, Palaeoclimatology, Palaeoecology 291 (1-2), 11-39.

Scott, A.C., Glasspool, I.J., 2007. Observations and experiments on the origin and formation of inertinite group macerals. International Journal of Coal Geology 70 (1-3), 53-66.

Shearer, J.C., Moore, T.A., 1996. Effects of experimental coalification on texture, composition and compaction in Indonesian peat and wood. Organic Geochemistry 24 (2), 127-140.

Simoneit, B.R.T., Rogge, W.F., Mazurek, M.A., Standley, L.J., Hilderman, L.M., Cass, G.R., 1993. Lignin pyrolysis products, lignans, and resin acids as specific tracers of plant classes in emissions from biomass combustion. Environmental Science and Technology 27, 2533-2541.

Slater, B.J., McLoughlin, S., Hilton, J., 2015. A high-latitude Gondwana lagerstätte: The Permian permineralised peat biota of the Prince Charles Mountains, Antarctica. Gondwana Research 27, 1446-1473.

Snyman, C.P., 1989. The role of coal petrography in understanding the properties of South African coal. In: Pickhardt, W. (Ed.). Erich Stach Memorial Issue. International Journal of Coal Geology 14, 83-101.

Solum, M.S, Pugmire, R.J., Grant, D.M., 1989. $^{13}C$ Solid-state NMR of Argonne Premium Coals. Energy & Fuels 3, 187-193.

South African National Standards (SANS) 17246:2011 (ISO 17246:2010). Coal - Proximate analysis.

South African National Standards (SANS) 17247:2006 (ISO 17247:2005). Coal - Ultimate analysis.

South African National Standards (SANS) 1928:2009 (ISO 1928:2009). Solid mineral fuels - Determination of gross calorific value by the bomb calorific method, and calculation of net calorific value.

South African National Standards (SANS) 334:1992 (ISO 334:1992). Solid mineral fuels - Determination of total sulfur - Eschka method.

South African National Standards (SANS) 7404-2:2015 (ISO 7404-2:2009). Methods for the petrographic analysis of coals Part 2: Methods of preparing coal samples.

South African National Standards (SANS) 7404-3:2016 (ISO 7404-3:2009). Methods for the petrographic analysis of coals - Part 3: Method of determining maceral group.

South African National Standards (SANS) 7404-5:2016 (ISO 7404-5:2009). Methods for the petrographic analysis of coals - Part 5: Method of determining microscopically the reflectance of vitrinite.

South African National Standards (SANS) 7936:2010 (ISO 7936:1992). Hard coal – Determination and presentation of float and sink characteristics – General directions for apparatus and procedures.

Spiker, E.C., Hatcher, P.G., 1987. The effects of early diagenesis on the chemical and stable carbon isotopic composition of wood. Geochimica et Cosmochimica Acta 51, 1385-1391.

Stout, S.A., Spackman, W., 1989. Notes on the compaction of a Florida peat and the Brandon lignite as deduced from the study of compressed wood. International Journal of Coal Geology 11, 247-256.

Suggate, R.P., Dickinson, W.W., 2004. Carbon NMR of coals: the effects of coal type and rank. International Journal of Coal Geology 57, 1-22.

Supaluknari, S., Burgar, I., Larkins, F.P., 1990. High-resolution solid-state $^{13}C$ NMR studies of Australian coals. Organic Geochemistry 15 (5), 509-519.

Taylor, G.H., Teichmüller, M., Davis, A., Diessel, C.F.K., Littke, R., Robert, P., 1998. Organic Petrology. Gebrüder Borntraeger, Berlin, 704pp.

Teichmüller, M., 1989. The genesis of coal from the viewpoint of coal petrology. In: Lyons, P.C., Alpern, B., (Eds.). Peat and Coal: Origin, Facies, and Depositional Models. International Journal of Coal Geology 12, 1-87.

Unsworth, J.F., Fowler, C.S., Jones, L.F., 1989. Moisture in coal: 2. Maceral effects on pore structure. Fuel 68 (1), 18-26.

van Asselen, S., Stouthamer, E., van Asch, Th.W.J., 2009. Effects of peat compaction on delta evolution: A review on process, responses, measuring and modelling. Earth Science Reviews 92, 31-35.

Van Niekerk, D., Mathews, J.P., 2010. Molecular representations of Permian-aged vitrinite-rich and inertinite-rich South African coals. Fuel 89, 73-82.

Van Niekerk, D., Mitchell, G.D., Mathews, J.P., 2010. Petrographic and reflectance analysis of solvent-swelled and solvent-extracted South African vitrinite-rich and inertinite-rich coals. International Journal of Coal Geology 81, 45-52.

Van Niekerk, D., Pugmire, R.J., Solum, M.S., Painter, P.C., Mathews, J.P., 2008. Structural characterization of vitrinite-rich and inertinite-rich Permian-aged South African bituminous coals. International Journal of Coal Geology 76, 290-300.

Yang, H., Yan, R., Chen, H., Lee, D.H., Zheng, C., 2007. Characteristics of hemicellulose, cellulose and lignin pyrolysis. Fuel 86, 1781-1788.

# Chapter 4

## Using $\delta^{15}N$ and $\delta^{13}C$ and nitrogen functionalities to support a fire-origin for certain inertinite macerals in a No. 4 Seam Upper Witbank coal, South Africa

**ABSTRACT**

Fires are likely to have been central to the formation of certain inertinite macerals present in South African coals. To investigate this hypothesis, a medium rank C bituminous Witbank coal from the No. 4 Seam Upper was density-fractionated to yield inertinite-rich and vitrinite-rich samples. The parent coal comprises of 41.6 vol. % vitrinite and 48.5 vol. % inertinite. The vitrinite-rich sample is dominated by collotelinite and collodetrinite (81 vol. % vitrinite), and the inertinite-rich sample by fusinite, semifusinite, and inertodetrinite (63 vol. % inertinite). The $\delta^{15}N$ and $\delta^{13}C$ values and nitrogen functionalities were determined, and used to constrain early coal-formation pathways for the dominant macerals of the density-fractionated samples. The vitrinite-rich sample has a lower $\delta^{13}C$ relative to the inertinite-rich counterpart. However, the inertinite-rich sample has the lower $\delta^{15}N$ value, along with a lower concentration of N-quaternary and higher N-pyrrolic. Because these samples are of the same coal maturity, and the major macerals were derived from similar precursors, differences in $\delta^{15}N$ and $\delta^{13}C$ and nitrogen functionalities reflect differences in coal-formation pathways. Degradation of $^{13}C$-rich cellulose in wood through either charring or bacterial activity results in lower $\delta^{13}C$ values. The lower $^{14}N$ for the vitrinite-rich sample along with higher N-quaternary and N-pyridinic suggests cellulose degradation driven by bacterial activity. In contrast, the higher $^{14}N$ coupled with higher N-pyrrolic and N-oxide complexes for the inertinite-rich sample, suggests fusinite and semifusinite were formed through charring. Differences in charring conditions, including the moisture content of affected vegetation, are suggested to have determined whether fusinite or semifusinite was produced. Inertodetrinite is attributed to the disintegration of charred plant matter.

**Keywords:** Stable isotopes; X-ray photoelectron spectroscopy; Main Karoo Basin; Woody tissues; Bacterial degradation; Vitrinite; N-quaternary; N-pyrrolic; Fusinite; Semifusinite

### 4.1. Introduction

The Main Karoo Basin of South Africa contains coals rich in inertinite (Falcon, 1986; Hagelskamp and Snyman, 1988; Cadle et al., 1993; Snyman and Botha, 1993; O'Keefe et al.,

2013). Two viewpoints currently exist for the origin of the inertinite macerals. Earlier workers attributed the inertinite to the incomplete degradation of plant matter as a result of a cool, temperate climate along with aerial oxidation (Falcon, 1986; Hagelskamp and Snyman, 1988; Cadle et al., 1993; Snyman and Botha, 1993). Glasspool (2003a, 2003b) rejects this, instead arguing that the macerals are pyrogenic based on the description of fossil charcoal associated with coals of the Witbank Coalfield.

Macroscopic charcoal associated with clastic sedimentary rocks of the Vryheid Formation (Vereeniging Coalfield, South Africa) has also been documented by Jasper et al. (2013). Despite this, the now firmly entrenched view that the inertinite macerals present in the coals are oxidation- and cold climate-derived continues to persist and is often cited as fact in the published literature on South African coals (e.g., Van Niekerk et al., 2008; O'Keefe et al., 2013). The controversy stems, in part, from the glacial/post-glacial climatic conditions prevailing in Gondwana in contrast to the tropical conditions of Laurasia (Falcon, 1986; Snyman and Botha, 1993). The Gondwana conditions were previously assumed to have hindered the development of extensive wild and/or peat fires. The presence of charcoal contradicts this view.

The stable isotope composition of coal (e.g., $\delta^{15}N$ and $\delta^{13}C$) reflects the composition of the source vegetation as well as changes resulting from early diagenesis and subsequent coalification processes (Spiker and Hatcher, 1987; Rimmer et al., 2006; Skrzypek et al., 2010; Suto and Kawashima, 2016; Valentim et al., 2016). For iso-rank bituminous coal samples, $\delta^{13}C$ values rise with an increase in density, concomitant with an increase in inertinite content (Rimmer et al., 2006; Valentim et al., 2016). This reflects the aromatization of the coal macromolecule with the loss of the heavier $^{13}C$ atoms, suggested to be related to the preferential loss of aliphatics (Rimmer et al., 2006).

Coal macerals formed through the degradation of plant matter by organisms may not possess anatomical structures (Guo and Bustin, 1998; ICCP, 1998; Hower et al., 2013; Richardson et al., 2012; O'Keefe et al., 2013). At the same time, bacterial degradation preferentially eliminates the isotopically lighter $^{14}N$ (Spiker and Hatcher, 1987; Rimmer et al., 2006; Skrzypek et al., 2010). Based on these observations, it is implicit that macerals formed through bacterial degradation such as collotelinite and collodetrinite may be structureless and have higher $\delta^{15}N$ values relative to inertinite counterparts. With limited degradation, macerals derived through charring may

possess anatomical structures (Scott, 1989, 2010; Jones and Chaloner, 1991; Guo and Bustin, 1998; Scott and Glasspool, 2007), and possibly have a higher $^{14}N$ content (Tukerian et al., 1998; Bird and Ascough, 2012). In the absence of post-formation heating, for example, resulting from the emplacement of igneous intrusions, the $\delta^{15}N$ and $\delta^{13}C$ signatures imparted on botanical precursors by early coal-formation processes remain unaffected until the meta-anthracite rank (Valentim et al., 2016, and references therein). This implies that these isotopes can be used to constrain the early coal-formation pathways for macerals present in iso-rank bituminous coal samples (Spiker and Hatcher, 1987; Rimmer et al., 2006; Valentim et al., 2016).

In order to address the question of whether charring contributed to the formation of certain inertinite macerals present in Witbank coals, vitrinite-rich and inertinite-rich samples were prepared through density-fractionation using medium rank C bituminous coal (termed the "parent coal") from the No. 4 Seam Upper. The $\delta^{15}N$ and $\delta^{13}C$ values as well as the concentrations of nitrogen functionalities for the three samples were determined, and subsequently used to constrain the early origin pathways for the dominant macerals in the density-fractionated samples. A necessary assumption is that charring of Permian coal-forming vegetation fractionated the stable isotopes in a similar manner to what is observed in laboratory experiments using modern plants. Consequently, in addition to the measured isotopic values for the Witbank coals, the discussion also considers the relative shifts in $\delta^{15}N$ and $\delta^{13}C$ values previously observed by others during laboratory experiments on various modern woods. The nitrogen functionalities present in the samples, namely: N-pyridinic, N-pyrrolic, N-quaternary, and N-oxide complexes were also analysed using X-ray photoelectron spectroscopy (XPS), and used in conjunction with the stable isotope results.

Carbon-13 cross-polarization magic-angle-spinning solid-state nuclear magnetic resonance ($^{13}C$ CP-MAS SS NMR) and electron spin resonance (ESR) results for the coal samples used in the present study were reported in previous publications (Moroeng et al., 2018a, 2018b). These results (see section 4.3) were interpreted to be consistent with a fire-origin for specific inertinite macerals. Thus, this study attempts to provide additional evidence for a fire-origin for certain inertinite macerals occurring in the No. 4 Seam Upper, based on a single coal sample and density-fractionated products thereof. To the authors' knowledge, the present paper is the first to report on both the $\delta^{15}N$ and $\delta^{13}C$ values for South African coal. Although $\delta^{13}C$ values and

nitrogen functionalities have been reported (e.g., Gröcke et al., 2009; Suto and Kawashima, 2016; Phiri et al., 2017, 2018), the previous studies do not focus on the origin of macerals in the coals.

## 4.2. Methodology

### 4.2.1. Sample characterization

The run-of-mine medium rank C bituminous Permian coal sample (No. 4 Seam Upper) used in this study was obtained from a mine operating in the Witbank Coalfield, South Africa. The proximate, elemental, petrographic, and $^{13}C$ CP-MAS SS NMR results were reported in a previous publication (Moroeng et al., 2018), and the relevant data are provided in the present study for context, where applicable. Following crushing, density-fractionation was undertaken to create a vitrinite-rich (RD = 1.3) and an inertinite-rich (RD = 1.8) sample following South African National Standard (SANS) 7936 (2010), while a portion of the original coal was set aside to represent the "parent sample". Witbank coals generally have a low liptinite content (below 5 vol. %), and it was expected that this maceral group would have a minor influence on the efficiency of the density-separation procedure.

The three samples were prepared for petrographic analysis as polished blocks following SANS standard 7404-2 (2015), and the maceral point-count was conducted following SANS standard 7404-3 (2016) using a Zeiss AxioImager m2M reflected light microscope retrofitted with Hilgers Diskus Fossil components and software, at a total magnification of 500x using immersion oil. The mean random vitrinite reflectance (%RoVmr) was determined for the parent sample following SANS 7404-5 (2016). Proximate, gross calorific value, and elemental (C, H, N, O, and S) analyses were conducted at a commercial laboratory (Bureau Veritas, Centurion, South Africa) following recommended SANS standards (SANS 334, 1992; SANS 17247, 2006; SANS 1928, 2009; SANS 17246, 2011).

### 4.2.2. De-carbonation

As the aim of this study is to quantify the organic $\delta^{15}N$ and $\delta^{13}C$ values and nitrogen functionalities of the coal samples, the presence of carbon- and nitrogen-bearing minerals are a possible contaminant. Valentim et al. (2016) note that $NH_4$-rich illite is typically associated with high rank coals. As a result, this mineral is not expected to influence the measured geochemical parameters due to the low rank of the coal sample. In order to remove carbonate minerals, and

thus minimize their contribution to the measured $\delta^{13}C$ values, the samples were treated with hydrochloric acid (HCl), following procedures documented by Gröcke et al. (2009). The samples were milled to a particle size of –212 µm. Approximately 30 g of each sample was weighed into a 1 L polypropylene beaker, and 400 mL of 6 M HCl introduced into each beaker and left for 24 h. The solution was then filtered-out using a Buchner Funnel. Subsequently, the coal product was washed several times with ultra-pure water (Milli-Q) to remove the acid. The HCl-treated samples are hereafter referred to as "de-carbonated", whereas the untreated counterparts are termed "original".

### 4.2.3. X-ray fluorescence

X-ray fluorescence (XRF) was used to assess the efficiency of the de-carbonation procedure focusing on major elements. An ash product of approximately 0.7 g was prepared for each of the original and de-carbonated samples prior to the analysis. Borate fusion discs were prepared and analyzed with a wavelength-dispersive XRF spectrometer, namely a "MagiX PRO" running under the "SuperQ" software version 5.3A, both from PANalytical. The XRF was calibrated with mixtures of pure chemicals (oxides) and with certified reference materials using a fundamental parameters model.

### 4.2.4. $\delta^{15}N$ and $\delta^{13}C$ stable isotopes

A range of aliquots for each of the samples were weighed using a Mettler Toledo M5 micro-balance and placed in pre-cleaned tin capsules. All capsules were cleaned using toluene prior to the weighing of samples. Each sample was weighed out at the following weight classes; 0.6 mg, 0.8 mg, and 1.2 mg. For each weight class, three sub-samples were weighed and analyzed. Thus, a total of nine sub-samples per coal (n = 9) were subjected to isotopic analysis. This was undertaken to ensure that statistically representative isotopic measurements for each sample were obtained.

Isotopic analysis was undertaken using a Flash EA 1112 Series coupled to a Delta V Plus stable light isotope ratio mass spectrometer via a ConFlo IV system (all equipment supplied by Thermo Fisher, Bremen, Germany), housed at the UP Stable Isotope Laboratory, Mammal Research Institute, University of Pretoria. Two laboratory running standards (Merck Gel: $\delta^{13}C$ = –20.26‰, $\delta^{15}N$ = 7.89‰, %C = 41.28, %N = 15.29, and DL-Valine: $\delta^{13}C$ = –10.57‰, $\delta^{15}N$ = –6.15‰, %C = 55.50, %N = 11.86) and a blank sample were run after every eleven unknown samples.

Data corrections were done using the values obtained for the Merck Gel during each run. The values for the DL-Valine standard provide the precision error for each run. The precision error for $\delta^{15}N$ was 0.07 ‰ and 0.1‰ for $\delta^{13}C$. These running standards are calibrated against international standards: National Institute of Standards & Technology (NIST): NIST 1557b (Bovine liver); NIST 2976 (Mussel tissue); and, NIST 1547 (Peach leaves). All results are referenced to Vienna Pee-Dee Belemnite (VPDB) for carbon isotope values, and to Air for nitrogen isotope values. Results are expressed in delta notation (δX) using a per mille (‰) scale, using the standard equation:

$$\delta X\ (‰) = [(R_{sample}/R_{standard})-1]x1000 \qquad \text{(Eq. 4.1)}$$

Where X = $^{15}N$ or $^{13}C$ and R = $^{15}N/^{14}N$ or $^{13}C/^{12}C$, respectively.

### 4.2.5. Determination of nitrogen functionalities using X-ray photoelectron spectroscopy

The XPS analyses were conducted on the original samples at a particle size of –212 µm. $NH_4$-rich illite was considered immaterial, given the low rank of the coal (Valentim et al., 2016, and references therein). Furthermore, Phiri et al. (2017) found that demineralization has a negligible impact on the nitrogen functionalities of South African bituminous coals determined using XPS. For the parent, inertinite-rich, and vitrinite-rich samples, a representative sub-sample was prepared for this analysis using a rotary splitter.

The XPS analyses were conducted at the Centre for Microscopy and Microanalysis, The University of Queensland (Australia). The XPS analysis was undertaken using a Kratos Axis ULTRA X-ray Photoelectron Spectrometer incorporating a 165 mm hemispherical electron energy analyzer. The incident radiation was Monochromatic Al Kα X-rays (1486.6 eV) at 225 W (15 kV, 15 ma). Survey (wide) scans were taken at an analyzer pass energy of 160 eV and multiplex (narrow) high resolution scans at 40 eV. Survey scans were carried out over 1200-0 eV binding energy range with 1.0 eV steps and a dwell time of 100 ms. Narrow high-resolution scans were run with 0.05 ev steps and 250 ms dwell time.

Base pressure in the analysis chamber was $1.0x10^{-9}$ torr and during sample analysis $1.0x10^{-8}$ torr.

Atomic concentrations (At. %) were calculated using the CasaXPS version 2.3.14 software and a Shirley baseline with Kratos library Relative Sensitivity Factors (RSFs). Peak fitting of the high-

resolution data was also carried out using the CasaXPS software. Data was charge corrected using the -C-C- at 284.8 eV.

## 4.3. Results

### 4.3.1. General characterization

The vitrinite-rich sample has both the highest total carbon and nitrogen content as well as the highest H/C atomic ratio (Table 4.1, elemental analysis). The H/C atomic ratio of the vitrinite-rich sample (0.85) is consistent with what is expected from a vitrinite-rich coal when compared to an inertinite-rich counterpart at the rank of bituminous coal, with the lower ratio (0.74) of the inertinite-rich sample indicative of a greater aromatic fraction (Maroto-Valer et al., 1998; Van Niekerk et al., 2008; Moroeng et al., 2017).

**Table 4.1:** Proximate, gross calorific value, elemental (air dried), petrographic composition (mineral matter included basis) and mean random vitrinite reflectance (%RoVmr, standard deviation (std. dev.)) results for the parent coal, inertinite-rich and vitrinite-rich samples.

| | **Parent** | **Inertinite-rich** | **Vitrinite-rich** |
|---|---|---|---|
| **Proximate analysis (wt. %)** | | | |
| Moisture | 3.1 | 3.0 | 3.1 |
| Ash | 12.5 | 13.4 | 4.2 |
| Volatile matter | 30.7 | 28.5 | 38.6 |
| Fixed carbon | 53.7 | 55.1 | 54.1 |
| **Gross calorific value (MJ/kg)** | | | |
| Calorific value | 27.7 | 27.1 | 30.9 |
| **Elemental analysis (wt. %)** | | | |
| Carbon | 67.40 | 67.60 | 75.00 |
| Hydrogen | 4.40 | 4.17 | 5.33 |
| Nitrogen | 1.80 | 1.68 | 2.07 |
| Oxygen | 8.61 | 9.57 | 9.58 |
| Sulphur | 2.24 | 0.64 | 0.76 |
| H/C atomic ratio | 0.78 | 0.74 | 0.85 |
| **Petrographic analysis (vol. %)** | | | |
| Telinite | 0.2 | 0.0 | 2.4 |
| Collotelinite | 12.0 | 12.4 | 35.3 |
| Vitrodetrinite | 0.0 | 0.0 | 0.0 |
| Collodetrinite | 28.0 | 15.4 | 36.3 |
| Corpogelinite | 1.4 | 0.5 | 6.9 |
| Gelinite | 0.0 | 1.3 | 0.0 |
| Pseudovitrinite | 0.0 | 0.2 | 0.4 |
| **Total vitrinite** | **41.6** | **29.8** | **81.3** |
| | | | |
| Fusinite | 8.6 | 8.3 | 3.9 |
| Semifusinite | 18.3 | 28.9 | 4.7 |
| Micrinite | 0.4 | 0.2 | 0.0 |

| | | | |
|---|---|---|---|
| Macrinite | 0.2 | 0.2 | 0.4 |
| Secretinite | 1.2 | 1.2 | 0.6 |
| Funginite | 0.0 | 0.0 | 0.0 |
| Inertodetrinite | 19.8 | 23.8 | 1.8 |
| **Total inertinite** | **48.5** | **62.6** | **11.4** |
| | | | |
| Sporinite | 3.3 | 2.9 | 2.9 |
| Cutinite | 0.4 | 0.0 | 2.0 |
| Resinite | 0.0 | 0.0 | 0.2 |
| **Total liptinite** | **3.7** | **2.9** | **5.1** |
| | | | |
| Silicate | 3.1 | 3.1 | 0.2 |
| Suphide | 2.4 | 1.2 | 0.8 |
| Carbonate | 0.8 | 0.6 | 1.4 |
| **Total minerals** | **6.3** | **4.9** | **2.4** |
| | | | |
| **%RoVmr** | **0.65** | | |
| **Std. Dev.** | **0.067** | | |

The maceral nomenclature adopted herein follows that of the International Committee for Coal and Organic Petrology for bituminous coals (ICCP, 1998, 2001; Pickel et al., 2017). The parent sample comprises of 41.6 vol. % total vitrinite and 48.5 vol. % total inertinite (Table 4.1, petrographic analysis). The density-fractionated samples were found to comprise of 81.3 vol. % vitrinite and 62.6 vol. % inertinite, respectively. Collotelinite and collodetrinite – with minor proportions of corpogelinite, telinite, and pseudovitrinite – are the most abundant macerals in the vitrinite-rich sample. In contrast, a high proportion of semifusinite and inertodetrinite were recorded for the inertinite-rich sample, along with an increased amount of fusinite. The observable mineral matter content is generally low, with silicates and sulphides constituting the major components. A very low concentration of carbonates was observed in these Witbank coal samples.

A 0.65 %RoVmr was determined on the parent sample (standard deviation = 0.067), confirming the sample as a medium rank C bituminous coal. Based on the low %RoVmr standard deviation, and the absence of petrographic features associated with rapid heating such as devolatilization vacuoles or extensive cracking, the coal sample has not been subjected to elevated temperatures due to igneous intrusions. As a result, and because the samples are derived from the same coal (and thus of the same maturity level), the $\delta^{15}N$ and $\delta^{13}C$ values can be used to constrain early coal-formation pathways for the dominant macerals of the density-fractionated samples (Rimmer et al., 2006; Valentim et al., 2016).

### 4.3.2. X-ray fluorescence

The XRF results for the ashed products of the original and de-carbonated coal samples are given in Table 4.2. The relatively low total values reflect minor elements that were not accounted for during the XRF analysis and, possibly, the volatilization of certain elements (e.g., sulphur) during borate fusion (Ling et al., 2014). Since carbonates would influence the accuracy of the measured $\delta^{13}C$ values, CaO (calcite) is used as proxy to assess the abundance of said minerals. The abundance of the CaO is significantly reduced in the de-carbonated samples suggesting a reduction in the total proportion of carbonate minerals.

**Table 4.2:** XRF results for ash products of the original and de-carbonated (DC) parent, inertinite-rich and vitrinite-rich samples, reported in mass %. Least limits of detection (LLDs) are about 0.05 mass %. Measurements below 0.05 mass % have been replaced with a dash ("-"). LLD for sulphur may be higher than 0.05 mass % $SO_3$.

| | **Parent** | **DC - Parent** | **Inertinite-rich** | **DC - Inertinite-rich** | **Vitrinite-rich** | **DC - Vitrinite-rich** |
|---|---|---|---|---|---|---|
| **$Al_2O_3$** | 27.92 | 21.88 | 31.17 | 26.14 | 29.14 | 22.91 |
| **BaO** | 0.07 | 0.09 | 0.06 | 0.08 | 0.21 | 0.38 |
| **CaO** | 1.65 | 0.55 | 1.07 | 0.47 | 8.87 | 3.57 |
| **$Cr_2O_3$** | 0.06 | - | - | - | 0.07 | 0.14 |
| **$Fe_2O_3$** | 17.71 | 20.39 | 2.91 | 3.40 | 6.36 | 14.20 |
| **$K_2O$** | 0.38 | 0.44 | 0.40 | 0.49 | 0.59 | 0.83 |
| **MgO** | 0.40 | 0.18 | 0.29 | 0.17 | 1.84 | 0.97 |
| **MnO** | - | - | - | - | 0.14 | - |
| **$Na_2O$** | - | 0.05 | - | - | 0.15 | 0.30 |
| **NiO** | - | - | - | - | - | 0.08 |
| **$P_2O_5$** | 0.33 | 0.35 | 0.32 | 0.35 | 0.59 | 0.65 |
| **$SiO_2$** | 47.58 | 52.00 | 54.26 | 61.90 | 39.36 | 35.68 |
| **$SO_3$** | 1.48 | 0.31 | 0.75 | 0.14 | 8.27 | 1.56 |
| **$TiO_2$** | 1.24 | 2.17 | 1.26 | 2.13 | 2.62 | 6.65 |
| **$V_2O_5$** | - | - | - | - | 0.09 | 0.22 |
| **Total** | 98.82 | 98.41 | 92.49 | 95.27 | 98.30 | 88.14 |

### 4.3.3. $\delta^{15}N$ and $\delta^{13}C$ values

The average $\delta^{15}N$ and $\delta^{13}C$ values (n = 9) for the three coal samples are presented in Table 4.3. The average $\delta^{13}C$ values for the samples are: –23.27‰ VPDB for the parent sample (std. dev. = 0.06); –23.13‰ VPDB for the inertinite-rich sample (std. dev. = 0.03); and, –23.68‰ VPDB for the vitrinite-rich sample (std. dev. = 0.02). With regards to the average $\delta^{15}N$ values (n = 9), the inertinite-rich sample has the lower value at 2.47‰ Air (std. dev. = 0.22), whereas the vitrinite-rich counterpart has a higher value of 3.30‰ Air (std. dev. = 0.16).

**Table 4.3:** $\delta^{15}N$ (Air) and $\delta^{13}C$ (Vienna Pee-Dee Belemnite, VPDB) isotopic values as well as total nitrogen (N) and carbon contents (C) for the parent, inertinite-rich and vitrinite-rich samples. Isotopic measurements for each sample were recorded on nine sub-samples (n = 9) and the average values (and standard deviation) are reported.

| Sample | Weight (mg) | $\delta^{15}N$ (‰) | Std. Dev. ($\delta^{15}N$) | N (%) | $\delta^{13}C$ (‰) | Std. Dev. ($\delta^{13}C$) | C (%) |
|---|---|---|---|---|---|---|---|
| **Parent** | 0.88 | 2.66 | 0.20 | 1.78 | -23.27 | 0.06 | 68.72 |
| **Inertinite-rich** | 0.92 | 2.47 | 0.22 | 1.70 | -23.13 | 0.03 | 67.05 |
| **Vitrinite-rich** | 0.89 | 3.30 | 0.16 | 2.02 | -23.68 | 0.02 | 73.21 |

The average $\delta^{15}N$ and $\delta^{13}C$ values (n = 9) for each sample along with the standard deviations are plotted in Figure 4.1. There is a degree of variability in the measured isotopic values for each sample as indicated by the standard deviations (denoted by the error bars). This may be interpreted to reflect sample heterogeneity (Table 4.1) as the samples have varying maceral proportions. The degree of variability appears to be greatest for the inertinite-rich and parent samples, possibly reflecting greater compositional heterogeneity.

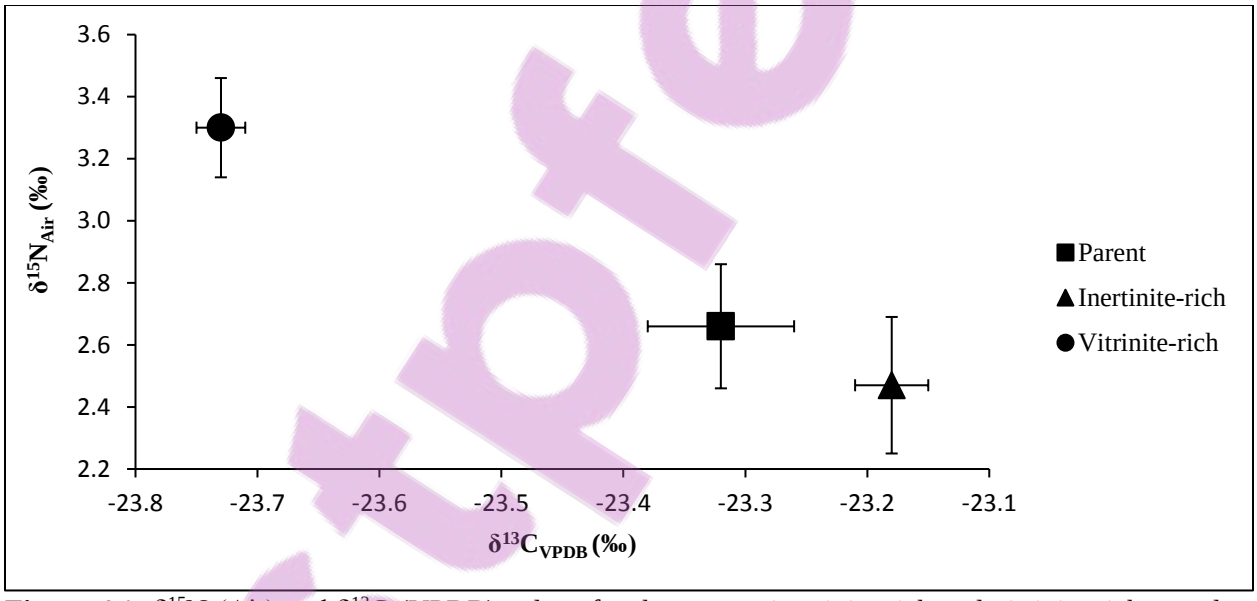


**Figure 4.1:** $\delta^{15}N$ (Air) and $\delta^{13}C$ (VPDB) values for the parent, inertinite-rich and vitrinite-rich samples. The measurements for each sample were taken nine times (n = 9) and the error bars denote the standard deviation.

Although the $\delta^{15}N$ and $\delta^{13}C$ values for the parent sample plot closest to the inertinite-rich sample, the values for the parent coal are largely intermediate between the density-fractionated samples (Figure 4.1), reflecting petrographic composition (Table 4.1). This suggests inherent differences between the $\delta^{15}N$ and $\delta^{13}C$ values of the density-fractionated samples.

The inertinite-rich sample has higher $\delta^{13}C$ values, between 0.50‰ VPDB and 0.60‰ VPDB (with an average of 0.55‰ VPDB) higher than the vitrinite-rich sample. The differences between these values are comparable with those previously reported by Rimmer et al. (2006) for density-fractionated samples (by density-gradient centrifugation) of a coal from the Blue Gem coal bed (Middle Pennsylvanian, Duckmantian (Westphalian B), Breathitt Formation), Southwestern Coal District, Eastern Kentucky, United States. The $\delta^{15}N$ values of the vitrinite-rich sample are higher than the other samples, at an average of 0.83‰ Air higher than the inertinite-rich sample.

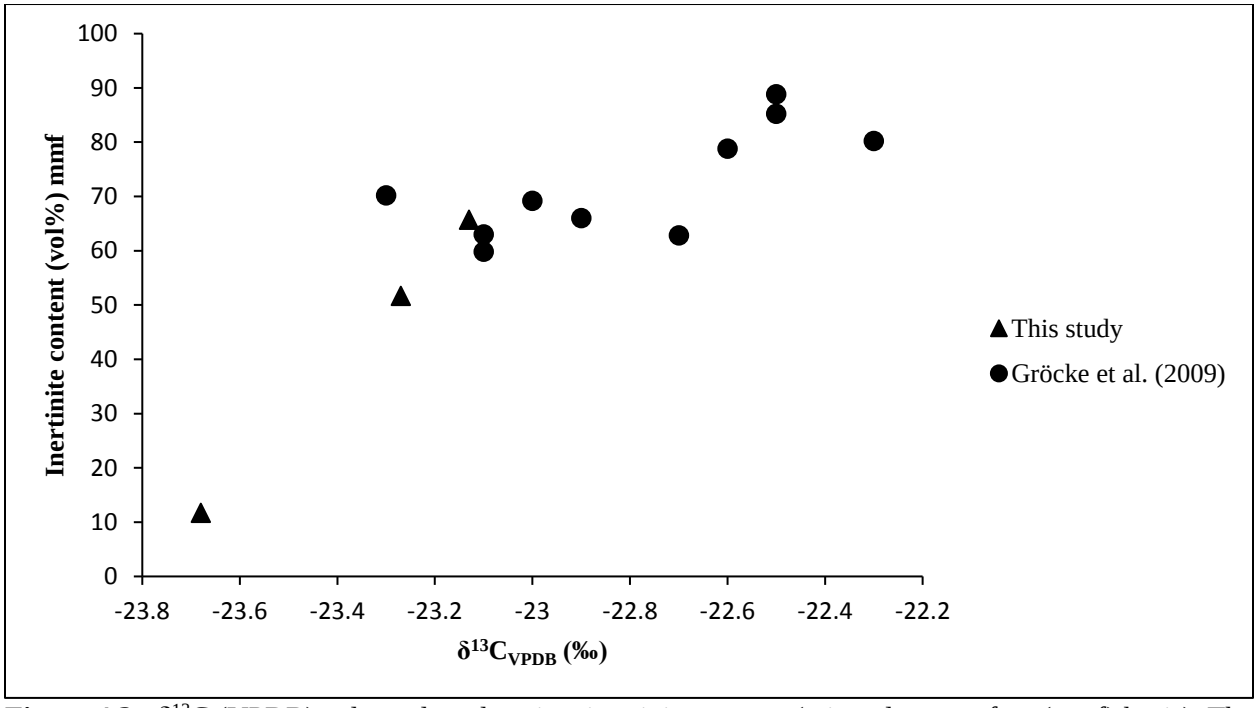


**Figure 4.2:** $\delta^{13}C$ (VPDB) values plotted against inertinite content (mineral-matter-free (mmf) basis). The triangles represent the average $\delta^{13}C$ values (n = 9) for the samples of the present study (Witbank Coalfield), and the circles denote values for coal samples as reported by Gröcke et al. (2009) (Highveld Coalfield).

The $\delta^{13}C$ values reported here are generally comparable to those previously reported by Gröcke et al. (2009) for dyke intruded coals from the No. 4 Lower Seam of the Highveld Coalfield, South Africa (Figure 4.2). Gröcke et al. (2009) concluded that the intrusion had limited impact on the $\delta^{13}C$ values, and found that the samples dominated by inertinite (max. 88.8 vol. % inertinite, mmf) generally had a higher $\delta^{13}C$ value (–22.7‰ VPDB) relative to samples dominated by vitrinite (–23.1‰ VPDB, 40.2 vol. % vitrinite). The values are also comparable to the South African regional average (–23.7 ± 0.7‰ VPDB) as reported by Suto and Kawashima (2016). It is interesting to note that the vitrinite-rich sample of the present study plots much

further left compared to the other coal samples, and that there is a general trend of higher $\delta^{13}C$ values with an increase in inertinite content (Figure 4.2). This is consistent with previous research publications based on American bituminous coals (e.g., Rimmer et al., 2006; Valentim et al., 2016).

Given that the dominant vitrinite and inertinite macerals in the density-fractionated samples may be derived from similar plant organs, i.e., wood (Hagelskamp and Snyman, 1988; ICCP, 1998, 2001; Hower et al., 2013; O'Keefe et al., 2013), the differences in the $\delta^{15}N$ and $\delta^{13}C$ values may be interpreted to reflect differences in early coal-formation pathways as opposed to differences associated with the compositions of precursor plant matter.

### 4.3.4. Nitrogen functionalities

The concentrations of different nitrogen functionalities in the coal samples are presented in Table 4.4. The XPS N 1s spectra for the parent, inertinite-rich, and vitrinite-rich samples were each deconvoluted into four sub-peaks, each with a binding energy of approximately 398.8 eV, 400.3 eV, 401.6 eV, and 402.2 – 403.2 eV corresponding to N-pyridinic, N-pyrrolic, N-quaternary, and N-oxide complexes, respectively. As has been done by other authors (e.g., Valentim et al., 2016; Phiri et al., 2017, 2018), the deconvoluted XPS N 1s spectra for each nitrogen functionality is denoted as N-6, N-5, N-Q, and N-X, respectively, in Table 4.4 and Figures 4.3, 4.4, and 4.5. For comparison, the measured spectra for the three samples are plotted together in Figure 4.6. Because of the poor signal-to-noise ratio, the XPS results for the parent coal (Figure 4.3) are largely excluded from the discussion henceforth.

The concentrations of nitrogen functionalities (N-6, N-5, N-Q, and N-X) between the three samples are variable. The vitrinite-rich sample has the higher proportion of both N-pyridinic (N-6 = 25.26 At. %) and N-quaternary (N-Q = 25.2 At. %). Although also high in the vitrinite-rich sample (N-5 = 42.88 At. %), the concentration of N-pyrrolic is much higher for the inertinite-rich sample at N-5 = 48.58 At. %. Similarly, the proportion of N-oxide complexes is slightly higher for the inertinite-rich sample (N-X = 8.17 At. %) relative to the vitrinite-rich counterpart (N-X = 6.66 At. %).

**Table 4.4:** XPS total nitrogen as well as nitrogen functionalities for the parent, inertinite-rich, and vitrinite-rich samples.

| | | **Parent** | **Inertinite-rich** | **Vitrinite-rich** |
|---|---|---|---|---|
| Total nitrogen (At. %) | | 1.13 | 1.49 | 1.53 |
| Nitrogen functionality (At. %) | Binding energy (eV) | | | |
| Pyridinic (N-6) | 398.8 | 18.98 | 21.61 | 25.26 |
| Pyrrolic (N-5) | 400.3 | 46.30 | 48.58 | 42.88 |
| Quaternary (N-Q) | 401.6 | 23.07 | 21.65 | 25.20 |
| N-oxide complexes (N-X) | 402.2 – 403.2 | 11.65 | 8.17 | 6.66 |

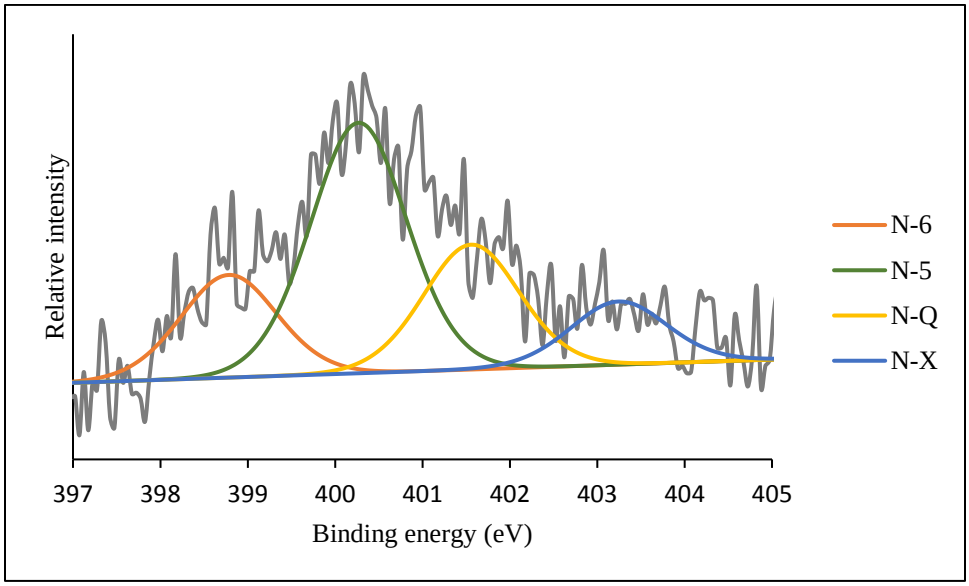


**Figure 4.3:** XPS N 1s spectra for the parent coal showing nitrogen functionalities denoted as N-5, N-6, N-Q, and N-X.

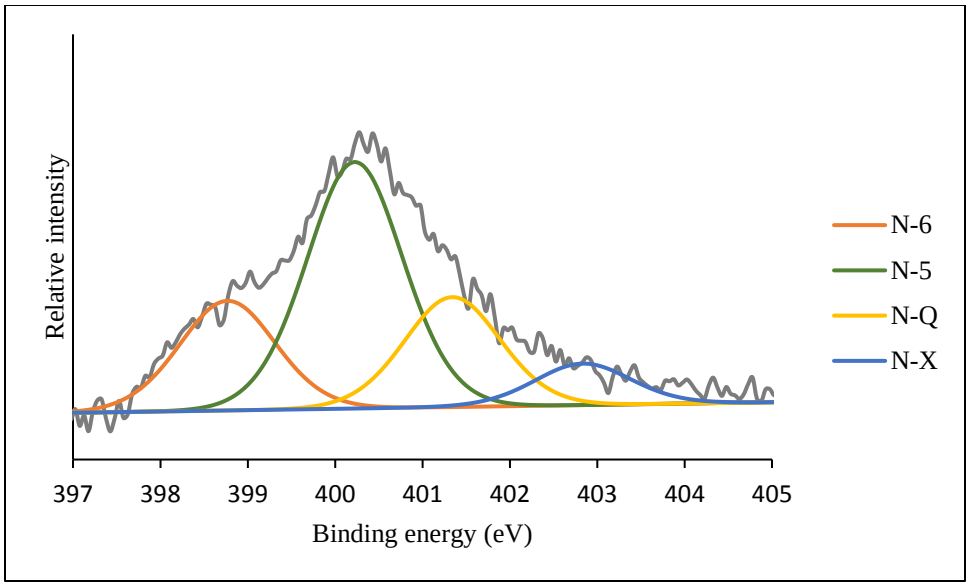


**Figure 4.4:** XPS N 1s spectra for the inertinite-rich sample showing nitrogen functionalities denoted as N-5, N-6, N-Q, and N-X.

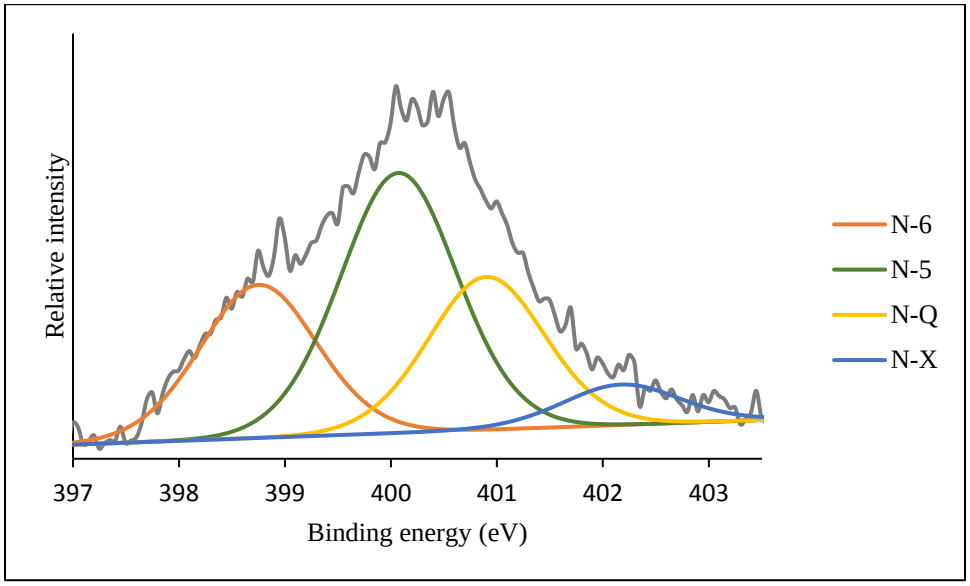


**Figure 4.5:** XPS N 1s spectra for the vitrinite-rich sample showing nitrogen functionalities denoted as N-5, N-6, N-Q, and N-X.

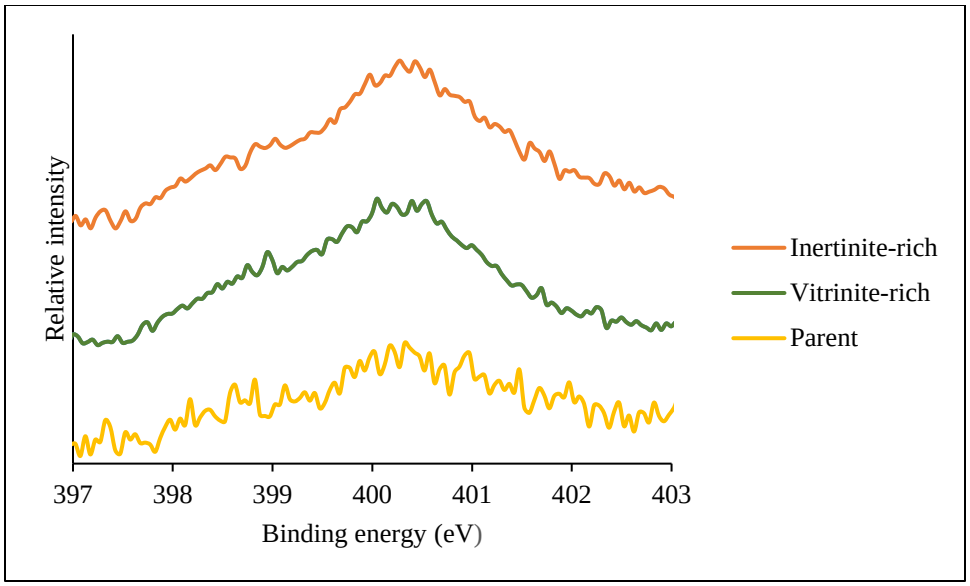


**Figure 4.6:** Measured XPS N 1s spectra for the inertinite-rich, vitrinite-rich, and parent samples.

The XPS data suggests that the concentration of some nitrogen functionalities is more dependent on maceral composition than others. For instance, N-pyrrolic appears most abundant in inertinite, whereas N-quaternary is more abundant in vitrinite. In contrast, although N-pyridinic is most abundant in the vitrinite-rich sample, this form of nitrogen is lowest in the parent coal despite this sample having a higher proportion of vitrinite than the inertinite-rich sample. This may suggest some degree of independence between N-pyridinic and maceral group composition. Similarly, N-oxides complexes in these samples do not appear to follow a trend related to maceral group composition.

Furthermore, the vitrinite-rich sample has a proportion of inertinite (11.4 vol. %) which may have contributed to the N-pyrrolic and N-oxide complexes contents of this sample. Similarly, the inertinite-rich sample is also comprised of 29.8 vol% vitrinite. The lack of correlation between some nitrogen functionalities and maceral composition – also reported by Valentim et al. (2016) for coals from the Peach Orchard coal bed, southern Magoffin County (Kentucky, United States) – may be related to differences in bulk nitrogen contents determined during elemental analysis (Table 4.1) and the surface nitrogen concentrations as determined using XPS (Table 4.4) (Kelemen et al., 2006).

## 4.4. Discussion

### 4.4.1. $\delta^{13}C$ signatures of Witbank coals and C3 plants

The $\delta^{13}C$ signatures of organic matter derived from C3 plants is controlled by local conditions such as plant species, topographical position, latitude/altitude, soil moisture content, irradiance, and the degree of reuse of respired $CO_2$ (Bird and Ascough, 2012, and references therein). Glossopterid gymnosperms (among others, e.g. heterosporous lycopods) were the most important Gondwana coal-forming plants (Falcon, 1986; Glasspool, 2003a, 2003b; Jasper et al., 2013; Ruckwied et al., 2014), and the C3 photosynthesis pathway as suggested by the $\delta^{13}C$ values of the Witbank coals is consistent with this. Plants with C4 and crassulacean acid metabolism (CAM) photosynthesis pathways only became abundant within the last 8 Myr (Kohn, 2010), and their contribution coal-formation in the Permian would thus have been negligible.

According to Kohn (2010), a C3 isotopic value of between –26‰ VPDB and –27‰ VPDB is most appropriate for plants growing in dry climatic conditions. Southern Hemisphere climatic conditions during Gondwana times are interpreted to have been highly varied – ranging from cold, to cool, to temperate (Falcon, 1986; Cairncross, 2001; Cadle et al., 1993; Snyman and Botha, 1993; Jasper et al., 2013), becoming progressively warmer, specifically during formation of the No. 4 Seam of the Witbank Coalfield (Ruckwied et al., 2014). The water levels within the peat-forming environments are also interpreted to have been variable, comprising wet and drier periods (Falcon, 1989; Glasspool, 2003b; Ruckwied et al., 2014). The interchange between the wet and dry periods would have given rise to mostly vitrinite and inertinite macerals respectively (Glasspool, 2003b; Moroeng et al., 2018), accounting for the general alternation of bright and dull bands observed in the coals (Falcon, 1989).

In their study, Suto and Kawashima (2016) mapped the $\delta^{13}C$ values for coals of various ages from around the globe. They found that the Tertiary coals of Indonesia had the lowest $\delta^{13}C$ average value (–27.4 ± 0.8‰ VPDB), whereas South African Permian counterparts had the highest (–23.7 ± 0.7‰ VPDB), and that there is a general trend of an increase in $\delta^{13}C$ with age between the two extreme values. The variation in $\delta^{13}C$ values with coal age is termed “age effect”, and is related to changes in the $\delta^{13}C$ composition of atmospheric $CO_2$ through time (Suto and Kawashima, 2016), and possibly changes in vegetation over Earth’s history. In addition to other parameters controlling the $\delta^{13}C$ of organic matter derived from C3 plants, the relatively

higher $\delta^{13}C$ values reported for the Witbank coals of the present study possibly also reflect the fluctuating water levels as well as the variable climatic conditions prevailing during the development of the coal-forming vegetation, and during the time of subsequent peatification processes.

### 4.4.2. Contribution of different plant tissues to the isotopic values of the coal samples

The isotopic signatures of modern plants are variable between the different organs, for example, between trunks, branches, and leaves (Hall et al., 2008; Bird and Ascough, 2012). However, the dominance of macerals overwhelmingly derived from woody tissues in the coal samples of the present study, including collotelinite, collodetrinite, semifusinite, and fusinite (Table 1), suggests that the contribution of other plant organs to the overall stable isotope values is minimal. The proportion of macerals derived from non-woody, particularly plant organ/tissue-specific precursors such as corpogelinite, gelinite, secretinite, and most liptinite macerals (ICCP, 1998, 2001; Pickel et al., 2017) is relatively low in both the parent and the density-fractionated samples. Funginite, derived from fungal tissues (ICCP, 2001), is completely absent in these Witbank coal samples. Because of the low proportion of these macerals and other inertinite macerals such as macrinite and micrinite, which have an origin specifically exclusive of charring of plant matter (ICCP, 2001; Hower et al., 2013; Richardson et al., 2012; O'Keefe et al., 2013; Valentim et al., 2016), the error their presence may introduce is considered negligible for the purpose of the current study.

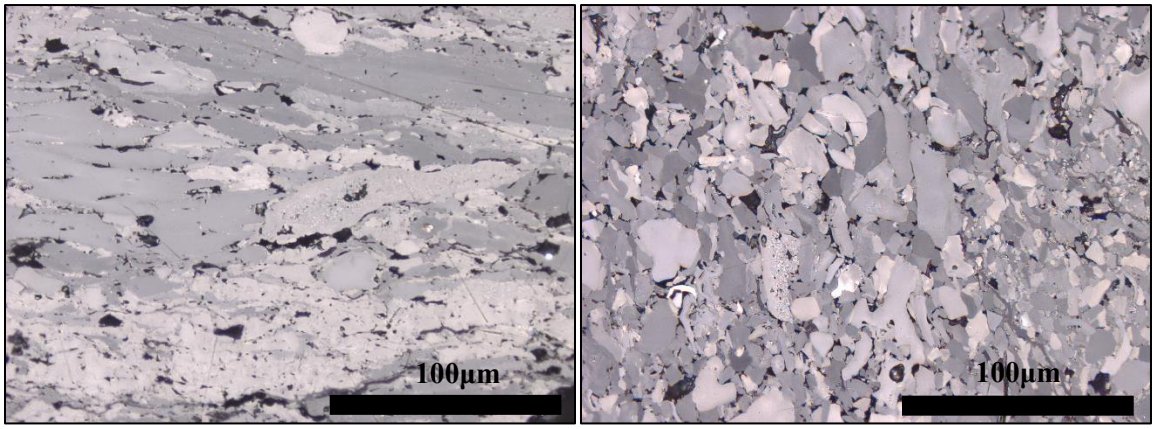


**Figure 4.7:** Inertodetrinite observed in the inertinite-rich sample. 500x magnification, reflected light with oil immersion. Scale is indicated.

Owing to the variety of macerals that may contribute to inertodetrinite formation (Hagelskamp and Snyman, 1988; ICCP, 2001; O'Keefe et al., 2013), the relatively high proportion of this

maceral in the parent and inertinite-rich samples of the present study (Table 4.1) may pose an interpretational challenge. This is because of the different plant tissues, with potentially different isotopic signatures, that may have contributed to the formation of this maceral. However, since inertodetrinite is a secondary maceral and is believed to represent fragmented particles of other macerals including fusinite and semifusinite (Figure 4.7) (Hagelskamp and Snyman, 1988; ICCP, 2001; O'Keefe et al., 2013), the precursor plant tissues to inertodetrinite are likely to have been similar to the precursors of the dominant, primary inertinite macerals.

Therefore, the starting isotopic composition of the woody precursors for the dominant inertinite and vitrinite macerals present in the samples can be interpreted to have been the same. As a result, the differences currently observed in the stable isotope values of the density-fractionated coal samples may be interpreted to reflect early coal-formation processes.

### 4.4.3. Implications of $\delta^{15}N$ and $\delta^{13}C$ values and nitrogen functionalities on coal-forming processes

Wood is composed of two principal components, lignin and cellulose, with the latter enriched in the isotopically heavier $^{13}C$ (Spiker and Hatcher, 1987; Whiticar, 1996; Czimczik et al., 2002; Bird and Ascough, 2012). Early biochemical coalification processes preferentially eliminate cellulose, selectively preserving the more resistant lignin (Teichmüller, 1989; Guo and Bustin, 1998; Czimczik et al., 2002), with the isotopic signature approaching that of the residual lignin (Spiker and Hatcher, 1987). During humification, the degradation of cellulose present in wood is driven by bacterial activity (Spiker and Hatcher, 1987; Teichmüller, 1989; Rimmer et al., 2006; Skrzypek et al., 2010). Cellulose-poor, wood-derived coal components may, therefore, be expected to be lower in $^{13}C$ relative to the precursor. It should be mentioned that humified matter derived from non-woody plants, e.g. moss (Sphagnum), may exhibit higher $\delta^{13}C$ values (Skrzypek et al., 2010) due to the inherently low cellulose content of the source vegetation in question (Plank, 1946).

The formation of vitrinite macerals is widely accepted to have occurred through the humification and gelification of wood (Spiker and Hatcher, 1987; Teichmüller, 1989; ICCP, 1998; Hower et al., 2013; O'Keefe et al., 2013). The higher $\delta^{15}N$ value (lower $^{14}N$) for the vitrinite-rich sample of the current study, relative to the inertinite-rich counterpart, suggests humification-related bacterial degradation where $^{14}N$ was preferentially eliminated (Spiker and Hatcher, 1987;

Rimmer et al., 2006; Skrzypek et al., 2010). The absence of anatomical structure in the vitrinite macerals (Figure 4.8) is also consistent with degradation by organisms, during which the anatomical structure of the botanical precursor would have been destroyed. Higher $\delta^{15}N$ values may also suggest an oxygenated peat-forming environment (Lehmann et al., 2002), which may suggest that some peat in the Witbank Coalfield accumulated in fresh-water and/or well-drained environments.

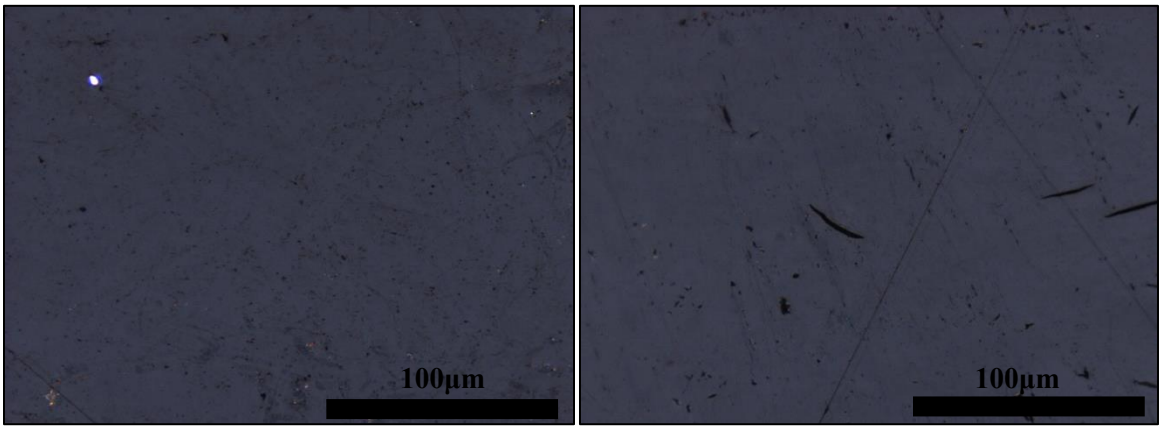


**Figure 4.8:** Vitrinite macerals with anatomical structure absent, observed in the vitrinite-rich sample. 500x magnification, reflected light with oil immersion. Scale is indicated.

In addition, for the vitrinite-rich sample, the low $^{14}N$ value corresponds with a higher proportion of both N-quaternary and N-pyridinic. According to Kelemen et al. (2006), N-quaternary is formed during vitrinization processes, whereas heating causes the destruction of this nitrogen functionality. Similarly, N-pyrrolic may be produced during the charring of plant matter (Schulten and Schnitzer, 1998, and references therein), as a result of the conversion of amines (Kelemen et al., 2006). The higher N-quaternary for the vitrinite-rich sample is consistent with vitrinization as a pathway for the dominant macerals of this sample. Although N-pyridinic may also be produced during charring of plant matter (Schulten and Schnitzer, 1998, and references therein; Kelemen et al., 2006), for the vitrinite-rich sample of the present study, the lower $^{14}N$ value along with the higher proportion of this nitrogen form suggests that the formation of the vitrinite macerals was driven primarily by bacterial activity in the presence $NH_3$.

The comparatively lower $\delta^{15}N$ value (higher $^{14}N$) of the inertinite-rich sample along with the higher concentration of N-pyrrolic and N-oxide complexes (Table 4.4), and the presence of anatomical structure in fusinite and semifusinite (Figure 4.9), suggests limited or no bacterial degradation of the source vegetation. In contrast to vitrinite formation, the formation of fusinite

and semifusinite is generally preceded by processes that are able to preserve the anatomical structures observed in these macerals (Figure 4.9). Although aerial oxidation in a cold climate setting has historically been cited for the formation of South African inertinite macerals in their entirety (Falcon, 1986; Hagelskamp and Snyman, 1988; Cadle et al., 1993; Snyman and Botha, 1993), the climate had warmed by time of the formation of the No. 4 Seam of the Witbank Coalfield (Ruckwied et al., 2014). Furthermore, there exists multiple pathways for the formation of the different macerals of the inertinite group (ICCP, 2001; Hower et al., 2013; O'Keefe et al., 2013), that are not accounted for by the singular oxidation pathway. As such, an alternative pathway could be responsible for the structures exhibited by the fusinite and semifusinite macerals of the coal seam assessed herein. Wood-charring produces structures that are greatly comparable to those observed in the inertinite macerals (Scott, 1989, 2010; Jones and Chaloner, 1991; Guo and Bustin, 1998; Glasspool, 2003a, 2003b; Scott and Glasspool, 2007; Ascough et al., 2010; Hower et al., 2013; Jasper et al., 2013), and may also account for the $\delta^{15}N$ and $\delta^{13}C$ values and the main nitrogen functionalities of the inertinite-rich sample (Schulten and Schnitzer, 1998, and references therein; Turekian et al., 1998; Czimczik et al., 2002; Kelemen et al., 2006; Rimmer et al., 2006; Ascough et al., 2008; Hall et al., 2008; Bird and Ascough, 2012).

The lower N-quaternary and higher N-pyrrolic of the inertinite-rich sample relative to the vitrinite-rich counterpart may be interpreted to reflect charring as a pathway for the formation of the dominant macerals of this sample (Schulten and Schnitzer, 1998, and references therein; Kelemen et al., 2006). The higher proportion of N-oxide complexes for the inertinite-rich sample may also be taken to consistent with this, suggesting exposure of the dominant macerals during the charring process.

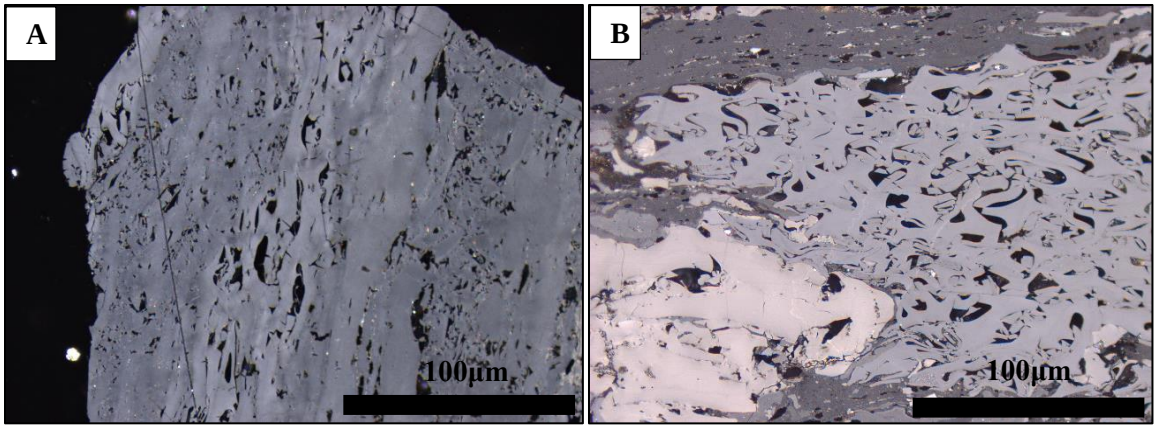


**Figure 4.9:** Inertinite macerals exhibiting anatomical structures, observed in the inertinite-rich sample. A – semifusinite; B – fusinite surrounded by other macerals. 500x magnification, reflected light with oil immersion. Scale is indicated.

A study discussing the presence of 6-aromatic carbon rings in the inertinite-rich sample, interpreted to be guaiacol and syringol – the principal products of low-temperature (below 400 °C) lignin pyrolysis (Asmadi et al., 2011; Kawamoto, 2017), has been published by Moroeng et al. (2018a). Further, Moroeng et al. (2018b) presented ESR results indicating that the inertinite-rich sample has a higher radical concentration relative to the vitrinite-rich counterpart, thus suggesting that the major organic components of the former sample were charred in their geologic history. Following on from the findings presented, and owing to: (1) the greater proportion of both N-pyrrolic and N-oxide complexes in the inertinite-rich sample relative to the vitrinite-rich counterpart; and, (2) the presence of charcoal within the Main Karoo Basin of South Africa (Glasspool, 2003a, 2003b; Jasper et al., 2013), the $\delta^{15}N$ and $\delta^{13}C$ values for the inertinite-rich sample of the present study are explained within the context of charring of plant matter.

With regards to $\delta^{13}C$, Hall et al. (2008) report a lower value relative to source vegetation following charring of modern yellowwoods (Podocarpus) at temperatures between 450 °C and 500 °C. Likewise, Czimczik et al. (2002) report a lower $\delta^{13}C$ value following charring of softwood (Pinus sylvestris L.) and hardwood (Betula pendula Roth). Similar observations were made by Turekian et al. (1998), though at lower temperatures (below 240 °C). This depletion of $\delta^{13}C$ is related to the thermal degradation of cellulose (Tukerian et al., 1998; Czimczik et al., 2002; Ascough et al., 2008; Hall et al., 2008; Bird and Ascough, 2012). Guo and Bustin (1998) report that cellulose is almost completely degraded following charring of wood at 320 °C for 40 minutes. Thermal reactions involving the lignin component, from which coal derives its

aromaticity (Spiker and Hatcher, 1987), would have given rise to the 6-aromatic carbon rings reported by Moroeng et al. (2018a) for the inertinite-rich sample.

Since the major components of the Witbank inertinite-rich sample were not subjected to bacterial degradation, as evidenced by present anatomical structure in the dominant inertinite macerals (Figure 9) and the lower concentration of N-quaternary (Table 4.4), the $\delta^{15}N$ of this coal sample may be expected to have remained relatively unaffected. Unlike $\delta^{13}C$, the $\delta^{15}N$ values of wood-derived charcoal are largely independent of photosynthetic pathway and composition of the original plant matter (Tukerian et al., 1998; Bird and Ascough, 2012). However, some conclusions can still be drawn based on the $\delta^{15}N$ value of the inertinite-rich sample of this study.

Particulate matter produced during charring of wood has higher $\delta^{15}N$ values relative to the source vegetation, and resultant charcoal (Tukerian et al., 1998). In contrast, the volatile phase ($NH_3$, $NO_x$, and $N_2O$) has lower values. During laboratory charring of plant matter (starting plant material Eucalyptus), Turekian et al. (1998) also observed a bimodal distribution of $\delta^{15}N$ depending on the heating temperature. This was ascribed to the presence of two distinct "nitrogen pools" in the plant matter, with one readily volatilized at low temperatures. The volatilization of free ammonia and the deamination of free amino acids were cited as being responsible for the higher $\delta^{15}N$ values at low-temperatures (Tukerian et al., 1998, and references therein; Bird and Ascough, 2012). At higher temperatures (above 200 °C) however, the $\delta^{15}N$ value of charred wood reverts back to the value of the source vegetation as demonstrated by Tukerian et al. (1998).

Because of the generally lower $\delta^{15}N$ values of the inertinite-rich sample relative to the vitrinite-rich counterpart, charring of the major inertinite macerals can be interpreted to have occurred at temperatures above 200 °C. In which case, the $\delta^{15}N$ value of the inertinite-rich sample may be taken to be comparable to that of the original plant matter. Alternatively, if lower temperatures were to be considered, the $\delta^{15}N$ value would have to be interpreted as higher relative to the source vegetation. Of course, the stable isotope composition of the source vegetation is unknown. An argument can also be made that the $\delta^{15}N$ value of inertinite-rich sample would either exceed or at least be comparable to that of the vitrinite-rich sample, if charring had occurred at lower temperatures. However, this is clearly not so.

If the greater degree of heterogeneity within the inertinite-rich sample (as evidenced by the comparatively larger standard deviation, Table 4.3 and Figure 4.1) also reflects differences within the inertinite maceral group, this may be attributed to differences in charring conditions and/or degrees of charring (Guo and Bustin, 1998; Ascough et al., 2008; Bird and Ascough, 2012). Lower $\delta^{13}C$ values may reflect relatively high temperature charring when compared to the higher $\delta^{13}C$ values of the same coal sample. The charring temperature would have determined whether fusinite or semifusinite was produced, possibly dependent on the moisture content of the affected vegetation (Glasspool, 2003b; Hower et al., 2013; Moroeng et al., 2018a, 2018b). The abundance of semifusinite in South African coals, exhibiting different levels of reflectance even within a singular coal sample (Hagelskamp and Snyman, 1988; Snyman and Botha, 1993), can be interpreted to suggest differences in the extent of charring of mostly wet source vegetation, perhaps also indicative of charring of standing vegetation (Glasspool, 2003b).

Glasspool (2003b) previously proposed peat charring for the formation of the inertinite macerals of the No. 2 Seam (Witbank Coalfield) based on the comparably high reflectance of both cell lumens and infilling gelified material. However, for the coal sample of the No. 4 Seam Upper of this study, high reflecting macerals with absent anatomical structures are only minor components. The presence of anatomical structure in the inertinite macerals suggests charring prior to humification-related degradation (Guo and Bustin, 1998; Hower et al., 2013). Therefore, for fusinite and semifusinite, the charred plant matter would subsequently have been deposited into a swamp with humified and/or gelified vitrinite-forming peat already present, near the site where the material was charred, possibly indicative of crown fires when considering the charring of standing vegetation. In the case of the smaller fragments that gave rise to inertodetrinite, the charred material could subsequently have been mechanically reworked by sedimentary processes (wind, water and/or gravity).

### 4.5. Conclusion

Certain inertinite macerals present in the coal assessed in this study are likely to have a fire-origin, contrary to the aerial oxidation pathway proposed by earlier workers. The coal sample was density-fractionated to create a vitrinite-rich and an inertinite-rich sub-sample. Collodetrinite and collotelinite were abundant in the vitrinite-rich sample (81 vol% total vitrinite), whereas the inertinite-rich sample was dominated by fusinite, semifusinite, and inertodetrinite (63 vol% total

inertinite). Because these samples were iso-rank, differences in the isotopic values and proportions of nitrogen functionalities were considered to reflect the early coal-formation pathways for the dominant macerals in each of the density-fractionated samples. Following the determination of $\delta^{15}N$ and $\delta^{13}C$ and nitrogen functionalities, it was found that:

- The vitrinite-rich sample has a comparatively lower $\delta^{13}C$ and higher $\delta^{15}N$ value than the inertinite-rich sample. The loss of $^{14}N$ was attributed to the degradation of plant matter through bacterial activity. The absence of morphology in the vitrinite macerals and the higher N-quaternary for this sample is consistent with this interpretation.
- Fusinite and semifusinite possess anatomical structures, and a relatively lower $\delta^{15}N$ value for the inertinite-rich sample. This was interpreted to reflect limited degradation of plant matter by organisms. The higher concentration of N-pyrrolic and N-oxide complexes for the inertinite-rich sample possibly reflect charring.
- Moreover, charring of plant matter is typically invoked to account for the preserved anatomical structure of inertinite macerals. Charred plant matter also has a lower $\delta^{13}C$ signature relative to the botanical precursor. However, the $\delta^{15}N$ may remain similar to that of the source vegetation, dependent on charring conditions. The lower $\delta^{15}N$ value of the inertinite-rich sample suggest charring at temperatures above 200 °C.
- Inertodetrinite present in the samples was suggested to have formed through the reworking of charred plant matter.

Thus, although based on a single parent coal sample, the $\delta^{15}N$ and $\delta^{13}C$ values and the concentration of nitrogen functionalities for the inertinite-rich sample relative to vitrinite-rich counterpart were interpreted to support a fire-origin for the major inertinite macerals (specifically fusinite and semifusinite) of the coal from the No. 4 Seam Upper, Witbank Coalfield. These results support the conclusions reached by Moroeng et al. (2018a, 2018b) using $^{13}C$ CP-MAS SS NMR and ESR on the same samples.

### 4.6. References

Ascough, P.L., Bird, M.I., Scott, A.C., Collinson, M.E., Cohen-Ofri, I., Snape, C.E., Le Manquais, K., 2010. Charcoal reflectance measurements: implications for structural characterization and assessment of diagenetic alteration. Journal of Archaeological Science 37, 1590-1599.

Ascough, P.L., Bird, M.I., Wormald, P., Snape, C.E., Apperley, D., 2008. Influence of production variables and starting material on charcoal stable isotopic and molecular characteristics. Geochimica et Cosmochimica Acta 72, 6090-6102.

Asmadi, M., Kawamoto, H., Saka, S., 2011. Thermal reactions of guaiacol and syringol as lignin model aromatic nuclei. Journal of Analytical and Applied Pyrolysis 92, 88-98.

Bird, M.I., Ascough, P.L., 2012. Isotopes in pyrogenic carbon: A review. Organic Geochemistry 42, 1529-1539.

Cadle, A.B., Cairncross, B., Christie, A.D.M., Roberts, D.L., 1993. The Karoo Basin of South Africa: type basin for coal-bearing deposits of southern Africa. International Journal of Coal Geology 23, 117-157.

Cairncross, B., 2001. An overview of the Permian (Karoo) coal deposits of Southern Africa. Journal of African Earth Sciences 33, 529-562.

Czimczik, C., Preston, C.M., Schimdt, M.W.I., Werner, R.A., Schulze, E.-D., 2002. Effects of charring on mass, organic carbon, and stable carbon isotope composition of wood. Organic Geochemistry 33, 1207-1223.

Diessel, C.F.K., 1992. Coal-Bearing Depositional Systems. Springer-Verlag, Berlin Heidelberg. 721pp.

Falcon, R.M.S., 1986. A brief review of the origin, formation, and distribution of coal in southern Africa. In: Anhaeusser, C.R., Maske, S. (Eds.), Mineral Deposits of Southern Africa, Vols. I and II. Geological Society of South Africa, Johannesburg, pp. 1879-1898.

Falcon, R.M.S., 1989. Macro-and micro-factors affecting coal-seam quality and distribution in southern Africa with particular reference to the No. 2 seam, Witbank coalfield, South Africa. International Journal of Coal Geology 12 (1-4), 681-731.

Glasspool, I., 2003a. Palaeoecology of selected South African export coals from the Vryheid Formation, with emphasis on the role of heterosporous lycopods and wildfire derived inertinite. Fuel 82, 959-970.

Glasspool, I.J., 2003b. Hypautochthonous–allochthonous coal deposition in the Permian, South African, Witbank Basin No. 2 seam; a combined approach using sedimentology, coal petrology and palaeontology. International Journal of Coal Geology 53, 81-135.

Gröcke, D.R., Rimmer, S.M., Yoksoulian, L.E., Cairncross, B., Tsikos, H., van Hunen, J., 2009. No evidence for thermogenic methane release in coal from the Karoo-Ferrar large igneous province. Earth and Planetary Science Letters 277, 204-212.

Guo, Y., Bustin, R.M., 1998. FTIR spectroscopy and reflectance of modern charcoals and fungal decayed woods: implications for studies of inertinite in coals. International Journal of Coal Geology 37, 29-53.

Hagelskamp, H.H.B., Snyman, C.P., 1988. On the origin of low-reflecting inertinites in coals from the Highveld Coalfield, South Africa. Fuel 67, 307-313.

Hall, G., Woodborne, S., Scholes, M., 2008. Stable carbon isotope ratios from archaeological charcoal as palaeoenvironmental indicators. Chemical Geology 247 (3-4), 384-400.

Hower, J.C., O'Keefe, J.M.K., Wagner, N.J., Dai, S., Wang, X., Xue, W., 2013. An investigation of Wulantuga coal (Cretaceous, Inner Mongolia) macerals: Paleopathology of faunal and fungal invasions into wood and the recognizable clues for their activity. International Journal of Coal Geology 114, 44-53.

International Committee for Coal and Organic Petrology (ICCP)., 1998. The new vitrinite classification (ICCP System 1994). Fuel 77 (5), 349-358.

International Committee for Coal and Organic Petrology (ICCP)., 2001. The new inertinite classification (ICCP System 1994). Fuel 80 (4), 459-471.

Jasper, A., Guerra-Sommer, M., Abu Hamad, A.M.B., Bamford, M., Cerruti Bernardes-de-Oliveira, M.E., Tewari, R., Uhl, D., 2013. The burning of Gondwana: Permian fires on the southern continent – A palaeobotanical approach. Gondwana Research 24 (1), 148-160.

Jones, T.P., Chaloner, W.G., 1991. Fossil charcoal, its recognition and palaeoatmospheric significance. Palaeogeography, Palaeoclimatology, Palaeoecology (Global and Planetary Change Section) 97, 39-50.

Kawamoto, H., 2017. Lignin pyrolysis reactions. Journal of Wood Science 63 (2), 117-132.

Kelemen, S.R., Afeworki, M., Gorbaty, M.L., Kwiatek, P.J., Sansone, M., Walters, C.C., 2006. Thermal Transformations of Nitrogen and Sulfur Forms in Peat Related to Coalification. Energy & Fuels 20, 635-652.

Kohn, M.J., 2010. Carbon isotope composition of terrestrial C3 plants as indicators of (paleo)ecology and (paleo)climate. Proceedings of the National Academy of Sciences of the United States of America 107 (46), 19691-19695.

Lehmann, M.F., Bernasconi, S.M., Barbieri, A., McKenzie, J.A., 2002. Preservation of organic matter and alteration of its carbon and nitrogen isotope composition during simulated and in situ early sedimentary diagenesis. Geochimica et Cosmochimica Acta 66 (20), 3573-3584.

Ling, M-.X., Liu, Y., Zhang, H., Sun, W., 2014. Sample Preparation and X-Ray Fluorescence Analysis of Sulfide Ores. Analytical Letters 47, 1598-1605.

Maroto-Valer, M.M., Andresén, J.M., Snape, C.E., 1998. Verification of the linear relationship between carbon aromaticities and H/C ratios for bituminous coals. Fuel 77 (7), 783-785.

Moroeng, O.M., Roberts, R.J., Bussio, J.P., Dixon, R.D., 2017. Self-heating Potential of Coal Inferred from Elemental Data – A Case Study of the Witbank Coalfield of South Africa. Energy & Fuels 31 (11), 11811-11817.

Moroeng, O.M., Keartland, J.M., Roberts, R.J., Wagner, N.J., 2018b. Characterization of coal using electron spin resonance: implications for the formation of inertinite macerals in the Witbank Coalfield, South Africa. International Journal of Coal Science & Technology 5 (3), 385-398.

Moroeng, O.M., Wagner, N.J., Brand, D.J., Roberts, R.J., 2018a. A Nuclear Magnetic Resonance study: Implications for coal formation in the Witbank Coalfield, South Africa. International Journal of Coal Geology 188, 145-155.

O'Keefe, J.M.K., Bechtel, A., Christanis, K., Dai, S., DiMichele, W.A., Eble, C.F., Esterle, J.S., Mastalerz, M., Raymond, A.L., Valentim, B.V., Wagner, N.J., Ward, C.R., Hower, J.C., 2013. On the fundamental difference between coal rank and coal type. International Journal of Coal Geology 118, 58-87.

Phiri, Z., Everson, R.C., Neomagus, H.W.J.P., Wood, B.J., 2017. The effect of acid demineralising bituminous coals and de-ashing the respective chars on nitrogen functional forms. Journal of Analytical and Applied Pyrolysis 125, 127-135.

Phiri, Z., Everson, R.C., Neomagus, H.W.J.P., Wood, B.J., 2018. Transformation of nitrogen functional forms and the accompanying chemical-structural properties emanating from pyrolysis of bituminous coals. Applied Energy 216, 414-427.

Pickel, W., Kus, J., Flores, D., Kalaitzidis, S., Christanis, K., Cardott, B.J., Misz-Kennan, M., Rodrigues, S., Hentschel, A., Hamor-Vido, M., Crosdale, P., Wagner, N., ICCP., 2017. Classification of liptinite – ICCP System 1994. International Journal of Coal Geology 169, 40-61.

Plank, N., 1946. The Nature of Cellulose in Sphagnum. American Journal of Botany 33 (5), 335-337.

Richardson, A.R., Eble, C.F., Hower, J.C., O'Keefe, J.M.K., 2012. A critical re-examination of the petrology of the No. 5 Block coal in eastern Kentucky with special attention to the origin of inertinite macerals in the splint lithotypes. International Journal of Coal Geology 98, 41-49.

Rimmer, S.M., Rowe, H.D., Taulbee, D.N., Hower, J.C., 2006. Influence of maceral content on $\delta^{13}C$ and $\delta^{15}N$ in a Middle Pennsylvanian coal. Chemical Geology 225, 77-90.

Ruckwied, K., Götz, A.E., Jones, P., 2014. Palynological records of the Permian Ecca Group (South Africa): Utilizing climatic icehouse-greenhouse signals for cross basin correlations. Palaeogeography, Palaeoclimatology, Palaeoecology 413, 167-172.

Schulten, H.-R., Schnitzer, M., 1998. The chemistry of soil organic nitrogen: a review. Biology and Fertility of Soils 26, 1-15.

Scott, A.C., 1989. Observations on the nature and origin of fusain. International Journal of Coal Geology 12, 443-475.

Scott, A.C., 2010. Charcoal recognition, taphonomy and uses in palaeoenvironmental analysis. Palaeogeography, Palaeoclimatology, Palaeoecology 291, 11-39.

Scott, A.C., Glasspool, I.J., 2007. Observations and experiments on the origin and formation of inertinite group macerals. International Journal of Coal Geology 70 (1-3), 53-66.

Skrzypek, G., Jezierski, P., Szynkiewicz, A., 2010. Preservation of primary stable isotope signatures of peat-forming plants during early decomposition – observation along an altitudinal transect. Chemical Geology 273, 238-249.

Slater, B.J., McLoughlin, S., Hilton, J., 2015. A high-latitude Gondwana lagerstätte: The Permian permineralised peat biota of the Prince Charles Mountains, Antarctica. Gondwana Research 27, 1446-1473.

Snyman, C.P., Botha, W.J., 1993. Coal in South Africa. Journal of African Earth Sciences 16 (1/2), 171-180.

South African National Standards (SANS) 17246:2011 (ISO 17246:2010). Coal - Proximate analysis.

South African National Standards (SANS) 17247:2006 (ISO 17247:2005). Coal - Ultimate analysis.

South African National Standards (SANS) 1928:2009 (ISO 1928:2009). Solid mineral fuels - Determination of gross calorific value by the bomb calorific method, and calculation of net calorific value.

South African National Standards (SANS) 334:1992 (ISO 334:1992). Solid mineral fuels - Determination of total sulfur - Eschka method.

South African National Standards (SANS) 7404-2:2015 (ISO 7404-2:2009). Methods for the petrographic analysis of coals Part 2: Methods of preparing coal samples.

South African National Standards (SANS) 7404-3:2016 (ISO 7404-3:2009). Methods for the petrographic analysis of coals - Part 3: Method of determining maceral group.

South African National Standards (SANS) 7404-5:2016 (ISO 7404-5:2009). Methods for the petrographic analysis of coals - Part 5: Method of determining microscopically the reflectance of vitrinite.

South African National Standards (SANS) 7936:2010 (ISO 7936:1992). Hard coal – Determination and presentation of float and sink characteristics – General directions for apparatus and procedures.

Spiker, E.G., Hatcher, P.G., 1987. The effects of early diagenesis on the chemical and stable carbon isotopic composition of wood. Geochimica et Cosmochimica Acta 51 (6), 1385-1391.

Suto, N., Kawashima, H., 2016. Global mapping of carbon isotope ratios in coal. Journal of Geochemical Exploration 167, 12-19.

Teichmüller, M., 1989. The genesis of coal from the viewpoint of coal petrology. In: Lyons, P.C., Alpern, B. (Eds.), Peat and Coal: Origin, Facies, and Depositional Models. International Journal of Coal Geology 12, 1-87.

Turekian, V.C., Macko, S., Ballentine, D., Swap, R.J., Garstang, M., 1998. Causes of bulk carbon and nitrogen isotopic fractionations in the products of vegetation burns: laboratory studies. Chemical Geology 152, 181-192.

Valentim, B., Algarra, M., Guedes, A., Ruppert, L.F., Hower, J.C., 2016. Notes on the origin of copromacrinite based on nitrogen functionalities and $\delta^{13}C$ and $\delta^{15}N$ determined on samples from the Peach Orchard coal bed, southern Magoffin County, Kentucky. International Journal of Coal Geology 160-161, 63-72.

Van Niekerk, D., Pugmire, R.J., Solum, M.S., Painter, P.C., Mathews, J.P., 2008. Structural characterization of vitrinite-rich and inertinite-rich Permian-aged South African bituminous coals. International Journal of Coal Geology 76, 290-300.

Whiticar, M.J., 1996. Stable isotope geochemistry of coals, humic kerogens and related natural gases. International Journal of Coal Geology 32, 191-215.

# Chapter 5

## Comparative study of a vitrinite-rich and an inertinite-rich Witbank coal using pyrolysis-gas chromatography, South Africa

**ABSTRACT**

The study aims to compare iso-rank vitrinite-rich and inertinite-rich coal samples to understand the impact of coal-forming processes on pyrolysis chemistry. A medium rank C bituminous coal was density-fractionated to create a vitrinite-rich and an inertinite-rich sub-sample. The vitrinite-rich sample has 83 vol. % total vitrinite (mineral-matter-free basis), whereas the inertinite-rich counterpart has 66 vol. % total inertinite. The vitrinite-rich sample is dominated by collotelinite and collodetrinite. Fusinite, semifusinite, and inertodetrinite are the main macerals of the inertinite-rich sample. For three samples, molecular chemistry was evaluated using a pyrolysis gas chromatograph (py-GC) equipped with a thermal desorption unit (TDU) coupled to a time of flight (TOF) mass spectrometer (MS) (py-GC/MS) and solid-state nuclear magnetic resonance ($^{13}$C CP-MAS SS NMR). The pyrolysis products of the coal samples are generally similar, comprised of low and high molecular weight alkanes, alkylbenzenes, alkylphenols, and alkyl-subtituted polycyclic aromatic hydrocarbons, though the vitrinite-rich sample is chemically more diverse. The lack of diversity exhibited by the inertinite-rich sample upon pyrolysis may be interpreted to suggest that major components were heated in their geologic history. Based on the $^{13}$C CP-MAS SS NMR analysis, the inertinite-rich sample has a greater fraction of phenolics, reflected in the py-GC/MS results as substituted and unsubstituted derivatives. The greater abundance of phenolics for the inertinite-rich sample may suggest a fire-related origin for the dominant macerals of this sample. The $C_2$-alkylbenzene isomers (p-xylene and o-xylene) were detected in the pyrolysis products for the vitrinite-rich and inertinite-rich samples, though more abundant in the former. The presence of these in both samples likely reflects common source vegetation for the dominant vitrinite and inertinite macerals.

**Keywords:** Py-TD-GC-TOFMS; Main Karoo Basin; Pyrolysis products; $^{13}$C CP-MAS SS NMR; Molecular chemistry; Phenolics; Xylene ($C_2$-alkylbenzene) isomers.

## 5.1. Introduction

The organic chemistry of coal is a complex product of the various progenitors for the individual macerals. During peatification, diagenesis, and subsequent coalification processes, the original vegetation is decomposed, altered, and ultimately transformed into coal. South African coals occurring in the Main Karoo Basin (MKB) are generally rich in inertinite with variable proportions of vitrinite, a relationship which may considered to be the inverse of that observed in most northern hemisphere coals (Falcon, 1986; Snyman and Botha, 1993; O'Keefe et al., 2013). The formation of the inertinite-rich Karoo-aged coals need to be understood in terms of the original material, and the origin pathways along which the inertinite and vitrinite macerals evolved.

Most vitrinite macerals are derived from the humification and gelification of woody tissues composed of lignin, cellulose, and a hemicellulose fraction (Teichmüller, 1989; van Krevelen, 1993; Hatcher and Clifford, 1997; ICCP, 1998; O'Keefe et al., 2013). Instead of the wood itself, other vitrinite macerals such as corpogelinite and gelinite are derived primarily from cell wall secretions and the contents thereof, or alternatively, from humic gels infilling cells, pores, and fissures (ICCP, 1998; O'Keefe et al., 2013). The origin of inertinite macerals is variable for the different macerals belonging to this group (van Krevelen, 1993; ICCP, 2001), derived through multiple origin pathways (O'Keefe and Hower, 2011; Hower et al., 2011a, 2013; O'Keefe et al., 2013; Moroeng et al., 2018). However, there is some general consensus that some macerals of this group, such as fusinite and semifusinite, formed through the charring of woody plant matter (Austen et al., 1966; Scott, 1989, 2002, 2010; Diessel, 1992; ICCP, 2001; Glasspool, 2003a, 2003b; Scott and Glasspool, 2007; Hower et al., 2013; O'Keefe et al., 2013; Moroeng et al., 2018). Other authors contend that semifusinite may also form through the aerial oxidation of parechymatous and xylem tissues of plants (Falcon, 1986; Falcon and Snyman, 1986; Hagelskamp and Snyman, 1988; Snyman, 1989; Cadle et al., 1993; Snyman and Botha, 1993; Taylor et al., 1998; ICCP, 2001). Other inertinite macerals form through the degradation of plant matter by organisms (macrinite), and from the remains of the organisms (funginite) (Moore et al., 1996; Moore and Shearer, 1997; ICCP, 2001; Hower et al., 2009, 2011b; Richardson et al., 2012), or from the partially digested excretion and/or regurgitation products (so-called copromacrinite) of said organisms (Hower et al., 2011a, 2013; O'Keefe et al., 2013; Valentim et al., 2016). Inertodetrinite represents reworked plant matter that would have produced primary

inertinite macerals, and secretinite reflects extreme oxidation or charring of resin and humic gels (ICCP, 2001; O'Keefe et al., 2013).

The organic chemical composition of coal, with coal being a product of most kingdoms of life (Hower et al., 2009, 2011b), is thus informed by: (1) the various botanical and zoological precursor materials; (2) processes that altered the matter during peatification, diagenesis, and subsequent coalification processes; (3) the level of coal maturity; as well as, (4) the depositional environment in its entirety, what Hower et al. (2011b, p. 187) term the "total environment". Various analytical techniques have been used in an attempt to elucidate the chemistry of the maceral components of coal. Although there are numerous studies reporting on the pyrolysis-gas chromatography mass spectrometry results for various macerals, and especially vitrinite-rich coals of the northern hemisphere (e.g., Meuzelaar et al., 1984; Senftle et al., 1986; Senftle and Larter, 1987: Nip et al., 1988, 1992; Eglinton et al., 1990, 1991; Boreham and Powell, 1991; Powell et al., 1991; van Krevelen, 1993, and references therein; Hartgers et al., 1994; Veld et al., 1994; Han et al., 1995; Odden and Barth, 2000; Davidson, 2004, and references therein; Sun and Horsfield, 2005; Liu and Peng, 2008; al Sandouk-Lincke et al., 2014; Zieger et al., 2018), studies using South African coals which are typically dominated by inertinite macerals are comparatively uncommon.

Fabiańska and Kruszewska (2003) used liquid gas chromatography-mass spectrometry (GC-MS) in an investigation into the biomarker distribution of coals from various South African coalfields. Pone et al. (2007) report spontaneous combustion by-products determined using gas chromatography for coals of the Witbank and Sasolburg Coalfields. Amongst other analytical techniques, Van Niekerk et al. (2008) used flash-pyrolysis gas chromatography mass spectrometry (flash-pyrolysis GC/MS) to compare the organic chemical structure of vitrinite-rich Waterberg and inertinite-rich Highveld coals. Sehume et al. (2017) used gas chromatography (GC) with flame-ionization detection (FID) to assess the quality of phenol-derived liquids from a Waterberg bituminous coal. There also appears to be concerted efforts to address the lack of studies on the chemical-structural properties of South African coals using advanced analytical methods such as solid-state nuclear magnetic resonance (NMR), wide angle X-ray diffraction-carbon fraction analysis (WAXRD-CFA), fourier transform infrared spectroscopy (FTIR), computer controlled scanning electron microscopy (CCSEM), matrix assisted laser desorption

ionization-time-of-flight mass spectrometry (MALDI-TOF-MS), X-ray photoelectron spectroscopy (XPS), high-resolution transmission electron microscopy (HRTEM), small-angle X-ray scattering (SAXS), and others (e.g., Van Niekerk et al., 2008; Van Niekerk and Mathews, 2010; Malumbazo et al., 2011; Strydom et al., 2011; Hattingh et al., 2013; Coetzee et al., 2015; Okolo et al., 2015; Roberts et al., 2015; Louw et al., 2016; Moroeng et al., 2018; Phiri et al., 2018).

The main purpose of the present study is to examine differences and/or similarities in the organic molecular chemistry of iso-rank coals, a vitrinite-rich and an inertinite-rich coal, using a pyrolysis gas chromatograph (py-GC) equipped with a thermal desorption unit (TDU) coupled to a time of flight (TOF) mass spectrometer (MS) (py-GC/MS) in order to understand the effect of source vegetation and origin pathways on coal pyrolysis products. As liptinite normally accounts for a minor proportion of the coals of the MKB (Falcon and Snyman, 1986; Kruszewska, 2003; Van Niekerk et al., 2008), it is omitted from the present discussion. A medium rank C bituminous Witbank coal from the No. 4 Seam Upper was density-fractionated to create the required samples, enhancing compositional differences between the samples without introducing rank-dependent variations. Along with the widely used carbon-13 cross-polarization magic-angle-spinning solid-state nuclear magnetic resonance analysis ($^{13}$C CP-MAS SS NMR), py-GC/MS is used to investigate the organic molecular chemistry of the samples. The $^{13}$C CP-MAS SS NMR results of these samples (including spectra) were reported by Moroeng et al. (2018). However, aside from the aromatic cluster sizes, other $^{13}$C CP-MAS SS NMR chemical-structural parameters are not explored by Moroeng et al. (2018).

## 5.2. Samples and analytical methods

### 5.2.1. Samples and preparation

A run-of-mine coal sample (weighing approximately 50 kg) was obtained from the No. 4 Seam Upper, Witbank Coalfield. Following crushing, a quarter of the original sample was reserved to represent the "parent" coal sample. The parent sample was density-fractionated at an RD of 1.3 and 1.8 to create the required vitrinite-rich and inertinite-rich samples, respectively, following South African National Standard (SANS) 7936 (2010).

### 5.2.2. Proximate, elemental, and petrographic analysis

The proximate (moisture, ash, volatile matter, and fixed carbon) and elemental analyses (C, H, N, O, and S) were undertaken at a commercial laboratory (Bureau Veritas, Centurion, South Africa) following prescribed SANS standards (SANS 334, 1992; SANS 17247, 2006; SANS 17246, 2011).

The samples were prepared for petrographic analysis as polished blocks following SANS 7404-2 (2015). The maceral analysis was undertaken following SANS 7404-3 (2016) by means of a 500 point-count, using a Zeiss AxioImager m2M reflected light microscope retrofitted with Hilgers Diskus Fossil components and software, at a total magnification of 500x using immersion oil. The mean random vitrinite reflectance (%RoVmr) of the coal was determined on the parent sample by a 100 point-count on collotelinite, following SANS 7404-5 (2016).

### 5.2.3. Nuclear magnetic resonance analysis

The $^{13}C$ CP-MAS SS NMR methodology is described extensively by Moroeng et al. (2018), and will only be briefly described in the present study.

$^{13}C$ CP-MAS SS NMR coupled with dipolar dephasing (CP-MAS/DD) was used to compare the coal samples, following the method described by Solum et al. (1989). These two experiments were performed on each sample to determine the structural differences between the parent coal, vitrinite-rich, and inertinite-rich samples. The structural parameters were calculated based on Solum et al. (1989) and Suggate and Dickinson (2004). The spectra were acquired using an Agilent VNMRS 500 MHz two-channel NMR spectrometer using 4 mm zirconia rotors and a 4 mm Chemagnetics TM T3 HXY MAS probe. All CP spectra were recorded with the latest VnmrJ 4.2 instrument software at ambient temperature with optimized high-power proton decoupling; a relaxation delay of 3 s and 10 000 scans were collected for obtaining sufficient signal-to-noise ratio. The power parameters were optimized for the Hartmann-Hahn match; the radio frequency fields were $\gamma CB1C = \gamma HB1H \approx 56$ kHz. The contact time selected for CP was 2 ms. The free induction decay recorded 2000 points and was Fourier transformed with a 125 Hz line broadening. Magic-angle-spinning (MAS) rate of 12 kHz and Admantane was used as an external chemical shift standard with the upfield methyl peak-referenced to 38.4 ppm.

The DD experiments were carried out under the same CP parameters with the interrupted decoupling constant of the tancpxidref sequence set to 40 μs, after first evaluating an incremental array of 10-100 μs time constants.

Regarding spectra processing, the integration reset points were adapted from Solum et al. (1989) and Mestrenova 11.02 "preset integral regions table" was made to ensure that the exact same regions were integrated reproducibly. The individual spectra were each phased and baseline corrected manually before integration. All spectra were processed in the same manner and by the same person to minimize operator bias. The absolute integral values were transferred to a Microsoft Excel spreadsheet for calculation of the coal structural parameters as per Solum et al. (1989). No variable contact time was performed as suggested by Solum et al. (1989), because of the long acquisition times. A contact time of 2 ms was used for all experiments and a correction factor of 1.3, derived from Solum et al. (1989), was used to correct the intensity of the bridgehead aromatic carbons (peak 135-90 ppm for DD) for the loss of magnetization during the interrupted decoupling.

### 5.2.4. Pyrolysis-gas chromatography mass spectrometry analysis

The samples were milled to a particle size of –212 μm for the py-GC/MS analysis. The py-TD-GC-TOFMS system used in this study consisted of an Agilent 6890B (Agilent Technologies, USA) gas chromatograph and a Pegasus III TOF-MS (LECO, USA) with a Gerstel autosampler, and is housed at the University of South Africa (Department of Chemistry, Florida, Johannesburg).

The coal was pyrolyzed at 700 °C for 1 minute. Thermal desorption was then carried out from 40 °C to 350 °C (3 minute hold time) at 240 °C $min^{-1}$. The desorbed volatiles were cryogenically focused using a Gerstel cooled injection system (CIS) at −25 °C using liquid nitrogen. The analytes moved onto the GC column through the transfer line heated at 350 °C and then separated using a Restek Rxi-17Sil MS capillary column (30 m × 0.25 mm × 0.25 μm) with helium as the carrier gas at a constant flow rate of 1.4 mL $min^{-1}$ throughout the analysis. The initial oven temperature was 50 °C and held for 1 minute, then increased to 300 °C at a rate of 9 °C/min and held constant for 2 minutes. The injection port and transfer line temperatures were maintained at 300 °C and 310 °C, respectively.

Mass acquisition was from 50 to 650 mass units at 10 spectra $s^{-1}$ data acquisition rate. The electron energy was 70 eV whilst mass spectrometer transfer line and ion source temperatures were 310 °C and 225 °C respectively. Data acquisition and processing was carried out using ChromaTOF software version 4.0 (LECO, USA). Peak identification was made using library matching using the National Institute of Standards & Technology (NIST) mass spectral library.

## 5.3. Results and discussion

### 5.3.1. Proximate, elemental, and petrographic composition

The proximate, elemental, and petrographic data are presented in Table 5.1. Based on the proximate analysis, the parent coal, vitrinite-rich, and inertinite-rich samples have the similar moisture contents. The vitrinite-rich sample has the highest volatile matter content as well as the lowest ash content. With regards to volatile matter, the higher content for the vitrinite-rich sample relative to the inertinite-rich counterpart is in agreement with published literature for bituminous coals (van Krevelen, 1993; Van Niekerk et al., 2008, and references therein). The H/C atomic ratio, which is indicative of aromatic fraction, is also in agreement with published literature regarding the greater aromatic fraction of bituminous inertinite-rich coals relative to vitrinite-rich counterparts at similar rank (Maroto-Valer et al., 1994, 1998; Mazumdar, 1999; Davidson, 2004; Van Niekerk et al., 2008). The parent sample has the higher total sulphur content, which is significantly reduced in the density-fractionated samples, including the inertinite-rich sample despite the higher ash content. This suggests that the major form of sulphur in the parent coal is present as sulphide minerals (or other sulphur-bearing mineral phases), which reported to the 1.8 sink fraction, with organic sulphur comprising a minor proportion. The total nitrogen content of the samples is fairly comparable, though the vitrinite-sample has the slightly higher proportion of this chemical element.

**Table 5.1:** Proximate, elemental (air dried), and maceral composition (mmf = mineral-matter-free basis) results for the parent coal, inertinite-rich and vitrinite-rich samples. %RoVmr = mean random vitrinite reflectance.

| | **Parent** | **Inertinite-rich** | **Vitrinite-rich** |
|---|---|---|---|
| **Proximate analysis (wt. %)** | | | |
| Moisture | 3.1 | 3.0 | 3.1 |
| Ash | 12.5 | 13.4 | 4.2 |
| Volatile matter | 30.7 | 28.5 | 38.6 |
| Fixed carbon | 53.7 | 55.1 | 54.1 |
| **Elemental analysis (wt. %)** | | | |

| | | | |
|---|---|---|---|
| Carbon | 67.40 | 67.60 | 75.00 |
| Hydrogen | 4.40 | 4.17 | 5.33 |
| Nitrogen | 1.80 | 1.68 | 2.07 |
| Oxygen | 8.61 | 9.57 | 9.58 |
| Sulphur | 2.24 | 0.64 | 0.76 |
| H/C atomic ratio | 0.78 | 0.74 | 0.85 |
| **Maceral composition (vol. %) mmf** | | | |
| Telinite | 0.2 | 0.0 | 2.5 |
| Collotelinite | 12.8 | 13.0 | 36.1 |
| Vitrodetrinite | 0.0 | 0.0 | 0.0 |
| Collodetrinite | 29.9 | 16.2 | 37.1 |
| Corpogelinite | 1.5 | 0.5 | 7.1 |
| Gelinite | 0.0 | 1.4 | 0.0 |
| Pseudovitrinite | 0.0 | 0.2 | 0.4 |
| **Total vitrinite** | **44.3** | **31.3** | **83.1** |
| | | | |
| Fusinite | 9.2 | 8.7 | 4.0 |
| Reactive semifusinite | 1.5 | 7.5 | 0.2 |
| Inert semifusinite | 18.0 | 22.9 | 4.6 |
| Micrinite | 0.4 | 0.2 | 0.0 |
| Macrinite | 0.2 | 0.2 | 0.4 |
| Secretinite | 1.3 | 1.3 | 0.6 |
| Funginite | 0.0 | 0.0 | 0.0 |
| Reactive inertodetrinite | 0.9 | 2.2 | 0.8 |
| Inert inertodetrinite | 20.3 | 22.8 | 1.0 |
| **Total inertinite** | **51.7** | **65.7** | **11.7** |
| | | | |
| Sporinite | 3.5 | 3.0 | 3.0 |
| Cutinite | 0.4 | 0.0 | 2.0 |
| Resinite | 0.0 | 0.0 | 0.2 |
| Alginite | 0.0 | 0.0 | 0.0 |
| Liptodetrinite | 0.0 | 0.0 | 0.0 |
| Exsudatinite | 0.0 | 0.0 | 0.0 |
| **Total liptinite** | **3.9** | **3.0** | **5.2** |
| | | | |
| **%RoVmr** | **0.65** | | |
| **Std. Dev.** | **0.067** | | |

In terms of maceral group composition, the parent coal sample consists of 44.3 vol. % vitrinite and 51.7 vol. % inertinite (mineral-matter-free basis). This maceral group combination may be considered to be relatively enriched in vitrinite in comparison to most Witbank coals (e.g., Falcon and Snyman, 1986; Roberts et al., 2015), although comparable to a sample used by Okolo et al. (2015). The 0.65 %RoVmr (Std. Dev. = 0.067) indicates that the coal is medium rank C bituminous. As a result, the maceral nomenclature used follows that of the International Committee for Coal and Organic Petrology for bituminous rank coals (ICCP, 1998, 2001; Pickel

et al., 2017). Furthermore, the semifusinite and inertodetrinite macerals have been further subdivided into reactive and inert sub-macerals as is the convention for South African coals (Falcon and Snyman, 1986; Falcon and Ham, 1988; Hagelskamp and Snyman, 1988; Snyman, 1989; Okolo et al., 2015). The inertinite-rich sample comprises of 65.7 vol. % total inertinite macerals, wherein fusinite (8.7 vol. %), semifusinite (reactive = 7.5 vol. % and inert = 22.9 vol. %) and inertodetrinite (reactive = 2.2 vol. % and inert = 22.8 vol. %) are the principal inertinite macerals. In contrast, the vitrinite-rich counterpart is dominated by the vitrinite macerals (81.3 vol. % total vitrinite), collotelinite and collodetrinite, with lower proportions of telinite and corpogelinite. Because the dominant macerals of the density-fractionated samples were derived from similar plant organs, i.e. wood (ICCP, 1998, 2001; Hower et al., 2013; O'Keefe et al., 2013), the pyrolysis products of the samples may be expected to either be similar or different. This would depend on which is the overriding parameter between source vegetation and origin pathways determining the pyrolysis products of the coal samples.

### 5.3.2. Comparison of organic geochemistry of the vitrinite-rich and inertinite-rich samples

Along with py-GC/MS, $^{13}$C CP-MAS SS NMR was used to compare the molecular chemistry of the coal samples. Moroeng et al. (2018) concluded that the $^{13}$C CP-MAS SS NMR results are generally comparable with results obtained by others using advanced, direct polarization SS $^{13}$C NMR coupled with spectral-editing techniques, for example the results reported by Cao et al. (2011, 2013). The results of the $^{13}$C CP-MAS SS NMR analysis are given in Table 5.2. The greater aromatic fraction of inertinite-rich coals relative to vitrinite-rich counterparts at the bituminous rank is well-established (Maroto-Valer et al., 1994, 1998; van Krevelen, 1993; Davidson, 2004; Van Niekerk et al., 2008), and the results of the present study largely concur with this (Table 5.2). Further, the results indicate that the inertinite-rich sample has the marginally greater fraction of phenolics ($f_a^P$ = 0.13 vs. 0.09 for the vitrinite-rich sample). Although this sample has the greater overall aromatic fraction, the degree of alkyl substitution is greater for the aromatics of the vitrinite-rich sample. Despite lower overall aliphatic fraction ($f_{al}$), the inertinite-rich sample has a significantly higher proportion of aliphatic carbons bonded to oxygen ($f_{al}^o$ = 0.05 vs. 0.002 for the vitrinite-rich counterpart), along with a higher fraction of carbonyl/carboxyls ($f_a^{CO}$). The proportion of non-protonated carbons and methyl groups in aliphatic compounds is larger for the vitrinite-rich sample ($f_a^{N*}$ = 0.1) relative to the other samples. The number of attachments per cluster ($\sigma + 1$) is larger for the inertinite-rich sample in

comparison to the vitrinite-rich counterpart. Therefore, the $^{13}C$ CP-MAS SS NMR chemical-structural parameters for the density-fractionated samples are markedly different, reflecting the greater aromatic fraction and oxygen-bearing functionalities for the inertinite-rich sample as well as the greater degree of alkyl substitution of aromatics for the vitrinite-rich sample. Moreover, aside from the average aromatic cluster size (C) for the inertinite-rich sample the $^{13}C$ CP-MAS SS NMR results are generally comparable with results obtained by others when evaluating the chemical-structural parameters for vitrinite-rich and inertinite-rich South African bituminous coals (e.g., Van Niekerk et al., 2008; Okolo et al., 2015; Roberts et al., 2015).

**Table 5.2:** Chemical structural parameters from solid-state 13C CP-NMR for the parent coal, inertinite-rich, and vitrinite-rich samples (Moroeng et al., 2018).

| | **Parent** | **Inertinite-rich** | **Vitrinite-rich** |
|---|---|---|---|
| $f_a$ | 0.73 | 0.72 | 0.68 |
| $f_a^*$ | 0.64 | 0.52 | 0.65 |
| $f_{al}$ | 0.27 | 0.28 | 0.32 |
| $f_{al}^o$ | 0.084 | 0.05 | 0.002 |
| $f_a^{CO}$ | 0.09 | 0.19 | 0.04 |
| $f_a^P$ | 0.09 | 0.13 | 0.09 |
| $f_a^S$ | 0.13 | 0.11 | 0.17 |
| $f_a^N$ | 0.39 | 0.25 | 0.48 |
| $f_a^H$ | 0.25 | 0.28 | 0.17 |
| $f_a^B$ | 0.17 | 0.01 | 0.22 |
| $f_a^{N*}$ | 0.05 | 0.04 | 0.10 |
| $f_{al}^H$ | 0.22 | 0.24 | 0.22 |
| $X_b$ | 0.26 | 0.02 | 0.34 |
| **C** | 13.9 | 5.80 | 17.3 |
| **#Cluster/100** | 4.58 | 9.10 | 3.74 |
| **σ + 1** | 4.77 | 2.59 | 6.87 |

Parameters: $f_a$ – Fraction Aromatics, $f_a^*$ – Corrected Fraction Aromatics (excl. CO), $f_{al}$ – Fraction Aliphatics, $f_{al}^o$ – Fraction Aliphatic C's bonded to oxygen, $f_a^{CO}$ – Fraction CO, $f_a^P$ – Fraction Phenolics, $f_a^S$ – Fraction Alkylated Aromatics, $f_a^N$ – Fraction Non-Protonated C's in aromatic region, $f_a^H$ – Fraction Protonated C's in aromatic region, $f_a^B$ – Fraction Bridgehead C's, $f_a^{N*}$ – Fraction Non-Protonated C's + Methyl groups in Aliphatics, $f_{al}^H$ – Aliphatic CH+CH2, $X_b$ – Mole fraction of Aromatic Bridgehead C's, C – Average # of Aromatic C's per cluster, #Cluster/100 – Average # of clusters per 100 Aromatic C's, σ + 1 – # of attachment per cluster.

The pyrolysis chromatograms for the parent, inertinite-rich, and vitrinite-rich coal samples are presented in Figures 5.1, 5.2, and 5.3, respectively. Of the compounds detected during the py-GC/MS analysis, chemical compounds with an abundance (area %) greater than 1% are given in Table 5.3. These compounds represent 75%, 78%, and 71% of the pyrolysis products detected for the parent, inertinite-rich, and vitrinite- rich samples, respectively. The chemical compounds presented were identified with a similarity of more than 70%, and are arranged in order of

increasing retention time in Table 5.3 to aid with peak identification on the chromatographs. For relatively simple compounds common in the pyrolysis products for the three samples such as phenol, benzene, xylene isomers, and fluorene, the py-GC/MS retention times are greatly comparable (Table 5.3). Differences appear to become more prominent for larger and/or more substituted compounds, thus with higher retention times.

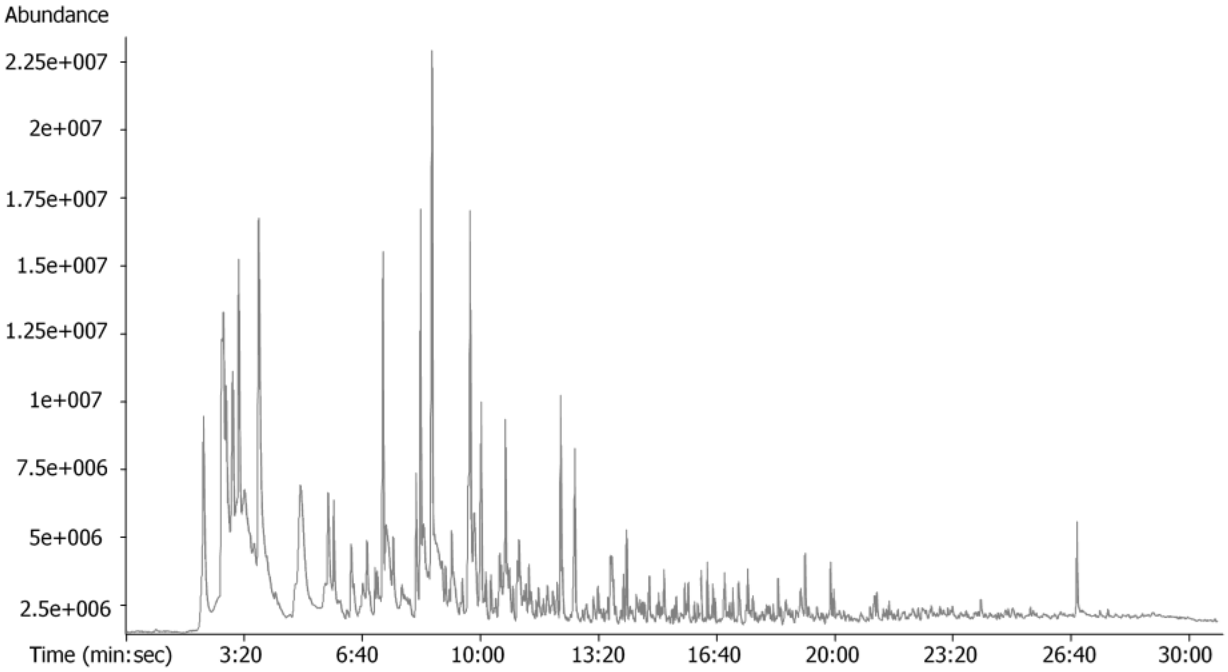


**Figure 5.1:** Total ion chromatogram for the parent coal sample.

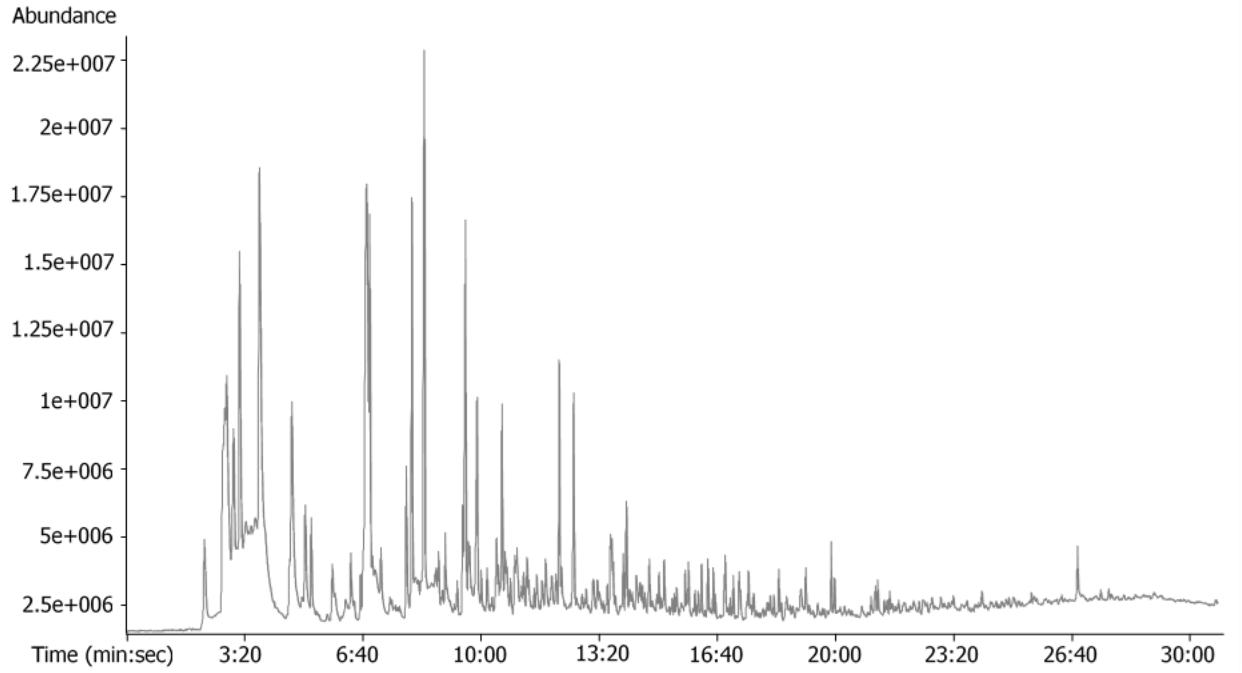


**Figure 5.2:** Total ion chromatogram for the inertinite-rich sample.

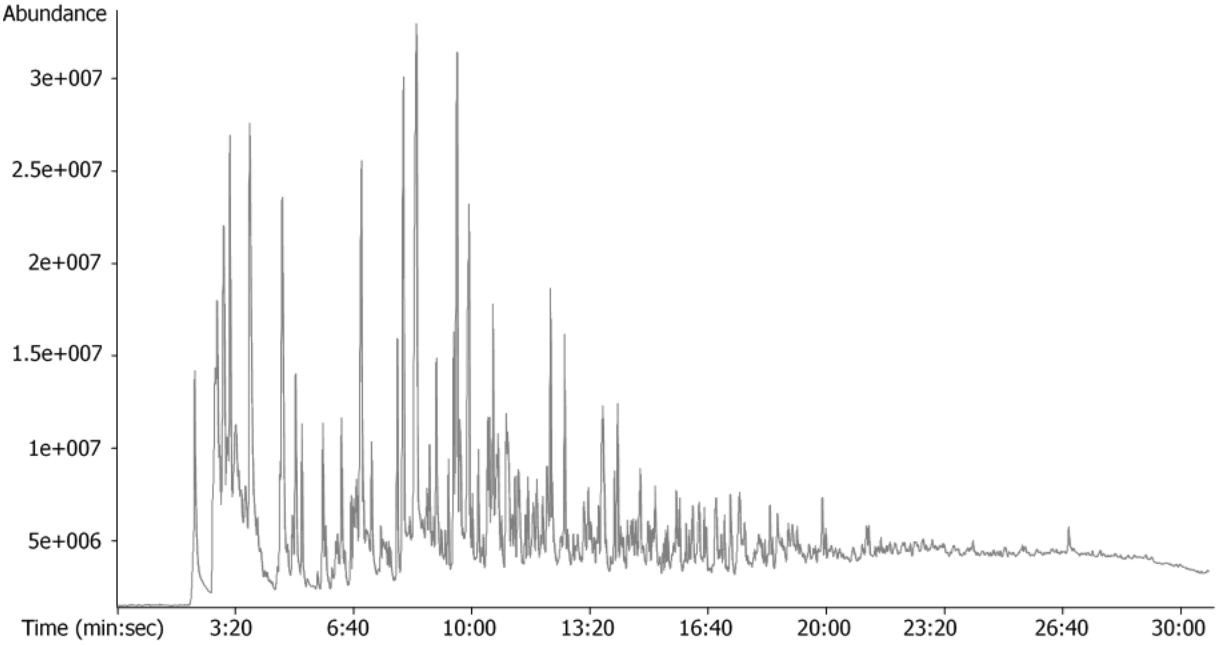


**Figure 5.3:** Total ion chromatogram for the vitrinite-rich sample.

The pyrolysis products of the coal samples of the present study generally comprise of similar compounds reported for various coals from around the world (Table 5.3) (e.g., Meuzelaar et al., 1984; Sentfle and Larter, 1987; Eglinton et al., 1991; Powell et al., 1991; Nip et al., 1988, 1992; van Krevelen, 1993, and references therein; Hartgers et al., 1994; Veld et al., 1994; Zieger et al.,

2018), and South Africa (Van Niekerk et al., 2008). The aliphatic fraction of the pyrolysis products is comprised of a range of low molecular weight (carbon number, $C_4$) to relatively high molecular weight ($C_{30}$) cyclic and branched alkanes and alkenes. With the aid of flash-pyrolysis GCMS, Van Niekerk et al. (2008) reported long-chain alkane and alkene compounds ranging up to $C_{23}$ for vitrinite-rich Waterberg and inertinite-rich Highveld bituminous coals. Further, the pyrolysis products of the vitrinite-rich Waterberg sample were reported to comprise of a greater proportion of aliphatic compounds relative to the inertinite-rich sample (Van Niekerk et al., 2008), consistent with the $^{13}C$ CP-MAS SS NMR results of this study (Table 5.2).

The aromatic fraction of the pyrolysis products for the samples of the present study comprise of a significant amount of substituted and unsubstituted 6-aromatic carbon ring functional groups. For the inertinite-rich sample, the abundance of these monocyclic rings is confirmed by the $^{13}C$ CP-MAS SS NMR results (Table 5.2), specifically the average number of aromatic carbons per cluster (C). The most abundant polycyclic aromatic hydrocarbons (PAHs) detected in the pyrolysis products are naphthalene and flourene, similar to the results obtained by Zieger et al. (2018) for vitrinites of the Carboniferous from the Ruhr Basin, Northwest Germany.Other larger PAHs such as pyrene, anthracene, and phenanthrene are present in minor amounts, hence their exclusion from Table 5.3. The PAHs mostly occur as alkyl-substituted derivatives, consistent with other studies (e.g., Van Niekerk et al., 2008; Zieger et al., 2018).

Ethane-tribromo- and trichloromethane (halogenated hydrocarbons) were also detected during the analysis. Of these, the latter is common to all the samples, whereas the former is only present in the pyrolysis products of the inertinite-rich sample. Despite the fact that the parent coal and the inertinite-rich sample have comparable ash contents, the inertinite-rich sample has a lower total sulphur content. This may be interpreted to suggest that the organic sulphur content of the coals is lower, assuming that the sulphides reported in the 1.8 sink fraction as previously suggested. This is also supported by the minor sulphur-bearing organic compounds (e.g., 3, 4-Epoxytetrahydrothiophene-1, 1-dioxide for the parent coal) detected during the py-GC/MS analysis. Likewise, nitrogen-bearing compounds (e.g., 1H-Pyrrole, 2-methyl-) were detected with a low abundance. However, it should be mentioned that Phiri et al. (2018) observed the dependence of pyrrolic nitrogen on pyrolysis temperature.

Through visual inspection, it becomes evident that the pyrolysis chromatogram for the parent coal (Figure 5.1) is most comparable to that of the inertinite-rich sample (Figure 5.2), likely reflecting similarities in petrographic composition (Table 5.1). The chromatograph for vitrinite-rich sample (Figure 5.3) is markedly different, exhibiting greater chemical diversity in comparison to the other samples, possibly resulting from the greater aliphatic fraction and alkyl substitution as reflected in the $^{13}C$ CP-MAS SS NMR results (Table 5.2). Van Niekerk et al. (2008) also observed marked differences in the molecular chemistry for vitrinite-rich Waterberg and inertinite-rich Highveld coal samples, with greater variability observed for the former sample, thus in agreement with the finding of the present study. Further, most compounds detected during the py-GC/MS analysis (Figure 5.3) appear to be generally more abundant in the vitrinite-rich sample. Because the coals used by Van Niekerk et al. (2008) were obtained from two different coalfields, an argument could be made that differences between vitrinite-rich Waterberg and inertinite-rich Highveld also reflect differences in source vegetation and/or depositional environments. However, the results of the present study may be taken to contradict such an interpretation, instead suggesting inherent differences in the pyrolysis products for the vitrinite and inertinite macerals.

**Table 5.3:** Compounds detected (abundance > 1%) using py-GC/MS for the parent, inertinite-rich, and vitrinite-rich samples. The compounds were identified with a similarity of more than 70%, and are arranged in order of increasing retention time (R.T.).

| Parent sample | | Inertinite-rich | | Vitrinite-rich | |
|---|---|---|---|---|---|
| **R.T. (min:sec)** | **Compound name** | **R.T. (min:sec)** | **Compound name** | **R.T. (min:sec)** | **Compound name** |
| 02:11.2 | Trichloromethane | 02:11.4 | Trichloromethane | 02:10.9 | Trichloromethane |
| 02:45.4 | 3,4-Epoxytetrahydrothiophene-1,1-dioxide | 02:42.9 | 2-Butene | 02:44.8 | Methyl vinyl ketone |
| 02:49.5 | Cyclopropylacetylene | 02:45.6 | Methyl vinyl ketone | 02:46.5 | Ethyl 3-methylbut-3-enyl carbonate |
| 02:59.4 | 4-Penten-1-ol, 3-methyl- | 02:47.0 | 1,4-Pentadiene | 02:49.1 | 1-Buten-3-yne, 2-methyl- |
| 03:10.9 | Benzene | 02:49.6 | 1,3-Cyclopentadiene | 02:59.0 | Norpseudoephedrine |
| 03:44.5 | Toluene | 02:59.5 | 4-Penten-1-ol, 3-methyl- | 03:00.3 | 3-Hexen-1-yne |
| 04:55.3 | p-Xylene | 03:01.0 | 1,3-Cyclohexadiene | 03:10.4 | 1,5-Hexadien-3-yne |
| 05:42.3 | o-Xylene | 03:11.0 | Benzene | 03:44.0 | 1,5-Heptadien-3-yne |
| 06:47.8 | Benzene, 1,2,3-trimethyl- | 03:44.6 | 1,5-Heptadien-3-yne | 04:38.9 | p-Xylene |
| 07:15.1 | Phenol | 04:39.3 | p-Xylene | 05:01.6 | o-Xylene |
| 08:11.1 | Benzene, 1-propynyl- | 05:02.0 | o-Xylene | 06:19.1 | Benzene, 1,2,3-trimethyl- |
| 08:18.7 | Phenol, 2-methyl- | 06:45.9 | Ethene, tribromo- | 06:53.1 | Phenol |
| 08:38.2 | Phenol, 3-methyl- | 06:51.5 | Phenol | 07:53.5 | Indene |
| 09:39.1 | 1H-Indene, 1-methyl- | 07:53.3 | Benzene, 1-propynyl- | 08:04.3 | Phenol, 2-methyl- |
| 10:01.3 | Phenol, 3,5-dimethyl- | 08:02.7 | Phenol, 2-methyl- | 08:26.4 | Phenol, 3-methyl- |
| 10:42.4 | Naphthalene | 08:24.0 | Phenol, 3-methyl- | 08:59.8 | Phenol, 2,3-dimethyl- |
| 11:05.6 | Phenol, 4-ethenyl-, acetate | 09:33.3 | Phenol, 2,3-dimethyl- | 09:29.1 | Benzene, 1-butynyl- |
| 11:22.4 | Phenol, 2-ethyl-6-methyl- | 09:33.6 | Cycloprop[a]indene, 1,1a,6,6a-tetrahydro- | 09:34.0 | Phenol, 2,4-dimethyl- |
| 12:39.8 | 1H-Indene, 1-ethylidene- | 09:53.3 | Phenol, 3,5-dimethyl- | 09:35.2 | Paradrine |
| 14:34.5 | Naphthalene, 2,6-dimethyl- | 10:35.1 | Naphthalene | 10:35.7 | Azulene |
| 17:37.6 | Fluorene | 12:12.2 | Naphthalene, 1-methyl- | 10:41.3 | Catechol |
| 26:49.9 | Squalene | 12:36.1 | Resorcinol | 11:18.7 | Phenol, 2-ethyl-6-methyl- |
| | | 12:36.6 | 1H-Indene, 1-ethylidene- | 12:12.8 | Benzene, 1-propynyl- |
| | | 14:06.2 | Naphthalene, 2,6-dimethyl- | 12:37.0 | Tetracyclo[2.2.1.0(2,6).0(3,5)]heptane-7-spiro-2'-cyclopropene |
| | | 14:44.8 | Naphthalene, 2,3-dimethyl- | 13:40.9 | 1H-Indenol |
| | | 17:37.4 | Fluorene | 14:06.7 | Naphthalene, 2,6-dimethyl- |
| | | | | 17:37.8 | Fluorene |

The varied pyrolysis products for the vitrinite-rich sample, as reflected in Figure 5.3, may be interpreted to suggest that humification and gelification processes result in the formation of chemical compounds able to give off diverse products upon pyrolysis. Similarly, the lack of diversity for inertinite-rich sample (Figure 5.2) may reflect the origin pathway for the dominant inertinite macerals. Moroeng et al. (2018) proposed that the dominant inertinite macerals of the coal samples of the present study were formed through charring of plant matter. Accepting charring as an origin pathway for these macerals, this process would likely have resulted in the volatilization of certain chemical species, which were driven off, and are currently reflected by the lack of chemical diversity in the chromatogram for the inertinite-rich sample (Figure 5.2). In which case, the inertinite macerals may essentially be interpreted to have been pre-pyrolyzed in their geologic history as a result of the origin pathway, prior to the py-GC/MS analysis. Further, the lack of chemical diversity for the pyrolysis products of the inertinite-rich sample may also be interpreted to suggest the dominant inertinite macerals, fusinite, semifusinite, and inertodetrinite, have similar origin pathways and source vegetation, especially considering that this sample also has a significant proportion of vitrinite (31.3 vol. % – mineral-matter free). The lack of diversity may therefore be taken to be consistent with the view that inertodetrinite represents fusinitized and semifusinitized plant matter that was subsequently fragmented (Hagelskamp and Snyman, 1988; ICCP, 2001; O'Keefe et al., 2013).

In addition, various other workers have argued for a fire-origin for certain inertinite macerals such as fusinite and semifusinite (Austen et al., 1966; Scott, 1989, 2002, 2010; Diessel, 1992, 2010; ICCP, 2001; Glasspool, 2003a, 2003b; Scott and Glasspool, 2007; Hower et al., 2013; Jasper et al., 2013; O'Keefe et al., 2013). Along with inertodetrinite, these are the abundant inertinite macerals of the Witbank coals of this study. The greater proportion of phenolics for the inertinite-rich sample (Table 5.2) may also be consistent with a fire-origin for the major inertinite macerals of this sample as concluded by Moroeng et al. (2018). This is based on the fact that pyrolysis experiments using lignin-rich wood at temperatures below 400 °C produces phenolic moieties (Asmadi et al., 2011; Kawamoto, 2017). However, the phenolic moieties produced during the pyrolysis experiments are methoxy-substituted. The absence of methoxy-substituted phenols in the pyrolysis products of the inertinite-rich sample, in particular, may suggest that the methoxy functionalities were either expelled during the course of coalification (Austen et al., 1966; Sentfle and Larter, 1987; Nip et al., 1988; van Krevelen, 1993, and references therein) or

alternatively, as a result of pyrolytic cleavage during the py-GC/MS analysis (Pan et al., 2015). It should be noted that methoxy-substituted phenols have been observed in low rank coals (Sentfle and Larter, 1987, and references therein; van Krevelen, 1993, and references therein).

Despite the diversity exhibited by the vitrinite-rich sample, the pyrolysis products identified for three samples of this study are generally similar (Table 5.2). The abundance of the compounds identified appear to vary between the samples (Figures 5.1 to 5.3), possibly depending on the dominant macerals of the each coal sample. This observation is consistent with the findings of Nip et al. (1992) for single maceral fractions (cutinite, resinite, sporinite, vitrinite, pseudovitrinite, semifusinite, and fusinite) of the Carboniferous from Brazil (Block seam, Roaring Creek Mine, Parke County) prepared using density gradient centrifugation. For the present study, phenolic compounds are a prominent example of a functional group reflected in the py-GC/MS and $^{13}C$ CP-MAS SS NMR results. According to Powell et al. (1991), phenolics are abundant in the pyrolysis products of low-rank coals as opposed to higher rank counterparts. Similar observations were made by Senftle et al. (1986) using vitrinite concentrates from the Lower Kittanning Seam (Pennsylvania), ranging in maturity from high volatile bituminous to low volatile bituminous. The fraction of phenolics for all three coal samples of this study comprises of a range unsubstituted and substituted (e.g., Phenol, 3, 5-dimethyl-; Phenol, 2-ethyl-6-methyl-) derivatives.

Nip et al. (1988) found that p-xylene and m-xylene were the major $C_2$-alkylbenzenes in the pyrolysis products of vitrinite and inertinite macerals from the Lower and Middle Yorkshire Coalfield (UK), whereas o-xylene was observed to be a major product of liptinite pyrolysis. This finding contrasts somewhat with the results of the present study. In the first instance, m-xylene was not detected in the pyrolysis products of the Witbank coal samples. Secondly, p-xylene and o-xylene were detected in the pyrolysis products for the parent, vitrinite-rich, and inertinite-rich samples, though in varying proportions. For the three samples, p-xylene was consistently observed to be more abundant than o-xylene.

Given that the inertinite-rich and vitrinite-rich samples are products of the same coal, differences in the proportions of the xylene isomers present in the pyrolysis products reflect differences between the major maceral groups, and not rank-dependent differences (Nip et al., 1988). This may be taken to suggest that for Witbank coals, p-xylene and o-xylene are the major pyrolysis

products for vitrinite macerals in particular. Alternatively, if the xylene isomers are pyrolysis products for the dominant inertinite macerals as well, this would have to be interpreted to suggest that origin pathways for the vitrinite and inertinite macerals produce chemical species that are able to give off the xylene isomers during pyrolysis. Although forming through different pathways, the dominant inertinite and vitrinite macerals of the samples are derived primarily from the woody tissues of plants, and the xylene isomers are thought to be derived from the lignin component of the wood (Nip et al., 1988). As a result, the presence of xylene isomers in the pyrolysis products for the vitrinite-rich and inertinite-rich samples may suggest that these reflect the comparable source vegetation as opposed to the different origin pathways (Sentfle and Larter, 1987).

Assuming that the xylene isomers reflect source vegetation for macerals present in these Witbank coals, the detection of largely similar pyrolysis products for both the vitrinite-rich and inertinite-rich samples may be interpreted to suggest a continuum in chemical composition between the dominant vitrinite and inertinite macerals (Nip et al., 1992). Because collotelinite, collodetrinite, fusinite, and semifusinite have similar botanical precursors, similarities in the pyrolysis products of these macerals may be expected as suggested by Powell et al. (1991). For South African coals, this has been established based chiefly on petrographic observations. As an example, the semifusinite component of South African coals is typically subdivided into a reactive and an inert sub-maceral (Falcon and Snyman, 1986; Falcon and Ham, 1988; Hagelskamp and Snyman, 1988; Snyman, 1989; Okolo et al., 2015). The subdivision accounts for reactive semifusinite possessing petrographic and chemical properties more comparable to vitrinite, whereas the inert counterpart possesses properties similar to fusinite of the same coal sample.

According to Nip et al. (1992), pyrolysis products can be used as a “fingerprint” to discriminate between different macerals. In this regard, the findings of the present study may be considered somewhat inconclusive and thus warrant further investigation, specifically with the use of advanced maceral separation techniques. This derives from the differences observed in the chromatograms for inertinite-rich and vitrinite-rich samples, suggesting differences in molecular composition which may be obscured by the relative impurity of the coal samples. With purer maceral fractions, it may be possible to assign pyrolysis products to specific macerals with a

higher degree of confidence. However, it should be mentioned that even for largely pure maceral fractions prepared using density-gradient centrifugation from the Argonne Premium Coal Sample Program (for example, fractions comprised of 96.5 vol. % liptinite, 100 vol. % vitrinite, and 99 vol. % inertinite, respectively), Hartgers et al. (1994) encountered difficulties with assigning pyrolysis products to specific macerals, instead suggesting assignment on the basis of an assemblage of functional groups detected.

### 5.4. Conclusion

The study evaluated the organic geochemistry of a vitrinite-rich and an inertinite-rich sample derived from a medium rank C bituminous coal (derived from the same coal, i.e., iso-rank) from the No. 4 Seam Upper of the Witbank Coalfield (South Africa) using pyrolysis py-GC/MS and $^{13}C$ CP-MAS SS NMR. The vitrinite-rich sample (81.3 vol. % vitrinite, mineral-matter-free basis) had an abundance of collotelinite and collodetrinite. In contrast, the inertinite-rich counterpart (65.7 vol. % inertinite) was dominated by fusinite, and variable proportions of both the reactive and inert semifusinite and inertodetrinite sub-macerals. Pyrolysis products for the vitrinite-rich and inertinite-rich samples generally comprised of similar organic molecules, although the former sample was more diverse and had a greater abundance of most compounds. The lack of diversity for the inertinite-rich sample was interpreted to suggest that the dominant macerals were pre-pyrolyzed in their geologic history, thus supporting a fire-origin for the specific macerals. According to the $^{13}C$ CP-MAS SS NMR analysis, the inertinite-rich sample had a higher fraction of phenolics, which comprised of a range of substituted and unsubstituted functionalities along with polycyclic aromatic compounds (PAHs) reflected in the py-GC/MS results. The abundance of phenolics for the inertinite-rich sample was also interpreted to be consistent with a fire-origin for the dominant inertinite macerals. The $C_2$-alkylbenzene isomer, p-xylene, was observed to be more abundant in the samples than o-xylene, whereas m-xylene was not detected. The xylene isomers are likely derived from the lignin component of woody plant matter, the precursor for the dominant vitrinite and inertinite macerals of the coal samples, thus suggesting that the isomers reflect source vegetation. The relative petrographic impurity of the samples rendered the assignment of the compounds to specific macerals difficult.

### 5.5. References

al Sandouk-Lincke, N.A., Schwarzbauer, J., Hartkopf-Fröder, C., Volk, H., Fuentes, D., Young, M., Littke, R., 2014. The effect of different pyrolysis temperatures on organic microfossils,

vitrain and amber - A comparative study between laser assisted- and Curie Point-pyrolysis-gas chromatography/mass spectrometry. Journal of Analytical and Applied Pyrolysis 107, 211-223.

Asmadi, M., Kawamoto, H., Saka, S., 2011. Thermal reactions of guaiacol and syringol as lignin model aromatic nuclei. Journal of Analytical and Applied Pyrolysis 92, 88-98.

Austen, D.E.G., Ingram, D.J.E. Given, P.H., Binder, C.R., Hill, L.W., 1966. Electron Spin Resonance Study of Pure Macerals. In: Given, P.H. (Ed.), Coal Science, Advances in Chemistry, 55. American Chemical Society, Washington DC, pp. 344-362.

Boreham, C.J., Powell, T.G., 1991. Variation in pyrolysate composition of sediments from the Jurassic Walloon Coal Measures, eastern Australia as a function of thermal maturation. Organic Geochemistry 17 (6), 723-733.

Cadle, A.B., Cairncross, B., Christie, A.D.M., Roberts, D.L. 1993. The Karoo Basin of South Africa: type basin for coal-bearing deposits of southern Africa. International Journal of Coal Geology 23, 117-157.

Cao, X., Chappell, M.A., Schimmelmann, A., Mastalerz, M., Li, Y., Hu, W., Mao, J., 2013. Chemical structure changes in kerogen from bituminous coal in response to dike intrusions as investigated by advanced solid-state $^{13}C$ NMR spectroscopy. International Journal of Coal Geology 108, 53-64.

Cao, X., Mastalerz, M., Chappell, M.A., Miller, L.F., Li, Y., Mao, J., 2011. Chemical structures of coal lithotypes before and after $CO_2$ adsorption as investigated by advanced solid-state $^{13}C$ nuclear magnetic resonance spectroscopy. International Journal of Coal Geology 88 (1), 67-74.

Coetzee, G.H., Sakurovs, R., Neomagus, H.W.J.P., Morpeth, L., Everson, R.C., Mathews, J.P., Bunt, J.R., 2015. Pore development during gasification of South African inertinite-rich chars evaluated using small angle X-ray scattering. Carbon 95, 250-260.

Davidson, R.M., 2004. Studying the structural chemistry of coal. IEA Clean Coal Centre. 121pp.

Diessel, C.F.K., 1992. Coal-Bearing Depositional Systems. Springer-Verlag, Berlin Heidelberg, 721pp.

Diessel, C.F.K., 2010. The stratigraphic distribution of inertinite. International Journal of Coal Geology 81 (4), 251-268.

Eglinton, T.I., Larter, S.R., Boon, J.J., 1991. Characterisation of kerogens, coals and asphaltenes by quantitative pyrolysis-mass spectrometry. Journal of Analytical and Applied Pyrolysis 20, 25-45.

Eglinton, T.I., Sinninghe Damsté, J.S., Kohnen, M.E.L., de Leeuw, J.W., 1990. Rapid estimation of the organic sulphur content of kerogens, coals and asphaltenes by pyrolysis-gas chromatography. Fuel 69, 1394-1404.

Fabiańska, M.J., Kruszewska, K.K.J., 2003. Relationship between petrographic and geochemical characterisation of selected South African coals. International Journal of Coal Geology 54 (1-2), 95-114.

Falcon, M.S., Snyman, C.P., 1986. An Introduction to Coal Petrography: Atlas of Petrographic Constituents in the Bituminous Coals of Southern Africa. Geological Society of South Africa, Johannesburg. 27pp.

Falcon, R.M.S., 1986. A brief review of the origin, formation, and distribution of coal in southern Africa. In: Anhaeusser, C.R., Maske, S. (Eds.), Mineral Deposits of Southern Africa, Vols. I and II. Geological Society of South Africa, Johannesburg, pp. 1879-1898.

Glasspool, I., 2003a. Palaeoecology of selected South African export coals from the Vryheid Formation, with emphasis on the role of heterosporous lycopods and wildfire derived inertinite. Fuel 82, 959-970.

Glasspool, I.J., 2003b. Hypautochthonous–allochthonous coal deposition in the Permian, South African, Witbank Basin No. 2 seam; a combined approach using sedimentology, coal petrology and palaeontology. International Journal of Coal Geology 53, 81-135.

Hagelskamp, H.H.B., Snyman, C.P., 1988. On the origin of low-reflecting inertinites in coals from the Highveld Coalfield, South Africa. Fuel 67, 307-313.

Han, Z., Kruge, M.A., Crelling, J.C., Stankiewicz, B.A., 1995. Organic geochemical characterization of the density fractions of a Permian torbanite. Organic Geochemistry 22 (1), 39-50.

Hartgers, W.A., Sinninghe Damste, J.S., de Leeuw, J.W., Ling, Y., Dyrkacz, G.R., 1994. Molecular Characterization of Flash Pyrolyzates of Two Carboniferous Coals and Their Constituting Maceral Fractions. Energy & Fuels 8 (5), 1055-1067.

Hatcher, P.G., Clifford, D.J., 1997. The organic geochemistry of coal: from plant materials to coal. Organic Geochemistry 27 (5-6), 251-257, 259-274.

Hattingh, B.B., Everson, R.C., Neomagus, H.W.J.P., Bunt, J.R., Van Niekerk, D., Jordaan, J.H.L., Mathews, J.P., 2013. Elucidation of the Structural and Molecular Properties of Typical South African Coals. Energy & Fuels 27 (6), 3161-3172.

Hower, J.C., O'Keefe, J.M.K., Eble, C.F., Raymond, A., Valentim, B., Volk, T.J., Richardson, A.R., Satterwhite, A.B., Hatch, R.S., 2011a. Notes on the origin of inertinite macerals in coal: Evidence for fungal and arthropod transformations of degraded macerals. International Journal of Coal Geology 86 (2-3), 231-240.

Hower, J.C., O'Keefe, J.M.K., Eble, C.F., Volk, T.J., Richardson, A.R., Satterwhite, A.B., Hatch, R.S., Kostova, I.J., 2011b. Notes on the origin of inertinite macerals in coals: Funginite associations with cutinite and suberinite. International Journal of Coal Geology 85 (1), 186-190.

Hower, J.C., O'Keefe, J.M.K., Wagner, N.J., Dai, S., Wang, X., Xue, W., 2013. An investigation of Wulantuga coal (Cretaceous, Inner Mongolia) macerals: Paleopathology of faunal and fungal invasions into wood and the recognizable clues for their activity. International Journal of Coal Geology 114, 44-53.

Hower, J.C., O'Keefe, J.M.K., Watt, M.A., Pratt, T.J., Eble, C.F., Stucker, J.D., Richardson, A.R., Kostova, I.J., 2009. Notes on the origin of inertinite macerals in coals: Observations on the importance of fungi in the origin of macrinite. International Journal of Coal Geology 80 (2), 135-143.

International Committee for Coal and Organic Petrology (ICCP). (1998). The new vitrinite classification (ICCP System 1994). Fuel 77 (5), 349-358.

International Committee for Coal and Organic Petrology (ICCP). (2001). The new inertinite classification (ICCP System 1994). Fuel 80 (4), 459-471.

Jasper, A., Guerra-Sommer, M., Abu Hamad, A.M.B., Bamford, M., Cerruti Bernardes-de-Oliveira, M.E., Tewari, R., Uhl, D., 2013. The burning of Gondwana: Permian fires on the southern continent – A palaeobotanical approach. Gondwana Research 24 (1), 148-160.

Kawamoto, H., 2017. Lignin pyrolysis reactions. Journal of Wood Science 63 (2), 117-132.

Kruszewska, K.J., 2003. Fluorescing macerals in South African coals. International Journal of Coal Geology 54, 79-94.

Liu, D., Peng, P., 2008. Possible chemical structures and biological precursors of different vitrinites in coal measure in Northwest China. International Journal of Coal Geology 75 (4), 204-212.

Louw, E.B., Mitchell, G.D., Wang, J., Winans, R.E., Mathews, J.P., 2016. Constitution of Drop-Tube-Generated Coal Chars from Vitrinite- and Inertinite-Rich South African Coals. Energy & Fuels 30 (1), 112-120.

Malumbazo, N., Wagner, N.J., Bunt, J.R., Van Niekerk, D., Assumption, H., 2011. Structural analysis of chars generated from South African inertinite coals in a pipe-reactor combustion unit. Fuel Processing Technology 92 (4), 743-749.

Maroto-Valer, M.M., Andresén, J.M., Snape, C.E., 1998. Verification of the linear relationship between carbon aromaticities and H/C ratios for bituminous coals. Fuel 77 (7), 783-785.

Maroto-Valer, M.M., Love, G.D., Snape, C.E., 1994. Relationship between carbon aromaticities and H/C ratios for bituminous coals. Fuel 73 (12), 1926-1928.

Mazumdar, B.K., 1999. On the relationship between carbon aromaticities and H/C ratios for bituminous coals. Fuel 78, 1239-1241.

Meuzelaar, H.L.C., Harper, A.M., Hill, G.H., Given, P.H., 1984. Characterization and classification of Rocky Mountain coals by Curie-point pyrolysis mass spectrometry. Fuel 63 (5), 640-652.

Moore, T.A. Shearer, J.C., Miller, S.L., 1996. Fungal origin of oxidized plant material in the Palangkaraya peat deposit, Kalimantan Tengah, Indonesia: Implications for 'inertinite' formation in coal. International Journal of Coal Geology 30, 1-23.

Moore, T.A., Shearer, J.C., 1997. Evidence for Aerobic Degradation of Palangka Raya Peat and Implications for its Sustainability. In: Rieley, J.O., Page, S.E., (Eds.). Tropical Peatlands. Samara Publishing Limited, Cardigan, pp. 157-167.

Moroeng, O.M., Wagner, N.J., Brand, D.J., Roberts, R.J., 2018. A Nuclear Magnetic Resonance study: Implications for coal formation in the Witbank Coalfield, South Africa. International Journal of Coal Geology 188, 145-155.

Nip, M., De Leeuw, J.W., Crelling, J.C. 1992. Chemical structure of bituminous coal and its constituting maceral fractions as revealed by flash pyrolysis. Energy & Fuels 6 (2), 125-136.

Nip, M., De Leeuw, J.W., Schenck, P.A., 1988. The characterization of eight maceral concentrates by means of Curie point pyrolysis-gas chromatography and Curie point

pyrolysis-gas chromatography-mass spectrometry. Geochimica et Cosmochimica Acta 52 (3), 637-648.

Odden, W., Barth, T., 2000. A study of the composition of light hydrocarbons ($C_5$-$C_{13}$) from pyrolysis of source rock samples. Organic Geochemistry 31 (2-3), 211-229.

O'Keefe, J.M.K., Bechtel, A., Christanis, K., Dai, S., DiMichele, W.A., Eble, C.F., Esterle, J.S., Mastalerz, M., Raymond, A.L., Valentim, B.V., Wagner, N.J., Ward, C.R., Hower, J.C., 2013. On the fundamental difference between coal rank and coal type. International Journal of Coal Geology 118, 58-87.

Okolo, G.N., Neomagus, H.W.J.P., Everson, R.C., Roberts, M.J., Bunt, J.R., Sakurovs, R., Mathews, J.P., 2015. Chemical-structural properties of South African bituminous coals: Insights from wide angle XRD-carbon fraction analysis, ATR-FTIR, solid state $^{13}C$ NMR, and HRTEM techniques. Fuel 158, 779-792.

Pan, S., Hui, S., Liang, L., 2015. Depolymerization Model for Coal Devolatilization: Bridges and Side Chains as the Reaction Centers. Energy & Fuel 29, 2162-2176.

Phiri, Z., Everson, R.C., Neomagus, H.W.J.P., Wood, B.J., 2018. Transformation of nitrogen functional forms and the accompanying chemical-structural properties emanating from pyrolysis of bituminous coals. Applied Energy 216, 414-427.

Pickel, W., Kus, J., Flores, D., Kalaitzidis, S., Christanis, K., Cardott, B.J., Misz-Kennan, M., Rodrigues, S., Hentschel, A., Hamor-Vido, M., Crosdale, P., Wagner, N., ICCP., 2017. Classification of liptinite – ICCP System 1994. International Journal of Coal Geology 169, 40-61.

Pone, J.D.N., Hein, K.A.A., Stracher, G.B., Annegarn, H.J., Finkleman, R.B., Blake, D.R., McCormack, J.K., Schroeder, P., 2007. The spontaneous combustion of coal and its by-products in the Witbank and Sasolburg coalfields of South Africa. International Journal of Coal Geology 72 (2), 124-140.

Powell, T.G., Boreham, C.J., Smyth, M., Russell, N., Cook, A.C., 1991. Petroleum source rock assessment in non-marine sequences: pyrolysis and petrographic analysis of Australian coals and carbonaceous shales. Organic Geochemistry 17 (3), 375-394.

Richardson, A.R., Eble, C.F., Hower, J.C., O'Keefe, J.M.K., 2012. A critical re-examination of the petrology of the No. 5 Block coal in eastern Kentucky with special attention to the origin

of inertinite macerals in the splint lithotypes. International Journal of Coal Geology 98, 41-49.

Roberts, M.J., Everson, R.C., Neomagus, H.W.J.P., Van Niekerk, D., Mathews, J.P., Branken, D.J., 2015. Influence of maceral composition on the structure, properties and behaviour of chars derived from South African coals. Fuel 142, 9-20.

Scott, A.C., 1989. Observations on the nature and origin of fusain. International Journal of Coal Geology 12, 443-475.

Scott, A.C., 2002. Coal petrology and the origin of coal macerals: a way ahead? International Journal of Coal Geology 50, 119-134.

Scott, A.C., 2010. Charcoal recognition, taphonomy and uses palaeoenvironmental analysis. Palaeogeography, Palaeoclimatology, Palaeoecology 291, 11-39.

Scott, A.C., Glasspool, I.J., 2007. Observations and experiments on the origin and formation of inertinite group macerals. International Journal of Coal Geology 70 (1-3), 53-66.

Sehume, T.Z., Strydom, C.A., Bunt, J.R., Schobert, H.H., 2017. Effectivity of Phenol during Solvent Extraction of a South African Bituminous Coal under Mild Conditions. Energy & Fuels 31 (12), 13655-13665.

Senftle, J.T., Larter, S.R., 1987. Comparative geochemistry of vitrinite kerogens from Carboniferous and Tertiary provinces. Organic Geochemistry 11 (5), 407-409.

Senftle, J.T., Larter, S.R., Bromley, B.W., Brown, J.H., 1986. Quantitative chemical characterization of vitrinite concentrates using pyrolysis-gas chromatography. Rank variation of pyrolysis products. Organic Geochemistry 9 (6), 345-350.

Snyman, C.P., 1989. The role of coal petrography in understanding the properties of South African coal. In: Pickhardt, W., (Ed.). Erich Stach Memorial Issue. International Journal of Coal Geology 14, 83-101.

Snyman, C.P., Botha, W.J. 1993. Coal in South Africa. Journal of African Earth Sciences 16 (1/2), 171-180).

Solum, M.S, Pugmire, R.J., Grant, D.M. 1989. $^{13}C$ Solid-state NMR of Argonne Premium Coals. Energy & Fuels 3, 187-193.

South African National Standards (SANS) 17246:2011 (ISO 17246:2010). Coal - Proximate analysis.

South African National Standards (SANS) 17247:2006 (ISO 17247:2005). Coal - Ultimate analysis.

South African National Standards (SANS) 334:1992 (ISO 334:1992). Solid mineral fuels - Determination of total sulfur - Eschka method.

South African National Standards (SANS) 7404-2:2015 (ISO 7404-2:2009). Methods for the petrographic analysis of coals Part 2: Methods of preparing coal samples.

South African National Standards (SANS) 7404-3:2016 (ISO 7404-3:2009). Methods for the petrographic analysis of coals - Part 3: Method of determining maceral group.

South African National Standards (SANS) 7404-5:2016 (ISO 7404-5:2009). Methods for the petrographic analysis of coals - Part 5: Method of determining microscopically the reflectance of vitrinite.

South African National Standards (SANS) 7936:2010 (ISO 7936:1992). Hard coal – Determination and presentation of float and sink characteristics – General directions for apparatus and procedures.

Strydom, C.A., Bunt, J.R., Schobert, H.H., Raghoo, M., 2011. Changes to the organic functional groups of an inertinite rich medium rank bituminous coal during acid treatment processes. Fuel Processing Technology 92, 764-770.

Suggate, R.P., Dickinson, W.W., 2004. Carbon NMR of coals: the effects of coal type and rank. International Journal of Coal Geology 57, 1-22.

Sun, Y., Horsfield, B., 2005. Comparison of the Geochemical Characteristics of "Barkinite" and Other Macerals from the Dahe Mine, South China. Energy Exploration & Exploitation 23 (6), 475-494.

Taylor, G.H., Teichmüller, M., Davis, A., Diessel, C.F.K., Littke, R., Robert, P., 1998. Organic Petrology. Gebrüder Borntraeger, Berlin, 704pp.

Valentim, B., Algarra, M., Guedes, A., Ruppert, L.F., Hower, J.C., 2016. Notes on the origin of copromacrinite based on nitrogen functionalities and $\delta^{13}C$ and $\delta^{15}N$ determined on samples from the Peach Orchard coal bed, southern Magoffin County, Kentucky. International Journal of Coal Geology 160-161, 63-72.

van Krevelen, D.W., 1993. Coal: Typology - Chemistry - Physics – Constitution, third ed. Elsevier, Amsterdam, 979pp.

Van Niekerk, D., Mathews, J.P., 2010. Molecular representations of Permian-aged vitrinite-rich and inertinite-rich South African coals. Fuel 89, 73-82.

Van Niekerk, D., Pugmire, R.J., Solum, M.S., Painter, P.C., Mathews, J.P., 2008. Structural characterization of vitrinite-rich and inertinite-rich Permian-aged South African bituminous coals. International Journal of Coal Geology 76, 290-300.

Veld, H., de Leeuw, J.W., Sinninghe Damsté, J.S., Fermont, W.J.J., 1994. Molecular Characterization of Vitrinite Maturation as Revealed by Flash Pyrolysis Methods. In: Mukhopadhyay, P.K., Dow, W.G., (Eds.). Vitrinite Reflectance as a Maturity Parameter: Applications and Limitations. ACS Symposium Series 570, American Chemical Society, Washington DC, pp. 149-160.

Wang, R., Sun, R., Liu, G., Yousaf, B., Wu, D., Chen, J., Zhang, H., 2017. A review of the biogeochemical controls on the occurrence and distribution of polycyclic aromatic compounds (PACs) in coals. Earth-Science Reviews 171, 400-418.

Zieger, L., Littke, R., Schwarzbauer, J., 2018. Chemical and structural changes in vitrinites and megaspores from Carboniferous coals during maturation. International Journal of Coal Geology 185, 91-102.

# Chapter 6

## Summary and conclusions

Several origin pathways have been proposed for the formation of macerals belonging to the inertinite group. Of these pathways, charring of plant matter appears to be the most probable for the dominant macerals present in the No. 4 Seam Upper of the Witbank Coalfield. Other coalification pathways such as aerial oxidation, fungal activity, and freeze-drying, requiring either or both cold climate and low water-levels, may be considered unsuitable for the formation of inertinite macerals present in the aforementioned coal seam. The view that inertinite formation was preceded by charring of plant matter is also supported by the presence of charcoal within and around the coal seams of the Main Karoo Basin (MKB) of South Africa as documented by others (Glasspool, 2003a, 2003b; Jasper et al., 2013). Wood charring experiments have demonstrated that this process produces morphologies comparable to those exhibited by inertinite macerals (Guo and Bustin, 1998). In addition to the occurrence of macroscopic charcoal, petrological and geochemical evidence can be used to support a fire-origin for inertinite macerals.

Petrographic and several geochemical analytical techniques were selected to examine the sustainability of a fire-origin for the inertinite macerals present in a No. 4 Seam Upper coal from the Witbank Coalfield, South Africa. A medium rank C bituminous coal sample was obtained (the "parent") and density-fractionated to create an inertinite-rich and a vitrinite-rich sample. The analytical methods used include: (1) petrographic analysis (maceral, microlithotype, and mean random vitrinite reflectance); (2) electron spin resonance (ESR); (3) carbon-13 cross-polarization magic-angle-spinning solid-state nuclear magnetic resonance ($^{13}$C CP-MAS SS NMR); and, (4) stable nitrogen and carbon isotopes ($\delta^{15}$N and $\delta^{13}$C) and the concentration of nitrogen functionalities (N-pyridinic, N-pyrrolic, N-quaternary, and N-oxide complexes) determined using X-ray photoelectron spectroscopy (XPS). Lastly, the vitrinite-rich and inertinite-rich samples were also compared using molecular chemistry obtained from a pyrolysis gas chromatograph (py-GC) equipped with a thermal desorption unit (TDU) coupled to a time of flight (TOF) mass spectrometer (MS) (py-GC/MS).

- The vitrinite-rich and inertinite-rich density-fractionated samples comprised of 81 vol. % total vitrinite (dominated by collotelinite and collodetrinite) and 63 vol. % total inertinite (dominated by fusinite, semifusinite, and inertodetrinite), respectively. Moreover, the coal samples were dominated by monomacerals, corresponding to vitrite and inertite, respectively.

- Based on the ESR analysis, it was proposed that the botanical precursor to the major components of the inertinite-rich sample (fusinite, semifusinite, and inertodetrinite) underwent charring before incorporation into the peat-forming environment, as concluded by Austen et al. (1966) when comparing the radical concentration of fusinite-rich coals and fusinite-impoverished counterparts. The process of thermally-driven alteration is responsible for the higher radical content of inertinite-rich sample relative to the iso-rank vitrinite-rich counterpart. Given the dissimilarity between the ESR parameters of the parent and vitrinite-rich sample, it is suggested that the fire-derived inertinite macerals have a significant influence on the ESR properties of the coal studied.

- The NMR structural parameters were largely consistent with the interpretation that the inertinite macerals of the coal have a pyrogenic origin. The $^{13}C$ CP-MAS SS NMR structural parameters revealed the presence of 6-aromatic carbons per cluster in the inertinite-rich sample as opposed to 17 in the vitrinite-rich sample. However, the total population of the 6-carbon rings was greater in the inertinite-rich sample, hence greater overall fraction of aromaticity. The presence of 6-aromatic carbon rings in the inertinite-rich sample was interpreted to reflect the presence of guaiacol and syringol, the low-temperature pyrolysis products of lignin-rich wood (Asmadi et al., 2011; Kawamoto, 2017). Because wood charring depletes both moisture and cellulose, it was suggested that the compaction potential of heat-affected inertinite-forming plant matter was minimized such that the material remained relatively unaffected by confining pressure following burial. Fire-affected plant matter would therefore have been more rigid than unaffected matter, with the two forming inertinite and vitrinite macerals respectively. In addition to preservation of anatomical details (Scott, 1989), rigidity of charred wood appears to manifest through the preservation of monocyclic rings on a molecular level. In contrast, the rings in less rigid matter merge to form the polycyclic clusters present in the vitrinite-

rich coal used in this study. Physically, polymerization is accompanied by the destruction of cellular structure in the collotelinite- and collodetrinite-rich sample. Based on the $^{13}C$ CP-MAS SS NMR results, it was thus concluded that the dominant macerals of the inertinite-rich were formed through low-temperature charring.

- Based on the $\delta^{13}C$ values of the parent, inertinite-rich, and vitrinite samples, the coals were derived from C3 plants. The lower $^{14}N$ value for the vitrinite-rich sample along with the higher concentration of N-quaternary and N-pyridinic, and absence of anatomical structure in the major components of this sample, was interpreted to reflect bacterial degradation of plant matter (Schulten and Schnitzer, 1998, and references therein; Kelemen et al., 2006; Rimmer et al., 2006). In contrast, the higher $^{14}N$ value of the inertinite-rich sample coupled with the higher N-pyrrolic and N-oxide complexes, and the preserved structure of fusinite and semifusinite, suggested charring of plant matter (Schulten and Schnitzer, 1998, and references therein; Kelemen et al., 2006; Rimmer et al., 2006). Bacterial degradation and charring both deplete $^{13}C$-rich cellulose. However, the higher $\delta^{13}C$ of the inertinite-rich sample reflected partial as opposed to complete charring. Partial charring was thus suggested to have given rise to the high semifusinite content of South African coals of the MKB.

- Since the degree of combustion would have been determined by moisture, it was postulated that the formation of fusinite, low- and high-reflecting semifusinites was controlled, in part, by this parameter as well as the size of the fire-affected plant organ. A relatively small and dry plant organ would have been more readily and evenly charred than a large and wet plant organ. In the former, incomplete charring may have given rise to variously reflecting macerals separated by gradational contacts. Given sharp contact between fusinite and inert- and/or reactive-semifusinite, the precursor plant matter were suggested to have been separate and discrete. Additionally, dead and dried-out plant matter would have given rise to fusinite, whereas the higher moisture, potentially standing or recently deceased vegetation would have resulted in the formation of semifusinite with lower reflectances.

- The dominance of both fire-derived inertinite macerals and vitrinite (formed through humification and gelification) in the No. 4 Seam Upper Witbank coal was attributed to an

interchange between wet and dry periods. This was supported by the dominance of monomaceral microlithotypes over bi- and trimacerals. Vitrinite formation would have required wet and relatively long periods, whereas the formation of inertinite macerals through fires may have occurred during drier seasons and within shorter time-spans.

- Fusinite and semifusinite were interpreted to represent plant matter charred within or close to the peat-forming environment during periods of relatively low water levels. Alternatively, the presence of the primary, fire-derived macerals may be indicative of crown fires, i.e., the burning of standing vegetation. Inertodetrinite was attributed reworking of charring by sedimentary processes.

- In terms of organic molecular composition obtained using py-GC/MS, the pyrolysis products of the vitrinite-rich and inertinite-rich generally comprised of similar organic compounds such as low and high molecular weight alkanes, alkylbenzenes, alkylphenols, and alkyl-subtituted polycyclic aromatic hydrocarbons (Nip et al., 1992; van Krevelen, 1993, and references). This likely reflects a continuum in chemical composition between the dominant vitrinite and inertinite macerals present in the samples (Nip et al., 1992). However, p-xylene and o-xylene, derived from lignin, were found to be more abundant in the vitrinite-rich sample. As a result of the relative impurity of the samples, it was not possible to assign specific pyrolysis products to specific macerals present in the samples. The greater diversity exhibited by the vitrinite-rich sample relative to the inertinite-rich counterpart suggests that the major maceral components of the latter sample were heated in their geologic history. This process would likely have resulted in the volatilization some chemical species, which were largely absent during py-GC/MS analysis.

Regarding the hypothesis as articulated in Chapter 1 of this thesis, the geochemical data discussed herein are thus interpreted to support a fire-origin for the dominant inertinite macerals occurring in the No. 4 Seam Upper coal seam of the Witbank Coalfield. However, more research is required to assess if the results of this study are applicable to the MKB in its entirety, and the sub-basins thereof. The MKB of South Africa is geographically extensive, subdivided into distinct entities, each containing multiple coal seams. Thus, a considerable amount of work is still required in order to ascertain if the findings of this work are applicable to other coal seams and/or coalfields. Furthermore, the northwards coalfields (e.g., Waterberg and Soutpansberg)

typically have a greater proportion of vitrinite, suggesting that fires had a minor role in the formation of the macerals. In addition, the organic geochemistry of the coals should be investigated using advanced maceral separation techniques so that it may be possible to assign different geochemical properties to specific macerals present in the coals.

### 6.1. References


Asmadi, M., Kawamoto, H., Saka, S., 2011. Thermal reactions of guaiacol and syringol as lignin model aromatic nuclei. Journal of Analytical and Applied Pyrolysis 92, 88-98.

Austen, D.E.G., Ingram, D.J.E. Given, P.H., Binder, C.R., Hill, L.W., 1966. Electron Spin Resonance Study of Pure Macerals. In: Given, P.H. (Ed.), Coal Science, Advances in Chemistry, 55. American Chemical Society, Washington DC, pp. 344-362.

Glasspool, I., 2003a. Palaeoecology of selected South African export coals from the Vryheid Formation, with emphasis on the role of heterosporous lycopods and wildfire derived inertinite. Fuel 82, 959-970.

Glasspool, I.J., 2003b. Hypautochthonous–allochthonous coal deposition in the Permian, South African, Witbank Basin No. 2 seam; a combined approach using sedimentology, coal petrology and palaeontology. International Journal of Coal Geology 53, 81-135.

Guo, Y., Bustin, R.M., 1998. FTIR spectroscopy and reflectance of modern charcoals and fungal decayed woods: implications for studies of inertinite in coals. International Journal of Coal Geology 37, 29-53.

Jasper, A., Guerra-Sommer, M., Abu Hamad, A.M.B., Bamford, M., Cerruti Bernardes-de-Oliveira, M.E., Tewari, R., Uhl, D., 2013. The burning of Gondwana: Permian fires on the southern continent – A palaeobotanical approach. Gondwana Research 24 (1), 148-160.

Kawamoto, H., 2017. Lignin pyrolysis reactions. Journal of Wood Science 63 (2), 117-132.

Kelemen, S.R., Afeworki, M., Gorbaty, M.L., Kwiatek, P.J., Sansone, M., Walters, C.C., 2006. Thermal Transformations of Nitrogen and Sulfur Forms in Peat Related to Coalification. Energy & Fuels 20, 635-652.

Nip, M., De Leeuw, J.W., Crelling, J.C. 1992. Chemical structure of bituminous coal and its constituting maceral fractions as revealed by flash pyrolysis. Energy & Fuels 6 (2), 125-136.

Rimmer, S.M., Rowe, H.D., Taulbee, D.N., Hower, J.C., 2006. Influence of maceral content on $\delta^{13}C$ and $\delta^{15}N$ in a Middle Pennsylvanian coal. Chemical Geology 225, 77-90.

Schulten, H.-R., Schnitzer, M., 1998. The chemistry of soil organic nitrogen: a review. Biology and Fertility of Soils 26, 1-15.

Scott, A.C., 1989. Observations on the nature and origin of fusain. International Journal of Coal Geology 12, 443-475.

van Krevelen, D.W., 1993. Coal: Typology - Chemistry - Physics - Constitution, third ed. Elsevier, Amsterdam, 979pp.

# Chapter 7

## References


al Sandouk-Lincke, N.A., Schwarzbauer, J., Hartkopf-Fröder, C., Volk, H., Fuentes, D., Young, M., Littke, R., 2014. The effect of different pyrolysis temperatures on organic microfossils, vitrain and amber - A comparative study between laser assisted- and Curie Point-pyrolysis-gas chromatography/mass spectrometry. Journal of Analytical and Applied Pyrolysis 107, 211-223.

Ascough, P.L., Bird, M.I., Scott, A.C., Collinson, M.E., Cohen-Ofri, I., Snape, C.E., Le Manquais, K., 2010. Charcoal reflectance measurements: implications for structural characterization and assessment of diagenetic alteration. Journal of Archaeological Science 37, 1590-1599.

Ascough, P.L., Bird, M.I., Wormald, P., Snape, C.E., Apperley, D., 2008. Influence of production variables and starting material on charcoal stable isotopic and molecular characteristics. Geochimica et Cosmochimica Acta 72, 6090-6102.

Asmadi, M., Kawamoto, H., Saka, S., 2011. Thermal reactions of guaiacol and syringol as lignin model aromatic nuclei. Journal of Analytical and Applied Pyrolysis 92, 88-98.

Austen, D.E.G., Ingram, D.J.E., Given, P.H., Binder, C.R., Hill, L.W., 1966. Electron Spin Resonance Study of Pure Macerals. In: Given, P.H., (Ed.). Coal Science, Advances in Chemistry, 55. American Chemical Society, Washington DC, pp. 344-362.

Austen, D.E.G., Ingram, D.J.E., Tapley, J.G., 1958. The investigation of free radicals trapped in low temperature carbons. Transactions of the Faraday Society 54, 400-408.

Bamford, M.K., 2004. Diversity of the Woody Vegetation of Gondwanan Southern Africa. Gondwana Research 7 (1), 153-164.

Beidari, M., Lin, S.-J., Lewis, C., 2017. Decomposition Analysis of $CO_2$ Emissions from Coal-Sourced Electricity Production in South Africa. Aerosol and Air Quality Research 17, 1043-1051.

Belcher, C.M., Finch, P., Collinson, M.E., Scott, A.C., Grassineau, N.V., 2009. Geochemical evidence for combustion of hydrocarbons during the K-T impact event. Proceedings of the National Academy of Sciences of the United States of America 106 (11), 4112-4117.

Bergh, J.P., Falcon, R.M.S., Falcon, L.M., 2011. Trace element concentration reduction by beneficiation of Witbank Coalfield no. 4 Seam. Fuel Processing Technology 92 (4), 812-816.

Berner, R.A., 1999. Atmospheric oxygen over Phanerozoic time. Proceedings of the National Academy of Sciences of the United States of America 96 (20), 10955-10957.

Binet, L., Gourier, D., Derenne, S., Robert, F., 2002. Heterogeneous distribution of paramagnetic radicals in the insoluble organic matter from the Orgueil and Murchison meteorites. Geochimica et Cosmochimica Acta 66 (23), 4177-4186.

Bird, M.I., Ascough, P.L., 2012. Isotopes in pyrogenic carbon: A review. Organic Geochemistry 42, 1529-1539.

Boreham, C.J., Powell, T.G., 1991. Variation in pyrolysate composition of sediments from the Jurassic Walloon Coal Measures, eastern Australia as a function of thermal maturation. Organic Geochemistry 17 (6), 723-733.

Bowman, D.M.J.S., Balch, J.K., Artaxo, P., Bond, W.J., Carlson, J.M., Cochrane, M.A., D'Antonio, C.M., DeFries, R.S., Doyle, J.C., Harrison, S.P., Johnston, F.H., Keeley, J.E., Krawchuk, M.E., Kull, C.A., Marston, J.B., Moritz, M.A., Prentice, I.C., Roos, C.I., Scott, A.C., Swetnam, T.W., van der Werf, G.R., Pyne, S.J., 2009. Fire in the Earth System. Science, New Series 24 (5926), 481-484.

Bussio, J.P., Roberts, J.R., 2016. A large scale investigation into changes in coal quality caused by dolerite dykes in Secunda, South Africa-implications for the use of proximate analysis on a working mine. Journal of African Earth Sciences 117, 401-409.

Cadle, A.B., Cairncross, B., Christie, A.D.M., Roberts, D.L. 1993. The Karoo Basin of South Africa: type basin for coal-bearing deposits of southern Africa. International Journal of Coal Geology 23, 117-157.

Cairncross, B., 1989. Paleodepositional environments and tectonosedimentary controls of the postglacial Permian coals, Karoo Basin, South Africa. International Journal of Coal Geology 12 (1-4), 365-380.

Cairncross, B., 1990. Tectono-sedimentary settings and controls of the Karoo Basin Permian coals, South Africa. International Journal of Coal Geology 16 (1-3), 175-178.

Cairncross, B., 2001. An overview of the Permian (Karoo) coal deposits of Southern Africa. Journal of African Earth Sciences 33, 529-562.

Cairncross, B., Cadle, A.B., 1988. Palaeoenvironmental control on coal formation, distribution and quality in the Permian Vryheid Formation, East Witbank Coalfield, South Africa. International Journal of Coal Geology 9 (4), 343-370.

Cairncross, B., Hart, R.J., Wills, J.P., 1990. Geochemistry and sedimentology of coal seams from the Permian Witbank Coalfield, South Africa; a means of identification. International Journal of Coal Geology 16 (4), 309-325.

Cao, X., Chappell, M.A., Schimmelmann, A., Mastalerz, M., Li, Y., Hu, W., Mao, J., 2013. Chemical structure changes in kerogen from bituminous coal in response to dike intrusions as investigated by advanced solid-state $^{13}C$ NMR spectroscopy. International Journal of Coal Geology 108, 53-64.

Cao, X., Mastalerz, M., Chappell, M.A., Miller, L.F., Li, Y., Mao, J., 2011. Chemical structures of coal lithotypes before and after $CO_2$ adsorption as investigated by advanced solid-state $^{13}C$ nuclear magnetic resonance spectroscopy. International Journal of Coal Geology 88 (1), 67-74.

Chen, Y., Mastalerz, M., Schimmelmann, A., 2012. Characterization of chemical functional groups in macerals across different coal ranks via micro-FTIR spectroscopy. International Journal of Coal Geology 104, 22-33.

Coetzee, G.H., Sakurovs, R., Neomagus, H.W.J.P., Morpeth, L., Everson, R.C., Mathews, J.P., Bunt, J.R., 2015. Pore development during gasification of South African inertinite-rich chars evaluated using small angle X-ray scattering. Carbon 95, 250-260.

Czimczik, C., Preston, C.M., Schimdt, M.W.I., Werner, R.A., Schulze, E.-D., 2002. Effects of charring on mass, organic carbon, and stable carbon isotope composition of wood. Organic Geochemistry 33, 1207-1223.

Davidson, R.M., 2004. Studying the structural chemistry of coal. IEA Clean Coal Centre. 121pp.

De Goede, S., Rabe, T., Bekker, R., Mtongana, S., Edwards, J., 2010. Characterization of Combustion Chamber Deposits Formed in Direct Injection Spark Ignition (DISI) Engines during an On-road Vehicle. SAE International 2010-01-2155.

Diessel, C.F.K., 1992. Coal-Bearing Depositional Systems. Springer-Verlag, Berlin Heidelberg, 721pp.

Diessel, C.F.K., 2010. The stratigraphic distribution of inertinite. International Journal of Coal Geology 81 (4), 251-268.

Dyrkacz, G.R., Bloomquist, C.A.A., Ruscic, L., 1984. Chemical variations in coal macerals separated by density gradient centrifugation. Fuel 63, 1166-1173.

Dyrkacz, G.R., Horwitz, E.P., 1982. Separation of coal macerals. Fuel 61 (1), 3-12.

Edwards, J.C., Choate, P.J., 1993. Average Molecular Structure of Gasoline Engine Combustion Chamber Deposits Obtained by Solid-State $^{13}C$, $^{31}P$, and $^{1}H$ Nuclear Magnetic Resonance Spectroscopy. SAE International Technical Paper 932811.

Eglinton, T.I., Larter, S.R., Boon, J.J., 1991. Characterisation of kerogens, coals and asphaltenes by quantitative pyrolysis-mass spectrometry. Journal of Analytical and Applied Pyrolysis 20, 25-45.

Eglinton, T.I., Sinninghe Damsté, J.S., Kohnen, M.E.L., de Leeuw, J.W., 1990. Rapid estimation of the organic sulphur content of kerogens, coals and asphaltenes by pyrolysis-gas chromatography. Fuel 69, 1394-1404.

Erdenetsogt, B-.O., Lee, I., Ko, Y-.J., 2017. Carbon isotope analysis and a solid state $^{13}C$ NMR study of Mongolian lignite: Changes in stable carbon isotopic composition during diagenesis. Organic Geochemistry 113, 293-302.

Erdenetsogt, B-.O., Lee, I., Lee, S.K., Ko, Y-.J., Bat-Erdene, D., 2010. Solid-state C-13 CP/MAS NMR study of Baganuur coal, Mongolia: Oxygen-loss during coalification from lignite to subbituminous rank. International Journal of Coal Geology 82 (1-2), 37-44.

Fabiańska, M.J., Kruszewska, K.K.J., 2003. Relationship between petrographic and geochemical characterisation of selected South African coals. International Journal of Coal Geology 54 (1-2), 95-114.

Falcon, M.S., Snyman, C.P., 1986. An Introduction to Coal Petrography: Atlas of Petrographic Constituents in the Bituminous Coals of Southern Africa. Geological Society of South Africa, Johannesburg. 27pp.

Falcon, R., Ham, A.J., 1988. The characteristics of Southern African coals. The Journal of the South African Institute of Mining and Metallurgy 88 (5), 145-161.

Falcon, R.M., 1986b. Spontaneous combustion of the organic matter in discards from the Witbank coalfield. The Journal of the South African Institute of Mining and Metallurgy 86 (7), 243-250.

Falcon, R.M.S., 1986a. A brief review of the origin, formation, and distribution of coal in southern Africa. In: Anhaeusser, C.R., Maske, S., (Eds.). Mineral Deposits of Southern Africa, Vols. I and II. Geological Society of South Africa, Johannesburg, pp.1879-1898.

Falcon, R.M.S., 1989. Macro-and micro-factors affecting coal-seam quality and distribution in southern Africa with particular reference to the No. 2 seam, Witbank coalfield, South Africa. International Journal of Coal Geology 12 (1-4), 681-731.

Fowler, T.G., Bartle, K.D., Kandiyoti, R., 1987. Low temperature processes in a bituminous coal studied by in situ electron spin resonance spectroscopy. Fuel 66 (10), 1407-1412.

Glasspool, I., 2003a. Palaeoecology of selected South African export coals from the Vryheid Formation, with emphasis on the role of heterosporous lycopods and wildfire derived inertinite. Fuel 82, 959-970.

Glasspool, I.J., 2003b. Hypautochthonous–allochthonous coal deposition in the Permian, South African, Witbank Basin No. 2 seam; a combined approach using sedimentology, coal petrology and palaeontology. International Journal of Coal Geology 53, 81-135.

Glasspool, I.J., Scott, A.C., 2010. Phanerozoic concentrations of atmospheric oxygen reconstructed from sedimentary charcoal. Nature Geoscience Letters 3, 627-630.

Grandy, D.W., Petrakis, L., 1979. Esr investigation of free radicals in solvent-refined coal materials. Fuel 58, 239-240.

Gröcke, D.R., Rimmer, S.M., Yoksoulian, L.E., Cairncross, B., Tsikos, H., van Hunen, J., 2009. No evidence for thermogenic methane release in coal from the Karoo-Ferrar large igneous province. Earth and Planetary Science Letters 277, 204-212.

Guo, Y., Bustin, R.M., 1998. FTIR spectroscopy and reflectance of modern charcoals and fungal decayed woods: implications for studies of inertinite in coals. International Journal of Coal Geology 37, 29-53.

Haenel, M.W., 1992. Recent progress in coal structure research. Fuel 71, 1211-1223.

Hagelskamp, H.H.B., Snyman, C.P., 1988. On the origin of low-reflecting inertinites in coals from the Highveld Coalfield, South Africa. Fuel 67, 307-313.

Hall, G., Woodborne, S., Scholes, M., 2008. Stable carbon isotope ratios from archaeological charcoal as palaeoenvironmental indicators. Chemical Geology 247 (3-4), 384-400.

Han, Z., Kruge, M.A., Crelling, J.C., Stankiewicz, B.A., 1995. Organic geochemical characterization of the density fractions of a Permian torbanite. Organic Geochemistry 22 (1), 39-50.

Hancox, J.P., 2016. The Coalfields of South-Central Africa: A Current Perspective. In: Wilson, M.G.C., (Ed.). The Great Mineral Fields of Africa (Special Issue of the 35 IGC, Cape Town, South Africa 27 August – 4 September 2016). Episodes, Journal of International Geoscience 37 (2), 407-428.

Hancox, J.P., Götz, A.E., 2014. South Africa's coalfields – A 2014 perspective. International Journal of Coal Geology 132, 170-254.

Hartgers, W.A., Sinninghe Damste, J.S., de Leeuw, J.W., Ling, Y., Dyrkacz, G.R., 1994. Molecular Characterization of Flash Pyrolyzates of Two Carboniferous Coals and Their Constituting Maceral Fractions. Energy & Fuels 8 (5), 1055-1067.

Hatcher, P.G., Clifford, D.J., 1997. The organic geochemistry of coal: from plant materials to coal. Organic Geochemistry 27 (5-6), 251-257, 259-274.

Hattingh, B.B., Everson, R.C., Neomagus, H.W.J.P., Bunt, J.R., Van Niekerk, D., Jordaan, J.H.L., Mathews, J.P., 2013. Elucidation of the Structural and Molecular Properties of Typical South African Coals. Energy & Fuels 27 (6), 3161-3172.

Holland, M.J., Cadle, A.B., Pinheiro, R., Falcon, R.M.S., 1989. Depositional environments and coal petrography of the Permian Karoo Sequence: Witbank Coalfield, South Africa. International Journal of Coal Geology 11, 143-169.

Hope, G., Chokkalingam, U., Anwar, S., 2005. The stratigraphy and fire history of the Kutai Peatlands, Kalimantan, Indonesia. Quaternary Research 64, 407-417.

Hower, J.C., O'Keefe, J.M.K., Eble, C.F., Raymond, A., Valentim, B., Volk, T.J., Richardson, A.R., Satterwhite, A.B., Hatch, R.S., 2011a. Notes on the origin of inertinite macerals in coal: Evidence for fungal and arthropod transformations of degraded macerals. International Journal of Coal Geology 86 (2-3), 231-240.

Hower, J.C., O'Keefe, J.M.K., Eble, C.F., Volk, T.J., Richardson, A.R., Satterwhite, A.B., Hatch, R.S., Kostova, I.J., 2011b. Notes on the origin of inertinite macerals in coals: Funginite associations with cutinite and Suberinite, International Journal of Coal Geology 85 (1), 186-190.

Hower, J.C., O'Keefe, J.M.K., Wagner, N.J., Dai, S., Wang, X., Xue, W., 2013. An investigation of Wulantuga coal (Cretaceous, Inner Mongolia) macerals: Paleopathology of faunal and fungal invasions into wood and the recognizable clues for their activity. International Journal of Coal Geology 114, 44-53.

Hower, J.C., O'Keefe, J.M.K., Watt, M.A., Pratt, T.J., Eble, C.F., Stucker, J.D., Richardson, A.R., Kostova, I.J., 2009. Notes on the origin of inertinite macerals in coals: Observations on the importance of fungi in the origin of macrinite. International Journal of Coal Geology 80 (2), 135-143.

Hower, J.C., Wagner, N.J., 2012. Notes on the methods of the combined maceral/microlithotype determination in coal. International Journal of Coal Geology 95, 47-53.

Hower, J.C., Wagner, N.J., O'Keefe, J.M.K., Drew, J.W., Stucker, J.D., Richardson, A.R., 2012. Maceral types in some Permian southern African coals. International Journal of Coal Geology 100, 93-107.

Hu, J.Z., Solum, M.S., Taylor, C.M.V., Pugmire, R.J., Grant, D.M., 2001. Structural Determination in Carbonaceous Solids Using Advanced Solid State NMR Techniques. Energy & Fuels 15 (1), 14-22.

Hunt, J.W., Smyth, M., 1989. Origin of inertinite-rich coals of Australian cratonic basins. International Journal of Coal Geology 11, 23-46.

Ikoma, T., Ito, O., Tero-Kubota, S., 2002. Exploring Radicals in Carbonaceous Solids by Means of Pulsed EPR Spectroscopy. Energy & Fuels 16, 40-47.

International Committee for Coal and Organic Petrology (ICCP)., 1998. The new vitrinite classification. (ICCP System 1994). Fuel 77 (5), 349-358.

International Committee for Coal and Organic Petrology (ICCP)., 2001. The new inertinte classification (ICCP System 1994). Fuel 80 (4), 459-47.

Jasper, A., Guerra-Sommer, M., Abu Hamad, A.M.B., Bamford, M., Cerruti Bernardes-de-Oliveira, M.E., Tewari, R., Uhl, D., 2013. The burning of Gondwana: Permian fires on the southern continent – A palaeobotanical approach. Gondwana Research 24 (1), 148-160.

Jones, T.P., Chaloner, W.G., 1991. Fossil charcoal, its recognition and palaeoatmospheric significance. Palaeogeography, Palaeoclimatology, Palaeoecology (Global and Planetary Change Section) 97, 39-50.

Kawamoto, H., 2017. Lignin pyrolysis reactions. Journal of Wood Science 63 (2), 117-132.

Kelemen, S.R., Afeworki, M., Gorbaty, M.L., Kwiatek, P.J., Sansone, M., Walters, C.C., 2006. Thermal Transformations of Nitrogen and Sulfur Forms in Peat Related to Coalification. Energy & Fuels 20, 635-652.

Kirk, K.T., Farrell, R.L., 1987. Enzymatic "combustion": the microbial degradation of lignin. Annual Review of Microbiology 41, 465-505.

Kohn, M.J., 2010. Carbon isotope composition of terrestrial C3 plants as indicators of (paleo)ecology and (paleo)climate. Proceedings of the National Academy of Sciences of the United States of America 107 (46), 19691-19695.

Kolker, A., Senior, C., van Alphen, C., Koenig, A., Geboy, N., 2017. Mercury and trace element distribution in density separates of a South African Highveld (#4) coal: Implications for mercury reduction and preparation of export coal. International Journal of Coal Geology 170, 7-13.

Kruszewska, K.J., 2003. Fluorescing macerals in South African coals. International Journal of Coal Geology 54, 79-94.

Kwan, C.L., Yen, T.F., 1979. Electron Spin Resonance Study of Coal by Line Width and Line Shape Analysis. Analytical Chemistry 51 (8), 1225-1229.

Lehmann, M.F., Bernasconi, S.M., Barbieri, A., McKenzie, J.A., 2002. Preservation of organic matter and alteration of its carbon and nitrogen isotope composition during simulated and in situ early sedimentary diagenesis. Geochimica et Cosmochimica Acta 66 (20), 3573-3584.

Levine, D.G., Schlosberg, R.H., Silbernagel, B.G., 1982. Understanding the chemistry and physics of coal structure (A Review). Proceedings of the National Academy of Sciences of the United States of America 79, 3365-3370.

Ling, M-.X., Liu, Y., Zhang, H., Sun, W., 2014. Sample Preparation and X-Ray Fluorescence Analysis of Sulfide Ores. Analytical Letters 47, 1598-1605.

Liu, D., Peng, P., 2008. Possible chemical structures and biological precursors of different vitrinites in coal measure in Northwest China. International Journal of Coal Geology 75 (4), 204-212.

Liu, J., Jiang, X., Shen, J., Zhang, H., 2014. Chemical properties of superfine pulverized coal particles. Part 1. Electron paramagnetic resonance analysis of free radical characteristics. Advanced Powder Technology 25 (3), 916-925.

Louw, E.B., Mitchell, G.D., Wang, J., Winans, R.E., Mathews, J.P., 2016. Constitution of Drop-Tube-Generated Coal Chars from Vitrinite- and Inertinite-Rich South African Coals. Energy & Fuels 30 (1), 112-120.

Lusilao-Makiese, J., Tessier, E., Amouroux, D., Hlanganani, T., Chimuka, L., Cukrowska, E.M., 2012. Speciation of mercury in South African coals. Toxicological & Environmental Chemistry 94 (9), 1688-1706.

Malumbazo, N., Wagner, N.J., Bunt, J.R., Van Niekerk, D., Assumption, H., 2011. Structural analysis of chars generated from South African inertinite coals in a pipe-reactor combustion unit. Fuel Processing Technology 92 (4), 743-749.

Mao, J.D., Schimmelmann, A., Mastalerz, M., Hatcher, P.G., Li, Y., 2010. Structural Features of a Bituminous Coal and Their Changes during Low-Temperature Oxidation and Loss of Volatiles Investigated by Advanced Solid-State NMR Spectroscopy. Energy & Fuels 24 (4), 2536-2544.

Maroto-Valer, M.M., Andresén, J.M., Snape, C.E., 1998b. Verification of the linear relationship between carbon aromaticities and H/C ratios for bituminous coals. Fuel 77 (7), 783-785.

Maroto-Valer, M.M., Love, G.D., Snape, C.E., 1994. Relationship between carbon aromaticities and H/C ratios for bituminous coals. Fuel 73 (12), 1926-1928.

Maroto-Valer, M.M., Taulbee, D.N., Andresén, J.M., Hower, J.C., Snape, C.E., 1998a. Quantitative $^{13}C$ NMR study of structural variations within the vitrinite and inertinite maceral groups for a semifusinite-rich bituminous coal. Fuel 77 (8), 805-813.

Marynowski, L., Simoneit, B.R.T., 2009. Widespread Upper Triassic to Lower Jurrasic wildfire records from Poland: Evidence from charcoal and pyrolytic polycyclic aromatic hydrocarbons. Palaios 24 (12), 785-798.

Mastalerz, M., Bustin, R.M., 1994. Variation in reflectance and chemistry of vitrinite and vitrinite precursors in a series of Tertiary Coals, Arctic Canada. Organic Geochemistry 22(6), 921-933.

Mastalerz, M., Bustin, R.M., 1997. Variation in the chemistry of macerals in coals of the Mist Mountain Formation, Elk Valley coalfield, British Columbia, Canada. International Journal of Coal Geology 33 (1), 43-59.

Mastalerz, M., Hower, J.C., Taulbee, D.N., 2013. Variations in chemistry of macerals as reflected by micro-scale analysis of a Spanish coal. Geologica Acta 11 (4), 483-493.

Mazumdar, B.K., 1999. On the relationship between carbon aromaticities and H/C ratios for bituminous coals. Fuel 78, 1239-1241.

Meuzelaar, H.L.C., Harper, A.M., Hill, G.H., Given, P.H., 1984. Characterization and classification of Rocky Mountain coals by Curie-point pyrolysis mass spectrometry. Fuel 63 (5), 640-652.

Moore, T.A. Shearer, J.C., Miller, S.L., 1996. Fungal origin of oxidized plant material in the Palangkaraya peat deposit, Kalimantan Tengah, Indonesia: Implications for 'inertinite' formation in coal. International Journal of Coal Geology 30, 1-23.

Moore, T.A., Shearer, J.C., 1997. Evidence for Aerobic Degradation of Palangka Raya Peat and Implications for its Sustainability. In: Rieley, J.O., Page, S.E., (Eds.). Tropical Peatlands. Samara Publishing Limited, Cardigan, pp.157-167.

Moroeng, O.M., Roberts, R.J., Bussio, J.P., Dixon, R.D., 2017. Self-heating Potential of Coal Inferred from Elemental Data – A Case Study of the Witbank Coalfield of South Africa. Energy & Fuels 31 (11), 11811-11817.

Moroeng, O.M., Wagner, N.J., Brand, D.J., Roberts, R.J., 2018a. A Nuclear Magnetic Resonance study: Implications for coal formation in the Witbank Coalfield, South Africa. International Journal of Coal Geology 188, 145-155.

Moroeng, O.M., Keartland, J.M., Roberts, R.J., Wagner, N.J., 2018b. Characterization of coal using electron spin resonance: implications for the formation of inertinite macerals in the Witbank Coalfield, South Africa. International Journal of Coal Science & Technology 5 (3), 385-398.

Moroeng, O.M., Wagner, N.J., Hall, G., Roberts, R.J. (under review). Using $\delta^{15}N$ and $\delta^{13}C$ and nitrogen functionalities to support a fire-origin for certain inertinite macerals in a No. 4 Seam Upper Witbank coal, South Africa. Organic Geochemistry.

Nip, M., De Leeuw, J.W., Crelling, J.C. 1992. Chemical structure of bituminous coal and its constituting maceral fractions as revealed by flash pyrolysis. Energy & Fuels 6 (2), 125-136.

Nip, M., De Leeuw, J.W., Schenck, P.A., 1988. The characterization of eight maceral concentrates by means of Curie point pyrolysis-gas chromatography and Curie point pyrolysis-gas chromatography-mass spectrometry. Geochimica et Cosmochimica Acta 52 (3), 637-648.

Odden, W., Barth, T., 2000. A study of the composition of light hydrocarbons ($C_5$-$C_{13}$) from pyrolysis of source rock samples. Organic Geochemistry 31 (2-3), 211-229.

O'Keefe, J.M.K., Bechtel, A., Christanis, K., Dai, S., DiMichele, W.A., Eble, C.F., Esterle, J.S., Mastalerz, M., Raymond, A.L., Valentim, B.V., Wagner, N.J., Ward, C.R., Hower, J.C., 2013. On the fundamental difference between coal rank and coal type. International Journal of Coal Geology 118, 58-87.

O'Keefe, J.M.K., Hower, J.C., 2011. Revisiting Coos Bay, Oregon: A re-examination of funginite–huminite relationships in Eocene subbituminous coals. International Journal of Coal Geology 85 (1), 34-42.

Okolo, G.N., Neomagus, H.W.J.P., Everson, R.C., Roberts, M.J., Bunt, J.R., Sakurovs, R., Mathews, J.P., 2015. Chemical-structural properties of South African bituminous coals: Insights from wide angle XRD-carbon fraction analysis, ATR-FTIR, solid state $^{13}$C NMR, and HRTEM techniques. Fuel 158, 779-792.

Pan, S., Hui, S., Liang, L., 2015. Depolymerization Model for Coal Devolatilization: Bridges and Side Chains as the Reaction Centers. Energy & Fuel 29, 2162-2176.

Petrakis, L., Grandy, D.W., 1981. Free radicals in coals and coal conversion. 4. Investigation of the free radicals in selected macerals upon liquefaction. Fuel 60, 120-124.

Phiri, Z., Everson, R.C., Neomagus, H.W.J.P., Wood, B.J., 2017. The effect of acid demineralising bituminous coals and de-ashing the respective chars on nitrogen functional forms. Journal of Analytical and Applied Pyrolysis 125, 127-135.

Phiri, Z., Everson, R.C., Neomagus, H.W.J.P., Wood, B.J., 2018. Transformation of nitrogen functional forms and the accompanying chemical-structural properties emanating from pyrolysis of bituminous coals. Applied Energy 216, 414-427.

Pickel, W., Kus, J., Flores, D., Kalaitzidis, S., Christanis, K., Cardott, B.J., Misz-Kennan, M., Rodrigues, S., Hentschel, A., Hamor-Vido, M., Crosdale, P., Wagner, N., ICCP., 2017. Classification of liptinite – ICCP System 1994. International Journal of Coal Geology 169, 40-61.

Plank, N., 1946. The Nature of Cellulose in Sphagnum. American Journal of Botany 33 (5), 335-337.

Plumstead, E.P., 1961. Ancient plants and drifting continents. South African Journal of Science 57 (7), 173-181.

Pone, J.D.N., Hein, K.A.A., Stracher, G.B., Annegarn, H.J., Finkleman, R.B., Blake, D.R., McCormack, J.K., Schroeder, P., 2007. The spontaneous combustion of coal and its by-products in the Witbank and Sasolburg coalfields of South Africa. International Journal of Coal Geology 72 (2), 124-140.

Powell, T.G., Boreham, C.J., Smyth, M., Russell, N., Cook, A.C., 1991. Petroleum source rock assessment in non-marine sequences: pyrolysis and petrographic analysis of Australian coals and carbonaceous shales. Organic Geochemistry 17 (3), 375-394.

Qiu, N., Li, H., Jin, Z., Zhu, Y., 2007. Temperature and time effect on the concentrations of free radicals in coal: Evidence from laboratory pyrolysis experiments. International Journal of Coal Geology 69, 220-228.

Radlinski, A.P., Mastalerz, M., 2018. Neutron scattering study of vitrinite: Insights into sub-micrometer inclusions in North American Carboniferous coals of bituminous rank. International Journal of Coal Geology 186, 145-154.

Remy, W., Taylor, T.N., Hass, H., Kerp, H., 1994. Four hundred-million-year-old vesicular arbuscular mycorrhizae. Proceedings of the National Academy of Sciences of the United States of America 91 (25), 11841-11843.

Retcofsky, H.L., Stark, J.M., Friedel, R.A., 1968. Electron Spin Resonance in American Coals. Analytical Chemistry 40 (11), 1699-1704.

Retcosfky, H.L., Hough, M.R., Maguire, M.M., Clarkson, R.B., 1981. Nature of the Free Radicals in Coals, Pyrolyzed Coals, Solvent-Refined Coal, and Coal Liquefaction Products. In: Gorbaty, M.L., Ouchi, K., (Eds.). Coal Structure, Advances in Chemistry, 192. American Chemical Society, Washington DC, pp. 37-58.

Richards, J.M., Naude, G., Theron, S.J., McCullum, M., 2013. Petrological characterization of coal: an evolving science. The Journal of the Southern African Institute of Mining and Metallurgy 113, 865-875.

Richardson, A.R., Eble, C.F., Hower, J.C., O'Keefe, J.M.K., 2012. A critical re-examination of the petrology of the No. 5 Block coal in eastern Kentucky with special attention to the origin of inertinite macerals in the splint lithotypes. International Journal of Coal Geology 98, 41-49.

Rimmer, S.M., Rowe, H.D., Taulbee, D.N., Hower, J.C., 2006. Influence of maceral content on $\delta^{13}C$ and $\delta^{15}N$ in a Middle Pennsylvanian coal. Chemical Geology 225, 77-90.

Roberts, M.J., Everson, R.C., Neomagus, H.W.J.P., Okolo, G.N., Van Niekerk, D., Mathews, J.P., 2015a. The characterization of slow-heated inertinite- and vitrinite-rich coals from the South African coalfields. Fuel 158, 591-601.

Roberts, M.J., Everson, R.C., Neomagus, H.W.J.P., Van Niekerk, D., Mathews, J.P., Branken, D.J., 2015b. Influence of maceral composition on the structure, properties and behaviour of chars derived from South African coals. Fuel 142, 9-20.

Ruckwied, K., Götz, A.E., Jones, P., 2014. Palynological records of the Permian Ecca Group (South Africa): Utilizing climatic icehouse–greenhouse signals for cross basin correlations. Palaeogeography, Palaeoclimatology, Palaeoecology 413, 167-172.

Saiz-Jimenez, C., de Leeuw, J.W., 1986. Lignin pyrolysis products: Their structures and their significance as biomarkers. Organic Geochemistry 10, (4-6), 869-876.

Schulten, H.-R., Schnitzer, M., 1998. The chemistry of soil organic nitrogen: a review. Biology and Fertility of Soils 26, 1-15.

Scott, A.C., 1989. Observations on the nature and origin of fusain. International Journal of Coal Geology 12, 443-475.

Scott, A.C., 2002. Coal petrology and the origin of coal macerals: a way ahead? International Journal of Coal Geology 50, 119-134.

Scott, A.C., 2010. Charcoal recognition, taphonomy and uses in palaeoenvironmental analysis. Palaeogeography, Palaeoclimatology, Palaeoecology 291 (1-2), 11-39.

Scott, A.C., Glasspool, I.J., 2007. Observations and experiments on the origin and formation of inertinite group macerals. International Journal of Coal Geology 70 (1-3), 53-66.

Sehume, T.Z., Strydom, C.A., Bunt, J.R., Schobert, H.H., 2017. Effectivity of Phenol during Solvent Extraction of a South African Bituminous Coal under Mild Conditions. Energy & Fuels 31 (12), 13655-13665.

Senftle, J.T., Larter, S.R., 1987. Comparative geochemistry of vitrinite kerogens from Carboniferous and Tertiary provinces. Organic Geochemistry 11 (5), 407-409.

Senftle, J.T., Larter, S.R., Bromley, B.W., Brown, J.H., 1986. Quantitative chemical characterization of vitrinite concentrates using pyrolysis-gas chromatography. Rank variation of pyrolysis products. Organic Geochemistry 9 (6), 345-350.

Shearer, J.C., Moore, T.A., 1996. Effects of experimental coalification on texture, composition and compaction in Indonesian peat and wood. Organic Geochemistry 24 (2), 127-140.

Silbernagel, B.G., Gebhard, L.A., Dyrkacz, G.R., 1984b. Electron Spin Resonance of Isolated Coal Macerals. In: Petrakis, L., Fraissard, J.P., (Eds.). Magnetic Resonance. Introduction, Advanced Topics and Applications to Fossil Energy. D. Reidel Publishing Company, pp. 645-653.

Silbernagel, B.G., Gebhard, L.A., Dyrkacz, G.R., Bloomquist, C.A.A., 1986. Electron spin resonance of isolated coal macerals. Fuel 65, 558-565.

Silbernagel, B.G., Gebhard, L.A., Dyrkacz, G.R., Bloomquist, C.A.A., 1984a. Electron Spin Resonance of Isolated Coal Macerals, Preliminary Survey. In: Winans, R.E., Crelling, J.C., (Eds.). Chemistry and Characterization of Coal Macerals. ACS Symposium Series, American Chemical Society, Washington DC, pp. 121-135.

Simoneit, B.R.T., Rogge, W.F., Mazurek, M.A., Standley, L.J., Hilderman, L.M., Cass, G.R., 1993. Lignin pyrolysis products, lignans, and resin acids as specific tracers of plant classes in emissions from biomass combustion. Environmental Science and Technology 27, 2533-2541.

Skrzypek, G., Jezierski, P., Szynkiewicz, A., 2010. Preservation of primary stable isotope signatures of peat-forming plants during early decomposition – observation along an altitudinal transect. Chemical Geology 273, 238-249.

Slater, B.J., McLoughlin, S., Hilton, J., 2015. A high-altitude Gondwana lagerstätte: The Permian permineralised peat biota of the Prince Charles Mountains, Antarctica. Gondwana Research 27, 1446-1473.

Snyman, C.P., 1989. The role of coal petrography in understanding the properties of South African coal. In: Pickhardt, W., (Ed.). Erich Stach Memorial Issue. International Journal of Coal Geology 14, 83-101.

Snyman, C.P., Botha, W.J. 1993. Coal in South Africa. Journal of African Earth Sciences 16 (1/2), 171-180).

Solum, M.S, Pugmire, R.J., Grant, D.M., 1989. $^{13}C$ Solid-state NMR of Argonne Premium Coals. Energy & Fuels 3, 187-193.

South African National Standards (SANS) 17246:2011 (ISO 17246:2010). Coal - Proximate analysis.

South African National Standards (SANS) 17247:2006 (ISO 17247:2005). Coal - Ultimate analysis.

South African National Standards (SANS) 1928:2009 (ISO 1928:2009). Solid mineral fuels - Determination of gross calorific value by the bomb calorific method, and calculation of net calorific value.

South African National Standards (SANS) 334:1992 (ISO 334:1992). Solid mineral fuels - Determination of total sulfur - Eschka method.

South African National Standards (SANS) 7404-2:2015 (ISO 7404-2:2009). Methods for the petrographic analysis of coals Part 2: Methods of preparing coal samples.

South African National Standards (SANS) 7404-3:2016 (ISO 7404-3:2009). Methods for the petrographic analysis of coals - Part 3: Method of determining maceral group.

South African National Standards (SANS) 7404-5:2016 (ISO 7404-5:2009). Methods for the petrographic analysis of coals - Part 5: Method of determining microscopically the reflectance of vitrinite.

South African National Standards (SANS) 7936:2010 (ISO 7936:1992). Hard coal – Determination and presentation of float and sink characteristics – General directions for apparatus and procedures.

Spiker, E.G., Hatcher, P.G., 1987. The effects of early diagenesis on the chemical and stable carbon isotopic composition of wood. Geochimica et Cosmochimica Acta 51 (6), 1385-1391.

Steyn, M., Minnitt, R.C.A., 2010. Thermal coal products in South Africa. The Journal of Southern African Institute of Mining and Metallurgy 110 (10), 593-599.

Stout, S.A., Spackman, W., 1989. Notes on the compaction of a Florida peat and the Brandon lignite as deduced from the study of compressed wood. International Journal of Coal Geology 11, 247-256.

Strydom, C.A., Bunt, J.R., Schobert, H.H., Raghoo, M., 2011. Changes to the organic functional groups of an inertinite rich medium rank bituminous coal during acid treatment processes. Fuel Processing Technology 92, 764-770.

Suggate, R.P., Dickinson, W.W., 2004. Carbon NMR of coals: the effects of coal type and rank. International Journal of Coal Geology 57, 1-22.

Sun, Y., Horsfield, B., 2005. Comparison of the Geochemical Characteristics of “Barkinite” and Other Macerals from the Dahe Mine, South China. Energy Exploration & Exploitation 23 (6), 475-494.

Supaluknari, S., Burgar, I., Larkins, F.P., 1990. High-resolution solid-state $^{13}C$ NMR studies of Australian coals. Organic Geochemistry 15 (5), 509-519.

Suto, N., Kawashima, H., 2016. Global mapping of carbon isotope ratios in coal. Journal of Geochemical Exploration 167, 12-19.

Taylor, G.H., Teichmüller, M., Davis, A., Diessel, C.F.K., Littke, R., Robert, P., 1998. Organic Petrology. Gebrüder Borntraeger, Berlin, 704pp.

Teichmüller, M., 1989. The genesis of coal from the viewpoint of coal petrology. In: Lyons, P.C., Alpern, B., (Eds.). Peat and Coal: Origin, Facies, and Depositional Models. International Journal of Coal Geology 12, 1-87.

Turekian, V.C., Macko, S., Ballentine, D., Swap, R.J., Garstang, M., 1998. Causes of bulk carbon and nitrogen isotopic fractionations in the products of vegetation burns: laboratory studies. Chemical Geology 152, 181-192.

Unsworth, J.F., Fowler, C.S., Jones, L.F., 1989. Moisture in coal: 2. Maceral effects on pore structure. Fuel 68 (1), 18-26.

Valentim, B., Algarra, M., Guedes, A., Ruppert, L.F., Hower, J.C., 2016. Notes on the origin of copromacrinite based on nitrogen functionalities and $\delta^{13}C$ and $\delta^{15}N$ determined on samples from the Peach Orchard coal bed, southern Magoffin County, Kentucky. International Journal of Coal Geology 160-161, 63-72.

van Asselen, S., Stouthamer, E., van Asch, Th.W.J., 2009. Effects of peat compaction on delta evolution: A review on process, responses, measuring and modelling. Earth Science Reviews 92, 31-35.

van Krevelen, D.W., 1993. Coal: Typology - Chemistry - Physics - Constitution, third ed. Elsevier, Amsterdam, 979pp.

Van Niekerk, D., Mathews, J.P., 2010. Molecular representations of Permian-aged vitrinite-rich and inertinite-rich South African coals. Fuel 89, 73-82.

Van Niekerk, D., Mitchell, G.D., Mathews, J.P., 2010. Petrographic and reflectance analysis of solvent-swelled and solvent-extracted South African vitrinite-rich and inertinite-rich coals. International Journal of Coal Geology 81, 45-52.

Van Niekerk, D., Pugmire, R.J., Solum, M.S., Painter, P.C., Mathews, J.P., 2008. Structural characterization of vitrinite-rich and inertinite-rich Permian-aged South African bituminous coals. International Journal of Coal Geology 76, 290-300.

Veld, H., de Leeuw, J.W., Sinninghe Damsté, J.S., Fermont, W.J.J., 1994. Molecular Characterization of Vitrinite Maturation as Revealed by Flash Pyrolysis Methods. In: Mukhopadhyay, P.K., Dow, W.G., (Eds.). Vitrinite Reflectance as a Maturity Parameter: Applications and Limitations. ACS Symposium Series 570, American Chemical Society, Washington DC, pp. 149-160.

Wagner, N.J., Hlatshwayo, B., 2005. The occurrence of potentially hazardous trace elements in five Highveld coals, South Africa. International Journal of Coal Geology 63 (3-4), 228-246.

Wagner, N.J., Tlotleng, M.T., 2012. Distribution of selected trace elements in density fractionated Waterberg coals from South Africa. International Journal of Coal Geology 94, 225-237.

Wang, R., Sun, R., Liu, G., Yousaf, B., Wu, D., Chen, J., Zhang, H., 2017. A review of the biogeochemical controls on the occurrence and distribution of polycyclic aromatic compounds (PACs) in coals. Earth-Science Reviews 171, 400-418.

White, A., Davies, M.R., Jones, S.D., 1989. Reactivity and characterization of coal maceral concentrates. Fuel 68, 511-519.

Whiticar, M.J., 1996. Stable isotope geochemistry of coals, humic kerogens and related natural gases. International Journal of Coal Geology 32, 191-215.

Więckowski, A.B., Wojtowicz, W., Pilawa, B., 2000. EPR characteristics of petrographically complex coal samples from durain and clarain. Fuel 79, 1137-1141.

Yang, H., Yan, R., Chen, H., Lee, D.H., Zheng, C., 2007. Characteristics of hemicellulose, cellulose and lignin pyrolysis. Fuel 86, 1781-1788.

Zhou, Q., Liu, Q., Shi, L., Yuxin, Y., Liu, Z., 2017. Behaviors of coking and radicals during reaction of volatiles generated from fixed-bed pyrolysis of a lignite and a subbituminous coal. Fuel Processing Technology 161, 304-310.

Zieger, L., Littke, R., Schwarzbauer, J., 2018. Chemical and structural changes in vitrinites and megaspores from Carboniferous coals during maturation. International Journal of Coal Geology 185, 91-102.